UNIVERSITY OF NAPLES FEDERICO II

POLYTECHNIC SCHOOL AND OF BASIC SCIENCES

EDUCATIONAL AREA: MATHEMATICS, PHYSICS, NATURAL SCIENCES

PhD in Chemical Sciences

XXIX Cycle (2014-2017)

Nature-inspired phenolic systems for technological and biomedical applications

Dr. Mariagrazia Iacomino

Supervisor

Prof. Marco d'Ischia

Assessor

Prof. Orlando Crescenzi

Coordinator

Prof. Luigi Paduano

UNIVERSITA' DEGLI STUDI DI NAPOLI FEDERICO II

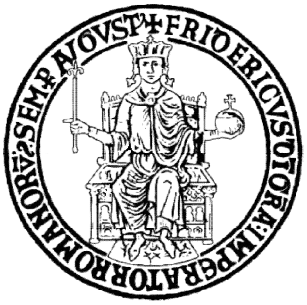

SCUOLA POLITECNICA E DELLE SCIENZE DI BASE

AREA EDUCATIVA: SCIENZE MATEMATICHE, FISICHE, NATURALI

Dottorato di Ricerca in Scienze Chimiche

XXIX Ciclo (2014-2017)

Sistemi fenolici ispirati alla Natura per applicazioni tecnologiche e biomediche

Dr. Mariagrazia Iacomino

Tutore

Prof. Marco d'Ischia

Relatore

Prof. Orlando Crescenzi

Coordinatore

Prof. Luigi Paduano

INDEX

List of publications

1. "Multifunctional thin films and coatings from caffeic acid and a cross-linking diamine." **M. Iacomino**, J.I. Paez, R. Avolio, A. Carpentieri, L. Panzella, G. Falco, E. Pizzo, M.E. Errico, A. Napolitano, A. Del Campo, M. d'Ischia, *Langmuir*, **2017**, *33*, 2096-2102, DOI: 10.1021/acs.langmuir.6b04079.

2. "Eumelanin broadband absorption develops from aggregation-modulated chromophore interactions under structural and redox control." R. Micillo, L. Panzella, **M. Iacomino**, G. Prampolini, I. Cacelli, A. Ferretti, O. Crescenzi, K. Koike, A. Napolitano, M. d'Ischia, *Sci Rep*., **2017**, *7*, DOI: 10.1038/srep41532.

3. "Tailoring melanins for bioelectronics: polycysteinyldopamine as an ion conducting redox-responsive polydopamine variant for pro-oxidant thin films." N.F. Della Vecchia, R. Marega, M. Ambrico, **M. Iacomino**, R. Micillo, A. Napolitano, D. Bonifazi, M. d'Ischia, *J. Mater Chem. C*., **2015**, *3*, 6525-6531, DOI: 10.1039/C5TC00672D.

Manuscripts in preparation

1. "Assessing the impact of carboxyl group esterification on the antioxidant activity, structural properties and stability of 5,6-dihydroxyindole-2-carboxylic acid melanins." R. Micillo, L. Panzella, **M. Iacomino**, O.Crescenzi, K. Koike, G. Monfrecola, A. Napolitano, M. d'Ischia (submitted).

2. "Resorcinol-switched autoxidation of dopamine: designing multifunctional fluorescence turn-on systems." **M. Iacomino**, C. T. Prontera,O. Crescenzi, M. d'Ischia, A. Napolitano. (submitted)

3. "Optimized preparation, chromophore stability and toxicity evaluation of the benzacridine pigments from reaction of chlorogenic acid with amino acids and proteins: toward the development of a green coloring agent for food." **M. Iacomino**, F. Weber, M. Gleichenhagen, V. Pistorio, L. Panzella, E. Pizzo, A. Schieber, M. d'Ischia, A. Napolitano. (submitted)

4. “A sulfur-based heteroatom replacement strategy for eumelanin manipulation: thiomelanin.” (in preparation)

Statement of candidate's contribution to jointly-published work

Chapter 2. *Structure-property-function relationships for the rational design of tailored melanins.*

The concepts presented in this chapter were reportedin the publication *"Eumelanin broadband absorption develops from aggregation-modulated chromophore interactions under structural and redox control"* R. Micillo, L. Panzella, **M. Iacomino**, G. Prampolini, I. Cacelli, A. Ferretti, O. Crescenzi, K. Koike, A. Napolitano, M. d'Ischia, presently in press on *Sci Rep*., **2017**, DOI: 10.1038/srep41532. I prepared precursors, carried out kinetic experiments and interpreted results.

The same chapter also reports main results from the submitted work *"Assessing the impact of carboxyl group esterification on the antioxidant activity, structural properties and stability of 5,6-dihydroxyindole-2-carboxylic acid melanins."* R. Micillo, L. Panzella, **M. Iacomino**, O.Crescenzi, K. Koike, G. Monfrecola, A. Napolitano, M. d'Ischia. I prepared 5,6-dihydroxyindole-2-carboxylic acid (DHICA) and the relative methyl ester (MeDHICA) monomers and deriving polymers, performed anti-oxidant activity assays, spectrophotometric and MALDI-MS characterization of synthetic eumelanines.

Chapter 3. *The S-substitution strategy for manipulation of catechol polymerization chemistry.*

The first section of this chapter is a partial representation of the paper *"Tailoring melanins for bioelectronics: polycysteinyldopamine as an ion conducting redox-responsive polydopamine variant for pro-oxidant thin films."* N.F. Della Vecchia, R. Marega, M. Ambrico, **M. Iacomino**, R. Micillo, A. Napolitano, D. Bonifazi, M. d'Ischia, *J. Mater Chem. C*., 2015, 3, 6525-6531, DOI: 10.1039/C5TC00672D.I prepared 5-S-cysteinyldopamine (CDA) monomer, collaborated to optimizing the dip-coating procedure to obtain pCDA thin films, and performed HPLC analysis of pro-oxidant properties of p(CDA) films.

Still unpublished results regarding a *sulfur-based heteroatom replacement strategy for eumelanin manipulation* are also summarized. This work was conceived by Professor Marco

d'Ischia in collaboration with Professor Daniel Ruiz Molina of the Catalan Institute of Nanoscience and Nanotechnology in Bellaterra (Barcelona, Spain). During my 3 months stage (September-December 2016), I synthesized and characterized 3,4-dihydroxyphenylethanthiol (DHPET) and 5,6-dihydroxybenzothiophene (DHBT) as sulphur-replaced analogs of eumelanin precursors. I also carried out purification and preliminary characterization of the oligomers andpolymers. The manuscript is currently in preparation.

Chapter 4. *Multifunctional mussel-inspired biomaterials and molecular systems by amine-controlled oxidative polymerization of natural catechols*

This chapter follows closely work that has been published as *"Multifunctional thin films and coatings from caffeic acid and a cross-linking diamine."* **M. Iacomino**, J.I. Paez, R. Avolio, A. Carpentieri, L. Panzella, G. Falco, E. Pizzo, M.E. Errico, A. Napolitano, A. Del Campo, M. d'Ischia, *Langmuir*, 2017, DOI: 10.1021/acs.langmuir.6b04079.I performed substrate coating experiments, UV-vis and ATR/FT-IR spectroscopy, I also run metal binding and dye adsorption evaluation assays.

The second section of this chapter isa representation of a related project on the *optimized preparation, chromophore stability and toxicity evaluation of the benzacridine pigments from reaction of chlorogenic acid with amino acids and proteins*. These results are reported in a manuscript under submission. I performed all the reported experiments except for LC-MS-MS analysis and toxicity tests on cells.

Chapter 5. *Dopamine-based multifunctional fluorescence turn-on systems.*

This chapter reports the results presented in the manuscript under submission *"Resorcinol-switched autoxidation of dopamine: designing multifunctional fluorescence turn-on systems."* **M. Iacomino**, C. T. Prontera, O. Crescenzi, M. d'Ischia, A. Napolitano. I synthesized and characterized the reported compounds by NMR and LC-MS spectrometry, UV-vis, fluorescence and FT-IR spectroscopy. I also performed the dip-coating procedures to obtain BisRes/DA thin films.

ABSTRACT

The imitation of Nature's chemical principles and logics has emerged as a competitive strategy for the design and implementation of functional molecular systems and biomaterials for innovative technological and biomedical applications. A unique source of inspiration in this context is offered by phenols, polyphenols and especially catechols, in view of their disparate biological roles. In the last decades, great interest has been directed to understand structural, physical and chemical properties of melanins, the black or brownish-red insoluble polyphenolic pigments of human skin, hair, eyes and melanomas.[1–6] However, the extreme heterogeneity of their molecular systems and practical difficulties in their extraction and purification processes from natural sources, made their structural characterization and the definition of structure-properties relationships a most difficult task. To this aim, synthetic mimics of natural melanins that can be obtained by oxidative polymerization of dopamine (DA), DOPA, 5-S-cysteinyldopamine (CDA), 5,6-dihydroxyindole (DHI) or 5,6- dihydroxyindole carboxylic acid (DHICA) hold much promise for technological applications due to their peculiar properties which include a broad-band UV and visible absorption profile, redox properties, free radical scavenging ability and water-dependent hybrid electronic-ionic semiconduction.[2,3,6–11]

Of particular relevance for technological purposes is the black polymer produced by oxidation of dopamine, polydopamine (PDA) and inspired by mussels' unique ability to strongly adhere to rocks underwater via catechol and amine crosslinks from DOPA and lysine residues.[12–15] Because of its robustness, universal adhesion properties, biocompatibility, reversible and pH-switchable permselectivity for both cationic and anionic redox-active probe molecules, PDA-based coating technology has opened up the doorway to novel opportunities in the fields of bioengineering, nanomedicine, biosensing and organic electronics.[12,16–23]

So far, however, progress in polyphenol-, catecholamine- and melanin-based functional materials and systems has been limited by a number of gaps and issues, including:

a) the lack of rational strategies based on structure-property relationships for selectively enhancing functionality or imparting new technologically relevant properties to polydopamine and synthetic melanins tailored to applications.

b) the lack of detailed studies on the actual scope of previous observations in the literature on catecholamine oxidation chemistry and the coupling with carbon, nitrogen and sulfur nucleophiles;
c) the lack of unambiguous data about the specific structural factors underpinning the universal material independent sticking behavior of polydopamine and other mussel-inspired bioadhesives.

In the light of the foregoing, specific objectives of the present PhD project include:

1) The definition of key structure-property relationships in synthetic eumelanins for the development of rational strategies to enhance or tailor functionality for specific applications;
2) The synthesis and chemical characterization of innovative molecular systems and functional polymers based on rational manipulation of melanin precursors, including dopamine and 5,6-dihydroxyindole for adhesion, crosslinking and other applications;
3) The development of alternative mussel inspired systems for various applications based on the oxidative chemistry of cheap, easily accessible and non-toxic natural phenolic compounds such as caffeic acid and chlorogenic acid;
4) The rational design of novel fluorescence turn-on systems for sensing applications based on catecholamine oxidation chemistry and coupling with nucleophiles.

Main results can be summarized as follows:

1) The origin and structure-dependent differences of the main chromophores generated by oxidative polymerization of DHI and DHICA to melanin-type products have been elucidated by a combined experimental and computational approach based on an unprecedented set of dimeric precursors. An improved model for the origin of eumelanin broadband absorption properties has been proposed;
2) The impact of carboxyl group esterification on the structure and antioxidant activity of DHICA-melanins has been clarified for the first time, providing novel directions for the design of melanin-inspired antioxidants and functional systems;
3) The adhesion and pro-oxidant properties of the polymer deriving from CDA oxidation (pCDA) were reported in comparison with PDA. This material proved capable of accelerating the kinetics of autoxidation of glutathione in its reduced form (GSH), a property potentially useful for sensing applications;

4) Two new sulfur-containing analogs of dopamine and 5,6-dihydroxyindole were synthesized, 3,4-dihydroxyphenilethanethiol (DHPET) and 5,6-dihydroxybenzothiophene (DHBT), their oxidative chemistry was investigated and the spectrophotometric, morphological and electronic properties of the DHBT polymer (thiomelanin) were assessed in the frame of a proof-of-concept project on novel melanin-like materials. Part of this work was carried out during a 3-month stay at the Catalan Institute for Nanoscience and Nanotechnologies (ICN2, Bellaterra, Spain)
5) Novel mussel-inspired adhesive films and biocompatible coatings with good metal-chelating and dye adsorbing properties were rationally designed and characterized by the autoxidative coupling of the natural catechol caffeic acid with the long-chain hexamethylenediamine at pH 9. The same coupling chemistry was extended to chlorogenic acid and two amino acids, glycine and lysine, for the synthesis of biocompatible green pigments for food-related applications.
6) A pH-sensitive fluorescent thin film and a fluorescent polymer tag were designed and obtained by suitable optimization of the strongly fluorogenic reaction between dopamine and resorcinols. The reaction is efficient, develops from cheap and easily available compounds and can be extended to a range of resorcinol and catecholamine partners. Possible sensing of volatile amines with this fluorogenic system is disclosed.

Overall, these results fulfil the main objectives of the PhD project and expand the current repertoire of functional nature-inspired materials and systems.

Chapter 1

Introduction

1.1 Functional systems inspired by Nature

Observation of natural phenomena and organisms has been, through the centuries, a primary source of questions and therefore, of answers aimed at unraveling the complexity of such systems and mimic Nature solutions to solve human problems. Indeed, learning from Nature, researchers developed artificial materials and devices with advanced properties for sustainable and efficient technological and biomedical solutions. Figure 1.1.1 shows the constant increasing number of scientific works reporting advances in the field of Nature inspired materials through the last 10 years.

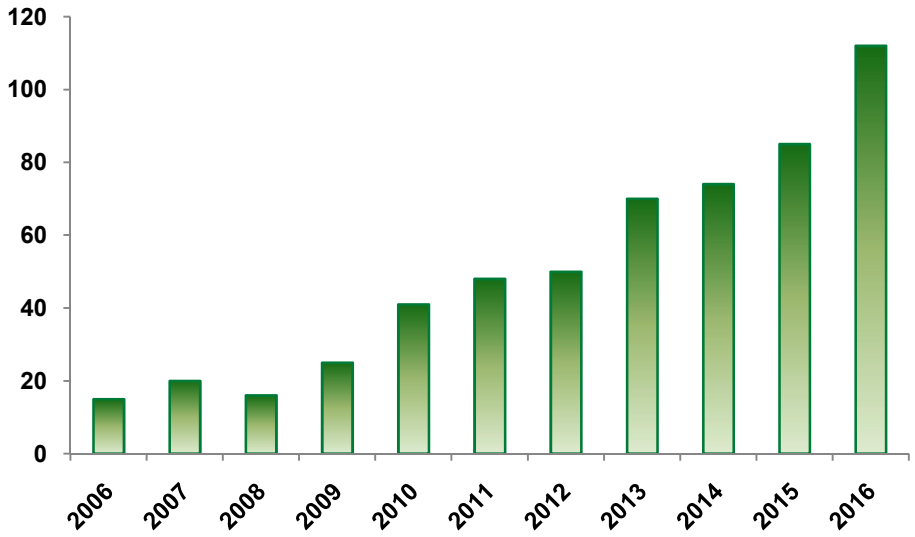

Figure 1.1.1 *Histrogram reporting the results of the research topic "nature inspired materials" analyzed by SciFinder analysis tool by year of publication.*

Investigation on biological systems pointed out their ability to exhibit extremely sophisticated features and properties that normally are not determined by their bulk properties, but more related to their intrinsic hierarchical micro/nanoscale architecture and abundant interfacial interactions. These latter, are mainly provided by highly specific weak interactions (*i.e.* hydrogen

bonding, coordination bonds, hydrophilic/hydrophobic interactions, π-stacking) than by strong covalent bonds.

This relationship between architecture, interfacial interactions, and properties of natural materials, supplies the inspiration to generate novel devices and materials, potentially useful for sensing, catalysis, transport, and other applications in medicinal or engineering science both in the biomedical or technological field.

Biomedical devices and technological applications. Natural evolution has led to highly functional assemblies of proteins, nucleic acids, and other (macro)molecules which perform complicated tasks that are still daunting for us to try to emulate. Tissue engineering and regenerative medicine has been taking great inspiration from the natural world. Of particular interest are biopolymeric matrices and bioactive nanosized fillers that thanks to their biodegradability, high mechanical strength, and similarities with extracellular matrices help in repair and regenerate damaged tissues and organs, especially to obtain bone-like implantable materials.[24–27]

Surface modification with biocompatible smart materials capable to improve cell attachment, proliferation and adhesion to tissues is an important issue in the context of biomedical applications because the biological response is often determined by biointerfacial interactions.[28]

Likewise, the design and realization of materials and coatings with tailored hydrophilicity/hydrophobicity properties is currently a hot topic of great technological relevance, and nature represents in this connection a uniquely rich source of inspiration for innovative solutions. The lotus leaf surface possesses a typical superhydrophobic ability and self-cleaning property due to branch-like nanostructures on top of the micropapillae.[29,30] Super-hydrophobicity is also found in the rose petal, that shows a strong adhesion force preventing water droplets rolling down thanks to a "raspberry-like" microstructure of its surface that allows drops penetration in the first levels of this fascinating structural organization.[31,32]

Besides hydrophobicity, optical properties are often associated with structured molecular architectures. The color of the feathers of a peacock or the wings of a butterfly are all caused by microstructures that exhibit periodic variations in dielectric constant in one, two or three dimensions. Color through structure can be found in a significant number of animals, particularly those living in poorly illuminated environments.[33] and they find relevant technological applications as, light manipulation, optical sensors, light–energy conversion, plasmonic materials with ultrahigh surface plasmon resonance (SPR) efficiency and metamaterials.[34,35]

Many examples of environment-friendly energy-storage materials have also been reported.[36] For example, inspired by the electron shuttles functioning in extracellular electron transfer via reversible redox-cycling, electrode materials with similar active functional groups have been explored.[37] Nature inspired frameworks for the development of solar cells,[38] photovoltaic materials,[39] and systems for artificial photosynthesis[40,41] also represent a highly active field of research.

The creation of such complex functionalities in bioinspired materials certainly depends on their multiscale structures and the rationale design of new, high performance materials requires a deep understanding of the underlying structure–property relationships. But, from the foregoing, it is clear that all of the above mentioned properties and functions are consequence of tailored molecular assemblies and interfaces with specific chemical and physical features that change and adapt in response to environmental cues. More in detail, functional changes at macroscopic scale are always the result of a response that occurs at the molecular level.

This response, in turn, depends in most cases on the dynamic interplay of interacting molecular systems endowed with great chemical versatility and responsiveness. In this context, polyphenols and especially catechols, represent most versatile molecular tools exploited by nature to fulfill a variety of roles and functions. Indeed, catechol-based compounds play a variety of roles in biological systems , such as antioxidant and free radical scavengers (e.g. natural polyphenols of plant origin), photoprotection (melanin pigments), molecular mediators and messengers (catecholamine neurotransmitters and hormones) and tissue strengthening via cross-linking (DOPA residues in mussel edulis foot proteins (mefp) and N-acetyldopamine in the sclerotization of insect cuticle).

Noticeable examples of natural catechol-based systems and derivatives can be classified in two main groups (Figure 1.1.2):

1. **Small molecules** as molecular mediators and messengers, including: catecholamine neurotransmitters and hormones, such as dopamine, norepinephrine and epinephrine and their metabolites and conjugates;

   products of metabolic transformation of steroids, such as the catecholestrogens;

   active structural components as N-acetyldopamine in the insect cuticle sclerotization;

   pigments as anthocyanines and flavonoids that confer to fruits and flowers their characteristic colours;[42]

anti-oxidants and free radical scavengers as hydroxytyrosol, pyrogallol, gallic, caffeic and chlorogenic acid derivatives, epicatechins, curcumin and anthocyanines;[29]

2. **Polyphenolic polymers** of plant origin as lignins, tannins, characterized by a marked structural diversity. Lignins derive from coniferyl and p-coumaryl alcohols and are investigated for their fuel value as well as to produce plastic-like materials. Tannins and related substances are used as clarifying agents in alcoholic drinks and as aroma ingredient in both alcoholic and soft drinks or juices, and find extensive uses in the wine industry,

   Polyphenolic polymers can also be found in animals. Noticeable examples include the melanins, the black (eumelanin) or reddish-brown (pheomelanin) pigments of human skin and hair, mammalian fur, bird feathers, cephalopod ink.

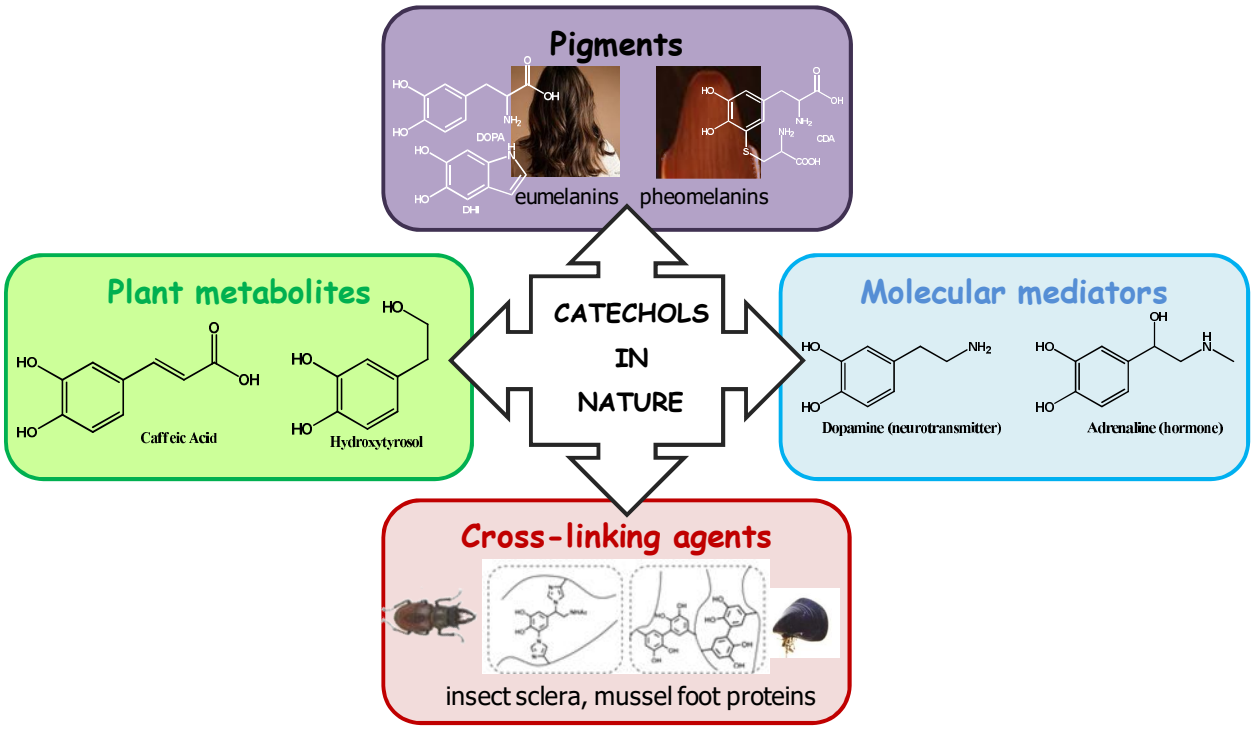

Figure 1.1.2 *Representative biological roles of catechols*.

Such a variety of diverse biological roles can be explained by the versatility of catechol chemistry.

1.2 Catechol chemistry

The presence of an *ortho* diphenol group confers to catechols a high oxidizability, slightly acidic properties under specific conditions, an electron-rich aromatic ring for electrophilic reactions and functionalization, and an ideal disposition for bidentate coordination and hydrogen bonding. As a result, catechol chemistry is largely dominated by metal chelating properties and redox equilibria. Moreover, upon conversion to semiquinone and quinone derivatives, catechols can turn into free radical intermediates and highly electrophilic species, respectively, becoming available for efficient coupling processes and for nucleophilic attack on the part of functional groups of biomolecules such as thiols, amines, as well as carbon nucleophiles including phenolic and catecholic rings. This peculiar chemistry is at the basis of a variety of biologically relevant processes, such as conjugation, polymerization, cross-linking and coupling that can be reproduced in vitro under mild biomimetic conditions. The nucleophilic character of the OH groups, moreover, makes them susceptible of important biological reactions such as sulfation, glucuronidation and methylation, e.g. by enzymes like catechol-O-methyl transferase (COMT) (Scheme 1.2.1).

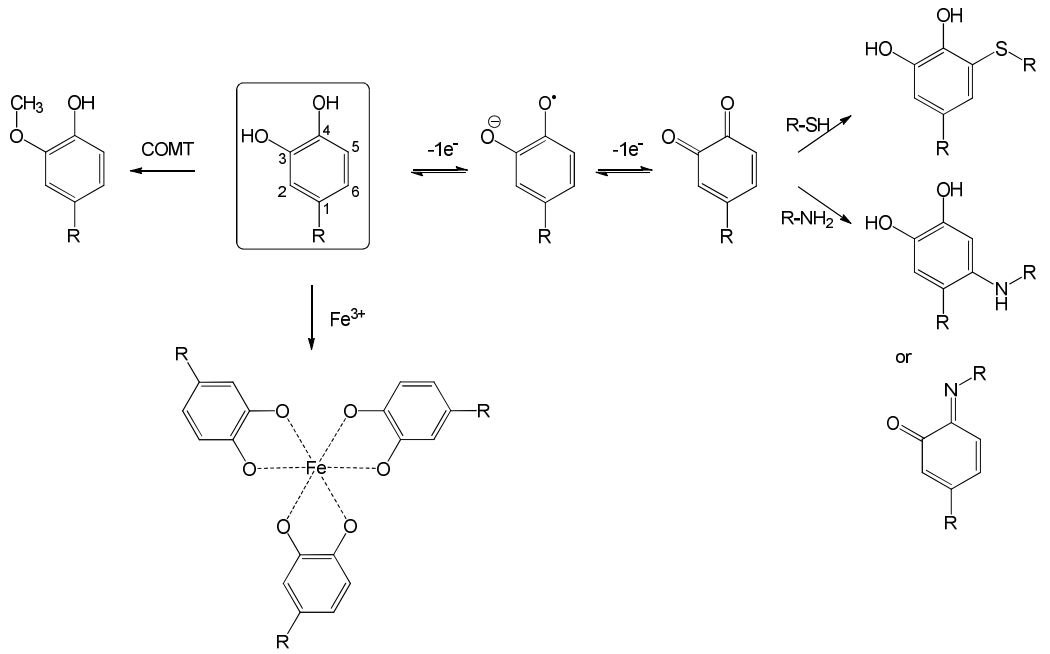

Scheme 1.2.1 *Catechol chemistry and biochemistry. The reaction with COMT involves preferentially catecholamines, therefore –R= alkylamino chain*.

Coordination chemistry. The catecholic *ortho* hydroxyl groups can donate non-bonding electron pair to many metal ions such as Fe^{2+}/Fe^{3+}, Cu^{2+}, Co^{2+}, Ni^{2+}, V^{3+}, Ga^{3+} to form reversible non-covalent complexes (chelates). The metal-to catechol complex stoichiometry is usually 1:1 and 1:2 for low-valent metals, while high-valent ions form 1:1, 1:2, and 1:3 complexes.[45]

The coordinative chemistry of catechols with iron (III) is particularly interesting, because the stability constants of bis- and tris- catechol–Fe^{3+} complexes are among the highest known for metal–ligand chelates.[46] Single molecule force measurements demonstrated that the catechol–Fe^{3+} bond is only slightly weaker than a covalent bond but, interestingly it can spontaneously reform after breaking.[47] Stoichiometry of the catechol–Fe^{3+} complexes has been deeply investigated as it seems to play a fundamental role in the underwater adhesion mechanism of mussels.[48–51] It has been found that catechol coordination chemistry is strictly controlled by pH via the deprotonation of the catecholic hydroxyl groups. The mono catechol–Fe^{3+} complexes dominate at pH lower than 5.6, bis at pH between 5.6 and 9.1, and tris at pH higher than 9.1.[13] The stoichiometry of the complex also depends on Fe^{3+} concentration: low iron (III) concentrations favour the tris-complex formation, while at high Fe^{3+} concentrations, the mono complex is formed.[46] Finally, the substituents on the catecholic aromatic ring affect the catechol–Fe^{3+} coordination by changing the pK_a values of the catechol analogues. Electron withdrawing substituents (e.g. $–NO_2$) result in lowering of the pK_a values (the pK_a values for nitrocatechol are 6.7 and 10.3; and for catechol are 9.1 and 14).[52] Thereby, nitro-substituted catechols form chelates and crosslinks at lower pH values.

Redox chemistry. Catechol redox systems involves the formation of quinone and hydroquinone type equilibrium species. In fully buffered media the quinone/hydroquinone redox process involves changes in the protonation state of the molecule, resulting in the observation that potentiometric or amperometric equilibrium potentials vary with pH. The pH dependence of the catechol redox process can be ascribed to a two proton−two electron ($2H^+$ $2e^–$) transfer, commonly known as a proton-coupled electron transfer reaction. This process is well represented in the "scheme of squares" shown in Scheme 1.2.2.[53] Under biological conditions, the redox reaction between catechol and oxygen, typically referred to as "autoxidation", is thermodynamically unfavourable because of the high activation energy barrier (530 mV). In natural systems, the obstacle of the catechol auto-oxidation, is overcome by the presence of enzymes (e.g. tyrosinase, horseradish peroxidase/H_2O_2) or metal ions (e.g. Fe^{3+}).[54]

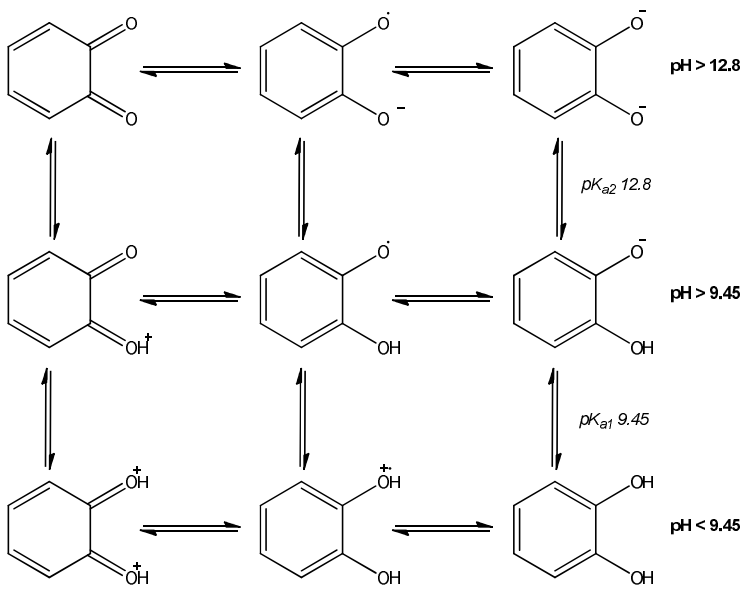

Scheme 1.2.2 *Catechols redox equilibria*.

Coupling with nucleophiles. Upon conversion to semiquinone and o-quinone derivatives, catechols can turn into free radical intermediates and highly electrophilic species, respectively, becoming available for efficient coupling processes and for nucleophilic attack on the part of functional groups such as thiols, amines, as well as carbon nucleophiles including phenolic and catecholic rings, allowing for conjugation, polymerization, cross-linking and coupling even under mild biologically-relevant conditions.

As mentioned previously, the reaction between catechols and amines is of vital importance in many natural biological processes, such as the cross-linking of adhesive proteins by marine organisms,[55] the formation of cytoskeleton by insects[56] and the biosynthesis of melanin.[8] For instance, in blue mussels, both DOPA and L-lysine are present in large quantities in mussel adhesive foot proteins (mfps). It has been proposed that the amino group in lysine side chains in mfps may react with the carbonyl groups of o-quinones to form catechol-amine adducts. The reaction between catechols and amines, together with all other possible reactions involving catechols (coordination with metal ions, cross-coupling with other nucleophiles), contributes to the fast solidification of freshly secreted mfps to form a tough and robust cuticle.[14]

Amines may react with o-quinones to form adducts either by addition or Schiff base formation. The factor that mainly determines which of these three reaction types will predominate, is the type of amine. In a Michael type addition an amine is attached to the catechol ring at the 6-position (see Scheme 1.2.1) to form amino-catechol coupling product. Three parameters can

affect the Michael-type addition: the pH, the type of catechol substituents and the basicity of the nucleophilic amines. In general, an increase in pH results in a higher reaction rate. Catechols with a substituent on the aromatic ring, have a reduced reactivity when compared to unsubstituted catechol, mostly dependent on the steric effect of the group. A third factor is the basicity of the nucleophilic amines: a more basic amine results in a higher reaction rate. In a Schiff base reaction the amine attacks the 1- or 2- position and an imine is created. Schiff base reactions are affected mainly by the pH.

Thiols can react with o-quinones by regioselective nucleophilic attack in the 2/5-position of the ring as shown in Scheme 1.2.1. Catechol–thiol adducts have been detected in many different natural systems. For instance, in the glue secreted by the sandcastle worm. The curing process of these proteins give raise to 5-S-cysteinyl-dopa units formed from dopa and cysteine during the setting process.[57] The addition efficiency of the reaction is increased by a higher oxidation rate of the catechols. Moreover, primary thiols with less steric hindrance exhibit a higher reactivity than secondary and tertiary thiols.

The o-quinone groups can also react via reverse dismutation to the unoxidized catechol, yielding two highly reactive semi-quinone radicals that can couple to form dimers via C-C crosslinks. The presence of such dimers has been assessed in many natural systems i.e. in mussels foot proteins.[58]

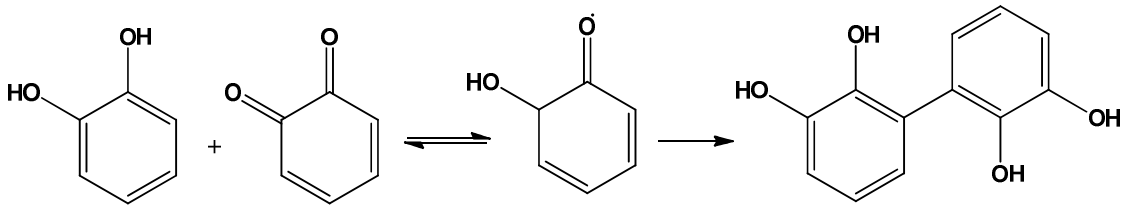

Scheme 1.2.3 *Crosslinking pathway via dismutation and aryloxyl coupling.*

Because of their chemically versatile structure, catechols and related systems are intensively investigated in the frame of supramolecular structures, metal chelating or cross-linking systems and polymers. Recent studies reported the design and biomimetic use of natural and synthetic catechols in biomedicine, analytical chemistry, nanotechnology and materials science, offering promising candidate structures for various technological applications.[59]

1.3 Catechol-based functional materials

The broad range of functional materials achievable thanks to the versatile catechol chemistry, can be classified in four main macroareas as recently proposed by *Ruiz-Molina et al.*:[59]

a) Hooks, in which catechol groups are incorporated into complex systems and serve as individual binding sites to isolated molecules;

b) Switches, in which catechol-based molecules are, under certain conditions, able to respond reversibly to external stimuli;

c) Anchors, in which they act as passive links to surfaces and/or covalent supports to other (functional) moieties;

d) Scaffolds, in which the catechol blocks constitute the framework for 2D or 3D structures, either by polymerization or self-assembly, which are functional on their own.

Hooks. Catechols reversible redox activity and their ability to strongly couple with metals and specific molecules enabled the preparation of many device applications. In particular, the ability of catechol groups to effectively coordinate transition metals has been extensively investigated for therapeutic, analytical and environmental applications. These include:

- artificial siderophores, intended as therapeutic agents specifically used for the treatment of both acute and chronic iron poisoning;[60]
- complexes with Gd^{3+} ions, as contrast agents in magnetic resonance imaging (MRI);[61]
- materials for chemo and biosensing, e.g. redox shuttles for NADH sensing electrodes,[62,63]
- physical or chemical stimuli-responsive hydrogels for applications as self-curing or wound healing materials.[64,65]

Switches. Several stimulus-controlled switches have been designed exploiting catechols coordination properties and redox chemistry for therapeutic, analytical and environmental applications. Noticeable examples are valence tautomeric (VT) materials for molecular electronics devices. VT materials are based on the modulation of internal electronic distribution of transition metal complexes upon application of different external stimuli.[66] Other significant applications include: a) sensitizer in dye-sensitized solar cells (DSSC), that improve the device efficiency;[67,68] b) development of electrochromic materials capable of reversible light absorption

in the NIR region upon the application of suitable redox potentials;[69] c) switchable catechol-modified chitosan films responsive to pH and voltage stimuli.[70,71] d) sensing of catecholamines by cross-coupling oxidation in the presence of resorcinol or its derivatives.[72,73]

Anchors. This represents the most significant field of application, therefore a large number of studies can be found in literature describing the use of catechols to anchor molecules or polymers to a large variety of surfaces, both nano/micro- and macroscopic. Many studies reported synthetic catechol-based polymeric structures with recognizable biomimetic features, among wich adhesiveness in wet condition is one of the most common. Few examples include: a) the preparation of water-soluble random copolymers of DOPA and lysine as wet adhesives;[74] b) the synthesis of copolymers of styrene and 3,4-dihydroxystyrene which were cross-linked by coordination with Fe^{3+} or by oxidation (periodate, permanganate and dichromate) to give layers with measured adhesion shear forces up to 1.2 MPa;[75] c) the preparation of hydrogels based on a branched DOPA-modified PEG polymer coordinated to Fe^{3+}, wich showed pH-dependent self-healing properties.[49]

Furthermore, many examples of surface functionalization have been reported in which catechols are meant as anchors to molecules, polymers or nanoparticles that demonstrate specific properties, allowing the preparation of different antibacterial[76,77] and antifouling[78,79] coatings.[80]

Scaffolds. Phenolic biopolymers, are a noticeable example of catechol-based scaffolds with a broad range of applications documented by a growing number of papers.[81] In the field of functional materials for organic electronics, bioelectronics and light harvesting, one of the most intriguing sources of inspiration is provided by the familiar property of the catecholamine metabolites DOPA and dopamine (DA) to generate on oxidation black insoluble biopolymers, commonly referred to as melanins or, more properly, ”eumelanins”.[1,82]

Originally stimulated by the central role in skin and eye pigmentation and its disorders, interest in melanin pigments has increased dramatically over the years to exceed the traditional boundaries of biology and medicine to include materials science. However, the notorious difficulties in the structural investigation of natural eumelanins, due primarily to the amorphous character, the marked insolubility in all solvents and the close association with the cellular ingredients of the biological matrix in which they are embedded, have traditionally dominated the chemists’ attitude toward these elusive pigments. For these reasons, considerable attention is currently being focused on synthetic eumelanin-like polymers for their possible application as soft, bioavailable and biocompatible functional materials.

Structurally related to melanins is the black polymer produced by oxidation of dopamine (DA) at pH 8.5 in the presence of oxygen reported for the first time by Messersmith, Lee and coworkers in 2007.[12] In an attempt to reproduce the high adhesion properties of mussel byssus, they described a universal eumelanin-like coating material, polydopamine (PDA), which can coat many types of surfaces, including superhydrophobic ones by a simple, one-step, dip-coating process that allows the substrate to become coated with a PDA film up to 50 nm thick within 24h.(Figure 1.3.1)

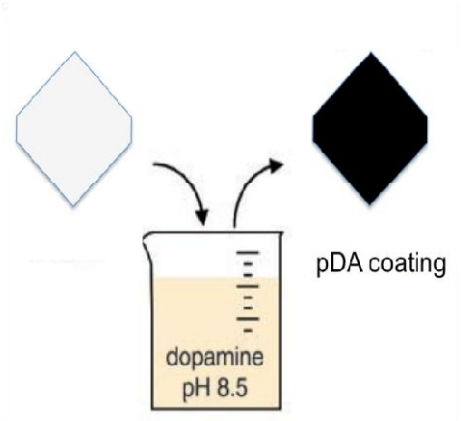

Figure 1.3.1 *Schematic illustration of thin film deposition of pDA by dip-coating an object into an alkaline dopamine solution.*[12]

This black synthetic eumelanin-like polymerdisplay intriguing physicochemical propertiessimilar to those of natural and synthetic melanins,[11] including a broad band visible absorption,[83] an intrinsic free radical character,[84,85] and a water-dependent, ionic-electronic hybrid conductor behaviour.[86] These properties prompted exploitation of PDA as multifunctional platforms for diverse technological applications, e.g. in organic electronics,[87] for the development of nanoparticles with free radical scavenging propertiesor for drug delivery;[20,88,89] in the setup of new systems for energy conversion, e.g. artificial photosynthetic mimics,[81] or as biointerface.[18,19,26]

1.4 Summary of state-of-the-art, and aims of the PhD project.

The above paragraphs provide the state of the art at the beginning of the present PhD project, which can be summarized as follows.

a) Nature inspired functional materials are attracting ever growing interest as long as our understanding of structure-properties relationships progresses. The possibility to investigate the structural and electronical properties of matter up to the nanometric scale allows us to recognize the chemical basis of natural processes and to apply them to solve technological issues.
b) Because of their versatile chemistry, catecholic compounds play a central role in a wide range of biological processes, spurring their exploitation in a variety of biomedical and technological fields. This state-of-affairs is exemplified by the burst of interest in materials science eumelanins and related material deriving from the autoxidation of dopamine (PDA) due to their outstanding physicochemical properties.

So far, however, progress in polyphenol-, catecholamine- and melanin-based functional materials and systems has been limited by a number of gaps and issues, including:

d) the lack of rational strategies based on structure-property relationships for selectively enhancing functionality or imparting new technologically relevant properties to polydopamine and synthetic melanins tailored to applications.
e) the lack of detailed studies on the actual scope of previous observations in the literature on catecholamine oxidation chemistry and the coupling with carbon, nitrogen and sulfur nucleophiles;
f) the lack of unambiguous data about the specific structural factors underpinning the universal material independent sticking behavior of polydopamine and other mussel-inspired bioadhesives.

In the light of the foregoing, specific objectives of the present PhD project include:

5) The definition of key structure-property relationships in synthetic eumelanins for the development of rational strategies to enhance or tailor functionality for specific applications;

6) The synthesis and chemical characterization of innovative molecular systems and functional polymers based on rational manipulation of melanin precursors, including dopamine and 5,6-dihydroxyindole for adhesion, crosslinking and other applications;
7) The development of alternative mussel inspired systems for various applications based on the oxidative chemistry of cheap, easily accessible and non-toxic natural phenolic compounds such as caffeic acid and chlorogenic acid;
8) The rational design of novel fluorescence turn-on systems for sensing applications based on catecholamine oxidation chemistry and coupling with nucleophiles.

Part of the work relating to research line 2) was carried out during a three-month stage in the laboratory of Professor Daniel Ruiz Molina at Catalan Institute for Nanoscience and Nanotecnology (ICN2, Bellaterra, Spain).

Overall, the results described in this thesis have led to significant advances in our understanding of eumelanin and PDA properties and have disclosed novel bioinspired functional materials and systems of potential technological and biomedical relevance.

Chapter 2

Structure-property-function relationships for the rational design of tailored melanins

2.1 Introduction

The structural and supramolecular bases of the characteristic broadband absorption spectrum of eumelanins accounting for their black or dark colorations have been the subject of intensive studies[5,89–95] because of their close relationship to key features of these polymers including the photoprotective and antioxidant properties, non-radiative UV energy dissipation mechanism,[96,97] the water dependent ionic-electronic conductivity,[85] and the paramagnetic state resulting in a permanent EPR signal.[2,7,98] Especially, their implications for the ability of eumelanins to convert the energy of the absorbed photon into non-photochemical dissipative processes is worthy of note for photoprotective mechanisms.[11,99]

According to a commonly accepted, yet simplistic view, natural eumelanins are heterogeneous polymers consisting of DHI and DHICA units linked through diverse bonding patterns[100,101] accounting for various levels of disorder (Figure 2.1.1).

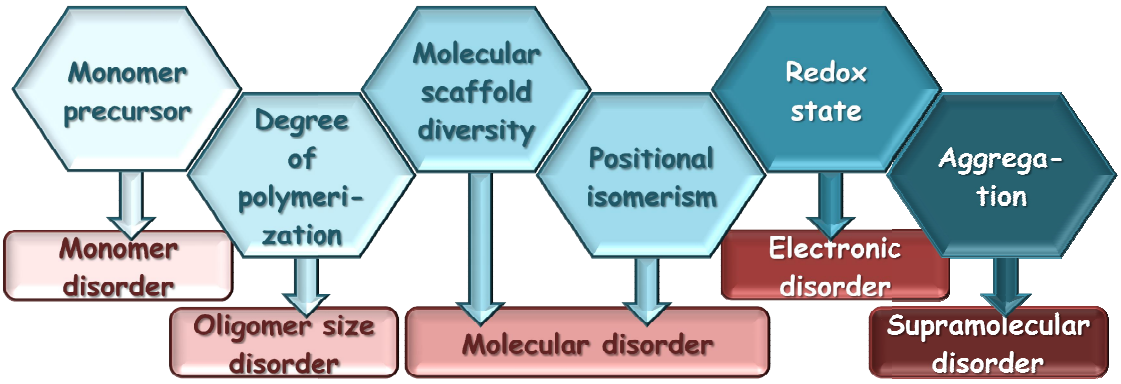

Figure 2.1.1 *Main levels of eumelanins disorder.*

The first level of disorder (chemical disorder)[4] relates to the possible participation in the polymerization process of different monomers, e.g. DHI, DHICA or open chain derivatives,

leading to a variety of oligomeric species that can develop complex ensembles of chromophores spanning the entire UV-visible range.

The second level of disorder relates to the variety of structures that can arise from a *single monomer*, due e.g., to molecular weight dispersion with polymerization (oligomers size disorder), molecular scaffold diversity due to positional isomerism, and conformational disorder reflecting atropisomerism, e.g., in DHICA oligomers (molecular disorder).

The third level of disorder (electronic disorder) refers to the existence of various possible oxidation states for each single oligomeric scaffold: for example, a dimer can exist in its fully reduced form and as one-electron, two-electron, three electron, and four electron (fully quinonoid) oxidation products. In principle, each oligomer (n-mer) can exist in 2n+1 different species, regardless of their stability. It is worth noting that it is the coexistence of oxidized and reduced moieties that is essential for the broadband visible-light absorption spectrum of eumelanins, as suggested by data from glycated water soluble eumelanin.[83] Thus, black color would depend not only on the degree of delocalization of π-electron conjugated chromophores[102,103] but also on intermolecular redox exchange and aggregation-dependent interchromophoric interactions. In this connection, computational studies suggested that the monotonic spectrum of eumelanin is due to delocalization of excitons over stacked DHI melanin.[104] The current view is that the optical eumelanin properties can be mimicked only by including catechol, semiquinone and quinone building blocks.[105]

The fourth level of disorder (supramolecular disorder) relates to the different modes of aggregation of oligomers as dictated by scaffold-dependent, redox state-controlled conformations (see Figure 2.1.2) and has a major impact on morphology and scattering properties.

In previous studies it was shown that poly(vinyl alcohol) (PVA) at 1% concentration can prevent precipitation of eumelanin thus allowing to disentangle intrinsic absorption properties due to chromophores from scattering effects. The results showed that besides the intrinsic chromophore component there is an extrinsic contribute that depends on the intermolecular perturbation[106] of π-electron systems and that is dominant in DHICA melanin, because of the lack of planar conformations.[7,107] These intrinsic and extrinsic contributes (Figure 2.1.2), together with local effects of geometric order and disorder,[108] would cooperate to generate the absorption spectrum of eumelanin.[86,104,108]

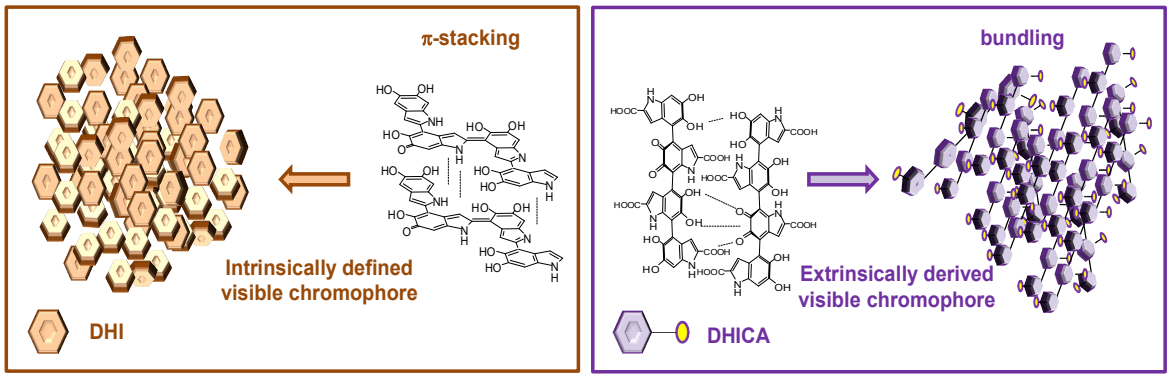

Figure 2.1.2 *Intrinsic and extrinsic contributions to eumelanin absorption properties.*

In order to elucidate the structure-properties relationships underlying the broadband spectrum and to dissect the contributions of the different levels of disorders, part of this thesis was directed to investigate and compare melanin chromophore formation from a collection of precursors featuring different substituents, molecular size (monomers and dimers) and shape (isomeric dimers). The dynamics of band broadening during eumelanin chromophore buildup and the role of chemical disorder were addressed by spectrophotometric experiments. In particular, two contributions to chemical disorder were considered: *structural disorder,* reflecting the variety of σ-scaffolds, and *redox disorder,* as determined by catechol-semiquinone-quinone mixing and π-electron perturbations. All data were interpreted with the support of DFT calculations (by Professor O. Crescenzi, Department of Chemical Sciences).

2.2 The dynamics of eumelanin chromophore evolution

Preliminary experiments were directed at comparing the generation and evolution of chromophores from DHI in the presence and in the absence of 1% PVA to prevent solid melanin precipitation.

To this aim, three oxidizing systems were used:

- Potassium ferricyanide in phosphate buffer at pH 7.0, $K_3[Fe(CN)_6]$, as a one-electron oxidant (2 molar eq.)
- Sodium periodate in phosphate buffer at pH 7.0, $NaIO_4$, operating as two–electron oxidant via cyclic ester formation with catechols (1 molar eq.)
- Ceric ammonium nitrate (CAN) in phosphate buffer at pH 3.0, $(NH_4)_2[Ce(NO_3)_6]$, operating by a one-electron transfer mechanism at acidic pH (2 molar eq.)

Oxidant concentration was based on a two-electron oxidation stoichiometry relative to the monomer, formally corresponding to *o*-quinone formation. Monomer consumption was checked by HPLC and was complete under these reaction conditions.

The results showed that ferricyanide and periodate can induce similar chromophoric changes and evolution kinetics while CAN induced a less intense chromophore, possibly ascribable to the inhibition of deprotonation at acidic pH (Figure 2.2.1).

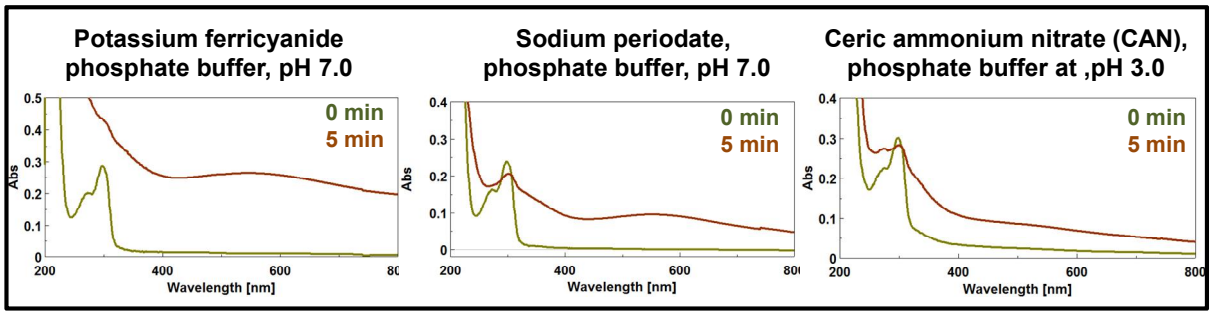

Figure 2.2.1 *Generation of chromophores from DHI (50 μM) using different oxidizing systems: potassium ferricyanide in phosphate buffer pH 7.0, sodium periodate in phosphate buffer at pH 7.0 or ceric ammonium nitrate (CAN) in phosphate buffer at pH 3.0.*

On this basis, ferricyanide was selected as the oxidant and oxidations were carried out with DHI and other selected monomers and dimers (Figure 2.2.2) at 50 μM concentration.

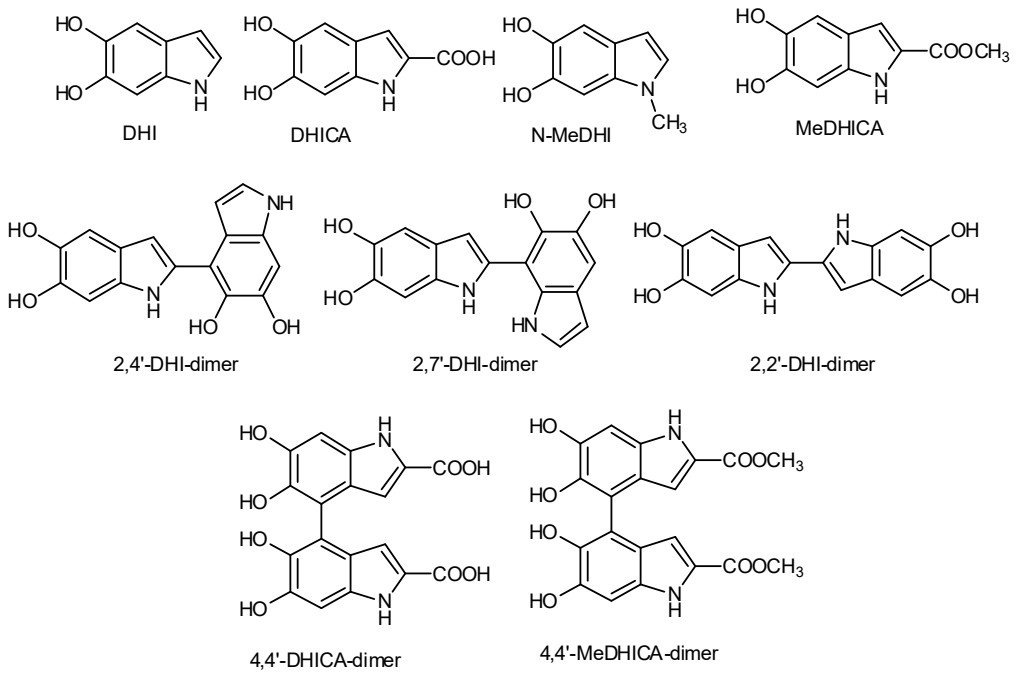

Figure 2.2.2 *Structures of monomers and dimers investigated in this thesis.*

Data from DHI oxidation over 24 hours reaction time showed the generation of a broad visible chromophore around 560 nm, referred to as melanochrome based on an old nomenclature (Figure 2.2.3).[82]

Further addition of 2 molar equivalents of potassium ferricyanide did not affect the maximum intensity and persistence of the chromophore suggesting the occurrence of oxidation processes unrelated to chromophoric species.

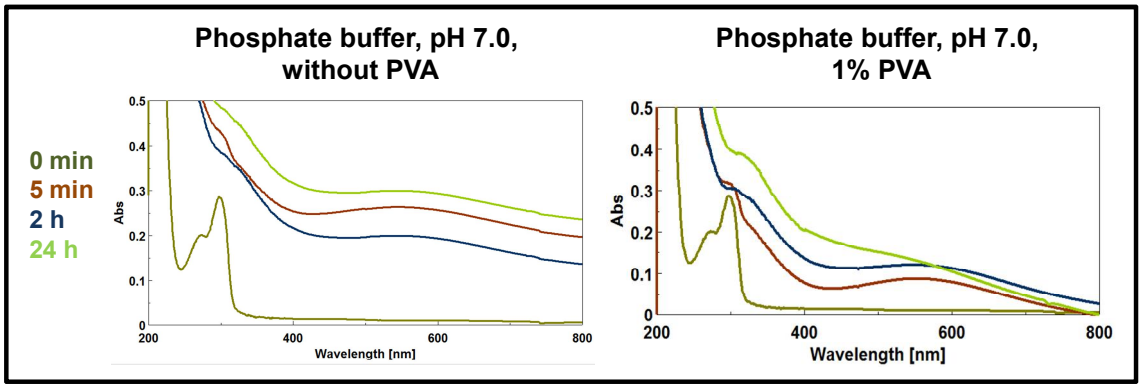

Figure 2.2.3 *Generation and evolution of chromophores from DHI (50 μM) oxidation by ferricyanide (2 molar equivalents) in the absence or the presence of 1% PVA.*

In order to quantify scattering contributions to the final spectra, spectra were recorded before and after filtration through a 0.45 micron nylon membrane. At 5 min spectral analysis did not show detectable absorption in filtrate.

Notably, all oxidation mixtures slowly darkened both in air and under an argon atmosphere due to broadening of the absorption band accompanied by extensive precipitation, as measured by filtration at 24 h. In the presence of 1% PVA melanin precipitation was inhibited at least in part, but melanochrome formation proceeded in a similar manner (Figure 2.2.4).

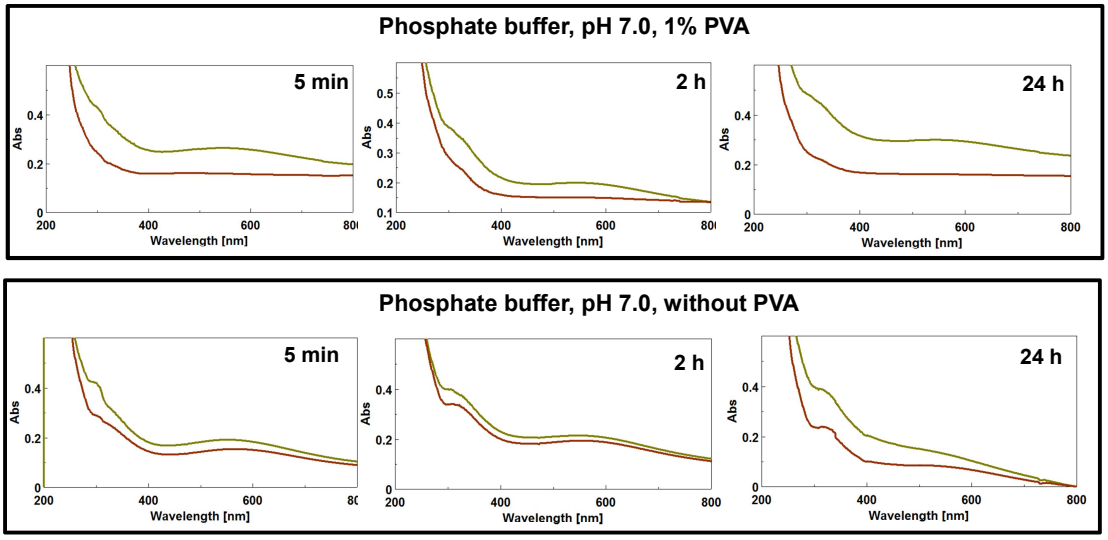

Figure 2.2.4 *UV-vis spectra of DHI (50 μM) oxidation mixtures by ferricyanide (2 molar equivalents) in the absence and in the presence of 1% PVA.* ***Green*** *traces were recorded before filtration,* ***brown*** *traces were recorded after filtration.*

These results allowed to identify three distinct phases of chromophore generation and evolution:

I) Fast generation of the melanochrome, whose absorption is mainly due to intrinsic chromophores.[109]

II) Slow band broadening process, mainly due to extrinsic contributions (i.e. intermolecular chromophore perturbations)

III) Melanin precipitation and consequent scattering.

While Phase I depends on the presence of the oxidant, phase II is oxygen independent. PVA allowed to disentangle contributions from phases II and III that otherwise would have been superposed.

Digital pictures in Figure 2.2.5 show the gradual darkening of the oxidation mixtures and the deposition of melanin pigment. At 5 min, it was possible to observe the development of a bluish coloration due to the melanochrome. The effect of PVA in preventing solid precipitation during phase III is well apparent from these comparative pictures.

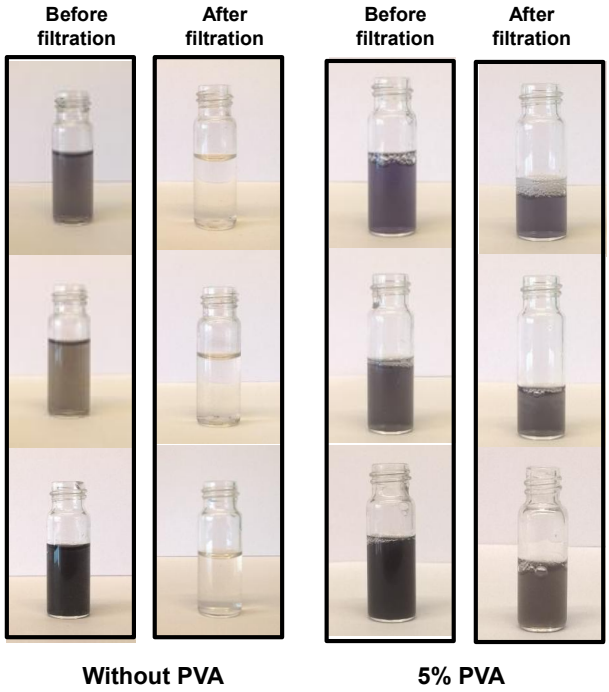

Figure 2.2.5 *Digital pictures of the reaction mixtures obtained by ferricyanide oxidation of DHI (500 μM) over 24 h in the absence and in the presence of 5% PVA.*

In order to examine the effect of ring substituents on the dynamics of DHI polymerization, the same experiment was performed on the N-methyl derivative of DHI (N-MeDHI), DHICA and MeDHICA.

The results show that the effect of the methyl group is negligible and the spectra are similar in the case of DHI and N-MeDHI (Figure 2.2.6).

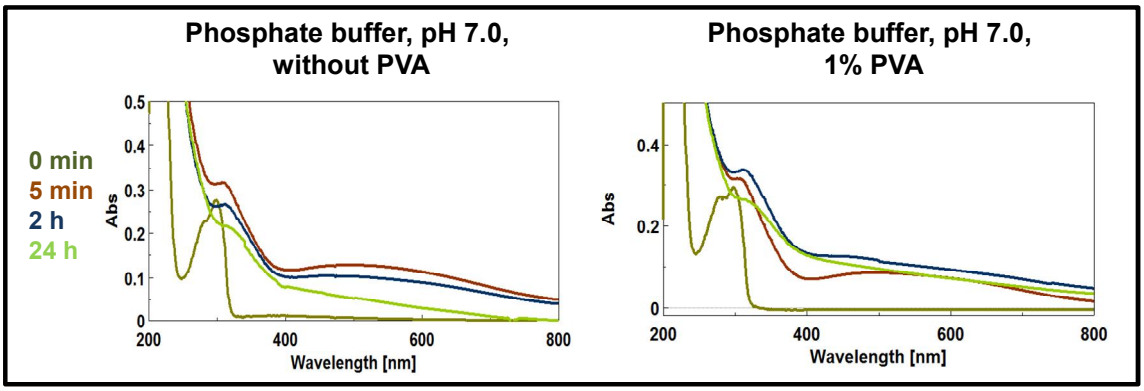

Figure 2.2.6 *Generation and evolution of chromophores from N-MeDHI (50 μM) oxidation by ferricyanide (2 molar equivalents) in the absence or in the presence of 1% PVA.*

In the case of DHICA a deep violet chromophore broadly centered between 500-550 nm and a well-defined UV absorbing band around 330 nm were observed both in the presence and in the absence of PVA (Figure 2.2.7). Spectra recorded at 5 min and 2h showed that the inhibition of aggregation by PVA delayed the decay of melanochrome.

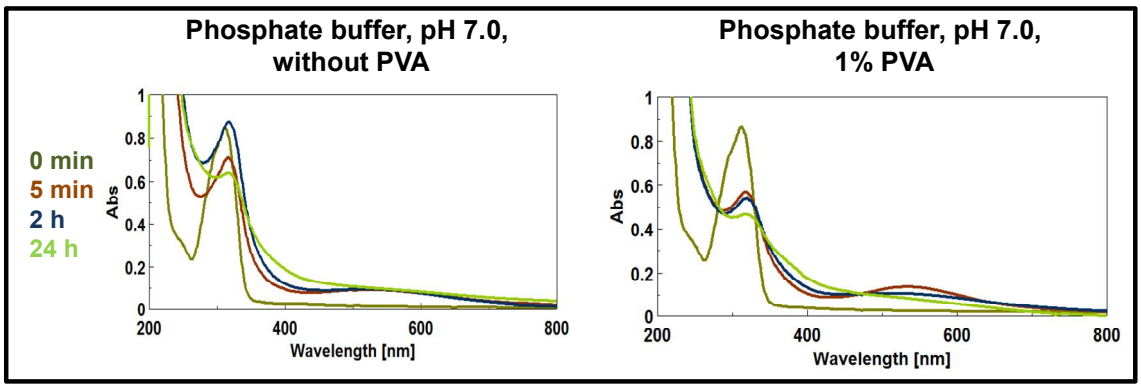

Figure 2.2.7 *Generation and evolution of chromophores from DHICA (50 μM) oxidation by ferricyanide (2 molar equivalents) in the absence or in the presence of 1% PVA.*

Digital pictures before and after filtration, in the presence and in the absence of PVA, confirmed the role of aggregation in color development (Figure 2.2.8).

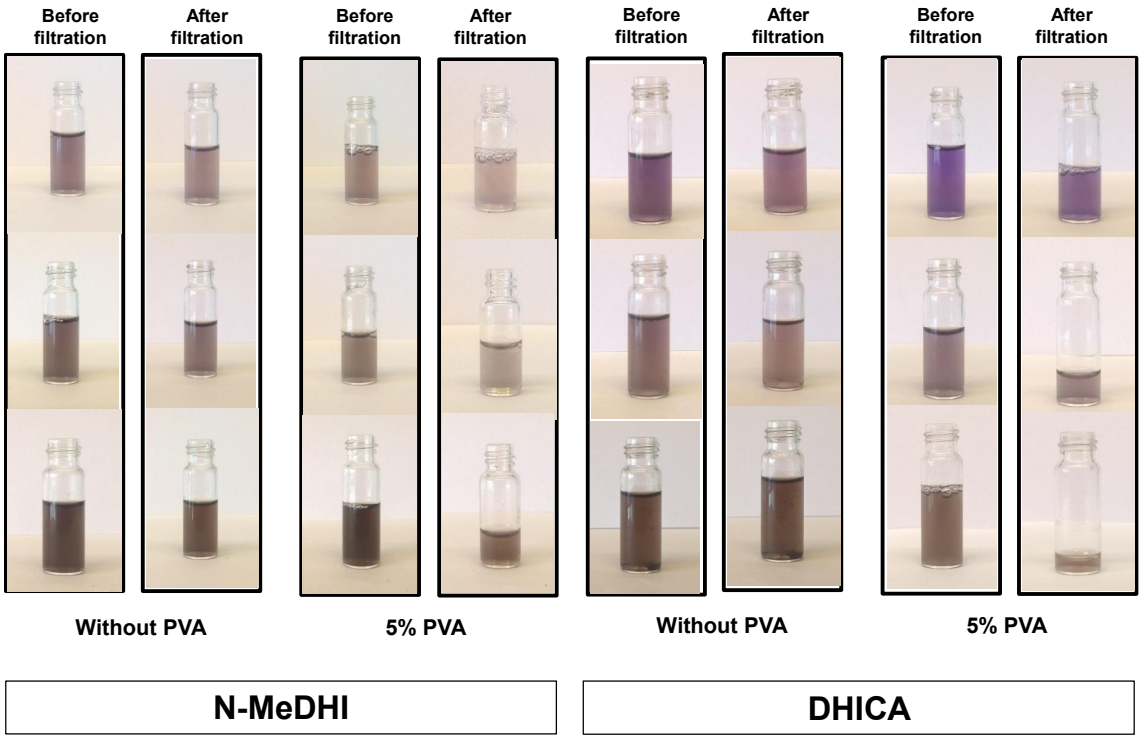

Figure 2.2.8 *Digital pictures of the mixtures obtained by ferricyanide oxidation of N-MeDHI or DHICA (500 μM) over 24 h in the absence and in the presence of 5% PVA.*

In contrast with the case of DHICA, MeDHICA did not lead to significant visible chromophores nor to an appreciable rise of scattering by oxidation with ferricyanide (Figure 2.2.9).

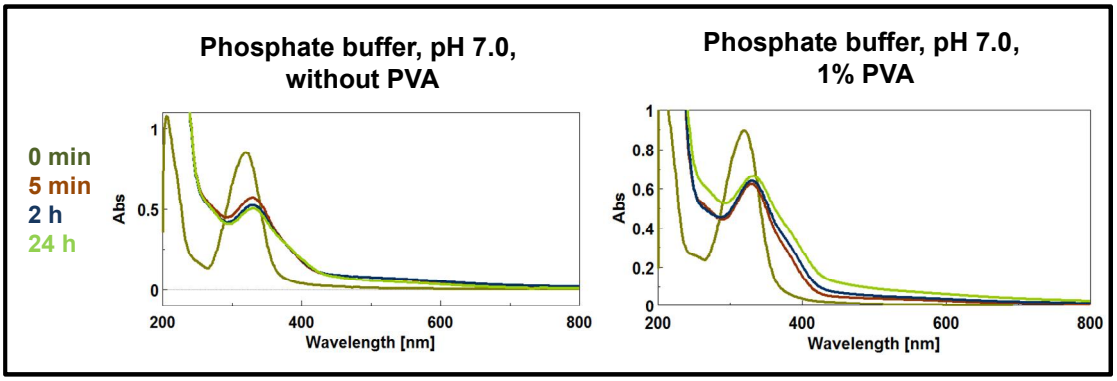

Figure 2.2.9 *Generation and evolution of chromophores from MeDHICA (50 μM) oxidation by ferricyanide (2 molar equivalents) in the absence or in the presence of 1% PVA.*

The lack of aggregated unsoluble materials was also confirmed by the lack of variations choromophore intensity by filtration (Figure 2.2.10).

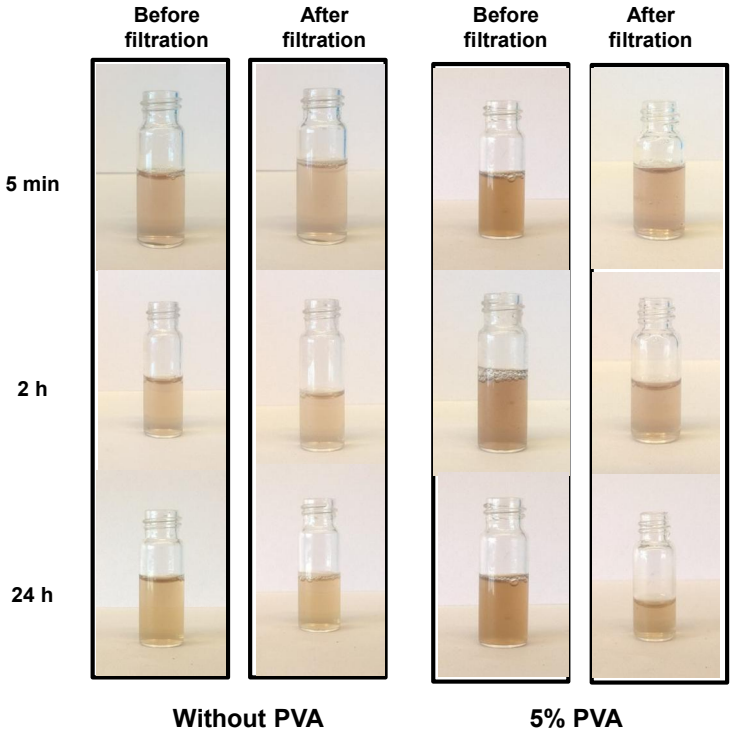

Figure 2.2.10 *Digital pictures of the oxidation mixtures obtained by ferricyanide oxidation of MeDHICA (500 μM) over 24 h in the absence and in the presence of 5% PVA.*

A complete set of the UV spectra recorded for N-MeDHICA, DHICA and MeDHICA is shown in Figure 2.2.11-13.

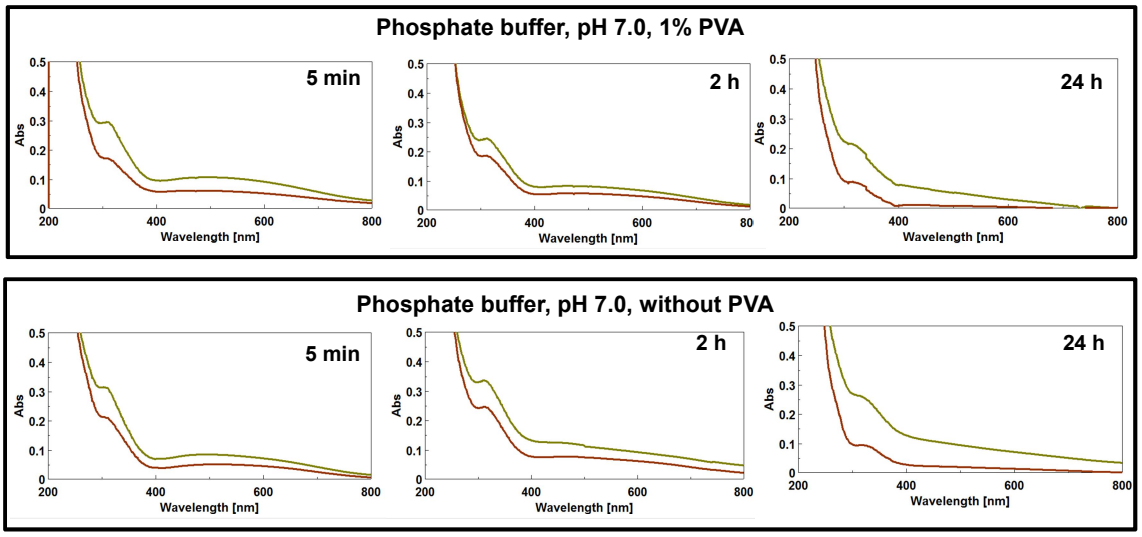

Figure 2.2.11 U*V-vis spectra of N-MeDHI (50 μM) oxidation mixtures by ferricyanide (2 molar equivalents) in the absence and in the presence of 1% PVA.* ***Green*** *traces were recorded before filtration,* ***brown*** *traces were recorded after filtration.*

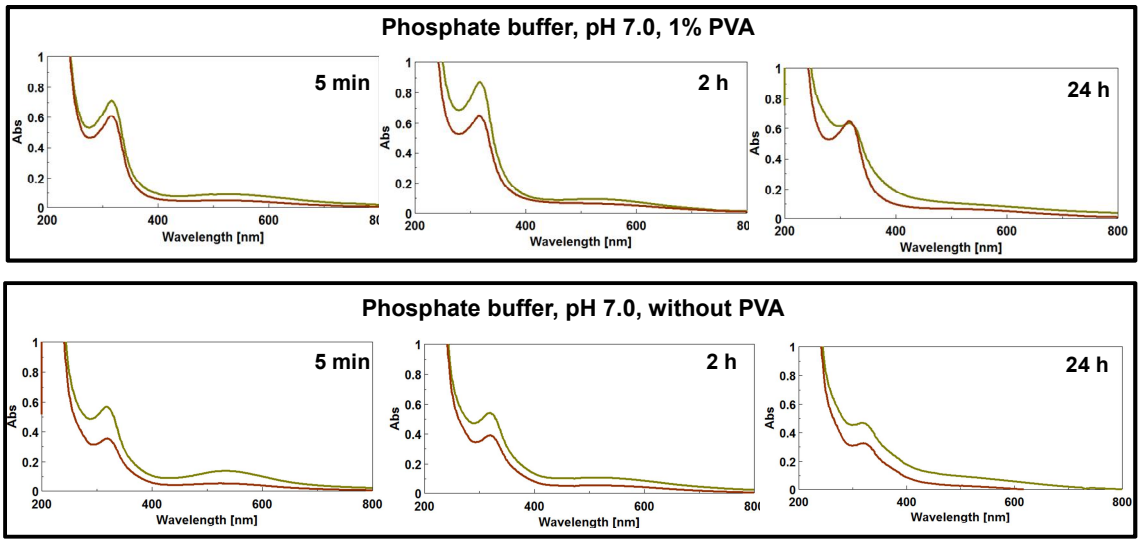

Figure 2.2.12 *UV-vis spectra of DHICA (50 μM) oxidation mixtures by ferricyanide (2 molar equivalents) in the absence and in the presence of 1% PVA.* ***Green*** *traces were recorded before filtration,* ***brown*** *traces were recorded after filtration.*

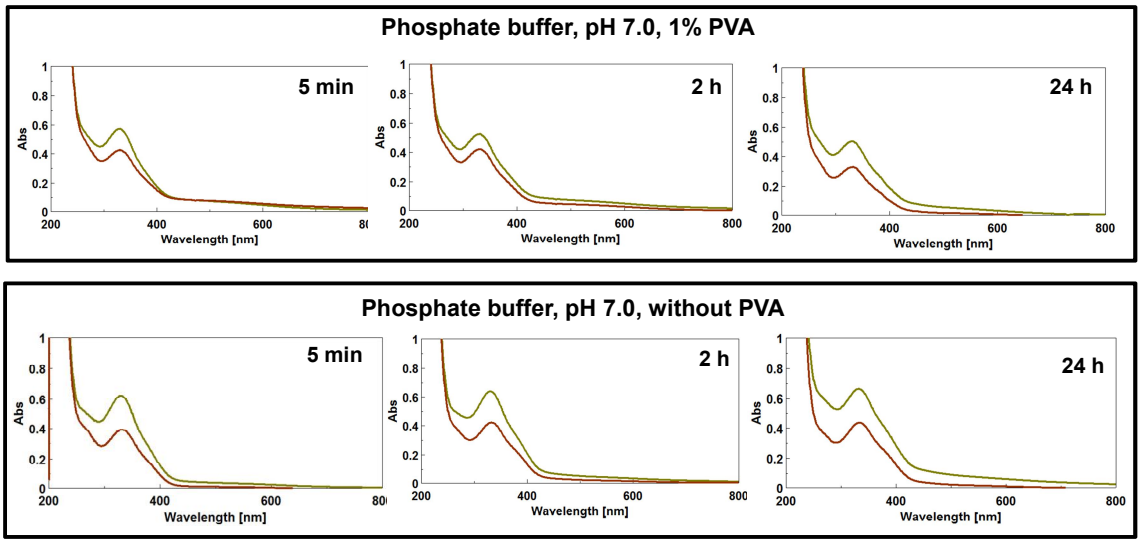

Figure 2.2.13 *UV-vis spectra of MeDHICA (50 μM) oxidation mixtures by ferricyanide (2 molar equivalents) in the absence and in the presence of 1% PVA.* ***Green*** *traces were recorded before filtration,* ***brown*** *traces were recorded after filtration.*

To assess the effect of molecular disorder as contributed by molecular weight dispersion and scaffold diversity, in a separate set of experiments oxidative polymerization was run on dimers and its spectrophotometric course compared to that of the corresponding monomers. Use of dimers would lead to a halved oligomer population with respect to monomers because of the lack of components with an odd number of units. In addition, constraints to scaffold diversity within each oligomer populations are posed by the dimer interring bond whereby only a fraction of the possible 2n-mers produced by oxidative polymerization of the monomer can be formed from each dimers.

Interestingly, marked differences were apparent in the early chromophores generated by the isomeric 2,4'-, 2,7'- and 2,2'- dimers of DHI both in the presence and in the absence of PVA (Figure 2.2.14).

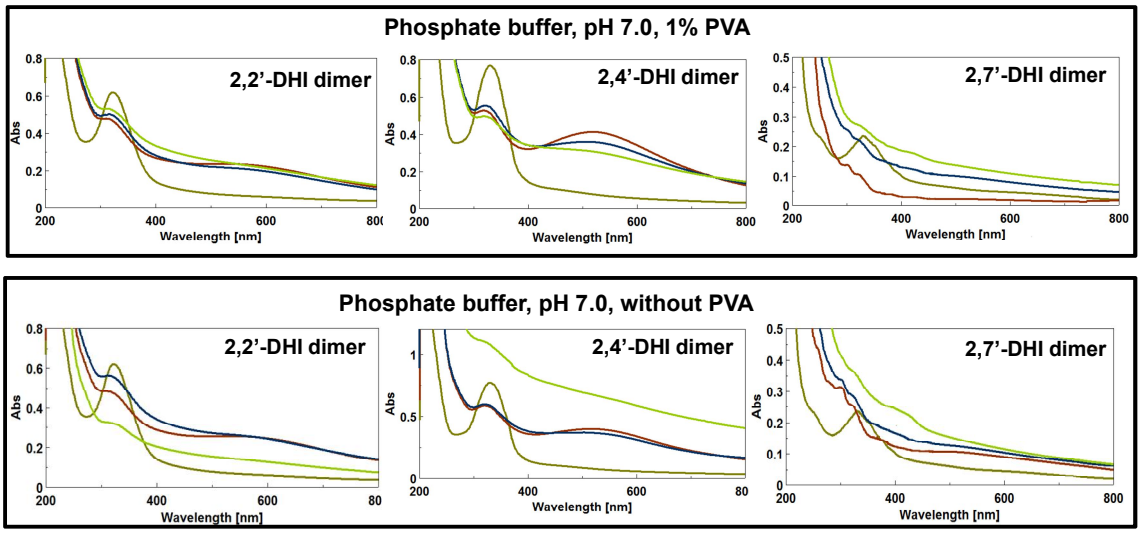

Figure 2.2.14 *UV-vis spectra of 2,2'-, 2,4'- and 2,7'-dimers of DHI (50 μM) oxidation mixtures by ferricyanide (2 molar equivalents) in the absence and in the presence of 1% PVA.*

The almost overlapping traces recorded at 5 min, 2 h and 24 h in the absence of PVA, suggest that the evolution of the melanochrome is faster in the case 2,2' dimer. It is concluded that in the first phase of chromophore evolution the way the indole units are bound is more important than the decrease in molecular weight dispersion.

Comparison of the spectra of the oxidation mixture of the 4,4'-dimer of DHICA with those of the monomer indicated a faster rate of melanochrome evolution (Figure 2.2.15). Similar was also the course of the oxidation of the 4,7'–dimer compared to the monomer (not shown).

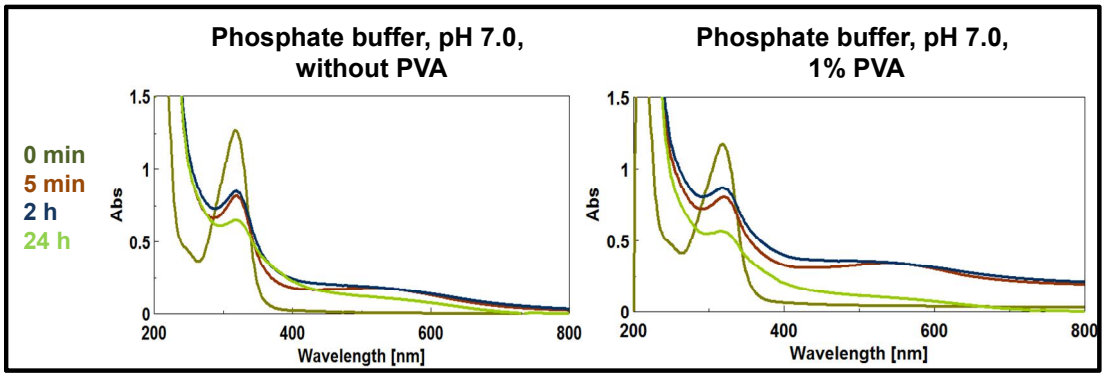

Figure 2.2.15 *Generation and evolution of chromophores from 4,4'-DHICA (50 μM) oxidation by ferricyanide (2 molar equivalents) in the absence or in the presence of 1% PVA.*

A complete set of UV spectra recorded for 2,4'-, 2,7'- and 2,2'-dimers of DHI and for the 4,4'-dimer of DHICA is shown in figures 2.2.16-19.

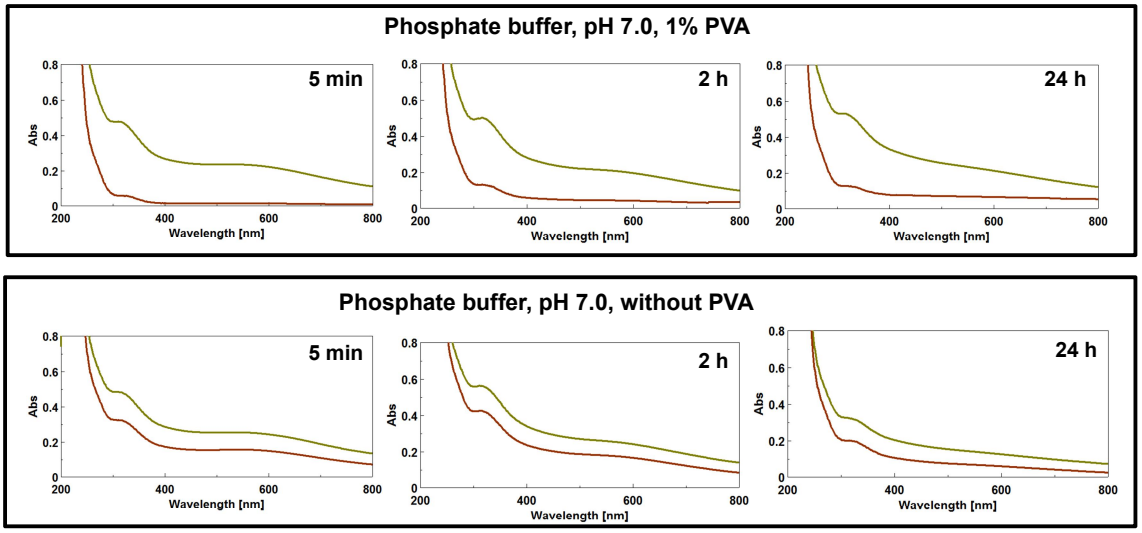

Figure 2.2.16 *UV-vis spectra of 2,2'-dimers of DHI (50 μM) oxidation mixtures by ferricyanide (2 molar equivalents) in the absence and in the presence of 1% PVA.* ***Green*** *traces were recorded before filtration,* ***brown*** *traces were recorded after filtration.*

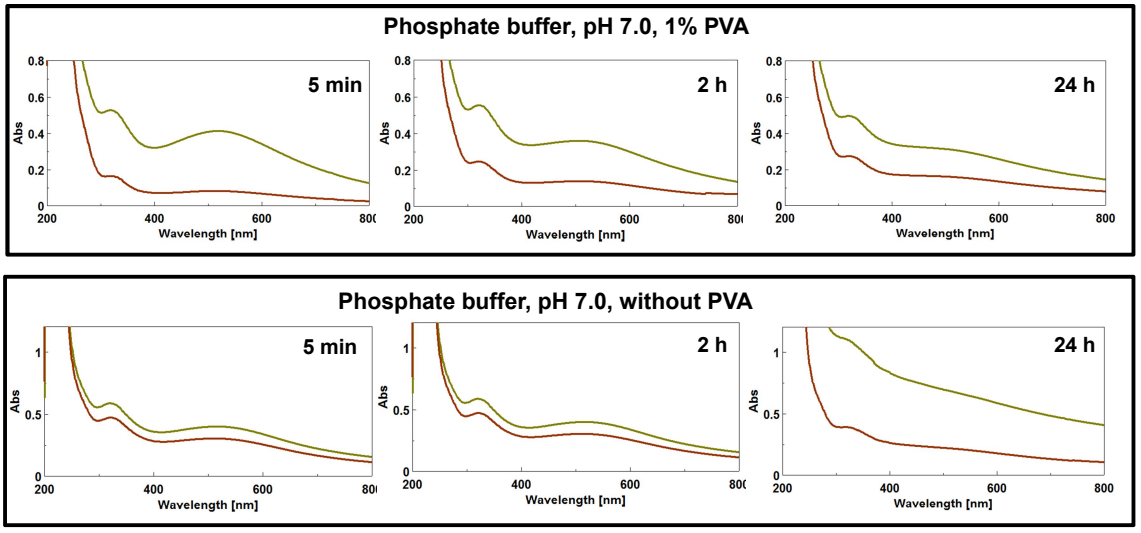

Figure 2.2.17 *UV-vis spectra of 2,4'-dimers of DHI (50 μM) oxidation mixtures by ferricyanide (2 molar equivalents) in the absence and in the presence of 1% PVA.* ***Green*** *traces were recorded before filtration,* ***brown*** *traces were recorded after filtration.*

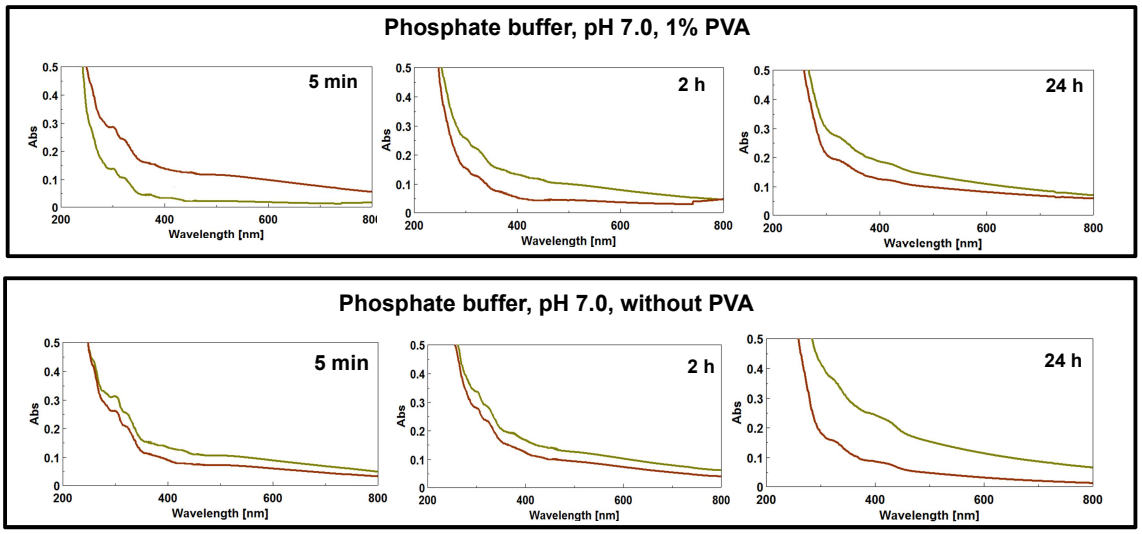

Figure 2.2.18 *UV-vis spectra of mixtures by ferricyanide oxidation (2 molar equivalents) of 2,7'-dimers of DHI (50 μM) in the absence and in the presence of 1% PVA.* ***Green*** *traces were recorded before filtration,* ***brown*** *traces were recorded after filtration.*

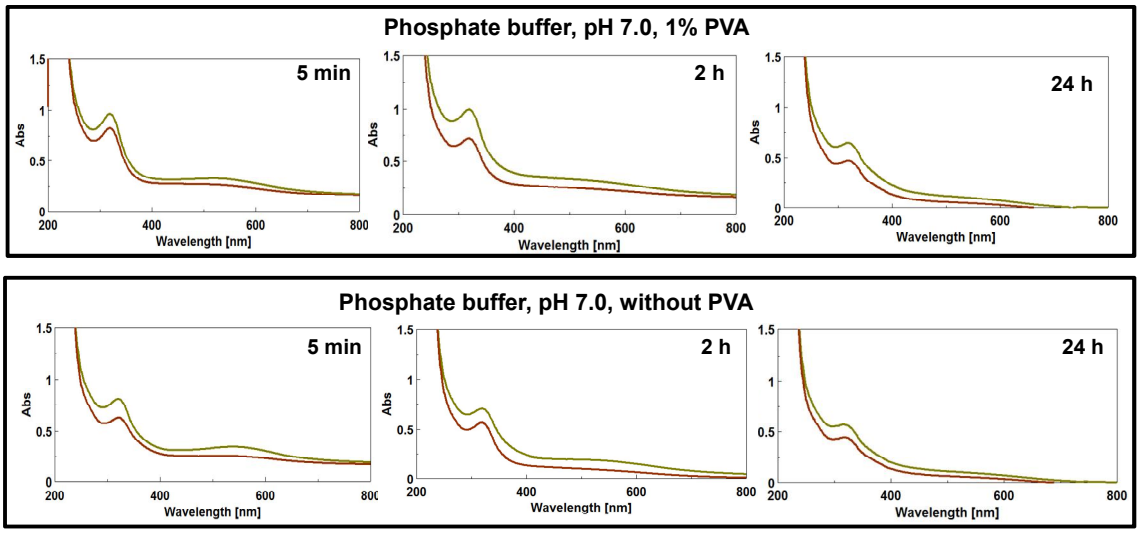

Figure 2.2.19 *UV-vis spectra of 4,4'-dimer of DHICA (50 μM) oxidation mixtures by ferricyanide (2 molar equivalents) in the absence and in the presence of 1% PVA.* ***Green*** *traces were recorded before filtration,* ***brown*** *traces were recorded after filtration.*

To compare the shapes of the final spectra of the polymers from dimers with those of the polymers from monomers, absorbance data at fixed visible wavelengths were normalized against the UV band at 300 nm and the resulting traces were matched against the theoretical monotonic profile (Figure 2.2.20).

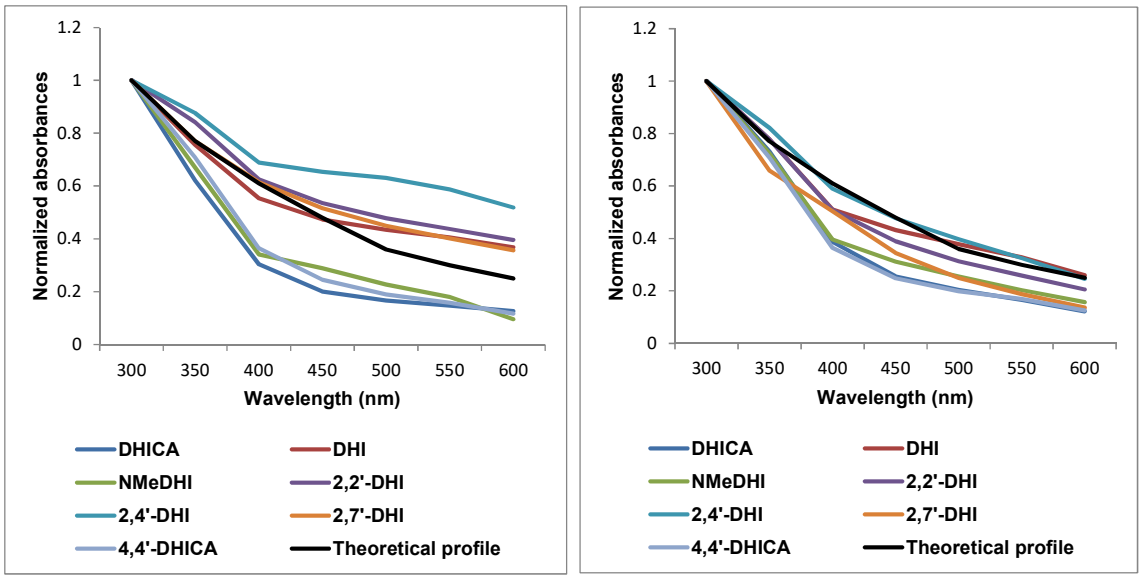

Figure 2.2.20 *Relative absorbance of the oxidation mixtures of the indole compounds at 24 h over the UV-visible region in the absence (left) and in the presence of 1% PVA (right). Values normalized against the absorbance at 300 nm for each mixture.*

DHICA and its dimer show a similar trend while the traces for DHI and its dimers are different, with more marked differences in the presence of PVA. The intensity of the visible chromophore decrease in the order 2,4'- > 2,2'- > 2,7'-isomers.

To clarify the role of monomer disorder in eumelanin formation, the course of oxidation mixtures of 3,4-dihydroxyphenylalanine (DOPA) and dopamine (DA) were investigated. Since DHI and DHICA are produced from DA and DOPA by a four electron oxidation process, 6 molar equivalent of potassium ferricyanide were used (Figure 2.2.21). These absorption profiles substantially lack the maximum due to melanochrome formation. The absorption in the visible range for DA is lower compared to DOPA, on account of its lower tendency to cyclize. The absorption maximum at around 420 nm observed in the spectra taken at 5 min is due to residual ferricyanide.

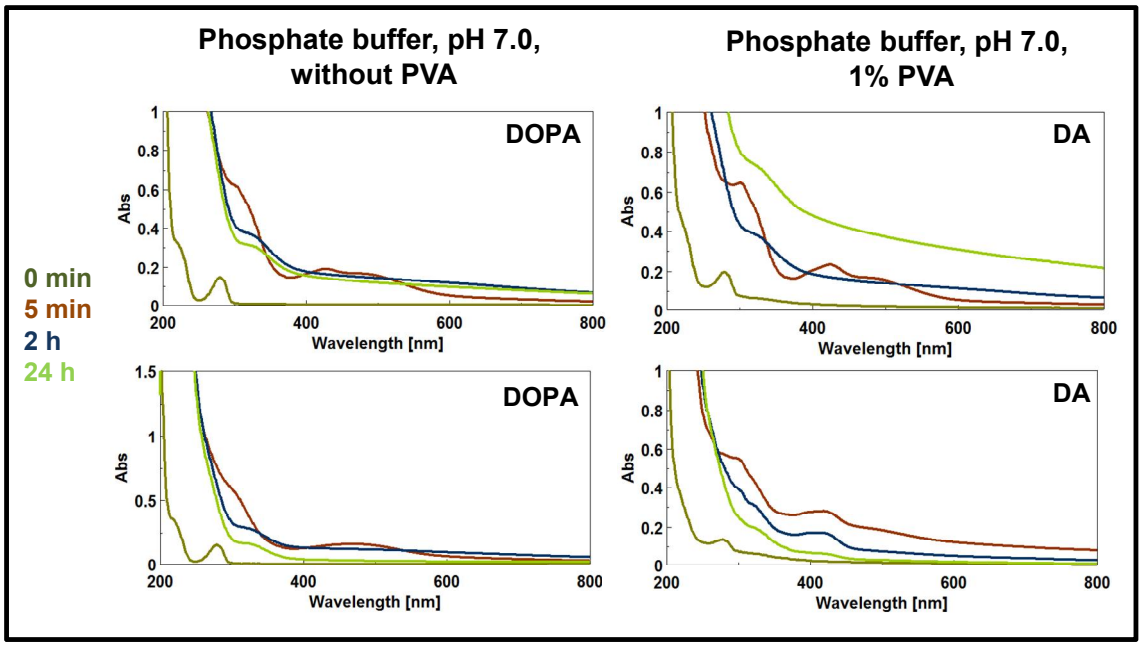

Figure 2.2.21 *Generation and evolution of chromophores from DOPA or DA (50 μM) oxidation by ferricyanide (6 molar equivalents) in the absence or in the presence of 1% PVA.*

Formal extinction coefficients (ε_f), were determined at 450, 550 and 650 nm for the chromophores produced at different reaction times in the presence of PVA.

$$\varepsilon_f = A/lc$$

(A is the absorbance, c is the initial monomer concentration and l is the optical path in cm)

Table 2.2.1 ***Formal extinction coefficients at different wavelengths and reaction times of the eumelanin chromophores investigated.***

Precursor(50 μM)	ε_f (450)	ε_f (550)	ε_f (650)	ε_f **ratio** 550/450	ε_f **ratio** 650/550
5 min					
DHI	2460	2909	2343	1.18	0.81
DHICA	1788	2618	1176	1.46	0.45
DOPA	3059	1267	256	0.41	0.20
DA	2589	1419	440	0.55	0.17
2 h					
DHI	3210	3369	2787	1.05	0.83
DHICA	1957	1990	1212	1.02	0.61
DOPA	3106	2478	1956	1.62	0.79
DA	1529	661	306	0.43	0.20
24 h					
DHI	3423	2603	1467	0.76	0.56
DHICA	2304	1493	705	0.65	0.47
DOPA	4042	2441	1316	0,60	0.54
DA	1915	967	344	0.50	0.36

a) DHI melanin exhibits higher formal extinction coefficients than DHICA melanin at 650 nm.

b) 650/550 nm coefficient ratios for DHICA are invariably lower than for DHI at each time;

c) 550/450 nm and 650/550 nm ratios at 5 min are respectively higher and lower for DHICA compared to DHI. This can be considered as a measure of melanochrome intensity and is consistent with a more defined band shape.

d) The 550/450 nm coefficient ratio decreases passing from 5 min to 2 h while 650/550 nm ratio increases. This can considered an index of band broadening.

The lower extinction coefficient at 550 nm after 5 min for DHICA relative to DHI confirms the important role of the carboxyl group in DHICA in inhibiting the development of the visible chromophore at all three phases. Moreover, DHICA chromophore is more defined than that of DHI.

The role of redox disorder. The possible occurrence of each structural component at different oxidation levels would imply a redox disorder.

Experiments aimed at probing susceptibility of eumelanin final chromophore to modification by oxidant or reducing agents can give indirect information about the average redox state. The addition of sodium dithionite or sodium borohydride to eumelanin samples produced in the presence of PVA caused a detectable decrease in the visible absorption (Figure 2.2.22).

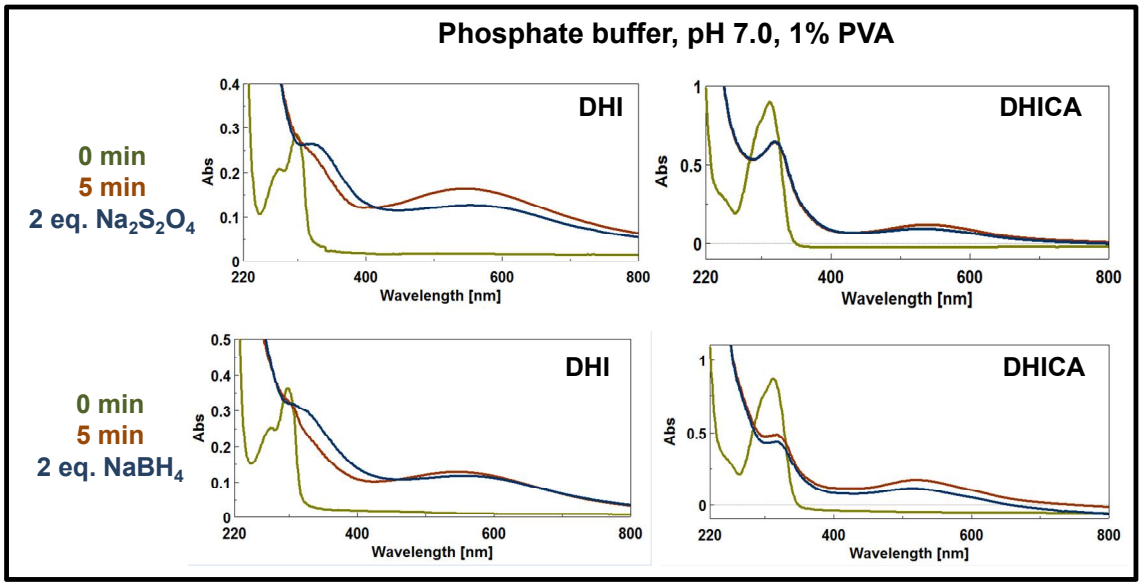

Figure 2.2.22 *Effect of addition of sodium dithionite or sodium borohydride to the oxidation mixtures of DHI or DHICA in the presence of 1% PVA.*

Despite the failure to attain complete color suppression, quinonoid species seem to be important determinants of the visible chromophores. Separate experiments carried out in the absence of PVA using an excess of reducing agents showed comparable decrease of the absorption in the visible region, indicating that the PVA chain does not affect the action of reducing agents.

Acidification to pH 2 caused a detectable ipsochromic shift of the visible chromophore of eumelanins and a bathochromic shift of the UV band (Figure 2.2.23). Alkalinization of the oxidation mixtures induced no detectable change. It is suggested that chromophoric species are present in an ionized quinonoid form at neutral pH.

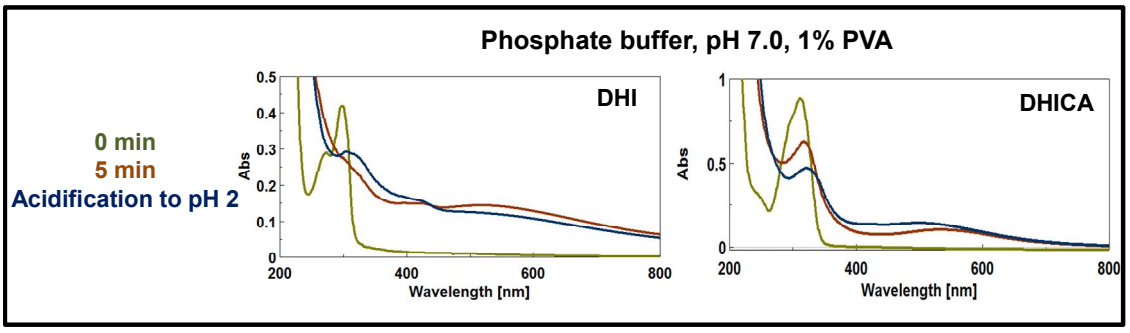

Figure 2.2.23 *Effect of acidification on the chromophores from DHI or DHICA oxidation mixtures (50 μM).*

These experiments overall confirmed the fundamental contribution of oxidized quinonoid units to eumelanin chromophore.

In a final set of experiments eumelanin samples prepared by ferricyanide oxidation of DHI or DHICA were exposed to the same concentration of the relevant monomer both in the presence or in the absence of PVA.

The addition of monomer DHICA to DHICA melanin and the addition of DHI to DHI melanin did not induce significant monomer conversion or chromophore change, suggesting the lack of redox activity for both the melanins (Figure 2.2.24).

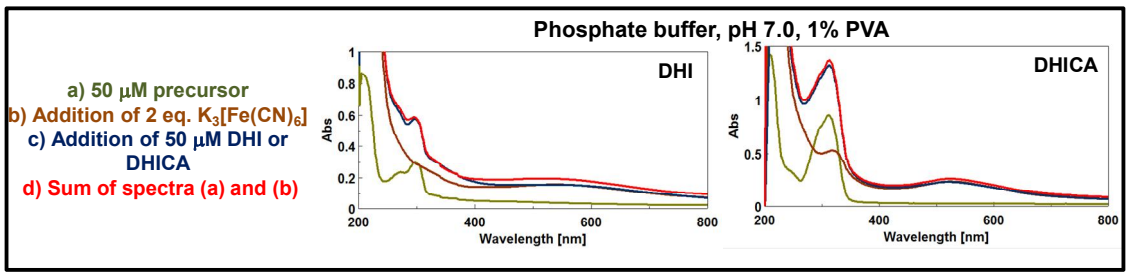

Figure 2.2.24 *Effect of addition of DHI and DHICA at 50 μM to the respective melanin generated in the presence of 1% PVA.*

In order to confirm the hypothesis that DHICA generates a poorly delocalized intrinsic chromophore and to prove the generation of extrinsic visible chromophores via intermolecular interaction of dimers from DHI and DHICA at different oxidation levels, computational studies were carried out in collaboration with the Institute of Chemistry of Organometallic Compounds

(ICCOM-CNR) and the Department of Chemistry and Industrial Chemistry of University of Pisa (Italy).

Preliminary calculations agree with experimental data[107,109] and confirm lack of visible absorption both in the case of DHI and DHICA monomers and dimers in the reduced catechol form (**HQ**), while the calculated spectra of the 2-electron oxidation products (**Q**) of DHI and DHICA dimers are different.

To consider the possible role of non-covalent intermolecular interactions between the intrinsic chromophores[110,111] a number of stacked configuration were assembled, for each of the investigated dimers, taking into account the coexistence[83,109] and the approach to each other of reduced and oxidized forms.

Three stacked conformers for each investigated species were selected after evaluating the reliability and accessibility of the possible conformations and their absorption spectra computed at TD-DFT level.

All **Q** forms of DHI dimers exhibit intense visible bands, that is particularly evident in the case of the planar 2,2' dimer (according with the evolution of chromophore in the absence of PVA), suggesting a strong influence of the stacking with a red-shift of main bands accompanied, especially at short stacking distances, by broadening and increased low-energy absorption. The same effect of band broadening was observed in the case of optimized geometry of the 2,4'-dimer. A remarkable effect due to stacking was predicted for the DHICA dimer. The spectrum of the **HQ**/**Q** complex obtained by approaching the dimers is different from the spectra of separated **HQ** and **Q** forms (virtually superimposable) and displays a marked bathochromic shift in the UV band.

These data support the existence of stabilizing intermolecular interactions causing the appearance of low energy transitions in the visible range.

As a further insight into chromophore development from oxidation of melanin precursors, in subsequent experiments autoxidation was run in the presence of biologically relevant metal ions. The oxidation was carried out in (4-(2-hydroxyethyl)-1-piperazineethanesulfonic acid) (HEPES) buffer at pH 7.5 in the presence of equimolar amounts of zinc, copper and iron ions. The course of the oxidation reaction was followed spectrophotometrically using the substrate at 50 μM concentration (Figure 2.2.25-28).

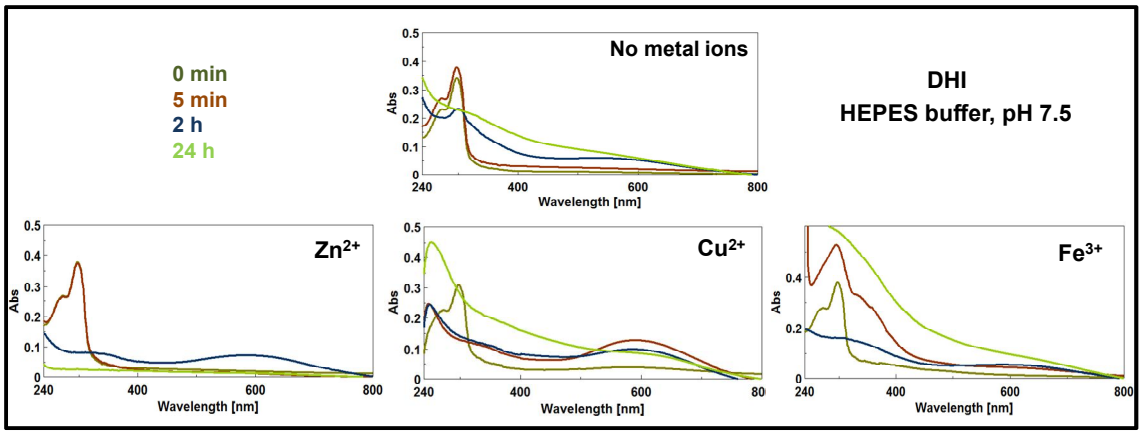

Figure 2.2.25 *Generation of chromophores from DHI in the presence and in the absence of 1 molar equivalent of Zn^{2+} or Cu^{2+} or Fe^{3+}.*

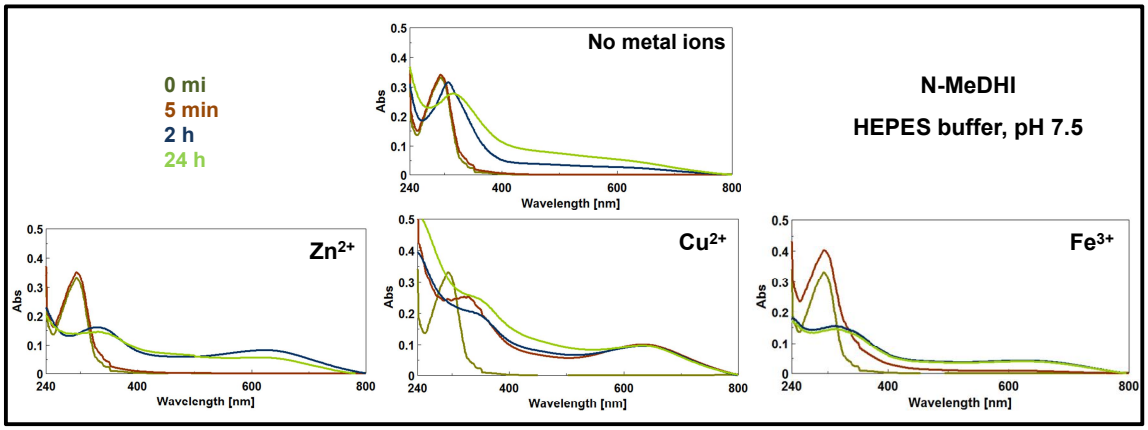

Figure 2.2.26 *Generation of chromophores from N-MeDHI in the presence and in the absence of 1 molar equivalent of Zn^{2+} or Cu^{2+} or Fe^{3+}.*

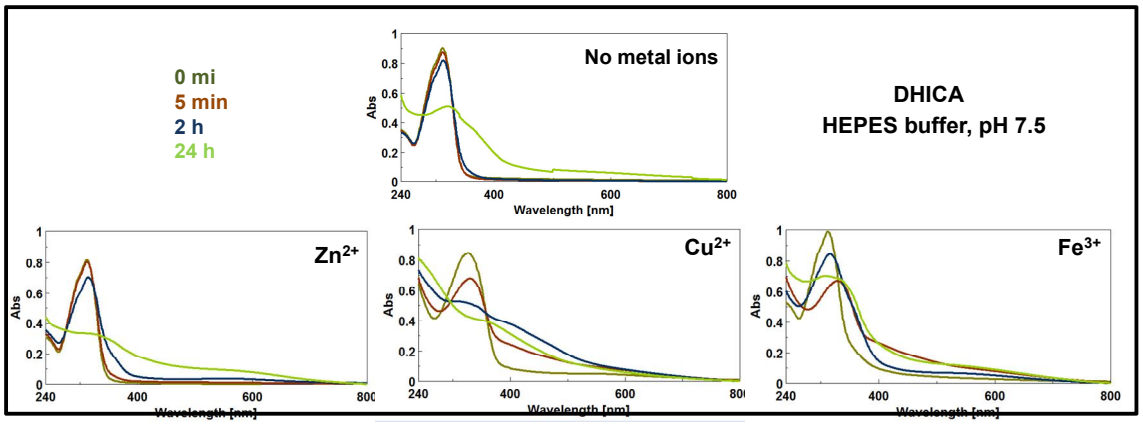

Figure 2.2.27 *Generation of chromophores from DHICA in the presence and in the absence of 1 molar equivalent of Zn^{2+} or Cu^{2+} or Fe^{3+}.*

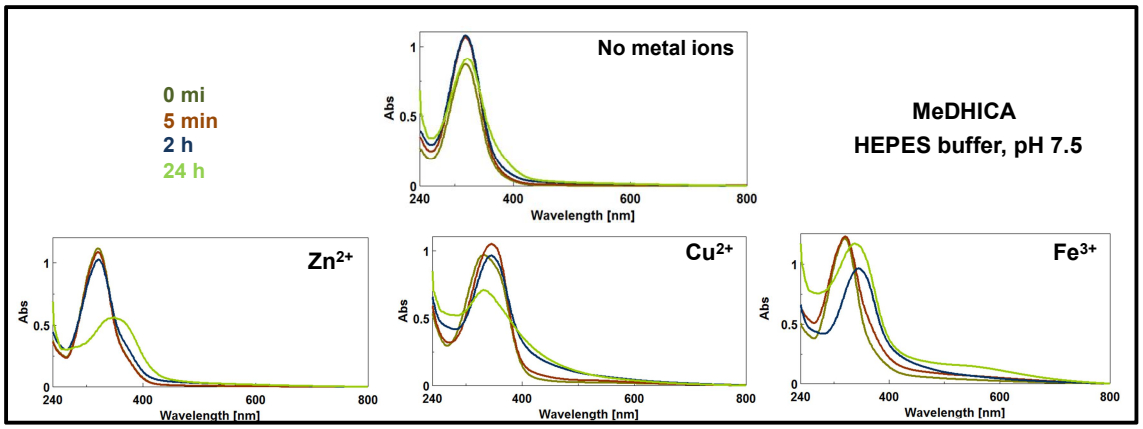

Figure 2.2.28 *Generation of chromophores from MeDHICA in the presence and in the absence of 1 molar equivalent of* Zn^{2+} *or* Cu^{2+} *or* Fe^{3+}.

Intense chromophores in the visible region were observed in oxidation mixtures catalyzed by metal ions. DHI and Me-DHI gave rise to more intense absorptions in the visible range under all the oxidation conditions. DHICA developed a visible chromophore only in the metal catalyzed oxidation whereas MeDHICA did not generate colors under the various oxidation conditions. In contrast to the case of zinc, copper and iron proved able to induce the decay of all the monomers within a few minutes suggesting a redox exchange between the indole and metal rather than aerobic oxidation. Purple to blue colors were observed for the reaction in the presence of copper in the case of both DHI and MeDHI, that are likely to arise from chelates of dimers or higher oligomers. By contrast in the presence of iron a brownish color prevailed. This is also well apparent in Figure 2.2.29 showing the colors of the oxidation mixtures in the presence of copper and iron ions at 10 min reaction time with the substrates at 100 μM. When treated with a reducing agent as sodium dithionite a complete discharge of the visible chromophore was observed for both DHI and DHICA with either metal ions suggesting that the chromophore derived from quinonoid forms of dimers or oligomers are possibly stabilized to further polymerization by the metal ions thus being more easily reducible.

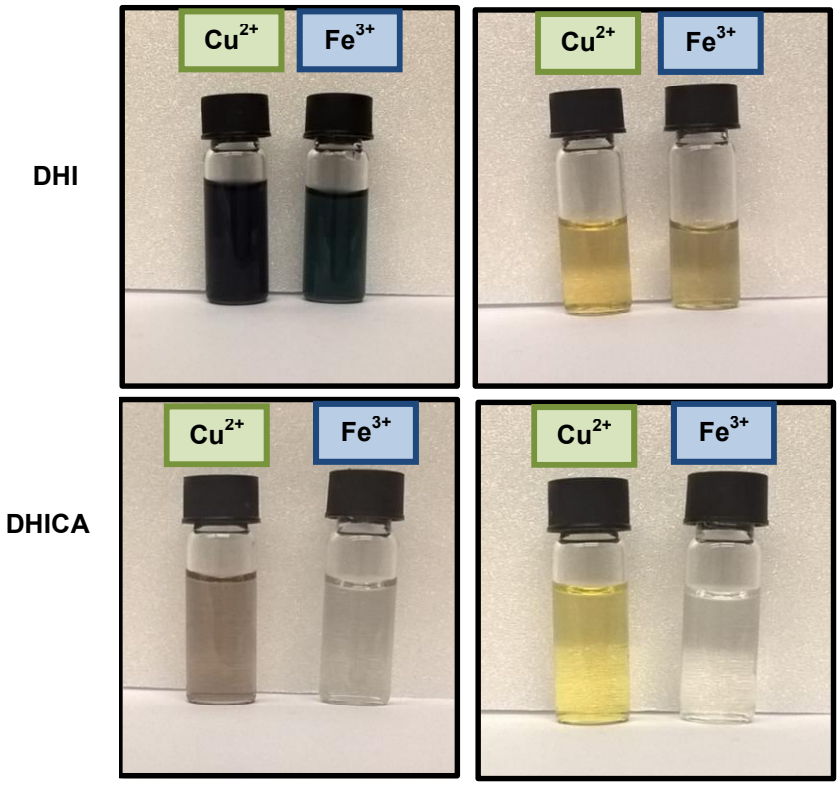

Figure 2.2.29 *Color of the oxidation mixtures of DHI or DHICA in the presence of equimolar metal ions with the substrate at 100 μM. Left: at 10 minutes reaction time; Right: soon after addition of excess dithionite.*

These experiments indicate that the presence of metal ions is an important determinant of transient and final chromophores and color properties.

Conclusions. The contribution of the structural (scaffold-controlled) and redox (π-electron-controlled) disorder to the unusual broadband absorption spectrum of eumelanins has been disentangled through an integrated experimental-theoretical approach based on poly(vinyl alcohol)-controlled polymerization of a large set of 5,6-dihydroxyindoles and related dimers. The results a) uncover the impact of the structural scaffold on eumelanin optical properties, disproving the widespread assumption of a universal monotonic chromophore; b) delineate eumelanin chromophore buildup as a three-step dynamic process involving the rapid generation of oxidized oligomers, termed melanochromes (phase I), followed by a slow oxidant-independent band broadening (phase II) leading eventually to scattering (phase III); c) point to a slow reorganization-stabilization of melanochromes via intermolecular redox interactions as the main determinant of visible broadband absorption; d) highlight the influence of metal cations on the chromophoric properties of melanins.

2.3 Effect of esterification on the antioxidant activity and oxidative polymerization of 5,6-dihydroxyindole-2-carboxylic acid

The effects of carboxyl group on eumelanin properties. One of the main variation that can be observed and that strongly affects melanin properties, is the presence or the absence of the carboxyl group in the precursors.[6]

The rearrangement of dopachrome to DHI or DHICA[112] constitutes an important branch in melanogenesis as carboxyl retention results in essential biological consequences such as antioxidant eumelanin properties that are enhanced in the case of DHICA melanin.[7] In vitro and at neutral pH, dopachrome spontaneously decomposes to give DHI and DHICA in a 70:1 ratio[113] but in the presence of dopachrome tautomerase or of metal cations, the formation of DHICA is favored.[114–117]

Oxidative polymerization of DHI and DHICA produces eumelanin via a wide range of oligomers, mainly coupled through 2,2'-, 2,4'-and 2,7'-bonding in the case of DHI,[118–120] through 4,4'-, 4,7'- and 7,7'-bonding in the case of DHICA (Figure 2.3.1). This different reactivity is due to the electron-withdrawing carboxylic acid group that decreases the nucleofilicity of the pyrrole moiety and the reactivity of the 3- position.[118,120]

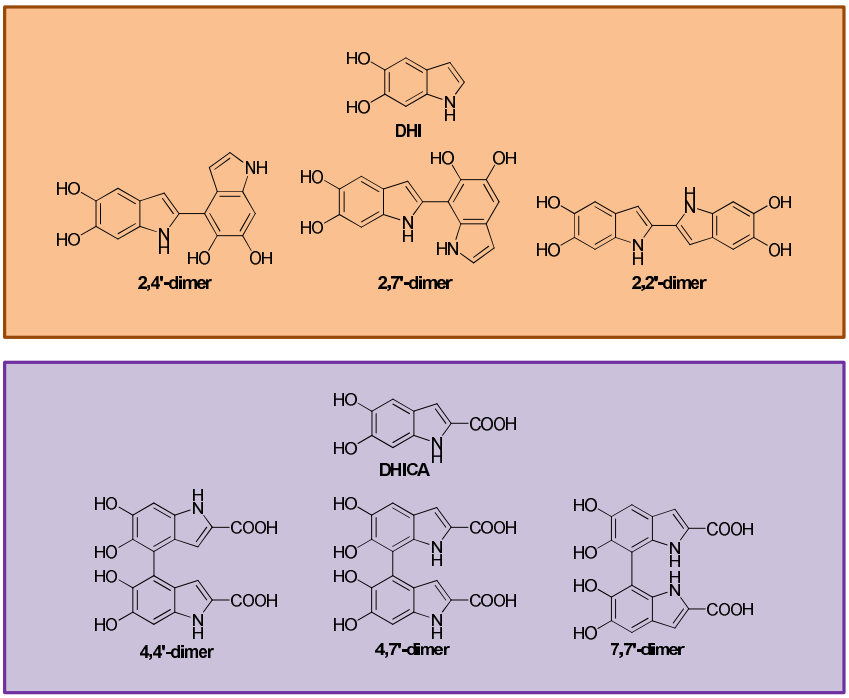

Figure 2.3.1 *DHI and DHICA dimers.*

While DHI oligomers exhibit a planar conformation with π-stacked supramolecular aggregates, DHICA mainly polymerizes through biphenyl-type bond, adopting a non-planar conformation with a hindered rotation at the inter-ring bonds, giving reason to atropisomerism.[121,10] Negative charges on the carboxylate groups reinforces this deviation from planarity, so while DHI oxidation produces planar species absorbing visible radiation, DHICA oligomers do not absorb above 400 nm because a significant interruption of π-electron delocalization.[107,109]

These structural differences between DHI and DHICA melanins strongly affect their physic-chemical properties. Mayor differences in DHICA and DHI monomers and polymers are comparatively summarized in Table 2.3.2.

Table 2.3.2 ***Comparison of the properties of eumelanins from carboxylated/non-carboxylated precursors.***

	DHI	**DHICA**
	Monomer characteristics	
Reactive sites	At least 4	Usually 2
Oxidizability	High	Low
	Polymer properties	
Solubility (neutral pH)	Nihil	Very slight
EPR signal intensity	Strong	Weak
Visible absorption	Intense	Poor
Photophysical properties	Efficient excited state decay	More efficient excited state decay
Chemical properties	Antioxidant	More potent antioxidant

Three features could account for differences in carboxylated or non carboxylated rich units in melanin:

- Lower number of reactive sites available for polymerization and cross-linking
- Lower oxidation potential
- Negative charge

This last characteristic can affect the structural properties of oligomers and their susceptibility to post-synthetic modifications. All these data suggest that retention of carboxyl group modulates pigment properties in eumelanins.

Effects of carboxylate esterification on eumelanin properties. In order to understand the role of the carboxyl group as determinant of the chemical properties of the 5,6-dihydroxyindole system, DHICA and its methyl ester (MeDHICA) were compared. Their conversion to eumelanin chromophore and their antioxidant properties were investigated.

Comparison of the autoxidation reaction of DHICA and MeDHICA (50 μM) in phosphate buffer (pH 8.5) showed in both cases a progressively decrease of the maximum of the indole at 320 nm with concomitant development of the featureless broadband absorption typical of melanins. However, a much slower rate was observed in the case of MeDHICA with the monomer indole still detectable at 48 h (Figure 2.3.2).

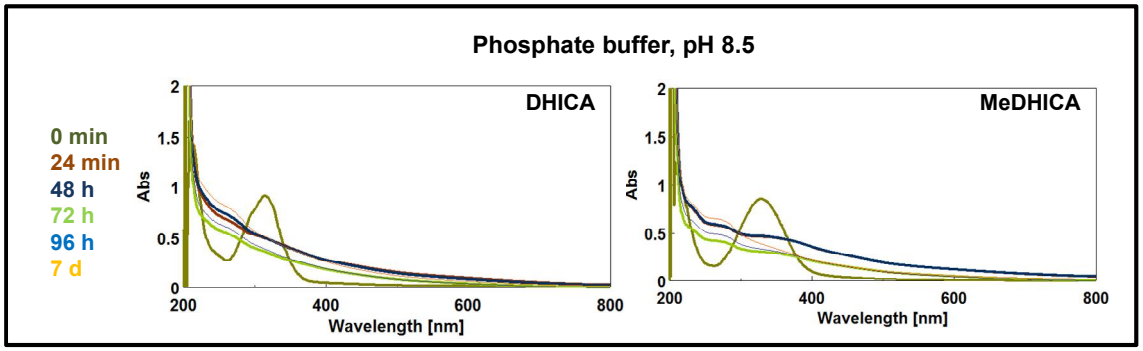

Figure 2.3.2 *Spectrophotometric course of the autoxidation mixture of DHICA or MeDHICA (50 mM) in 0.1 M phosphate buffer, pH 8.5.*

Monitoring the course of the oxidation by reverse phase HPLC, a complete consumption of the monomer was observed at 72 h, while at 48 h the decay of the starting indole was about 40%. The elutographic profile showed other more retained components of which the first eluted was clearly predominant (Figure 2.3.3). A similar product pattern is obtained using potassium ferricyanide as oxidant, while the addition of metal ions like copper or cobalt to the autoxidation mixture markedly accelerated the process, favoring the formation of the first eluted component, This latter was isolated by preparative HPLC from the oxidation mixture of the indole at 10 mM

concentration in the presence of equimolar cobalt sulphate in 0.2 M HEPES buffer pH 7.5 over 15 min reaction time.

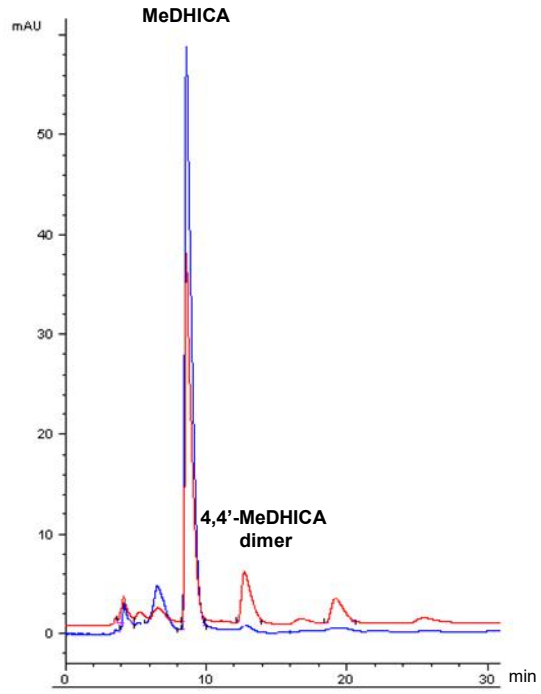

Figure 2.3.3 *HPLC profile of the MeDHICA oxidation mixture with UV detection (280 nm). Blue trace: t= 0; red trace: t= 48 h.*

The product was identified as the 4,4'-biindolyl based on NMR analysis in comparison with data reported for DHICA dimers.[9] Since the 4,4' dimer is the major oligomer also in the case of DHICA it can be concluded that the regioselectivity of the oxidative coupling observed for DHICA is not affected by derivatization of the carboxyl group.

Melanins from MeDHICA and DHICA, for comparison, were prepared using different oxidizing conditions including autoxidation in phosphate buffer at pH 8.5 and chemical oxidants like ferricyanide. The reaction was run until complete consumption of the monomer as determined by HPLC analysis. The oxidation mixtures were then acidified and the melanin pigment was separated by centrifugation.

The solubility properties of MeDHICA and DHICA melanins prepared by autoxidation were assayed in different organic solvents selected among those with high miscibility in water, using a test concentration of 0.3 mg/mL and stirring the materials in the appropriate solvent for 15 min. Digital pictures of the solution/suspension in methanol or dimethyl sulfoxide (DMSO) chosen as representative solvents are shown in Figure 2.3.4.

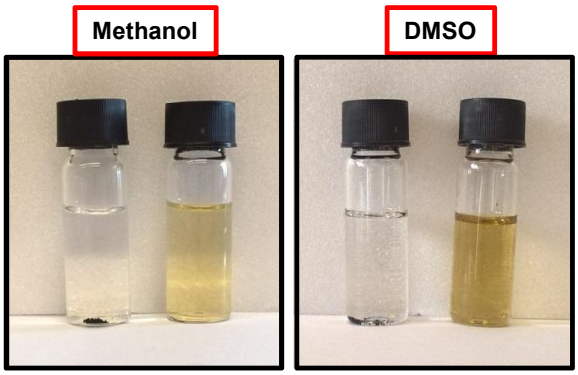

Figure 2.3.4 *Digital pictures of 0.3 mg/mL DHICA (left) or MeDHICA (right) melanin prepared by autoxidation and stirred in methanol or DMSO for 15 minutes.*

In DMSO, MeDHICA melanin proved to be completely soluble whereas DHICA melanin did not, while in methanol as well as in other solvents only a partial solubilization was obtained. Absorption spectra of the supernatants, after discarding the solid materials and appropriate dilution, showed a maximum around 330 nm in the case of MeDHICA melanin whose intensity correlated fairly well with the observed solubility in the solvents examined (Figure 2.3.5).

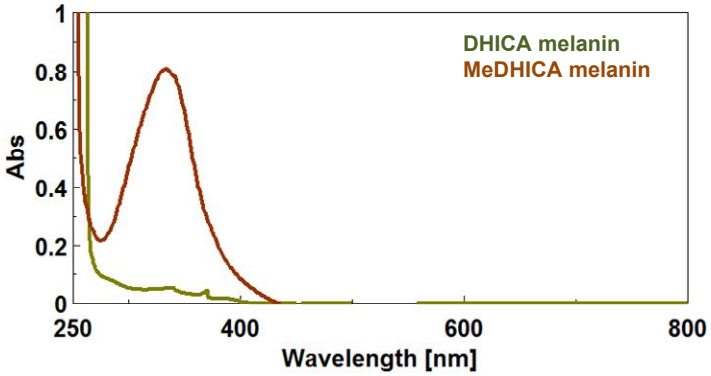

Figure 2.3.5 *Uv-vis spectra of DHICA and MeDHICA melanin in DMSO.*

Mass spectrometric analysis in the MALDI mode was run using 2,5-dihydroxybenzoic acid as the matrix, the melanin was applied to the plate from a fine suspension in ethanol obtained by homogenization in a glass to glass potter. The spectrum of the MeDHICA melanin prepared by aerobic oxidation displays a well distinct pattern of signals corresponding to oligomers from the dimer to the octamer, peaking at the trimer (Figure 2.3.6). Though it cannot be ruled out that other high molecular weight components are not detected by this methodology, the spectrum

provides evidence for a clean collection of intact oligomers as constituents of MeDHICA melanin. A similar though less defined spectrum was obtained for MeDHICA melanin prepared by ferricyanide oxidation (data not shown).

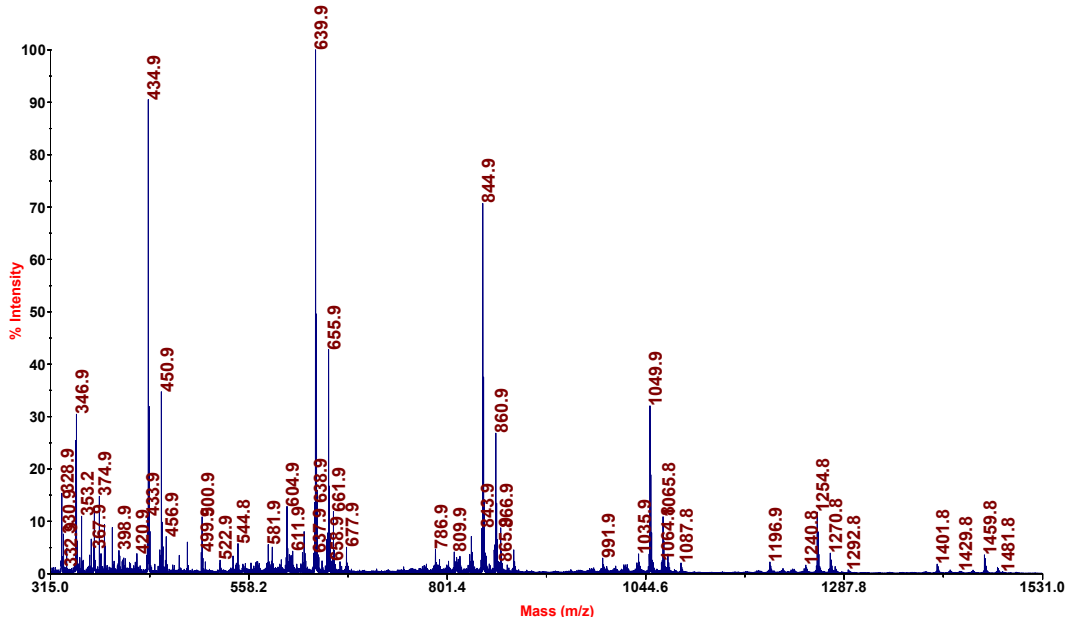

Figure 2.3.6 *MALDI spectrum of the MeDHICA melanin prepared by aerobic oxidation.*

EPR spectra of different MeDHICA melanins in comparison with one representative DHICA melanin were recorded. Almost identical g-values were exhibited by all melanins and signal amplitudes (ΔB) were comparable and relatively narrower (Table 2.3.3) compared with those reported for DHI and other melanins.[7]

Table 2.3.3 ***EPR spectral parameters for MeDHICA and DHICA melanin prepared under different conditions***

Sample	ΔB (G)	spin/g	g-factor
MeDHICA melanin (autoxidation)	4.4 ± 0.2	6.2×10^{18}	2.0029 ± 0.0002

MeDHICA melanin (ferricyanide)	4.0 ± 0.2	2.4×10^{18}	2.0029 ± 0.0002
DHICA melanin (autoxidation)	4.5 ± 0.2	8.2×10^{17}	2.0029 ± 0.0002

These data coupled with analysis of the power saturation curves (Figure 2.3.7) indicated a similar free radical character for the various melanins with a good degree of homogeneity and low dispersion of the free radical components.

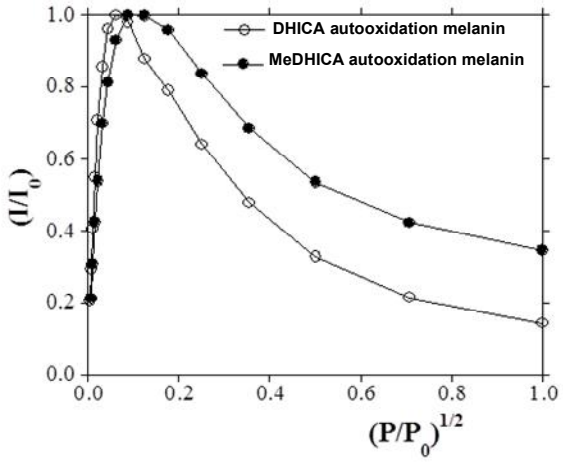

Figure 2.3.7 *Power saturation curves for MeDHICA and DHICA melanin prepared by auto oxidation.*

Spin densities of MeDHICA melanins were of higher magnitude with respect to DHICA melanin, suggesting the presence of radical centers arising from intermolecular aggregation *equilibria* of localized quinone and indole units inside the pigment backbone. Conversely, in DHI-melanin[7] the paramagnetic centers belong to extensively delocalized π-electron systems across largely planar scaffolds.[85]

Antioxidant properties of MeDHICA melanins (in comparison with respective monomers and 4,4' dimers) were assayed by two chemical tests, namely the 2,2-diphenyl-1-picrylhydrazy (DPPH),[122] an assay that measures the H-donor ability of a given species and the ferric reducing antioxidant power (FRAP),[123] which measures the ability of the antioxidant to reduce a Fe^{3+}-tripyridyltriazine complex to a dark blue Fe^{2+} complex with absorption maximum at 593 nm.

In the case of DPPH (Figure 2.3.8) the EC_{50} values (*i.e.* the dose of the material at which a 50% DPPH reduction is observed), were determined. Very low and similar values were obtained for both monomers, whereas for the dimer the values were comparable and as low as 2.4 μg/mL. This is in line with the high antioxidant potential of DHICA as reported in previous work by different assays which is substantially unaltered in the ester.

In the case of melanins, a fine suspension was obtained by homogenization in a glass/glass potter. MeDHICA melanin obtained by autoxidation proved to be a very effective antioxidant to an extent comparable or even higher with respect to DHICA melanin, but either pigment was less potent that their monomer or 4,4'-dimer.

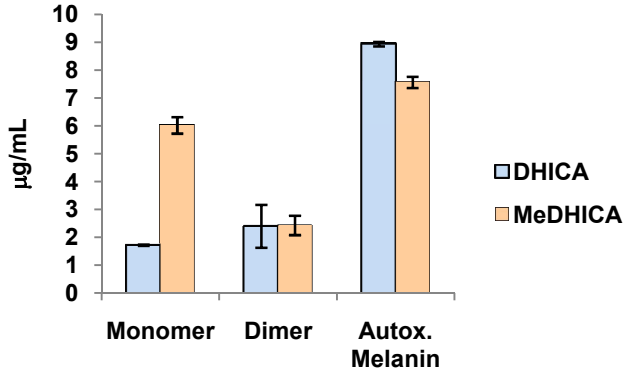

Figure 2.3.8 *EC_{50} values from DPPH assay on DHICA and MeDHICA monomers, dimers, and melanin prepared by autooxidation. Data are expressed as mean ± SD of three independent experiments, each performed in duplicate.*

In the case of FRAP (Figure 2.3.9), results were expressed as trolox equivalents and show comparable values in the case of the monomer and of the dimer, while MeDHICA melanin proved to be a stronger antioxidant than DHICA melanin.

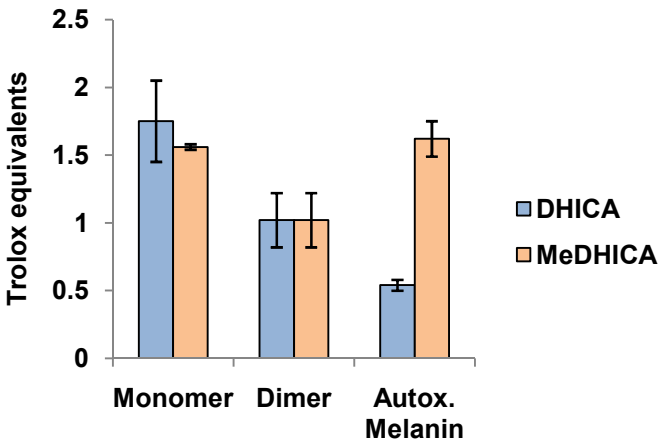

Figure 2.3.9 *Ferric reducing power of DHICA and MeDHICA monomers, dimers, and melanin prepared by autoxidation, expressed as trolox equivalents. Data are expressed as mean ± SD of three independent experiments, each performed in duplicate.*

These results suggest that the role of the carboxyl group in melanogenesis from DHICA is more complex than simply blocking the 2-position of the indole ring, and can be modulated through the control of ionization of carboxylate anion. Based on the behavior of the ester, it is suggested that suppression of carboxylic acid ionization under the acidic conditions of melanosome interior enhances antioxidant properties while hindering dark melanin formation. However, data presented in this paragraph are only preliminary and still underway.

2.4 Methods and experimental procedures

3,4-Dihydroxy-L-phenylalanine (L-DOPA), dopamine hydrochloride, hydrogen peroxide (30% v/v), potassium ferricyanide, sodium periodate, nickel sulfate eptahydrate, copper acetate, zinc sulfate heptahydrate, cobalt sulfate, ferric chloride,4-(2-hydroxyethyl)-1-piperazineethanesulfonic acid (HEPES), ceric ammonium nitrate (CAN), sodium dithionite, sodium borohydride, horseradish peroxidase (HRP; donor: H_2O_2oxidoreductase, EC 1.11.1.7) and sodium *tert*-butoxide, oleoyl chloride, triethylamine (TEA), anhydrous tetrahydrofuran (THF) 1,1-diphenyl-2-picrylhydrazyl (DPPH), 2,4,6-tris(2-pyridyl)-s-triazine, and 6-hydroxy-2,5,7,8-tetramethylchroman-2-carboxylic acid (trolox) were purchased from Sigma-Aldrich. All solvents were HPLC grade. Bidistilled deionized water was used throughout the study.

HPLC analyses were performed on a Agilent 1100 binary pump instrument equipped with and a SPD-10AV VP UV-visible detector using an octadecylsilane-coated column, 250 mm x 4.6 mm, 5 μm particle size (Phenomenex Sphereclone ODS) at 0.7 mL/min. Detection wavelength was set at 280 nm.

Analysis of oxidation mixtures of melanin precursors was performed using 1% formic acid: methanol 60:40 v/v as eluant in the case of MeDHICA and the following gradient in the case of DHICA: 1.5% formic acid (eluant A)/ methanol (eluant B) from 5 to 90% b, 0-45 min.

UV spectra were recorded on a Jasco V-730 Spectrophotometer.

EPR measurements were performed using an X-band (9 GHz) Bruker Elexys E-500 spectrometer (Bruker, Rheinstetten, Germany), equipped with a super-high sensitivity probe head.

Samples were transferred to flame-sealed glass capillaries which, in turn, were coaxially inserted in a standard 4 mm quartz sample tube. Measurements were performed at room temperature. The instrumental settings were as follows: sweep width, 100 G; resolution, 1024 points; modulation frequency, 100.00 kHz; modulation amplitude, 2.0 G. The amplitude of the field modulation was preventively checked to be low enough to avoid detectable signal over modulation. Preliminarily, EPR spectra were measured with a microwave power of ~0.5 mW to avoid microwave saturation of resonance absorption curve. Several scans, typically 16, were accumulated to improve the signal-to-noise ratio. Successively, for power saturation experiments, the microwave power was gradually incremented from 0.02 to 160 mW. The g value and the spin density were evaluated by means of an internal standard, Mn^{2+}-doped MgO, prepared by a synthesis protocol reported in literature.[124]

MALDI analysis mode was run on a AB Sciex TOF/TOF 5800 instrument using 2,5-dihydroxybenzoic acid as the matrix and the melanin applied to the plate from a fine suspension in ethanol obtained by homogenization in a glass to glass potter. Spectrum represents the sum of 15,000 laser pulses from randomly chosen spots per sample position. Raw data are analyzed using the computer software provided by the manufacturers and are reported as monoisotopic masses.

Preparation of 5,6-dihydroxyindole monomers. 5,6-dihydroxyindole (DHI),[125] 5,6-dihydroxyindole-2-carboxylic acid (DHICA)[125] and 5,6-dihydroxy-*N*-*methyl*indole (N-MeDHI) were prepared as described.[120]

MeDHICA was prepared starting from DOPA methylester prepared by reacting DOPA (2.0 g) in methanol (20 mL) with 96% sulfuric acid (2 mL) under reflux. After 24 h the mixture was allowed to cool and sodium bicarbonate was added to neutrality. The solution thus obtained was reacted in water with potassium ferricyanide under the same conditions used for preparation of DHI[125] and after 15 min extracted with ethyl acetate to give pure Me-DHICA (1.3 g, 61% yield).

Preparation of 5,6-dihydroxyindole dimers. 2,2'-biindolyl,[126] 2,4'-biindolyl and 2,7'-biindolyl from DHI were prepared as previously described with slight modifications. Briefly, a solution of DHI (300 mg, 2.0 mmol) in 0.05 M phosphate buffer (pH 6.8, 120 mL) was treated with horseradish peroxidase (36 U/mL) and H_2O_2 (266 μL of a 30% solution, 2.3 mmol). After 25 s, the oxidation reaction was stopped by addition of a solution of sodium dithionite and rapidly extracted with ethyl acetate. After acetylation of the residue obtained following evaporation of the combined organic layers with acetic anhydride-pyridine overnight at room temperature the mixture was fractionated by column chromatography (gradient elution, $CHCl_3$–ethyl acetate from 9:1 to 6:4) to afford the 2,7'-biindolyl (45 mg, 10% yield, > 95% pure) and the 2,4'-biindolyl (53 mg, 11%, > 95% pure) as acetylated derivative. For isolation of the 2,2'-biindolyl as the *O*-acetyl derivative (30 mg, 12% yield) DHI (150 mg, 1.0 mmol) was oxidized in air in 0.05 M HEPES buffer (pH 7.5) in the presence of $NiSO_4 \cdot 7H_2O$ (560 mg, 2.0 mmol). After acetylation treatment of the ethyl acetate extracts the residue was taken up in acetone and the product was recovered by filtration as white prisms.

4,4'-Biindolyl from DHICA was prepared as previously described[29] with modifications. A solution of DHICA (100 mg, 0.51 mmol) in 0.1 M HEPES buffer (pH 7.5, 495 mL) was treated with copper acetate (1 molar equivalent) and the reaction mixture was taken under vigorous stirring. After 10 min, the oxidation reaction was stopped by addition of sodium dithionite,

acidified to pH 2 and rapidly extracted with ethyl acetate. The residue obtained following evaporation of the combined organic layers was fractionated by preparative HPLC. (16 mg, 16% yield, >90% pure).

4,4'-Biindolyl from Me-DHICA was prepared as previously described[114] with modifications. A solution of Me-DHICA (110 mg, 0.51 mmol) in 0.2 M HEPES buffer (pH 7.5) (33 mL) was treated with cobalt sulfate (1 molar equivalent) and the reaction mixture was taken under vigorous stirring. After 20 min, the oxidation reaction was stopped by addition of sodium dithionite, acidified to pH 2 and rapidly extracted with ethyl acetate. The mixture was fractionated by preparative HPLC. (18 mg, 12% yield, >90% pure).

Oxidation of 5,6-dihydroxyindole monomers and dimers. 15 μL of a 10 mM solution of the appropriate indole monomer or 4,4'DHICA-dimer were added to 3 mL of 0.1 M phosphate buffer (pH 7.0) to reach a final concentration of 50 μM followed by 2 molar equivalents of potassium ferricyanide (30 μL of a 10 mM solution in water). In the case of DOPA and DA the reaction was carried out with 6 molar equivalent of ferricyanide. The reaction mixtures were taken under vigorous stirring and periodically analyzed by UV-vis spectrophotometry. Spectra were registered at 5 min, 2 h and 24 h. After 5 min in air, reaction mixtures were degassed and kept under stirring in an argon atmosphere.

In other experiments the reaction was performed:

i) in the presence of sodium periodate (1 molar eq.)

ii) in the presence of CAN (2 molar eq.) in 0.1 M phosphate buffer (pH 3.0).

iii) adding sodium dithionite or sodium borohydride after the addition of potassium ferricyanide (2 or 40 molar equivalents).

iv) in the presence of ferric chloride or zinc sulfate or copper acetate(1 molar eq.)in 0.2 M HEPES buffer

When required, oxidation mixtures were filtered through a 0.45 micron nylon membrane.

Substrate consumption was determined by HPLC analyses under the conditions described above.

When required the reaction was carried in 0.1 M phosphate buffer (pH 7.0) containing 1% poly(vinyl alcohol) (PVA) to prevent polymer precipitation.

In the case of acetylated dimers the following protocol was followed: 5 mL of a 3.6 mM solution of the acetylated dimer in methanol were treated under an argon atmosphere with sodium *tert*-butoxide (8 molar equivalents) and after 5 min the pH of the solution was taken to 2 by addition of 4 M HCl. 42 μL of the resulting mixture was added to 3 mL of 0.1 M phosphate buffer (pH

7.0) to reach a final concentration of 50 μM followed by 2 molar equivalents of potassium ferricyanide.

Preparation of melanin from DHICA and MeDHICA. Autoxidation melanins were obtained by autoxidation of 10 mM solutions of DHICA or MeDHICA in 0.1 M phosphate buffer at pH 8.5. The oxidation mixtures were allowed to stand at room temperature under vigorous stirring. Oxidation was halted at complete monomer consumption as determined by HPLC analysis and then acidified to pH 2. The melanin precipitate was collected by centrifugation (7000 rpm, 10 min, 4 °C) and was washed three times with 15 mL of 0.01M hydrocloridric acid (95% and 65% yield). In another set of experiments, 3 molar equivalents of potassium ferricyanide were added to 10 mM solutions of DHICA or MeDHICA in 0.1 M phosphate buffer at pH 7.0. The oxidation mixture was allowed to stand at room temperature under vigorous stirring for 10 min and then acified to pH 2. The melanin precipitates were collected by centrifugation (7000 rpm, 1020 min, 4 °C) and washed three times with 15 mL of 0.1 M hydrocloric acid (86% and 93% yield).

Test of the solubility of melanin from DHICA and MeDHICA. Melanin prepared by autoxidation from DHICA or MeDHICA (0.3 mg/mL) were suspended/dissolved in methanol or DMSO. The materials were stirred in the appropriate solvent for 15 min and UV-vis spectra of supernatants were registered after centrifugation (5000 rpm, 10 min, and 4 °C) and appropriate dilution.

2,2-Diphenyl-1-picrylhydrazy (DPPH) assay. The assay was performed as previously described.[122] Briefly, to a 200 μM DPPH solution in methanol, a proper amount of a methanolic suspension of each melanin homogenized with a glass/glass potter was added and rapidly mixed. The reaction was followed by spectrophotometric analysis measuring the absorbance at 515 nm after 10 min. Values are expressed as the EC_{50} i.e. the dose of the material at which a 50% DPPH reduction is observed,

Ferric reducing/antioxidant power (FRAP) assay. The assay was performed as described.[123] To a solution of FRAP reagent, a proper amount of a methanolic suspension of each melanin homogenized with a glass/glass potter was added and rapidly mixed. After 10 minutes, the absorbance at 593 nm was measured. Trolox was used as the standard and results were expressed as Trolox equivalents. The FRAP reagent was prepared freshly by mixing 0.3 M acetate buffer (pH 3.6), 10 mM 2,4,6-tris(2-pyridyl)-s-triazine in 40 mM HCl, and 20 mM ferric chloride in water, in the ratio 10:1:1, in that order.

Chapter 3

Sulfur-nitrogen replacement strategy for eumelanin manipulation

3.1 Introduction

The rational design of melanin-type functional materials and systems with tailored opto-electronic, free radical, antioxidant and metal chelating properties is currently a most active and challenging issue in materials science, nanotechnology and biomedicine. Since a decade ago, a prominent place in this field has been occupied by polydopamine (PDA), a eumelanin-type polymer inspired to mussel byssus with unusual underwater adhesion properties for surface functionalization and coating.[12] Material-independent adhesion layers produced with PDA can be exploited for the immobilization of biological molecules, production of self-assembled monolayers, nanoparticle modification, bio-optoelectronic materials, and fouling-resistant systems.[127] The processes and mechanisms underlying deposition of PDA coatings have been investigated in detail,[81,128–130] and the importance of specific cooperative effects between functional groups in the adhesion mechanisms has been emphasized, including mainly the coexistence of catechol/quinone and primary amine functionalities.[49] Because of ist robustness, universal adhesion properties and biocompatibility, PDA-based coating technology has opened up unprecedented opportunities in biomedicine and nanomedicine, e.g. nanoparticle functionalization, drug delivery and interfacing with cells.[81,131] The simple and accessible methodology for preparation of PDA particles and films provides moreover a unique tool for functionalization and post-modification, including deposition on metal films, self-assembly of monolayers, and grafting to macromolecules.

Recent work directed at elucidating PDA structure[128–130] revealed the presence of different functional units which account altogether for the extraordinarily versatile and multifunctional nature of this material, diplaying high affinity for biomolecules, metal ions, synthetic polymers and organic compounds.

Although the development of functional platforms capable of influencing the redox state of cells provides an attractive strategy for bioelectronic applications,[132,133] little attention has been placed so far to rationally designing bioinspired coating materials that combine the unique adhesion and film quality properties of PDA with intrinsic and tunable redox properties.

Another useful and versatile platform for the realization of bioinspired and biocompatible eumelanin-type polymers is provided by the 5,6-dihydroxyindole (DHI) system, the main building block of human pigments. Several studies have illustrated the manifold synthetic opportunities offered by the 5,6-dihydroxyindole system, including the acid-mediated conversion into triazatruxene scaffolds with electroluminescence properties.[87]

So far, however, progress in the exploitation of eumelanin-related systems in materials science has been hindered by the intrinsic complexity of these biopolymers, as determined by multiple levels of structural, redox and supramolecular disorder, as well as their instability to oxidative degradation, their hydration-dependent conductivity properties and the difficulty to control their π-electron properties, which overall limit their performances e.g. in electronic devices. The development of DHI analogs and derivatives amenable to chemical modification thus represents a desirable achievement both to improve the robustness and tailor the properties of eumelanin-type polymers.

Previous attempts toward this goal were mainly based on monomer modification by judicious choice of substituents and bonding patterns to control structural, optical and electronic properties of the conjugated polymer. Examples include substitution of the ring with iodine,[134] to stabilize the π-electron system of 5,6-indolequinone, or alkynyl groups, to provide conformationally-controlled π-electron delocalization. However, systematic studies aimed at clarifying the role of nitrogen in DHI π-electron system, its redox properties and oxidation reactivity, are so far missing.

In an attempt to set up a chemical manipulation strategy for controlling and tailoring the physicochemical properties of melanin-type materials, we focused our attention to the potential opportunities offered by the use of sulfur for rationally modifying monomer properties.

A main source of inspiration, to this aim, came from the unique physicochemical properties of pheomelanins, the sulfur-containing variant of melanin pigments implicated in the abnormal susceptibility of red-haired individuals to sunburn and skin cancer.[135,136] Chemical and biological evidence indicates that both natural and synthetic pheomelanin pigments not only are potent photosensitizers but can also promote depletion of key cellular antioxidants, such as glutathione and NADPH, and can induce DNA damage by oxygen-dependent, UV-independent mechanisms relying on redox cycling of 1,4-*2H*-benzothiazine units.[137–139]

In the pheomelanin pathway, 1,4-*2H*-benzothiazine units are generated by the oxidative cyclization of cysteine-catechol conjugates derived from attack of cysteine onto o-quinone intermediates (Scheme 3.1.1).

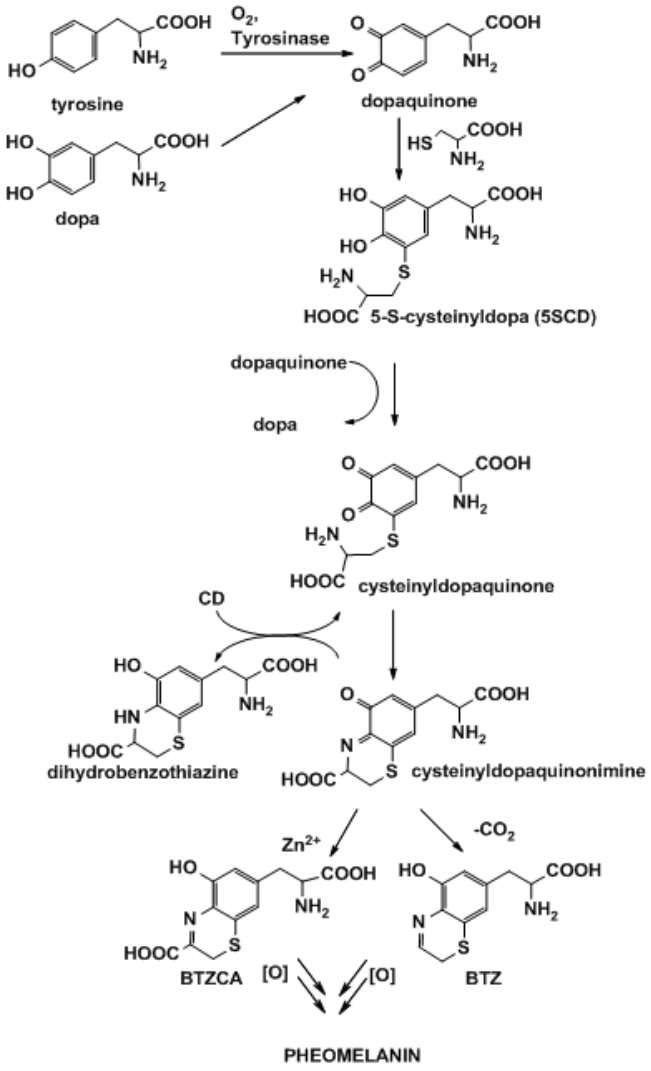

Scheme 3.1.1 *The pheomelanin biosynthetic pathway.*

Inspired by these properties, we recently developed the first PDA-based photoresponsive polymer by inclusion of the benzothiazine units of red hair pigments.[140] The new material, named polycisteynildopamine (PCDA), was obtained by oxidative polymerization of 5-S-cysteinyldopamine (CDA), an important dopamine metabolite precursor of the brain pigment neuromelanin, which gives on oxidation benzothiazine intermediates similar to pheomelanin building blocks (Scheme 3.1.2).[100,141]

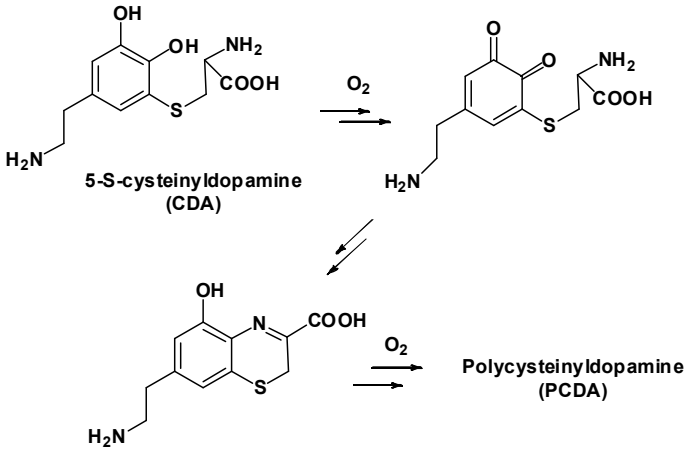

Scheme 3.1.2 *Structure and oxidation chemistry of CDA leading to PDCA.*[141]

Whit the aim to reach new insights in the structure-property relationships between eu/pheo-melanins and their dramatically different properties, another attractive approach was based on the replacement of nitrogen with sulfur both in the dopamine and DHI scaffolds that are, as already explained, the main monomer precursors of eumelanins.

Prior to our studies, systematic work aimed at clarifying the role of nitrogen in DHI π-electron system, its redox properties and oxidation reactivity, was missing. It was expected that a rational N-to-S replacement strategy could integrate and expand the current framework of structure-property-function relationships for eumelanin biopolymers and to set up novel rational strategies toward eumelanin manipulation and tailoring.

This chapter summarizes the results from two separate studies aimed at investigating the potential role of S-substitution and N-replacement in dopamine and DHI oxidative chemistry, as an entry to novel functional materials.

3.2 S-Csteinyl-substitution as a strategy for manipulating polydopamine properties.

The main rationale of this study was to produce a new PDA variant combining the adhesion enhancement capabilities of dopamine with the peculiar redox and photochemical properties of the 1,4-2H-benzothiazine system found in photoactive red hair pigments. As recently reported, synthetic pheomelanin-like materials can be easily fabricated by oxidation of 5-S-cysteinyldopamine (CDA), a product of DA metabolism resembling the pheomelanin precursor 5-S-cysteinyldopa but replacing the alanyl side chain with an ethylamine side chain on the catechol ring.[141] Reported in this section is:

a) the first use of a CDA polymer (pCDA) as a strongly adhesive variant of pDA for dip-coating of glass surfaces via autoxidation of CDA at pH 8.5, i.e. using the reported methodology for pDA;[16]
b) the morphological, and chemical characterization of pCDA thin films in comparison with pDA;
c) the ability of pCDA thin films to accelerate the autoxidation of two important natural reducing agents, glutathione and nicotinamide adenine dinucleotide (NADH), in analogy with the behaviour of aqueous suspensions of natural and synthetic pheomelanin polymers.

Surface functionalization with pCDA and thin film characterization. CDA, synthesized using a reported method,[142] was allowed to autoxidize at 10 mM concentration in 0.05 M bicarbonate buffer, pH 8.5 in the presence of quartz and other materials, e.g. glass, metal objects or plastic cuttings. Under these conditions, thin films of pCDA were deposited on their surfaces. Dip-coating of quartz surfaces with pCDA for various periods of time was thus compared with pDA films obtained under the same conditions, up to 24 h of polymerization time (Figure 3.2.1, digital picture). Solid state UV-visible spectra indicate the gradual polymerization and time dependent generation of a broad band at around 400 nm accounting for the lighter yellow-brown coloration of the pCDA films, with respect to pDA (Figure3.2.1).

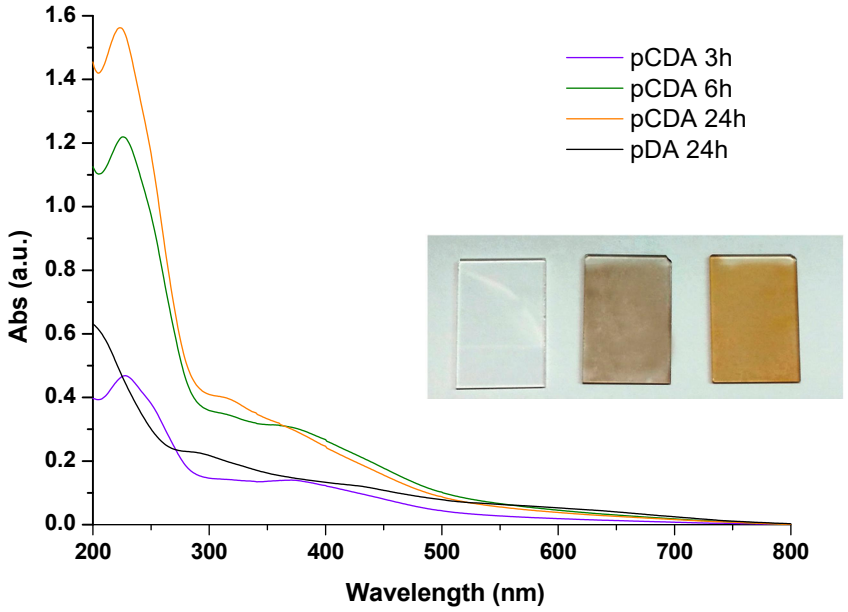

Figure 3.2.1 *Solid state UV-vis absorbance spectra of pCDA thin films on quartz obtained at 3, 6 and 24 h oxidation time and pDA at 24 h oxidation time. Digital picture of pDA (middle) and pCDA (right) thin films on quartz surfaces produced by oxidation of DA and CDA for 24 h against control, no coating (left).*

The morphology of pCDA versus pDA films was investigated by scanning electron microscopy (SEM) and tapping mode atomic force microscopy (AFM) analysis. AFM imaging of three areas of 1 mm^2 (randomly selected across the surface) revealed that the pCDA films are much smoother at the nanoscale compared to pDA films. Indeed, fewer agglomerates exceeding the average surface height (around 7 and 10 nm for pCDA and pDA, respectively) were detectable through this imaging method (Figure 3.2.2), along with narrower height value frequency distributions.

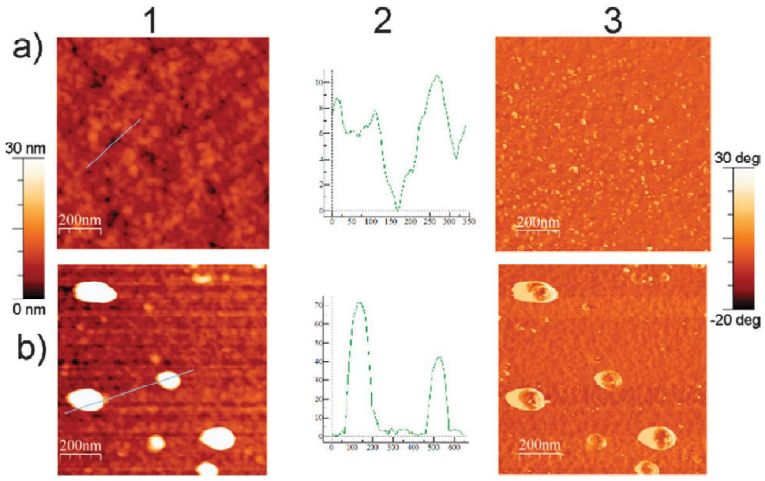

Figure 3.2.2 *Topography (1) height cross section profile (2) and phase (3) AFM images of pCDA-8 h (a) and pDA-8 h (b) surfaces. Analyses were performed in air at 298 K on 1 μm^2 areas.*

Water contact angles (WCAs) for thin films were also determined. After 8 h oxidation time WCA value was of 57.8 ± 0.5 for pCDA vs. 42.6 ± 2.8 for pDA, increasing to 73.8 ± 1.1 and64.0 ± 1.3, respectively, when films were left standing under an ambient atmosphere. This may suggest the presence of a certain level of moisture on the as prepared surfaces, and the convergence of the WCA value for the pDA surface toward the literature reported value of 65°.[143]

Detailed chemical characterization of pCDA was reported previously,[140] confirming the formation of benzothiazine and benzothiazole units similar to those found in natural and synthetic pheomelanin pigments. To substantiate this conclusion, and to probe possible structural modifications with time, pCDA thin films were investigated by X-ray photoelectron spectroscopy (XPS). The results confirmed complete retention of sulfur atoms during oxidative polymerization of

CDA, with limited variations in compositions (Figure 3.2.3), and complete stability of the sulfur-containing structural moieties during polymerization. No sulfur was consistently detected in pDA during polymerization. Overall, chemical and spectral data were consistent with the presence of benzothiazine units within the structure of pCDA as previously reported.[140]

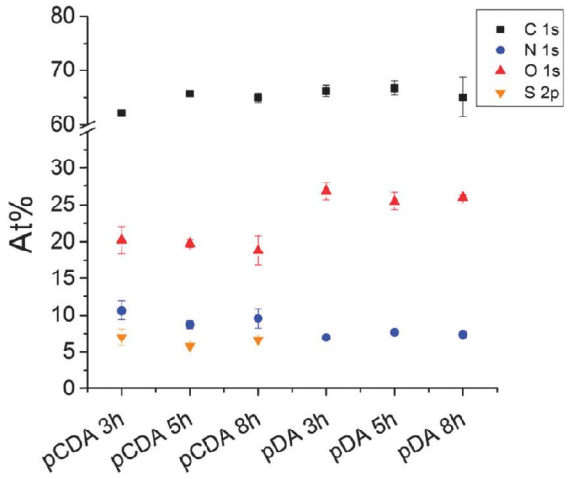

Figure 3.2.3 *XPS-based assessment of the organic moiety composition of pCDA and PDA films on to glass coverslips after 3, 5 and 8 hours of polymerization. Atomic percent (At%) are reported with black squares for C 1s, red pyramids for O 1s, blue circles for N 1s and orange triangles for S 2p.*

Prooxidant properties of pCDA thin films. Figure 3.2.4 shows the effect of pCDA thin films and suspensions on the autoxidation of glutathione (GSH), a primary cellular antioxidant, a substrate for detoxifying enzymes such as glutathione-S-tranferaseand glyoxalase, and a cofactor of glutathione peroxidase, and NADH, a central component of the respiratory chain and a critical index of the metabolic state of the mitochondria.

Data showed that pCDA either as a thin film or as suspension can markedly accelerate the autoxidation of GSH in phosphate buffer pH 7.4, leading to 65–80% depletion in less than 3 h incubation time, while PDA did not affect the reaction rate significantly. No accelerating effect was observed under an oxygen depleted atmosphere, indicating an essential role of oxygen in the pCDA-promoted oxidation of GSH. Similar though less marked effects were observed in the case of NADH.

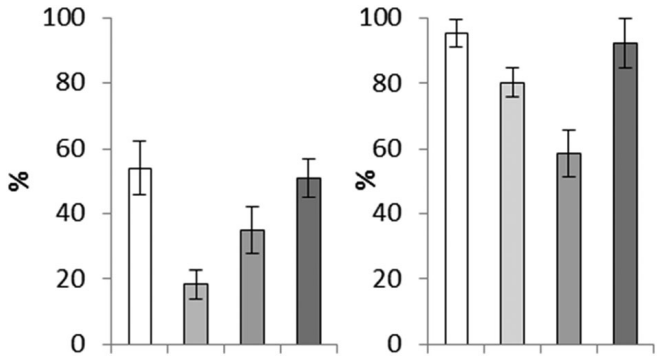

Figure 3.2.4 *Effect of pCDA on the autoxidation of GSH at 150 μM (left panel) and NADH at 300 μM (right panel) at 3 h reaction time in 0.1 M phosphate buffer pH 7.4 as determined by HPLC-ED/UV. Shown is residual GSH or NADH conc (%). Open bars: control; light grey bars: pCDA thin film; grey bars: pCDA as 0.05 mg/mL suspension; black bars: pDA thin film. Data are expressed as mean ± SD of three independent experiments, each performed in triplicate.*

Toward structure–property relationships for polydopamine-based biopolymers. Combining together the results of this and the previous study[140] some important analogies and differences between pCDA and pDA can be highlighted.

pCDA proved to be more competent to mediate electron exchange by chemical processes, e.g. with thiols, compared to pDA, but is less efficient in mediating electron transport. Such a difference can be ascribed to the different chemistry of the specific redox moieties of pDA and pCDA, namely the catechol–quinone and the o-aminophenol–o-quinoneimime couples. These related couples operate through free radical intermediates, namely semiquinone and semiquinone-imine (aminophenoxyl radicals), which are believed to be responsible for eumelanin and pheomelanin paramagnetic properties, respectively. It can be speculated that in pDA catechol/quinine couples tend to comproportionate in an irreversible hydration driven manner to give semiquinones that eventually furnish protons and electrons as free charge carriers (Scheme 3.2.1).[3]

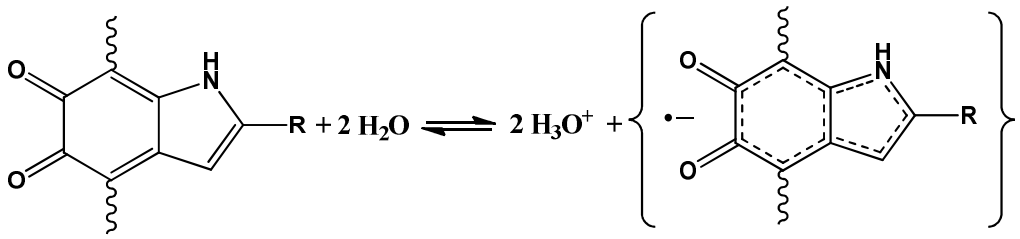

Scheme 3.2.1. *The comproportionation reaction.*

This process would evolve until the π-electron system attains an equilibrium condition in which redox exchange, e.g. with thiols, becomes increasingly difficult. Conversely, in pCDA electronic conduction would be limited by the lack of significant comproportionation processes, despite efficient shuttling between different redox states upon interaction with GSH and oxygen (Scheme 3.2.2).[135,136] In pCDA, ionic conductivity would be mainly due to proton transport and may be mediated by protonated amine groups, including the o-aminophenol groups of dihydrobenzothiazine moieties.

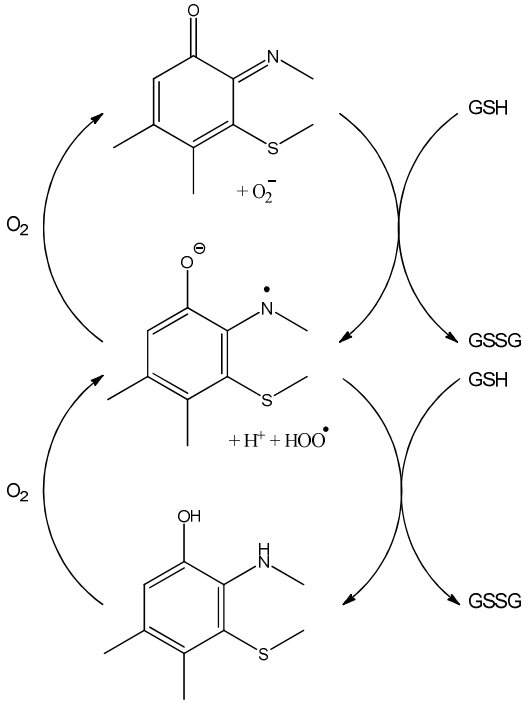

Scheme 3.2.2 *Schematic illustration of redox cycling mechanisms supposedly involved in pCDA prooxidant properties toward GSH.*

Conclusions. The combination of the unique adhesion properties of mussel inspired eumelanin-type pDA with the redox behaviour of benzothiazine systems of red human hair pigments led to the development of pCDA as a novel multifunctional material with remarkable adhesion and pro-oxidant properties. pCDA thin films proved capable of accelerating the kinetics of autoxidation of GSH, a property potentially useful for sensing applications, and is proposed as a novel melanin-based electroactive biomaterial for redox interactions with biomolecules, serving as a potential transducer of electrical, redox and luminous signals. More work is necessary to assess biocompatibility, however, based on the present and previous data, it can be suggested that while PDA may be suitable to implement signal transducing biointerfaces allowing for significant electron transport, pCDA may be exploited to implement photoresponsive bioelectronic components. The development of bio-devices capable of influencing the redox state of cells is also an attractive application of pCDA versus pDA.

3.3 Sulfur-based nitrogen-replacement strategy for eumelanin manipulation.

In the following section, we report a proof-of-concept investigation on the oxidative polymerization of 2-(3,4-dihydroxyphenyl)ethanethiol (DHPET), the thia-analog of dopamine, as well as of 5,6-dihydroxybenzothiophene (DHBT), the thia-analog of 5,6-dihydroxyindole in order to probe heteroatom replacement as a strategy to expand the scope of eumelanin-based functional materials (Figure 3.3.1).

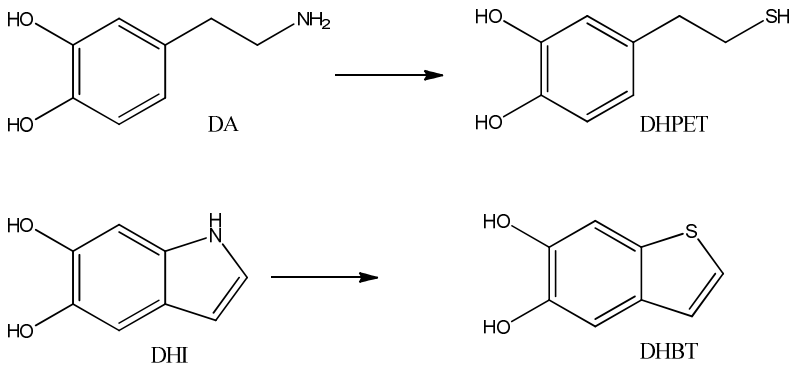

Figure 3.3.1 *Graphic representation of the N to S substitution strategy applied to dopamine (DA) and to 5,6-dihydroxyindole (DHI) leading to their thia-analog respectively, 5,6-dihydroxyphenylethanethiol (DHPET) and 5,6-dihydroxybenzothiophene (DHBT).*

The project was carried out in the frame of a collaboration with the Catalan Institute of Nanoscience and Nanotechnology (ICN2) in Bellaterra (Barcelona, Spain). Main goal of this project were:

a) To assess the nature of the oxidation products of DHPET and their intermediates under different oxidation conditions, with a view to verifying the possible generation of cyclized benzothiophene-like species;
b) To assess the oxidation products of DHBT under different oxidative conditions;
c) To investigate absorption, free radical and morphological properties of deriving polymeric materials compared to pDA, to define their melanin-like character and to assess whether it has antioxidant/free radical scavenger functions in standard assays.

Since this work is currently under completion and partly under consideration for patents, only a summary of main results is reported.

Synthesis of 2-(3,4-dihydroxyphenyl)ethanethiol (DHPET). In preliminary experiments, DHPET was synthesized and its oxidation chemistry was investigated under different conditions. Besides drawing a more defined set of structure-property-function relationships in eumelanin-type materials, specific aims of the experiments were:

a) to verify the feasibility of this approach as an expedient entry to DHBT via nucleophilic attack of the SH group onto the o-quinone groups;
b) to assess whether a pDA like material is formed regardless of DHBT formation, and to investigate its absorption, free radical and adhesion properties.

DHPET was efficiently synthesized as depicted in Scheme 3.3.1. The synthesis consists in three steps of which, only the first requires flash chromatography purification. The overall yield is of 77.5%.

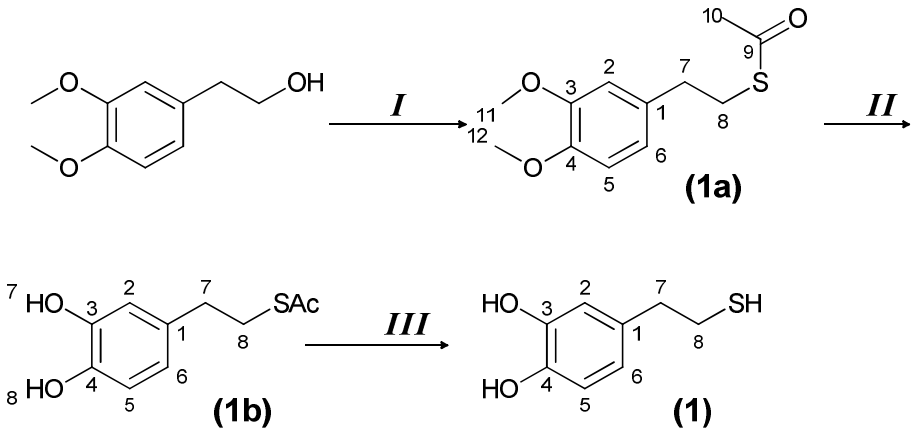

Scheme 3.3.1 *DHPET (**1**) synthetic route.*

Step I, **1a** is obtained as a brown oil after mesylation of 2-(3,4 –dimetoxyphenyl)ethanol and subsequent reaction of the mesylate intermediate with potassium thioacetate. Before step II, purification is needed by water/ethyl acetate extraction and flash silica chromatography.

Step II and III, the following two steps consist in deprotection of the catechol and thiol moieties by BBr_3 and HCl mediated hydrolysis of the metoxy groups and of the thioester, respectively. Interestingly, DHPET could not be achieved inverting the order of the deprotection reaction.

DHPET oxidation chemistry. DHPET autoxidation (1 mM) in 50 mM bicarbonate buffer at pH 8.5 was monitored by UV-visible analysis. After an initial red phase, attributable to the o-quinone, a brown insoluble precipitate was observed with almost complete loss of the catechol absorption. A similar behaviour was observed with $K_3[Fe(CN)_6]$. Attempts to reduce or acetylate the brown solid were however unsuccessful.

The oxidation of DHPET was then investigated at lower pH using $NaIO_4$ (2 eq) in phosphate buffer (pH 6.8) or $(NH_4)_2[Ce(NO_3)_6]$ (2 eq) in phosphate buffer pH 3 as the oxidants. In both cases, TLC of the extractable organic fraction ($CHCl_3$:AcOEt 8:2) showed a significant amount of unreacted thiol after 2 h.

Complete substrate conversion was observed using Horseradish Peroxidase (HRP)/H_2O_2 as the oxidizing system. TLC of the extractable organic fraction ($CHCl_3$:AcOEt 8:2) showed a distinct UV visible spot with no unreacted thiol left. Acetylation of the organic extract followed by purification of the resulting mixture on PLC led to the isolation of two main fractions which were analyzed by ^1H and ^{13}C NMR and ESI-Ion Trap mass spectrometry. For comparison, the mass spectrum of the monomer was also recorded.

The ESI mass spectrum of DHPET showed no pseudomolecular peak but a small peak at m/z = 169 $[(M-2)+H]^+$ suggesting loss of H_2, a common phenomenon with catechol compounds. MS-analysis of Fraction 1 showed a base peak at m/z 545 $[M + Na]^+$ (Figure 3.3.2A, left), compatible with a thiosulfinate derivative (**2**) (Figure 3.3.2B, left). Consistent with this conclusion was the ^1H-NMR spectrum revealing the effect of the sulfur stereogenic center on the adjacent CH_2 spin system. The hypothesized structure was confirmed by ^{13}C NMR analysis. MS-analysis of Fraction 2 showed a base peak at m/z 529 $[M + Na]^+$ (Figure 3.3.2A, right), compatible with a disulfide derivative (**3**) (Figure 3.3.2B, right). This conclusion was supported by the ^1H and ^{13}C NMR spectra that showed a highly symmetric distribution of NMR signals.

A)

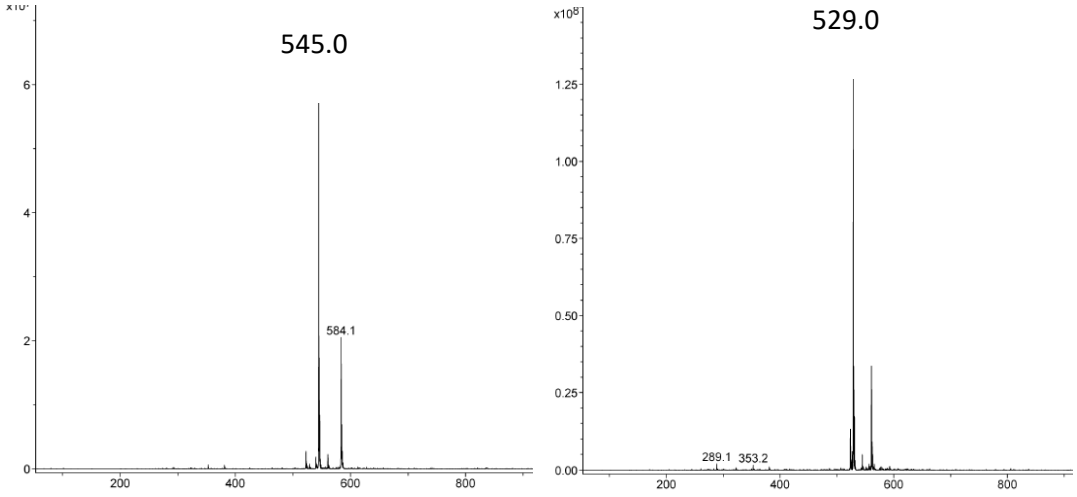

B)

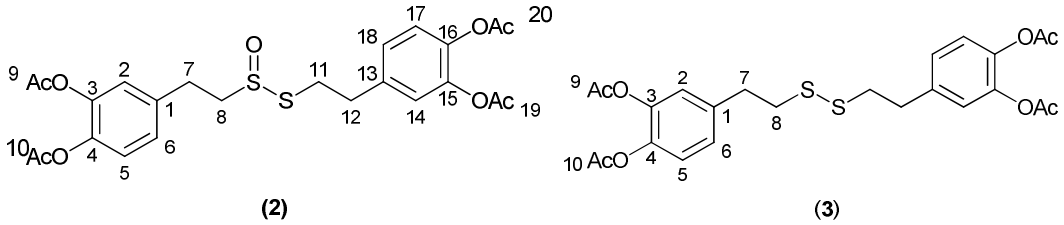

Figure 3.3.2 *A) MS-analysis of Fraction 1, left and Fraction 2, right. B) Hypothesized structures of main oxidation products from DHPET.*

Synthesis of 5,6-dihydroxy-2,3-diidrobezothiophene (H_2-DHBT). Based on these experiments, which ruled out DHPET oxidation as a viable route to the thia-analog of pDA, the synthesis of the target thiomelanin was next pursued by by-passing the cyclization stage through use of H_2-DHBT, the putative cyclization product of DHPET quinone. Synthesis of H_2-DHBT was achieved slightly modifing literature reported synthetic protocols.[144,145] The complete synthetic route is summarized in Scheme 3.3.2, it consist of six synthetic steps and three flash chromatography purifications leading to the desired product with an average overall yield of 40%. All intermediates were characterized by ^{1}H and ^{13}C NMR.

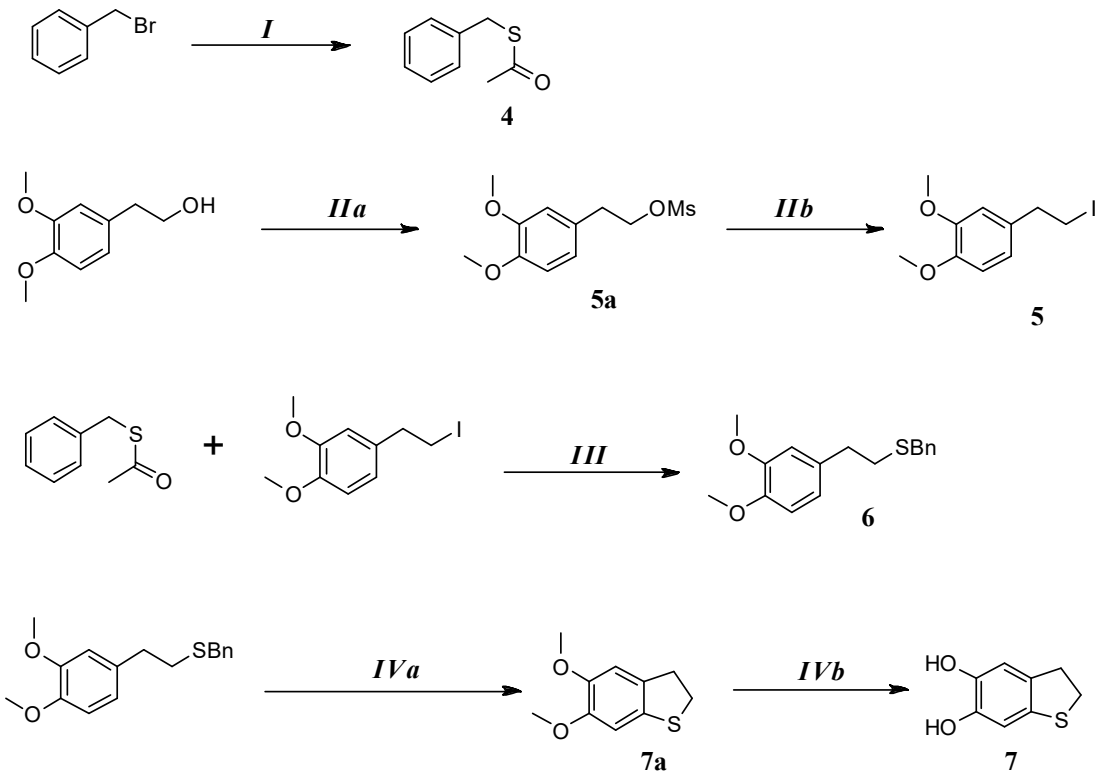

Scheme 3.3.2 *Synthetic scheme for H_2-DHBT.*

Step I. **4** is obtained from benzyl bromide by the nucleophilic substitution of the bromide group due to potassium thioacetate. **4** is recovered as a pale yellow oil by extraction (water/ethyl acetate) of the dried reaction mixture. *Steps IIa and IIb.* Intermediate **5** is obtained through two steps from 3,4-dimetoxyphenyl-1-ethanol. The primary alchol group is previously derivatized to mesylate (*IIa,* **5a**), then substituted to iodine using sodium iodide. Step *IIb* is followed by flash chromatography purification leading to **5** as a yellow oil. *Step III.* Intermediates **4** and **5** are then reacted in a 0.5 M NaOH/CH_3OH 1:2 mixture for 24 h to obtain **6** as a crystalline solid after water/CH_2Cl_2 extraction followed by flash chromatography purification (hexane : ethyl acetate 9:1). *Steps IVa and IVb.* Cyclization of the thio-ether **6**, is achieved by reaction with the ipervalent iodine reagent bis(trifluoroacetoxy)iodo benzene (BTIB) and BF_3-EtO_2. Hypervalent iodine reagents are reported as low toxic, ready available and easy handling chemicals to obtain sulfur-containing heterocycles from phenol ethers bearing an alkyl sulfide side chain. The hypotesized reaction mechanism is depicted in Scheme 3.3.3. The electron-rich aromatic ring is initially oxidized by the activated hypervalent iodine reagent via single electron transfer, then the sulfide side chain attacks the radical cation to exclusively form the isolable and stable sulfonium salt. The benzyl group was easily cleaved by treatment with $MeNH_2$ to give the corresponding sulfur-containing heterocycle (**7a**).[144]

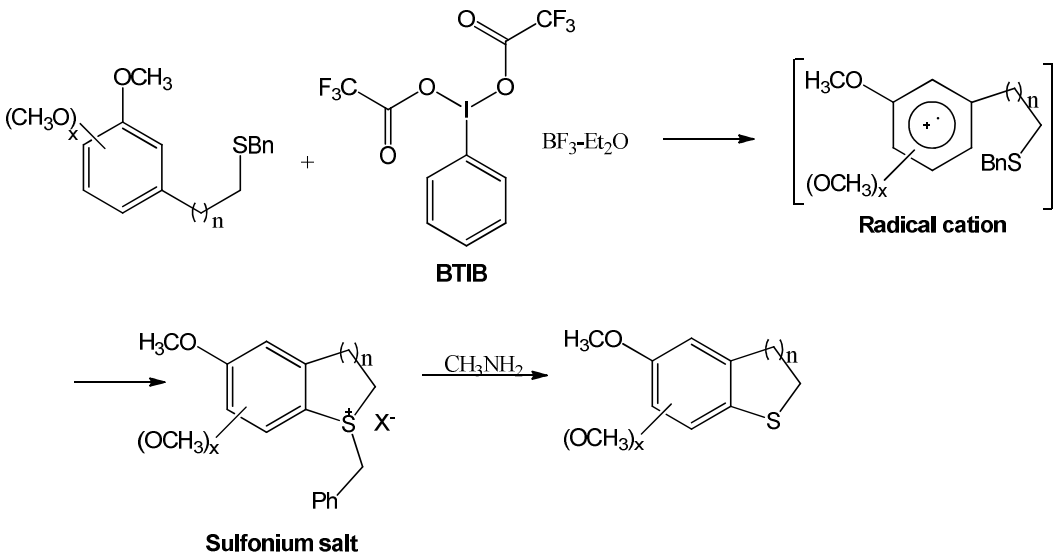

Scheme 3.3.3 *Proposed mechanism for the reaction between BTIB and phenol ethers bearing an alkyl sulfide sidechain to give sulphur-containing heterocycles.*[146]

The final product **7** (H_2-DHBT) is thus obtained by BBr_3 mediated deprotection of metoxyl groups. H_2-DHBT is recovered by extraction of the reaction mixture, no further purification is needed (yield: 90 %).

H_2-DHBT oxidation chemistry. Spectrophotometric analysis of the oxidation of H_2-DHBT was carried out on a UV-vis spectrophotometer mounting a diod array detector (DAD). In a first set of experiments, H_2-DHBT oxidation was promoted by $K_3[Fe(CN)_6]$ (2 m. eq.) in 50 mM phosphate buffer pH 7.4, spectra were recorded every 30 seconds. Figure 3.3.3 shows the fast generation of a deep red coloration (λ_{max} 480 nm), most likely due to the quinone, which slowly discharged within 1 minute (absorption maxima of $K_3[Fe(CN)_6]$ are also detectable at 220 and 350 nm).

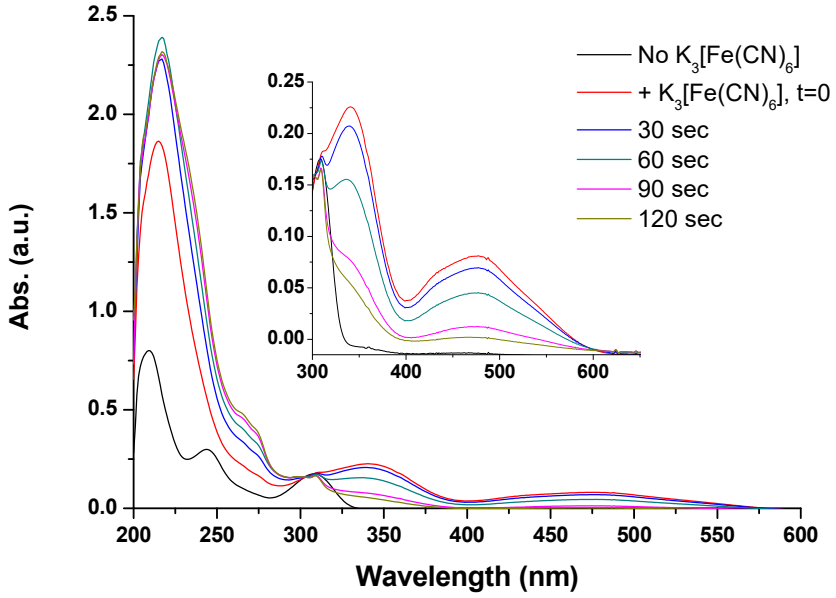

Figure 3.3.3 *Spectrophotometric analysis of 0.05 mM H_2-DHBT oxidation in 50 mM phosphate buffer pH 7.4, $K_3[Fe(CN)_6]$ (2 m. eq.).*

To avoid overlapping of the $K_3[Fe(CN)_6]$ UV-vis profile, in a second sets of experiments, the analysis was repeated in the absence of any oxidizing agent besides oxygen, at alkaline pH (autoxidative conditions). Figure 3.3.4 shows UV-vis spectra recorded every 30 seconds during the early stages of H_2-DHBT autoxidation in phosphate buffer at pH 8.8. It can be noticed the instantaneous raising of a maximum of absorption at 480 nm, slowly decreasing in absorption intensity over the following 2 minutes. Interestingly, analysis of the UV region of the spectrum reveals simultaneous increasing of an absorption maximum at 230 nm probably due to the formation of a different chromophoric specie.

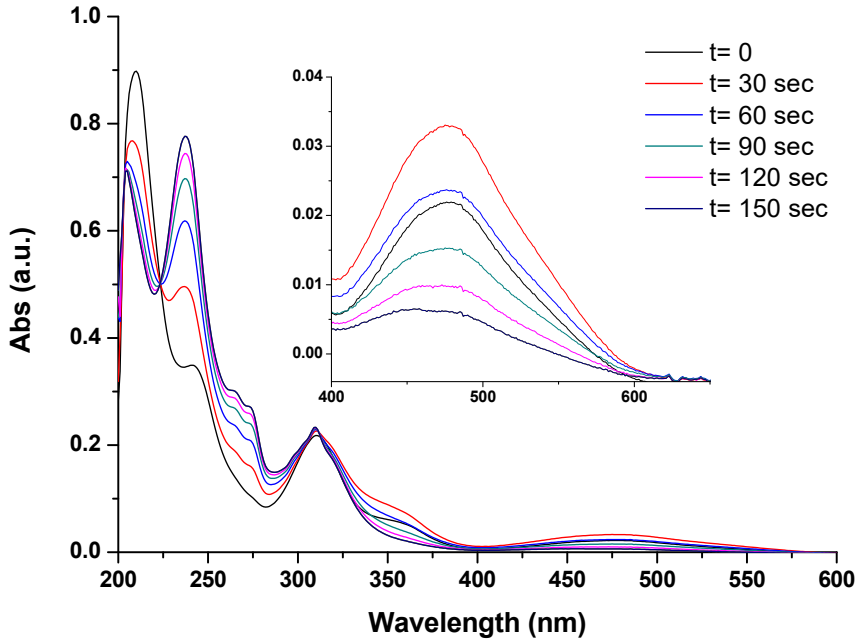

Figure 3.3.4 *Spectrophotometric analysis of 0.05 mM H_2-DHBT autoxidation in 50 mM phosphate buffer pH 8.8.*

To identify the oxidation products, H_2-DHBT was allowed to oxidize in air, in 50 mM phosphate buffer pH 7.4 under stirring for 24 h. Ethyl acetate extraction of the reaction mixture led to a light grey powder in 75% yield that upon ^{1}H, ^{13}C NMR and GC-MS analysis proved to be the aromatic heterocycle 5,6-dihydroxy[b]benzothiophene (DHBT). No traces of sulfur oxidized species or other oxidation products were detected (GC-MS and elemental analysis evidences, data not shown). Oxidation with potassium ferricyanide in 50 mM phosphate buffer pH 9.0 under argon atmosphere for 30 min allowed to isolate DHBT in higher yields (90 %).

The mechanism of the reaction involves oxidation of the catechol to the o-quinone followed by sequential isomerization steps based on proton shifts akin to the generation and isomerization of dopaminochrome to DHI.

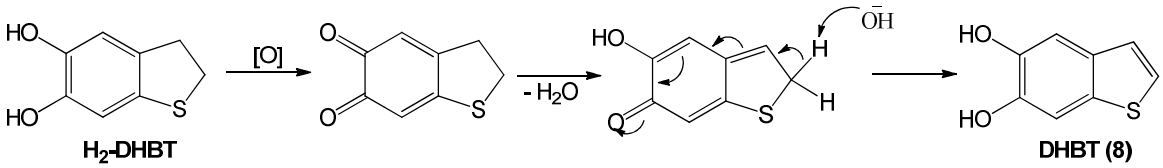

Scheme 3.3.4 *H_2-DHBT proposed oxidation and isomerization steps to DHBT.*

The oxidative chemistry of H_2-DHBT was then investigated in order to define whether the chemical oxidant or pH conditions could influence the nature of products. All reactions have been performed dissolving H_2-DHBT in CH_3OH and aqueous buffer in a closed vial, under Ar atmosphere. Three different oxidants have been tested:

- Horse radish peroxidise (HRP)/H_2O_2 (50 U mL^{-1}, 1eq, 50 mM phosphate buffer pH 7.7);
- $K_3[Fe(CN)_6]$ (1.7eq, 50 mM phosphate buffer pH 8.8);
- $(NH_4)Ce(NO_3)_6$ (1 eq, 50 mM phosphate buffer pH 3.5).

Reactions were monitored by HPLC. 0.1% formic acid –acetonitrile in 8:2 ratio was selected as eluant. H_2-DHBT retention time in the elutographic condition was about 6.5 min. In any oxidative condition, the major product was represented by a peak with R_t: 9.8 min assigned to the aromatic derivative DHBT by comparison with a standard solution of the isolated product. Further addition of any of the above mentioned oxidants, led to precipitation of solid material that upon extraction with ethyl acetate, proved to consist mainly of DHBT accompanied by other oxidation products with longer retention times. Oxidation of H_2-DHBT with the total amount of chemical oxidant led to the formation of the same species as inferred by HPLC analysis.

Accordingly, in order to assess the nature of the oxidation products, subsequent analysis were conducted on DHBT as starting material using controlled amount of oxidant. Reactions were monitored by HPLC (same eluting conditions as above). At reaction completion, (disappearing of the 9.7 min, DHBT peak) reaction mixtures were extracted with ethyl acetate and the dried organic layers acetylated using acetic anhydride and pyridine at room temperature overnight. Acetylated mixtures were analyzed by LC-MS. As inferred from HPLC-MS comparison of acetylated organic layers, the oxidant does not have any influence on products from DHBT (Figure 3.3.5, top). Although its oxidation is never complete probably due to solubility issues (precipitation of products and starting material), the formation of three different dimeric species (m/z: 521) was observed. As an example, Figure 3.3.5 (bottom) reports the mass spectrum of the product eluting at 31 min after DHBT oxidation with potassium ferricyanide.

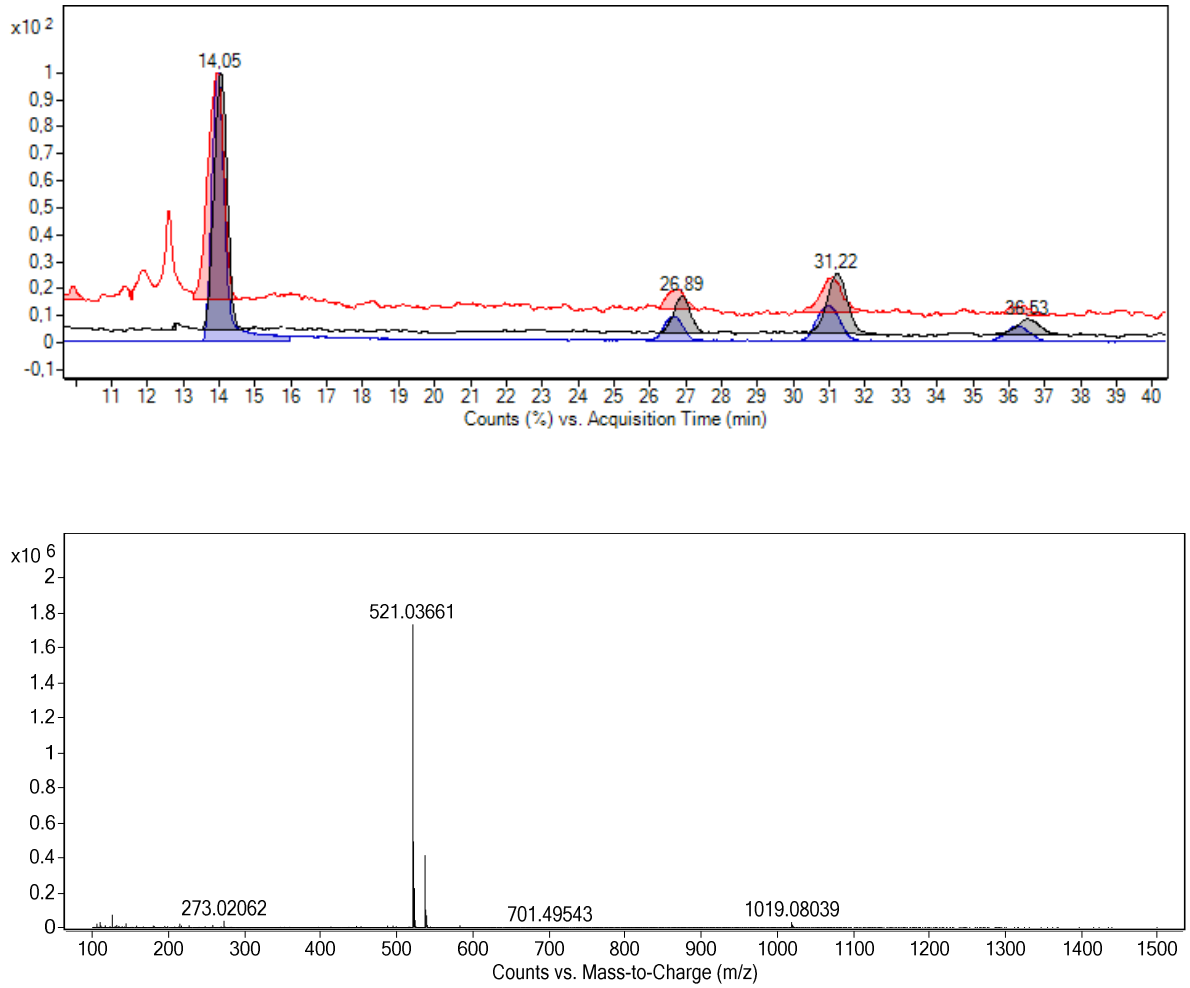

Figure 3.3.5 *Top) TIC traces of the acetylated ethyl acetate extracts from DHBT oxidation with (HRP)/H_2O_2 (50 U mL^{-1}, 1 eq, red), $K_3[Fe(CN)_6]$ (1 eq, black) or $(NH_4)Ce(NO_3)_6$ (1 eq, blue). Bottom) Representative MS spectrum of the acetylated dimeric species.*

In order to isolate the dimers, ferricyanide mediated oxidation was selected as the most convenient condition. The acetylated organic layer was then subjected to carefull purification by silica-gel chromatography (hexane : ethyl acetate 7:3). Although low yields, this purification step allowed to recover three fractions containing respectively: dimers, trimers and tetramers from DHBT. MALDI-TOF analysis of recovered fractions showed good separation of the oligomers in terms of size distribution however, ^{1}H NMR spectra confirmed the presence in each fraction of many isomeric species with the same m/z ratio (see experimental section).

Spectral, morphological and chemical properties of polyDHBT (thiomelanin, pDHBT). Under more forcing conditions, (e.g. 3 eq$K_3[Fe(CN)_6]$) oxidation of DHBT gave a highly insoluble greyish solid via dimeric and oligomeric intermediates that was collected by centrifugation and subjected to spectral and morphological analysis.

LDI-MS analysis of the mixture revealed the presence of oligomeric species ranging from the dimer (m/z $[M+Na]^+$= 353) up to the decamer ($[M+Na]^+$= 1664). A $[M+K]^+$ serie is also detectable (Figure 3.3.6). Spectral analysis revealed a substantial integrity of oligomer scaffolds without extensive degradative breakdown, as usually observed in the case of DHI polymers/melanins. Notably, inspection of m/z values indicated a prevalence of reduced catechol forms of the oligomers.

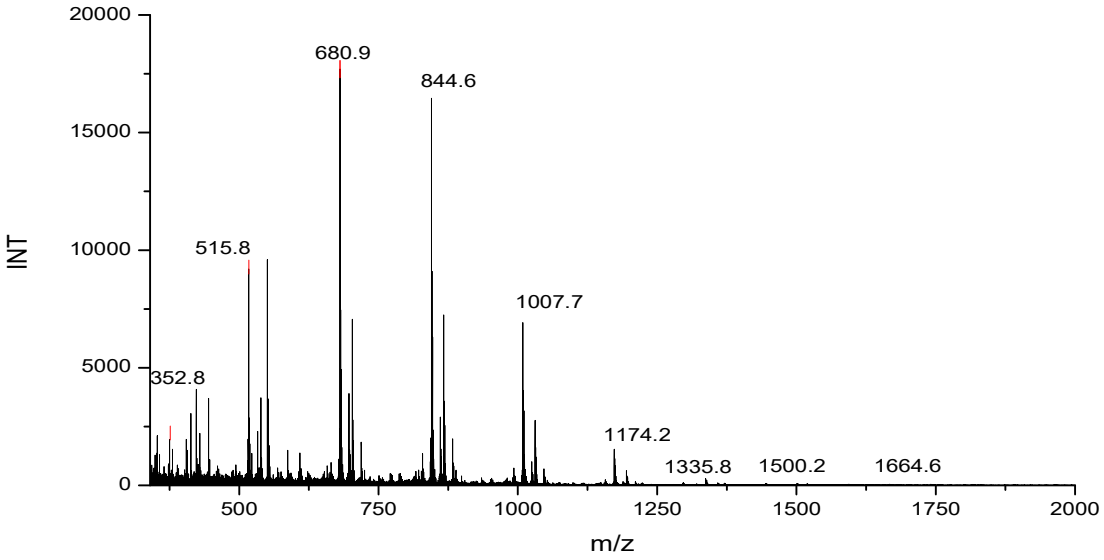

Figure 3.3.6 *MALDI-MS spectrum of pDHBT*

Consistent with this conclusion from MS data, the UV-visible absorption profile of thiomelanin in suspension indicated relatively poor visible extinction properties, on account of a low proportion of oxidized quinone-type species (Figure 3.3.7).

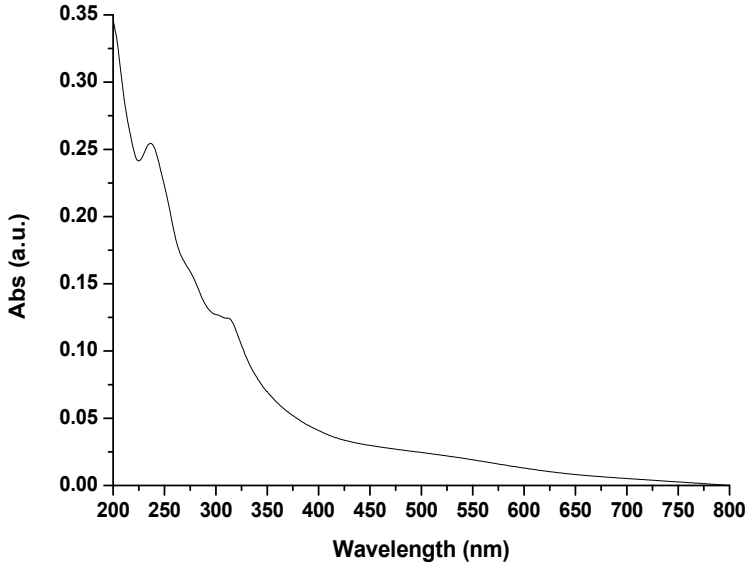

Figure 3.3.7 *UV-Vis spectra of a 0.25 mg/mL pDHBT suspension in 0.05 M carbonate buffer pH 9.*

ATR/FT-IR analysis of the polymeric material also revealed the presence of a broand band centered at 3600 cm $^{-1}$ mainly ascribable to phenolyc oxydril groups. Interestingly, it is not very dissimilar from the monomer spectrum (not reported) suggesting at least, a retention of its structural features.

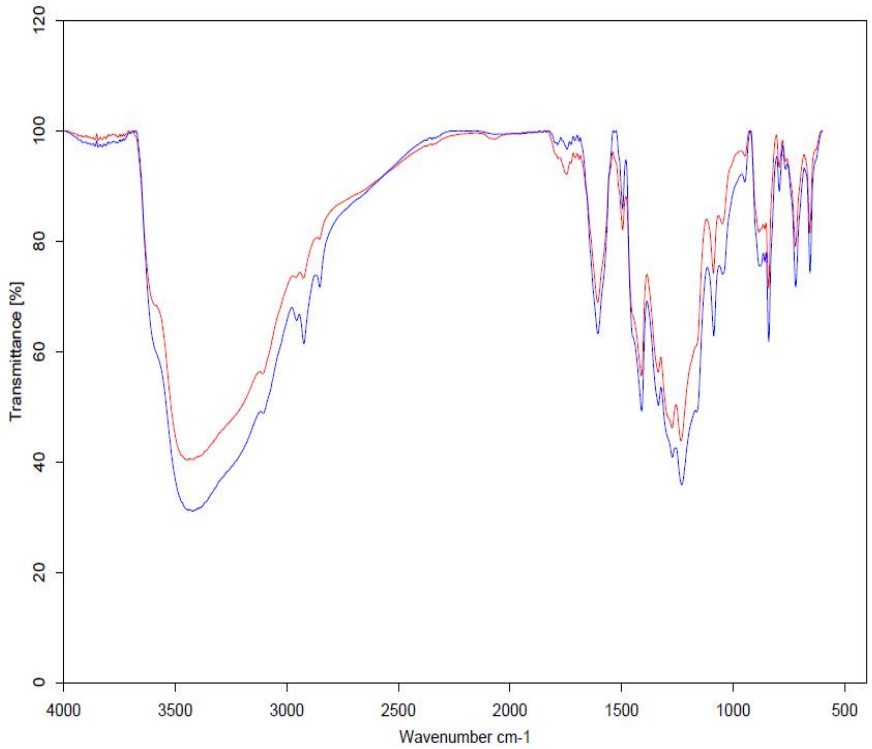

Figure 3.3.8 *ATR/FT-IR spectrum of DHBT (red trace) and pDHBT (blue trace).*

Figure 3.3.9 shows the EPR spectrum of a thiomelanin sample from ferricyanide oxidation of DHBT. Data showed a relatively intense signal much narrower than that of polydopamine and DHI melanin, indicating a lower degree of structural disorder and heterogeneity. This conclusion was confirmed by the power saturation curve, which was different from that of eumelanin samples, in line with a higher degree of structural and electronic homogeneity.

	g (±0.0003)	**ΔB [G] (±0.05 G)**	**Spin density [spin/g]**
pDHBT	2.0032	4.37	3.8×10^{17}
pDA	2.0035	4.8	
DHI melanin	2.0035	5.6	

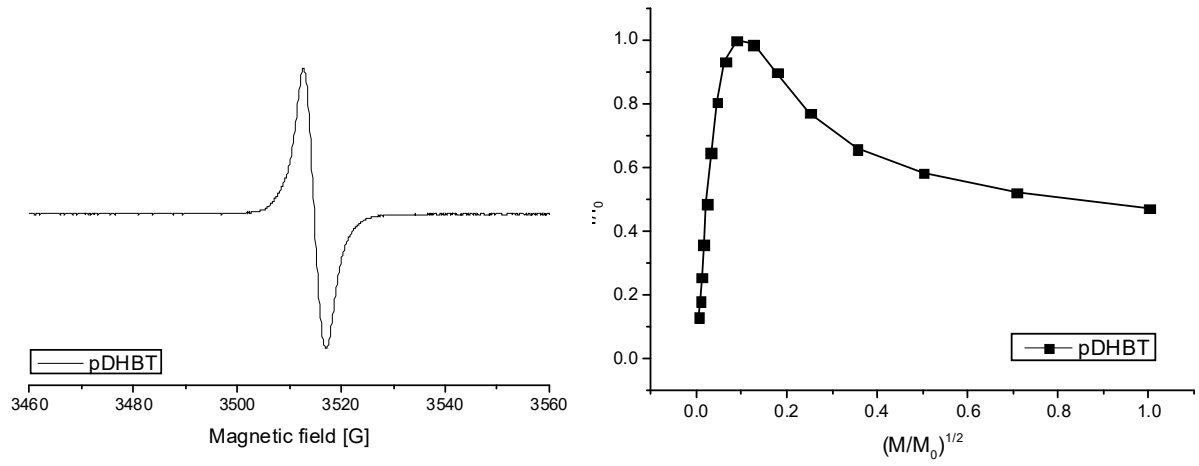

Figure 3.3.9 *EPR signal (left) and power saturation profile (right) of pDHBT.*

Conclusions. A proof-of concept study aimed at clarify structure-properties reletionships in eumelanin-like polymers was reported. Two new sulphur-substituted dopamine and 5,6-dihydroxyindole derivatives were synthesized, their oxidative chemistry was investigated and Spectrophotometric, morphological and electronical properties of DHBT-deriving polymer were preliminarly assessed. Compared to pDA or DHI melanin, thiomelanin showed less intense absorption in the visible region, less pronounced EPR properties and proved to consist of mixtures of oligomers up to the 10-mer (LDI-MS evidence). N-to-S heteroatom replacement is thus proposed as an efficient strategy for modifying and tailoring physical and chemical properties in eumelanin-type functional materials.

3.4 Experimental methods and supporting information

All reagents were obtained from commercial sources and used without further purification. Organic solvents were used as purchased. Water was of MilliQ® quality. Buffers were prepared by standard procedures. A Crison pH-meter equipped with a 5014 Crison electrode was used for pH measurements at room temperature.

UV-Vis absorption spectra were registered at room temperature on a V-560 JASCO spectrophotometer using calibrated 2 mL cuvettes and, for solid state samples, on a Cary 4000 UV-Vis spectrophotometer using the solid sample holder. ^{1}H-NMR and ^{13}C-NMR spectra were recorded in deuterated solvents at 400 MHz on a Bruker DRX 400 or Bruker Avance DRX 400 and at 500 MHz on a Varian Inova 500, δ values are reported in ppm and coupling constants are given in Hz. HPLC analyses for reaction monitoring were performed on an Agilent 1100 series instrument equipped with an LC-10AD VP pump and a G1314A UV-Vis detector using a Sphereclone C18 column (4.6 x 150 mm, 5 μm). LC-MS analysis was conducted on an ESI-TOF 1260/6230DA Agilent Technologies in positive ion mode. IR spectra were recorded on Nicolet 5700 FT-IR + Smart performer spectrometer mounting a Continuum FT-IR Microscope and on Bruker Optics TENSOR 27 FT-IR.

CDA was synthesized following a previously reported procedure.[147]

X-ray photoelectron spectroscopy (XPS). All the analysis were performed on a Thermo Scientific K-Alpha XPS system (Thermo Fisher Scientific, UK). Spectra were collected using a monochromatized Al-K α radiation (1486.6 eV). The surface emitted photoelectrons were analysed in a double-focusing hemispherical analyser and recorded on a multi-channel detector. All the spectra were acquired in the constant analyser energy mode. The ThermoScientific Avantage software (Thermo Fisher Scientific) was used for digital acquisition and data processing.

Water contact angle assessment (WCA). Static contact angle analyses were performed with 1 μL droplets for water, and carried out on a TBU90E Dataphysics contact angle goniometer.

Atomic Force Microscopy (AFM). Measurements were carried out on air at 298 K by using a Nanoscope V (model MMAFMLN, Digital Instrument Metrology Group). The tips used in all measurements were antimony-doped silicon cantilevers (T = 3.5–4.5 μm, L = 115–135 μm, f_o = 271–305 kHz, k = 20–80 N m^{-1}, Bruker) at a resonant frequency of ca. 280 kHz. The collected images were then analysed with WsxM 5.0 software (Nanotec Electronica S. L.) to acquire the cross-sectional values and profiles of the processed images.

Coating experiments. Glass coverslips, quartz slides or the other materials (cuttings of polyethyleneterephthalate (PET), coins) were dipped in a solution of either dopamine hydrochloride, or 5-S-cysteinyldopamine at 10 mM concentration in 0.05 M bicarbonate buffer, pH 8.5 and kept under stirring in air. At the proper times the coated materials were rinsed with deionized water and air dried.

GSH and NADH oxidation. A 150 μM solution of GSH or a 300 μM solution of NADH in 0.1 M phosphate buffer (pH 7.4) was allowed to stand at room temperature under vigorous stirring in the presence and in the absence of pCDA (1 mg) or pCDA thin film. Aliquots of the reaction mixtures were periodically withdrawn and analyzed by HPLC with UV and electrochemical detector.

EPR measurements were performed using an X-band (9 GHz) Bruker Elexys E-500 spectrometer(Bruker, Rheinstetten, Germany), equipped with a super-high sensitivity probe head. Samples were transferred to flame-sealed glass capillaries which, in turn, were coaxially inserted in a standard 4 mm quartz sample tube. Measurements were performed at room temperature. The instrumental settings were as follows: sweep width, 100 G; resolution, 1024 points; modulation frequency, 100.00 kHz; modulation amplitude, 2.0 G. The amplitude of the field modulation was preventively checked to be low enough to avoid detectable signal overmodulation. Preliminarily, EPR spectra were measured with a microwave power of ~0.5 mW to avoid microwave saturation of resonance absorption curve. Several scans, typically 16, were accumulated to improve the signal-to-noise ratio. Successively, for power saturation experiments, the microwave power was gradually incremented from 0.02 to 160 mW. The g value and the spin density were evaluated by means of an internal standard, Mn^{2+}-doped MgO, prepared by a synthesis protocol reported in literature.[124]

MALDI analysis was run on a AB Sciex TOF/TOF 5800 instrument using 2,5-dihydroxybenzoic acid as the matrix and the melanin applied to the plate from a fine suspension in ethanol obtained by homogenization in a glass to glass potter. Spectrum represents the sum of 15,000 laser pulses from randomly chosen spots per sample position. Raw data are analyzed using the computer software provided by the manufacturers and are reported as monoisotopic masses.

Synthesis and structural characterization of 3,4-dihydroxyphenyl ethanethiol (DHPET, 1). *Step I, Synthesis of S-3,4-dimethoxyphenethyl ethanethioate (***1a***).* To a solution of 2-(3,4 – dimetoxyphenyl)ethanol (1.5 g, 8.24 mmol) in dry tetrahydrofuran (THF, 42 mL) methanesulfonyl chloride (MsCl, 1.55 mL, 21.3 mmol) and triethylamine (Et_3N, 2.51 mL) were added dropwise under N_2 atmosphere. The reaction mixture was stirred at r.t. for 2 h. Potassium thioacetate (3 g)

was dissolved in dry DMF (36 mL). The latter solution was slowly added to the reaction mixture. After 4 h, the solvent was evaporated under reduced pressure and extracted (water/ethyl acetate), the combined organic layers were dried over anhydrous Na_2SO_4, evaporated and purified by flash silica chromatography (hexane:ethyl acetate 9:1). The desired product (**1a**) was obtained as a brown oil (2.6 mg, 87 % yield).

(**1a**): ^{1}H NMR (400 MHz, $CDCl_3$) δ 6.80 (d, *J* = 8.1 Hz, H-6), 6.77 (s, H-2), 6.73 (d, *J* = 8.0 Hz, H-5), 3.88 and 3.86 (s, H-11, H-12), 3.10 (t, *J* = 7.7 Hz, H-8), 2.81 (t, *J* = 7.7 Hz, H-7), 2.33 (s, H-10). ^{13}C NMR (91 MHz, $CDCl_3$) δ 193.2 (C-9), 149.0 (C-3), 148.0 (C-4), 133.0 (C-1), 122.0 (C-6), 115.2 (C-5), 112.1 (C-2), 56.1 and 55.8 (C-11, C-12) 36.1 (C-8), 33.2 (C-7), 30.3 (C-10).

*Step II, Synthesis of S-3,4-dihydroxyphenethyl ethanethioate (***1b***).* To a solution of **1a** (1.53 g, 5.88 mmol) in CH_2Cl_2 (24 mL) a 1 M solution of BBr_3 in CH_2Cl_2 (32 mL) was slowly added under N_2 atmosphere at -5 °C. After 6 h, the reaction mixture was extracted with water. The combined organic layers were dried over anhydrous Na_2SO_4 and evaporated to give **1b** (1.0 g, yield >> 99%). No further purification was needed.

(**1b**): ^{1}H NMR (400 MHz, $CDCl_3$) δ 6.82 (d, *J* = 8.0 Hz, H-6), 6.73 (s, H-2) 6.65 (d, *J* = 8.0 Hz, H-5), 2.82 (d, *J* = 6.6 Hz, H-7), 2.79 (d, *J* = 6.6 Hz, H-8), 2.07 (s, H-10).
^{13}C NMR (91 MHz, $CDCl_3$) δ 193.2 (C-9), 145.0 (C-3), 144.0 (C-4), 133.0 (C-1), 122.0 (C-6), 116.2 (C-5), 115.4 (C-2), 36.1 (C-8), 33.6 (C-7), 30.5 (C-10).

*Step III, Synthesis of S-3,4-dihydroxyphenyl ethanethiol (***DHPET, 1***).* To a solution of **1b** (1.0 g, 5.85 mmol) in CH_3OH (90 mL) 12 M HCl was added (50 drops). The mixture was left to react under stirring overnight under reflux. After 12 h, the solvent was evaporated under reduced pressure and the reaction extracted by water/ethyl acetate. DHPET was recovered without further purification as a brown oil (900 mg, yield = 90%).

(**1**): ^{1}H NMR (360 MHz, $CDCl_3$) δ 6.80 (d, *J* = 8.0 Hz, H-6), 6.77 (s, H-2), 6.73 (d, *J* = 8.0 Hz, H-5), 2.98 (t, *J* = 6.8 Hz, H-7), 2.85 (t, *J* = 6.8 Hz, H-8). ^{13}C NMR (91 MHz, $CDCl_3$) δ 149.0 (C-3), 148.1 (C-4), 131.0 (C-1), 121.0 (C-6), 120.9 (C-2), 112.2 (C-5), 38.7 (C-7), 35.2 (C-8).

Synthesis and structural characterization of 5,6-dihydrobenzo[b]thiophene (DHBT, 8).

*Step I, Synthesis of S-benzyl ethanethioate (***4***).* To a solution of benzyl bromide (1.26 g, 7.4mmol) in Acetone (20 mL) potassium thioacetate (0.9 g, 7.88 mmol) was added . The reaction mixture was

heated at reflux for 2h, evaporated and extracted with ethyl acetate, the combined organic layers were dried over anhydrous Na_2SO_4 and evaporated, affording **4** as a colourless oil (1.20 g, 99%).

(**4**): ^{1}H NMR (360 MHz, CD_3Cl) δ 7.29 (m, protoni aromatici), 4.12 (s, H-5), 2.35 (s, H-7). ^{13}C NMR (91 MHz, $CDCl_3$) δ 137.57 (C-1), 128.80 (C-3,3'), 128.63 (C-2,2'), 127.27 (C-4), 33.46 (C-7), 30.34 (C-5).

*Step IIa and IIb, Synthesis of 2-iodoethyl-3,4-dimethoxybenzene (***5***).* To a solution of 2-(3,4 – dimetoxyphenyl)ethanol (1.5 g, 8.24 mmol) in CH_2Cl_2 (20 mL) at 0 °C pyridine (0.73 mL, 9.06 mmol) and methanesulfonyl chloride (0.66 mL, 9.06 mmol) were added. The reaction mixture was stirred at rt for 12 h, poured into 5% aqueous HCl (12 mL), and extracted with CH_2Cl_2, the combined organic layer was dried over anhydrous Na_2SO_4, evaporated and used without further purification for the next step of the synthesis (yield: 85%).

(**5a**):

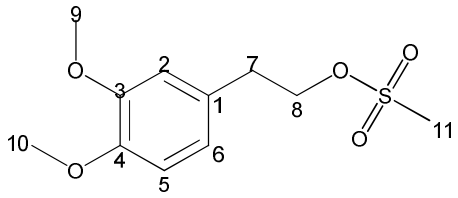

^{1}H NMR (360 MHz, $CDCl_3$) δ 6.80 (d, J = 8.0 Hz, H-6), 6.77 (s, H-2), 6.73 (s, H-5), 4.37 (t, J = 6.9 Hz, H-8), 3.86 (s, H-10), 3.84 (s,H-9), 2.98 (t, J = 6.8 Hz, H-7), 2.85 (s, H-11).^{13}C NMR (91 MHz, $CDCl_3$) δ 149.0 (C-3), 148.0 (C-4), 131.0 (C-1), 121.0 (C-6), 112.2 (C-5), 112.1 (C-2), 70.52 (C-8), 55.9 (C-10), 55.8 (C-9), 37.3 (C-11), 35.2 (C-7).

Subsequently, to a solution of 5a (2.0 g, 7.83mmol) in acetone NaI (1.76 g, 11.7mmol) was added. The mixture was heated at reflux overnight, cooled, and evaporated. The oily mixture was then added to water and extracted with CH_2Cl_2, the combined organic layers were dried over anhydrous Na_2SO_4 and evaporated. Flash chromatography of the crude mixture, with Hexane: Ethyl Acetate 9:1 as eluting system, afforded 1.39 g (61%) of **5** as a pale yellow oil.

(**5**):

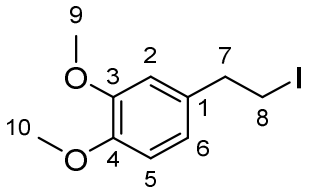

^{1}H NMR (360 MHz, $CDCl_3$) δ 6.8 (d, J = 8.1 Hz, H-6), 6.75 (s, H-2) 6.6 (d, J = 8.1 Hz, H-5), 3.9 (s, H-10), 3.8 (s, H-9), 3.3 (t, J = 7.8 Hz, H-8), 3.1 (t, J = 7.8 Hz, H-7). ^{13}C NMR (91 MHz, $CDCl_3$) δ 148.9 (C-3), 147.9 (C-4), 133.3 (C-1), 120.4 (C-6), 111.6 (C-2), 111.3 (C-5), 55.9 (C-9,10), 40.0 (C-8), 6.2 (C-7).

*Step III, Synthesis of benzyl(3,4-dimethoxyphenethyl)sulfane (***6***).*To a solution of **5** (1.2 g, 4.1 mmol) in MeOH (20 mL) at 0 °C 0.5 M NaOH in MeOH (10 mL) was slowly added and then a solution of **4** (0.68 g, 4.1mmol) in MeOH (10 mL). The reaction mixture was stirred at room temperature for 24 h, poured into water, and extracted with CH_2Cl_2, and the combined organic layers were dried over anhydrous Na_2SO_4 and evaporated. Flash chromatography of the crude mixture with Hexane: Ethyl Acetate 9:1 as eluting system, afforded 0.98 g (85%) of **6** as a colorless oil.

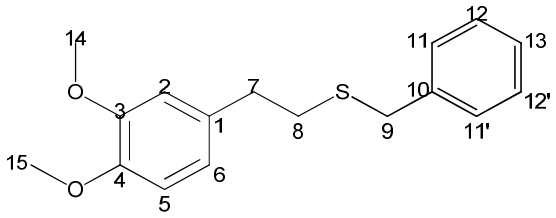

*Step IVa and IV, Synthesis of 1,2-dihydro-5,6-dihyroxybenzothiophene (***7***).* A DCM (66 mL) mixture of PIFA and BF_3-Et_2O is added dropwise to a solution of **6** (0.95 g, 3.3 momol) in DCM (95 mL) at -78 °C under N_2. The reaction is stirred for 20 minutes, then quenched with $MeNH_2$ (40%), stirred for 30 minutes and acidified with HCl 10% until pH 6.5. The mixture was extracted with CH_2Cl_2 and purified by flash chromatography using Hexane : Ethyl acetate 9:1 as eluting system affording to 0.4 g (63%) of 5,6-dimethoxy-2,3-dihydrobenzo[b]thiophene as a white solid.

(**7a**):

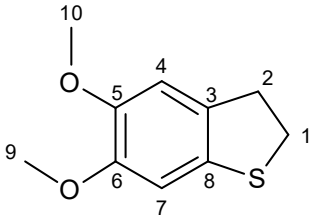

^{1}H NMR (360 MHz, $CDCl_3$) δ 6.8 (s, H-7), 6.7 (s, H-4), 3.84 (s, H-9), 3.83 (s, H-10), 3.4 (t, J = 7.7 Hz, H-2), 3.2 (t, J = 7.7 Hz, H-1). ^{13}C NMR (91 MHz, $CDCl_3$) δ 148.84 (C-6), 146.64 (C-5), 132.29 (C-3), 131.57 (C-8), 108.73 (C-4), 105.86 (C-7), 56.39 (H-11), 56.23 (H-10), 36.50 (C-1), 34.28 (C-2).

In the next reaction, BBr_3 (5 mL) was added dropwise to a solution of **7a** (0.17 g, 0.89 mmol) in DCM (4 mL), at 0 °C and under N_2 atmosphere. After 90 minutes, the reaction mixture was evaporated and extracted with H_2O/Diethyl Ether affording to 0.13 mg (90%) of **7** as a white solid.

(**7**):

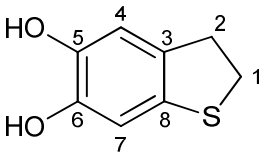

^{1}H NMR (360 MHz, CD_3OD) δ 6.66 (s, H-4), 6.58 (s, H-7), 3.27 (t, J = 7.7 Hz, H-1), 3.08 (t, J = 7.6 Hz, H-2). ^{13}C NMR (91 MHz, CD_3OD) δ 144.4 (C-5), 142.1 (C-6), 130.8 (C-3), 130.7 (C-8), 111.7 (C-4), 108.7 (C-7), 35.7 (C-1), 33.3 (C-2).

(**8**):

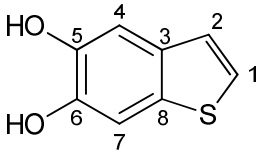

^{1}H NMR (360 MHz, CD_3OD) δ 7.23 (d, J = 5.4 Hz, H-1), 7.20 (s, H-7), 7.17 (s, H-4), 7.09 (d, J = 5.4 Hz, H-2). ^{13}C NMR (91 MHz, CD_3OD) δ 140.3 (C-5), 140.1 (C-6), 136.8 (C-8), 133.8 (C-3), 111.5 (C-4), 108.57 (C-7), 127.9 (C-2), 123.3 (C-1).

Oxidation of DHPET or DHBT. To a methanolic solution of DHPET or DHBT, the proper buffer was added to achieve the desired substrate concentration (1 or 10 mM). Different oxidative conditions were tested:

a) O_2 mediated oxidation in 0.05 M Na_2CO_3 buffer pH 8.5-9;
b) sodium periodate (1-2 molar eq.) in 0.1 M phosphate buffer (pH 7.4);
c) Cerium Ammonium Nitrate (1-2 molar eq.) in 0.1 M phosphate buffer (pH 3.0);
d) potassium ferricyanide (1-3 molar equivalents).
e) Horse radish peroxidise (HRP)/H_2O_2 (50 U mL^{-1}, 1eq) in 0.05 M phosphate buffer pH 7.7.

Substrate consumption was determined by HPLC analysis (0.1 % HCOOH-ACN 8:2).

Synthesis and structural characterization of DHPET dimers

Dimers were obtained oxidizing DHPET in the conditions described at line e) of the previous paragraph. Purification was achieved by Preparative Layer Chromatography (PLC), $CHCl_3$: AcOEt 8:2 was selected as eluant.

(**2**) R_f: 0.8, ^{1}H NMR (400 MHz, $CDCl_3$)

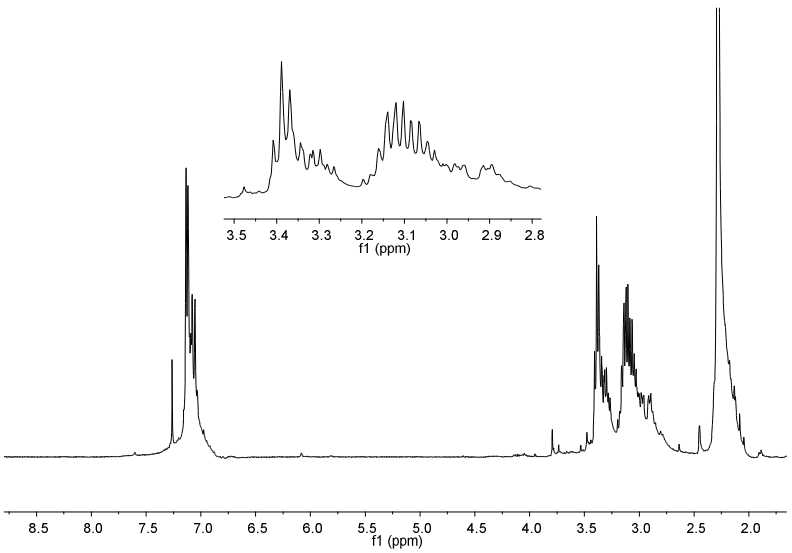

^{13}C NMR (101 MHz, $CDCl_3$) δ 168.5 (C-9), 142.1 (C-3), 141.0 (C-4), 137.9 (C-1), 137.1 (C-6), 127.0 (C-2), 123.6 (C-5), 56.70 (C-8), 39.6 (C-10), 36.7 (C-7), 34.1 (C-11), 20.8 (C-9).

(**3**): R_f: 0.6

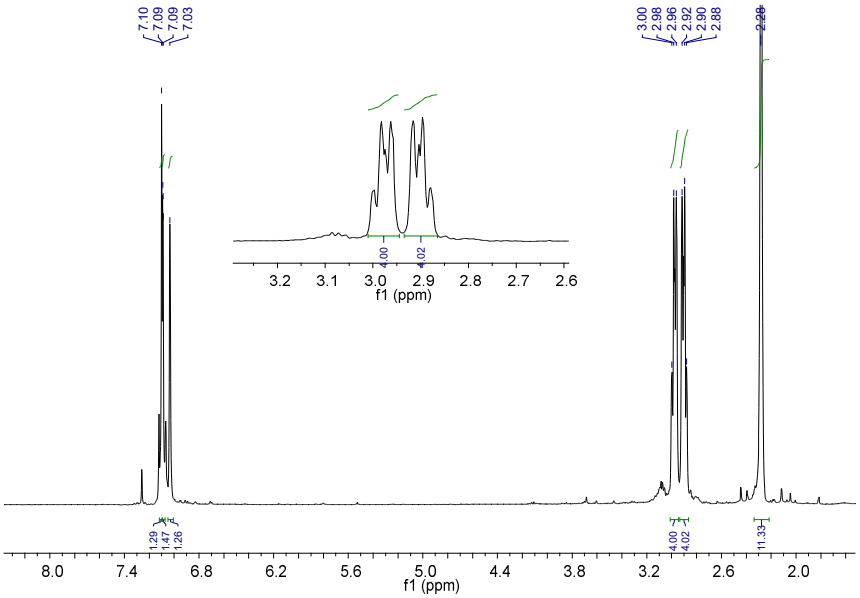

^{1}H NMR (400 MHz, $CDCl_3$) δ 7.10 (s, H-2), 7.09 (d, H-5), 7.03 (d, H-6), 3.01 – 2.94 (t, J= 2.98 Hz, H-7), 2.93 – 2.86 (t, J= 2.90 Hz, H-8), 2.28 (s, H-9). ^{13}C NMR (101 MHz, $CDCl_3$) δ 168.4 (C-9,10), 141.9 (C-3), 140.4 (C-4), 138.8 (C-1), 126.8 (C-6), 123.5,(C-2) 123.3 (C-5), 39.4 (C-8), 34.9 (C-7).

Synthesis and preliminar structural characterization of DHBT oligomers

Oligomers were obtained by DHBT oxidation with 2 eq of potassium ferrycianide following the procedure reported in the related paragraph. Purification of the reaction mixture was performed by silica gel chromatograph whit hexane:ethyl acetate 7:3 as the eluant. As no signals were detected in the high-field region, ^{1}H NMR spectra are reported as expansion of the low-field region. All ^{1}H NMR spectra are recorded at 400 MHz in $CDCl_3$.

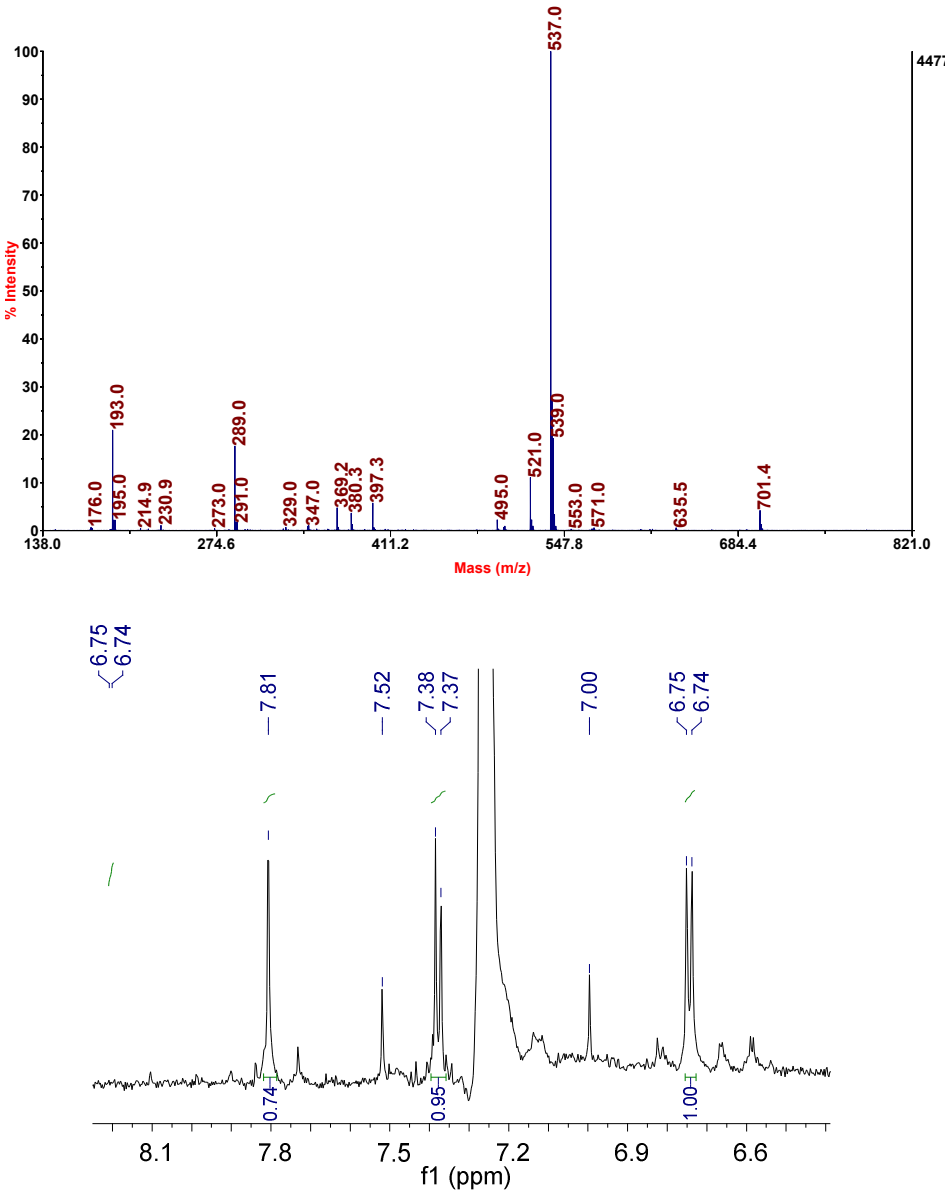

MALDI-MS and ^{1}H NMR spectra of DHBT dimers.

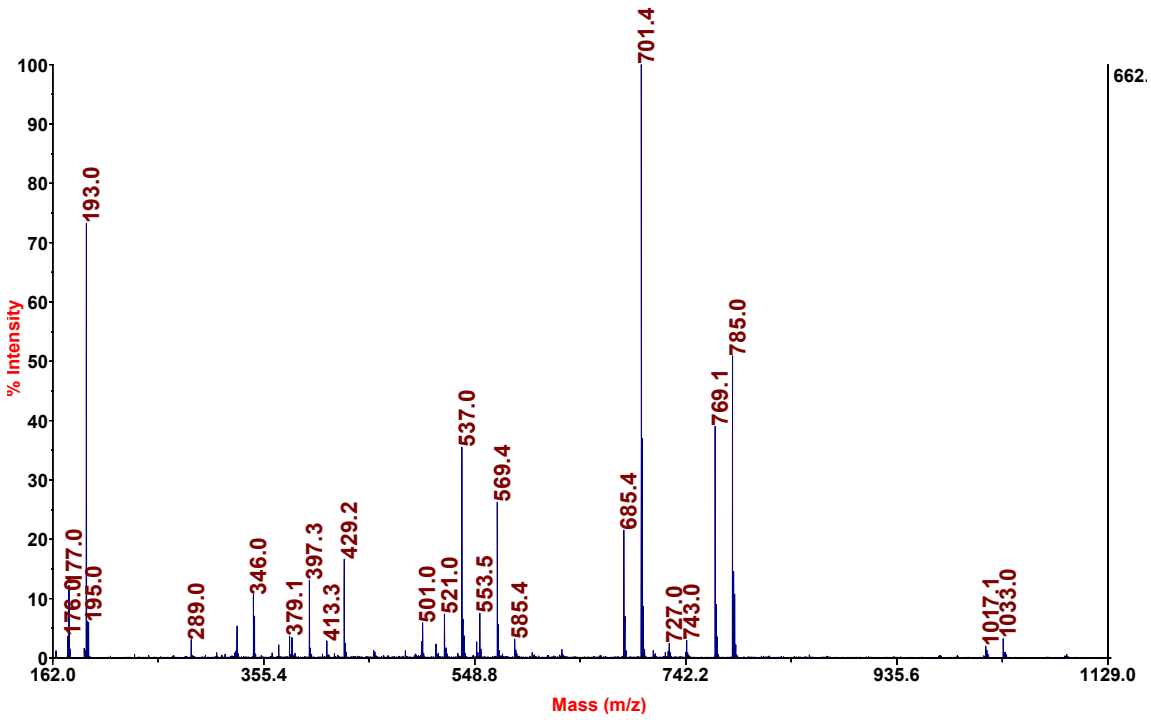

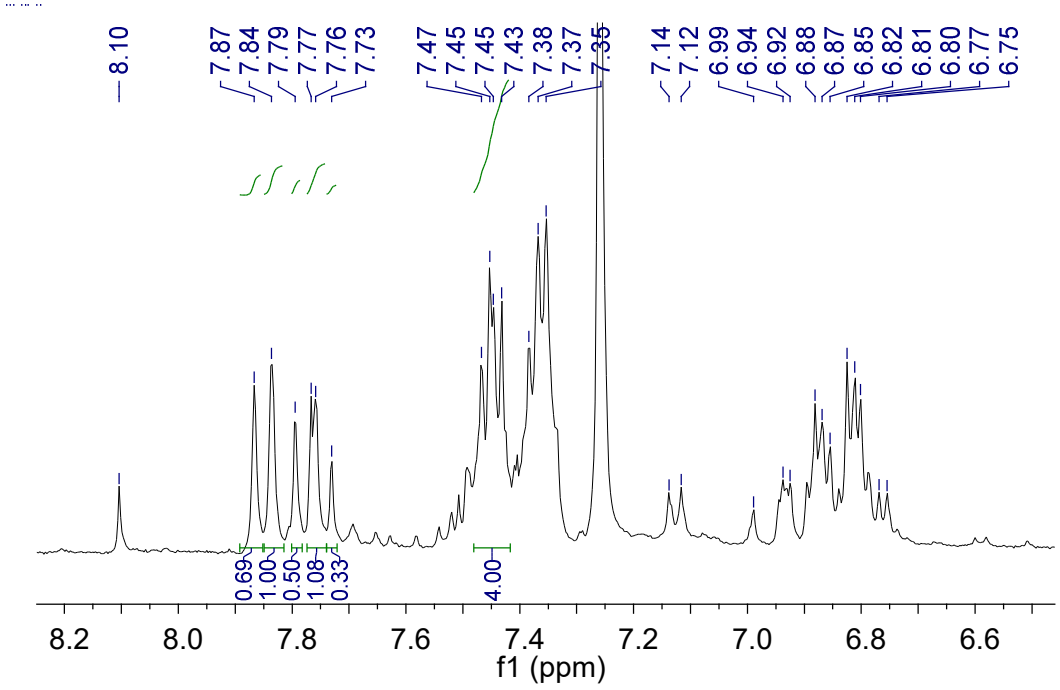

MALDI-MS and ^{1}H NMR spectra of DHBT trimers.

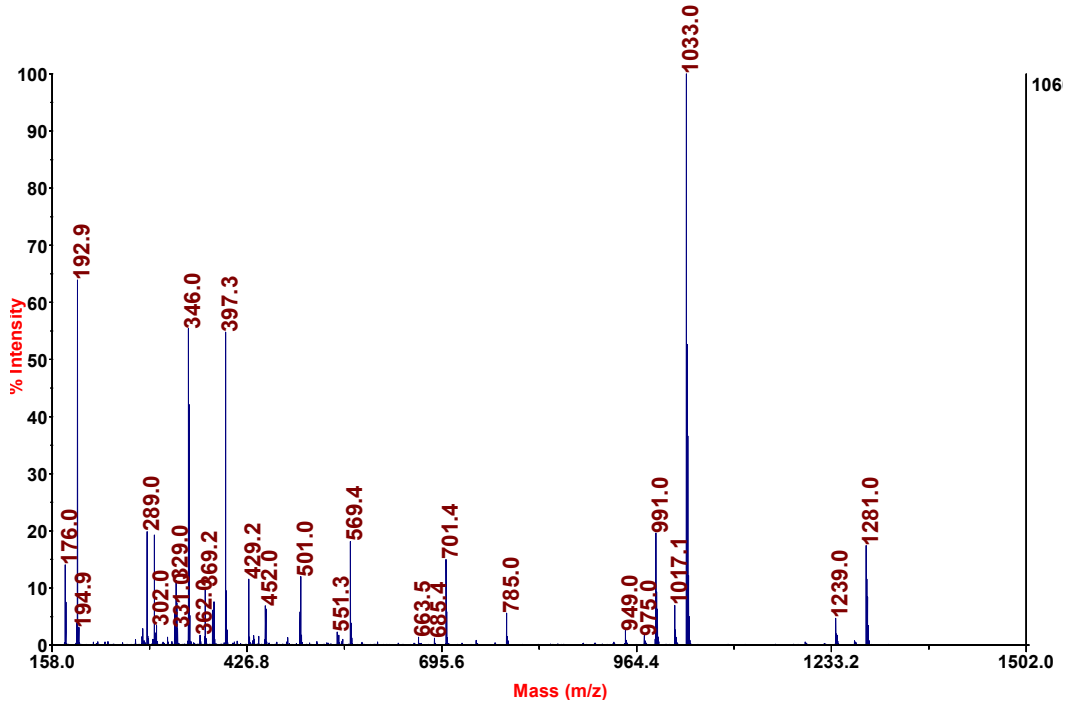

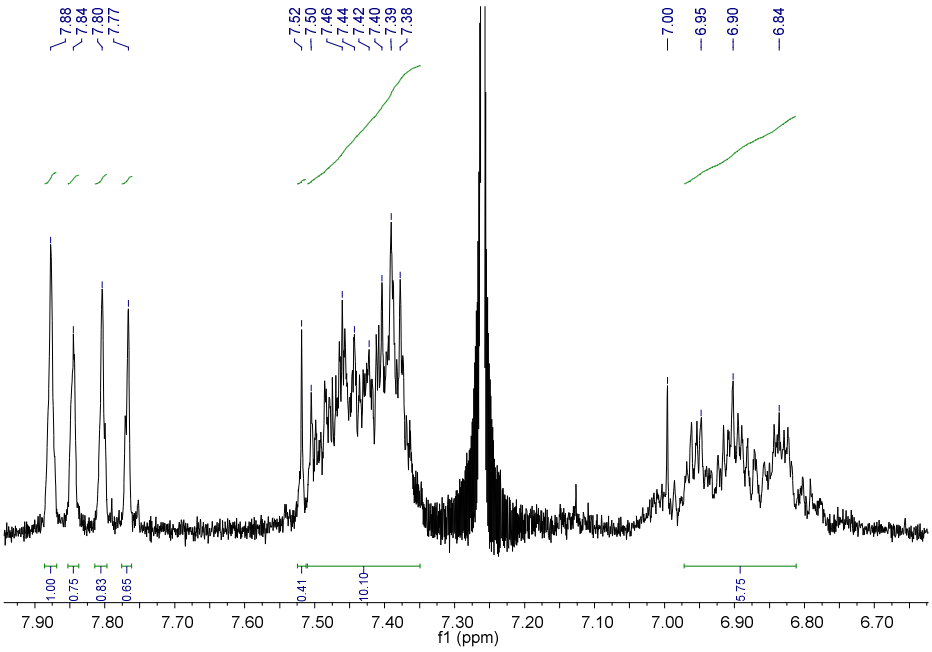

MALDI-MS and ^{1}H NMR spectra of DHBT tetramers.

Chapter 4

Multifunctional mussel-inspired biomaterials and molecular systems by amine-controlled oxidative polymerization of natural catechols

4.1 Introduction

As illustrated in detail in Chapter 1, catechol chemistry is largely dominated by

- redox equilibria with semiquinone radicals and highly electrophilic quinines capable of efficient coupling with nucleophilic functional groups such as thiols, amines, as well as carbon nucleophiles including phenolic and catecholic rings;
- metal chelation, especially towards biologically relevant ions such as Fe^{3+}, Zn^{2+} and Cu^{2+}.

These properties render catechol compounds versatile intermediates for conjugation, polymerization, cross-linking and coupling even under mild biologically-relevant conditions (Scheme 4.1.1).

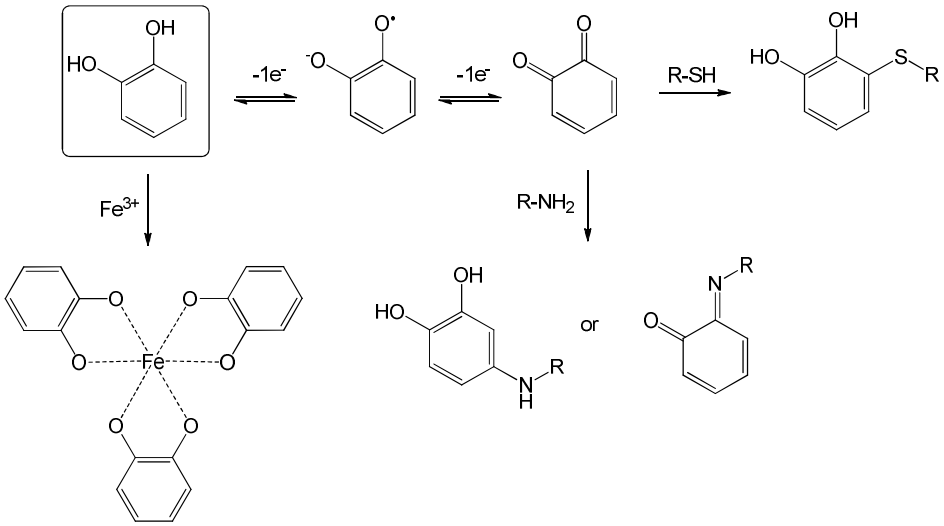

Scheme 4.1.1 *Catechol chemistry.*

In this chapter, the attention will be focused on the oxidatively-induced cross-linking reaction of catechols with amines/amino acids as a bio-inspired process of increasing impact for the design and development of functional biomaterials and systems.

By far, the most relevant example of such a reaction in nature comes from mussels' ability to cling to rocks underwater. Extensive biochemical studies of wet adhesion have demonstrated that the main players in this process are the proteins secreted by mussel byssus: mussel foot protein (mfp)-1 and mfp-5 which exhibit an unusually high content of DOPA and lysine residues.[14] These amino acids, in the slightly alkaline sea water, undergo fast oxidative coupling via amine-quinone reactions and are capable of establishing coordinative interactions with inorganic ions allowing strong adhesion.[13]

As previously mentioned, studies of the autoxidation of the catecholamine dopamine, featuring the catechol and amine functional groups of mussel byssus proteins, led to development of a black melanin-like adhesive polymer termed polydopamine (pDA), which can be used to coat any kind of surface.[12,16]

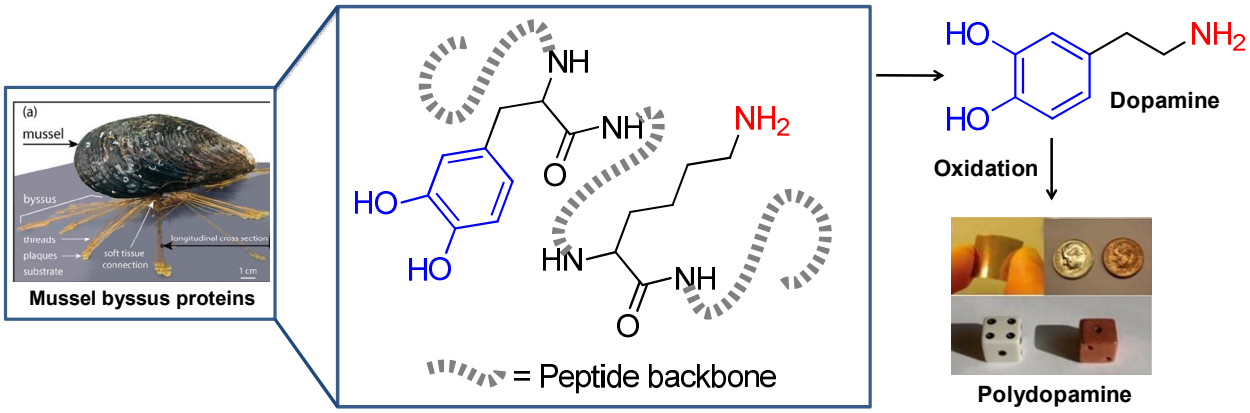

Figure 4.1.1 *Catechol and amino groups are the core reactive unit in mussels' and pDA adhesion mechanisms.*

Although PDA is currently the reference material for surface functionalization and coating, some issues relating to the toxicity of the precursor dopamine and the limited number of functional groups available for post-synthetic modification have prompted intense studies toward novel mussel-inspired surface chemistry beyond pDA-based technology. An attractive approach to this goal may be based on the development of alternative dip-coating methodologies based on separate catechol and amine components allowing access to tailored materials via rational combination of precursors.[148,149]

In this chapter, the results of proof-of-concept investigations are presented demonstrating that the combination of caffeic acid (CA), a cheap, non-toxic and easily accessible natural catechol, with

hexamethylenediamine (HMDA), as a lysine mimic, provides the basis for a novel, costly effective and simple methodology to achieve a biocompatible organic thin film which can adhere to a broad range of surfaces. The coating exhibits metal-chelating properties comparable to those of pDA and dye-adsorbing ability of potential interest for various applications.

Based on this chemistry, in a related series of experiments the preparation and characterization of green biocompatible coloring substances will also be reported, which take inspiration from the marked greening of some vegetables, such as sweet potato, burdock, and sunflower seeds shown during cooking, or other food processing e.g. alkali extraction of proteins from sunflower meal (Figure 4.1.2). Studies aimed at identifying the structure of the green pigment demonstrated that it is formed by the reaction between the esters of caffeic acid, expecially chlorogenic acid (CGA) and amino acids under enzymic conditions (mainly due to polyphenol oxidases) or alkaline aeration.[150,151]

Figure 4.1.2 *Picture of sunflower seeds before (left) and during (right) the alkaline protein extraction process.*

Since green synthetic food dyes have progressively been banned, e.g. triarylmethanegreen S (also E142) that is now still admitted only in Europe, the search for natural based colorants is nowadays very active. Moreover, apart from chlorophylls and the semisynthetic copper chlorophyllins (natural green 3, E141), this latter recently used also as food supplement for its additional benefical effects,[152] no other natural product-based colorants are available for green coloring.

On this basis, starting from a comparative analysis of the conditions of formation of the benzacridine pigment previously reported,[153,154] we developed a procedure for its purification and

evaluated the pH dependence and the thermal stability of the chromophore. Moreover, we demonstrated the straightforward formation of the pigment from protein and protein rich food matrices. Other possible applications of food relevance like sensing of fish deterioration were explored. The toxicity of these pigments was determined at different doses on two human cell lines like Caco-2 and HepG2 cells.

4.2 Thin films and coatings from caffeic acid and a cross-linking diamine

Autoxidation of caffeic acid (1 mM) at pH 8.5-9, in phosphate or bicarbonate buffer did not result in detectable coatings on glass or quartz, despite apparent polymerization with evident darkening of the mixture.[155] Likewise, no visible coating was observed upon addition of ammonia, Tris buffer, butylamine, dodecylamine or ethylenediamine to the catechol solution up to 50 mM concentration. However, in the presence of equimolar amounts of HMDA, the autoxidation of caffeic acid led to the deposition of greenish-blue films (λ_{max} 660 nm) on a glass surface within a few hours which could be detected by UV-vis spectrophotometry (Figure 4.2.1, left). Efficient HMDA-mediated deposition of CA films was observed also on quartz and other materials (Figure 4.2.1, right).

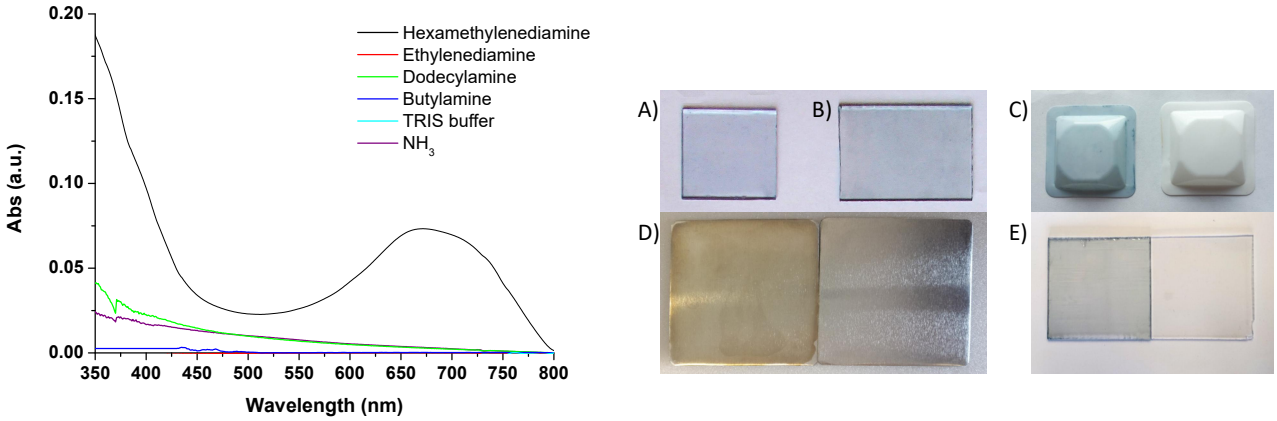

Figure 4.2.1 *UV-vis spectra of cover glasses dipped into 1 mM solution of CA in 50 mM Na_2CO_3 buffer in the presence of equimolar amounts of various amines over 3 hours and picture of CA/HMDA coated A) quartz, B) borosilicate glass, C) polystyrene with uncoated control, D) aluminum with uncoated control, E) polyethylene and uncoated polyethylene.*

Morphological characterization. Spectrophotometric monitoring of film deposition kinetics on a glass coverslip showed a steep increase of the absorbance at 660 nm over 6 hrs (Figure 4.2.2). 3 hour coated substrates were selected for morphological characterization. CA/HMDA thin films were characterized by atomic force microscopy (AFM, Figure 4.4.1), water contact angle (WCA), ellipsometry and X-ray photoemission spectroscopy (XPS) and the results were compared to pDA films produced in the presence of Tris and HMDA.CA/HMDA coatings were ca. 10 nm thick, smooth, and homogeneous and exhibited lower WCA than pDA/Tris films. pDA/HMDA films showed intermediate properties in terms of thickness and hydrophobicity, but a significantly higher roughness. XPS data showed a higher N content in the pDA films prepared in the presence of HMDA vs. those obtained in Tris buffer (Table 4.2.1).

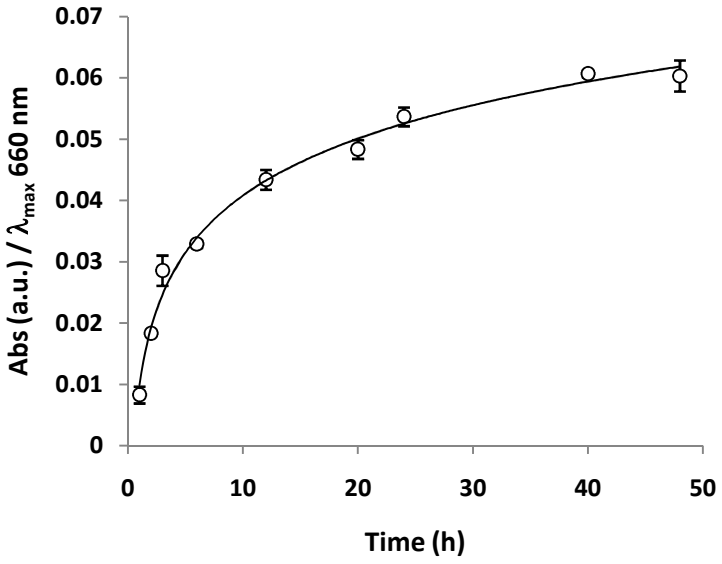

Figure 4.2.2 *Time course of the absorption at 660 nm of a glass coverslip dipped into 1:1 solution of CA and HMDA (5 mM) in 50 mM Na_2CO_3 buffer pH 9.*

Table 4.2.1 Characterization of thin films from CA/HMDA and PDA on silicon wafers.

Film	Thickness (nm)	Roughness (nm)	Water contact angle (deg)	Comp.(atom, %)
Caffeic acid/ HMDA	9.4 ± 0.4	1.0	69.4 ± 1.7	C 1s 54.5±0.4 O 1s 27.9±0.1 N 1s 3.8±0.1
PDA/ HMDA	16.9 ± 1.7	5.1	76.0 ± 2.0	C 1s 48.5±0.9 O 1s 29.9±0.5 N 1s 3.3±0.1
PDA/ Tris	23.7 ± 0.4	0.4	86.2 ± 1.2	C 1s 23.1±0.9 O 1s 48.2±0.5 N 1s 0.8±0.2

Data collected at Max Plank institute by Dr Julieta Paez and co-workers

Structural and electronical characterization. Based on these findings, the CA/HMDA film was next subjected to structural analysis to elucidate the chemical nature of the main species. To this aim, the greenish-blue precipitate obtained by autoxidation of CA in the presence of HMDA in bicarbonate buffer at pH 9 was collected, extensively washed and analyzed by ^{13}C and ^{15}N CP-MAS

NMR (Figure 4.2.3, spectra recorded by Dr. M.E. Errico and co-workers from the Institute of Chemistry and Technology of Polymers, National Council of Research (CNR), Pozzuoli, Italy) combined with ATR/FT-IR (Figure 4.4.2) and LDI/MALDI-MS (Figure 4.2.4). The ^{13}C NMR spectrum (Figure 4.2.3a) displayed aliphatic chain signals of HMDA denoting extensive incorporation of the diamine. Major bands at δ 95-105 indicated the presence of shielded aromatic carbons adjacent to amine groups. Signals at δ 125, 138 and 148 were attributed to aromatic ring signals. Intense sp^2 carbon bands at δ 168 and 175 were due to conjugated carbonyl and carboxyl groups. The ^{15}N NMR spectrum (Figure 4.2.3b) revealed an intense amine resonance and two broad bands around δ 90 and 120, consistent with shielded imine and heteroaromatic structures.[156] Overall, these data, integrated by LDI-MS analysis and supported by previous literature on the reactions of CA esters with amines,[150,151]described the CA/HMDA coating as consisting of a mixture of trioxygenated carboxylated benzacridinium derivatives including tethered dimeric species (Figure 4.2.5).Several trihydroxybenzacridine derivatives green in color had already been identified by reaction of caffeic acid esters (mostly chlorogenic acids) with different aminoacids,[154,157,158] but use of free carboxyl groups as in the CA/HMDA coating reaction may account for specific effects on product properties. A mechanistic path to the proposed structures including the decarboxylation step is shown in Figure 4.4.3.

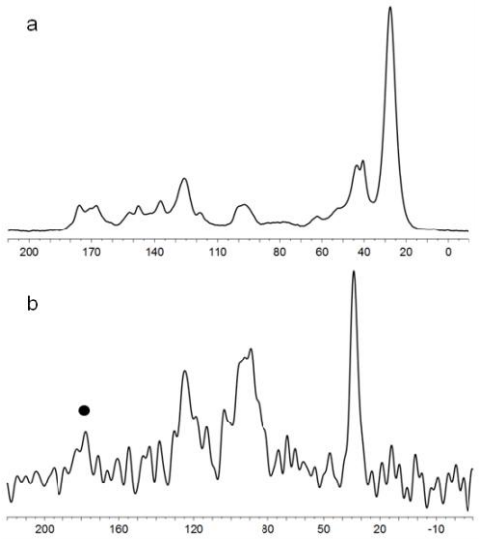

Figure 4.2.3 *^{13}C (a) and ^{15}N (b) CP-MAS NMR spectra of the CA/HMDA polymer. Spinning sidebands are marked by a dot.*

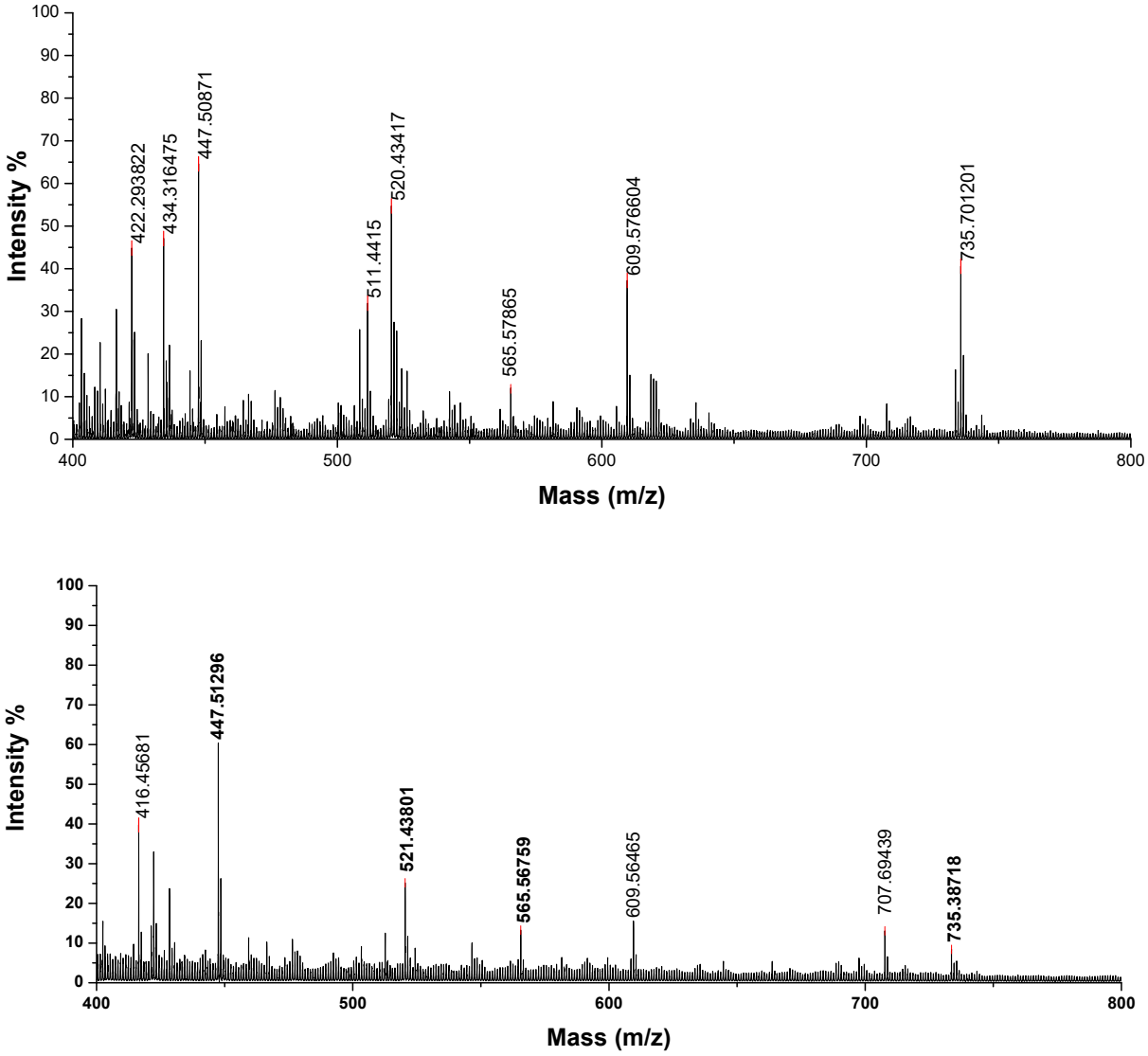

Figure 4.2.4 *MALDI-MS (top) and LDI-MS (bottom) spectra of the solid separated from the CA/HMDA mixture after centrifugation and washings with water. Molecular peaks that have been structurally assigned are in bold. In the case of MALDI-MS analysis, 2,5-dihydroxybenzoic acid was used as matrix. Sample preparation as described under experimental.*

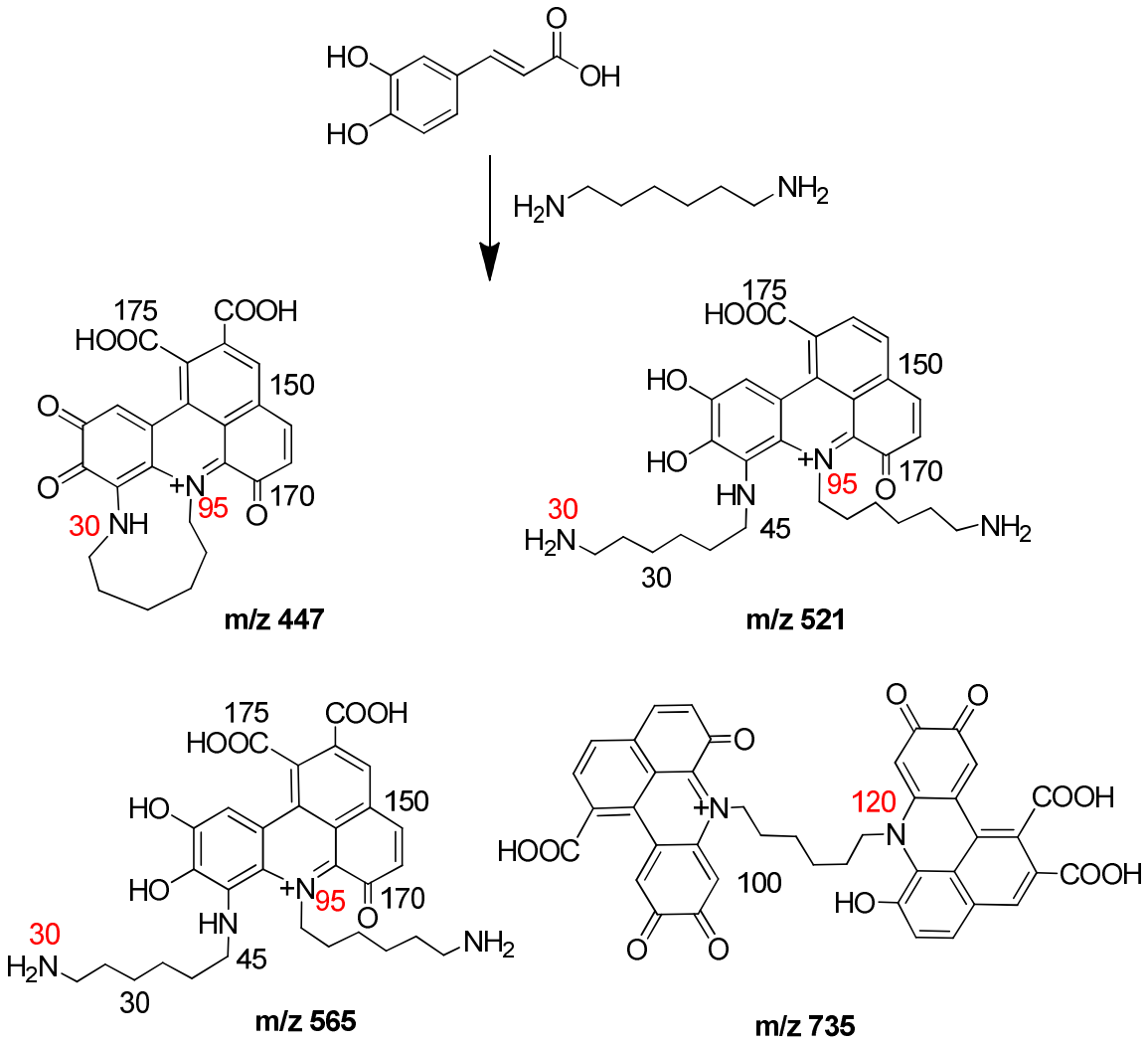

Figure 4.2.5. *Proposed structures for representative components of CA/HMDA films as inferred from LDI-MS. Shown are the m/z values for the pseudomolecular ions.* ^{13}C *NMR and* ^{15}N *(red) NMR resonance assignments are highlighted.*

Interestingly, electron paramagnetic resonance (EPR) spectra showed distinct paramagnetic properties, consistent with the occurrence of the polycyclic systems in different redox states, e.g. the catechol and quinone forms represented in Figure 4.2.5. Inspection of the EPR spectrum suggested mainly carbon-centered radicals (g= 2.0037) with negligible involvement of O-centered semiquinone radicals or of nitrogen centered radicals. Both the power saturation profile and the broad signal amplitude (ΔB= 6.47 G) were consistent with a high degree of heterogeneity (Table 4.2.2 and Figure 4.2.6).[7]

Table 4.2.2. Electron Paramagnetic Resonance (EPR) characterization of CA/HMDA solid material.

	ΔB (G)	**g**	**Spin density (spin/g)**
CA/HMDA	6.47±0.05	2.0037±0.0003	4.5×10^{17}

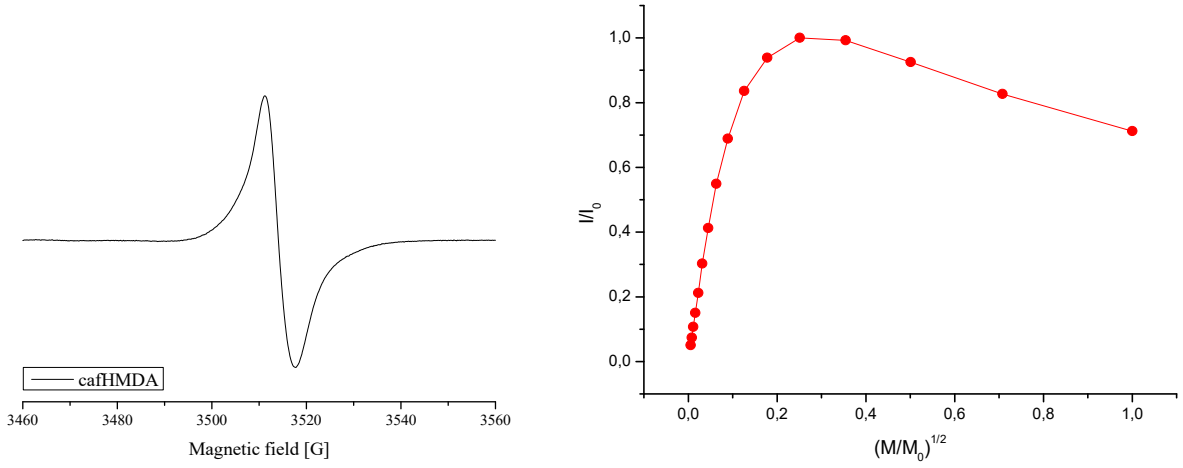

Figure 4.2.6. *EPR signal (left) and power saturation profile (right) of CA/HMDA solid material.*

Stability and pH-dependence. The chemical stability of the CA/HMDA films was tested under different conditions. Exposure of as prepared films to aqueous solutions containing hydrogen peroxide or reducing agents, such as or sodium borohydride, glutathione or dithiothreitol, did not result in detectable modification of the UV-visible absorption spectra (data not shown). Interestingly, acid vapors caused visible and color change from green to greysh, revertable by exposure to ammonia vapors, denoting pH-dependent chromophores (Figure 4.2.7). No detectable film detachment was induced by oxidative, reductive or acidic treatments.

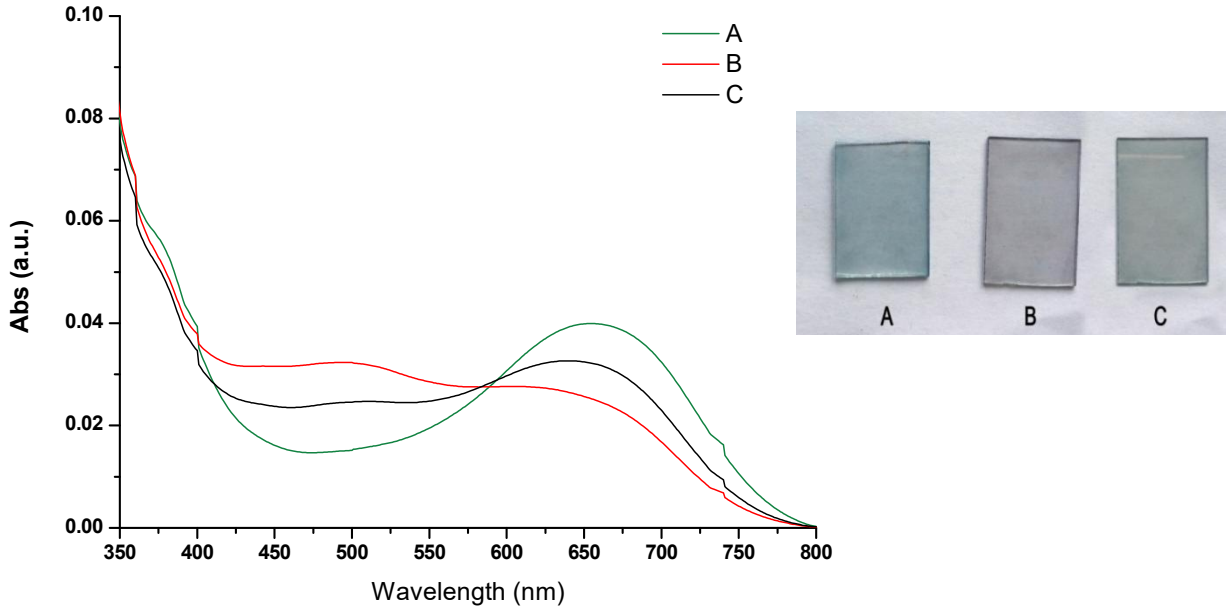

Figure 4.2.7 *UV-Vis spectra of CA/HMDA coated glass under neutral conditions (A), after exposure to HCl vapours (10 seconds, B), and further exposure to NH_3 vapours (10 seconds, C). Shown is a digital picture of the glass exposed to the different conditions.*

To clarify the structural requisites of the film-forming catechols, in further experiments CA was replaced with4-methylcatechol (MC) in the HMDA-containing mixture. A deep-yellow coating (λ_{max} 405 nm) was obtained (Figure 4.2.8) which on ellipsometric (Table 4.4.1) and spectral characterization (Figure 4.4.4-6) proved to consist of variously substituted quinine imine species deriving from nucleophilic addition of HMDA to MC deriving O-quinone moieties (Figure 4.2.9). No UV-detectable surface coating was observed in the absence of HMDA.

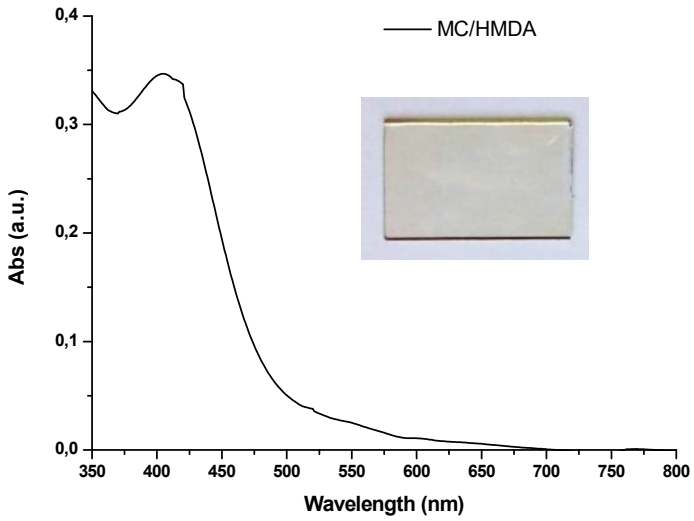

Figure 4.2.8 *UV-vis spectrum of a glass coverslip dipped into 1:1 solution of MC and HMDA (1 mM) in 50 mM Na_2CO_3 buffer pH 9 over 3 hours and picture of the MC/HMDA coated coverslip.*

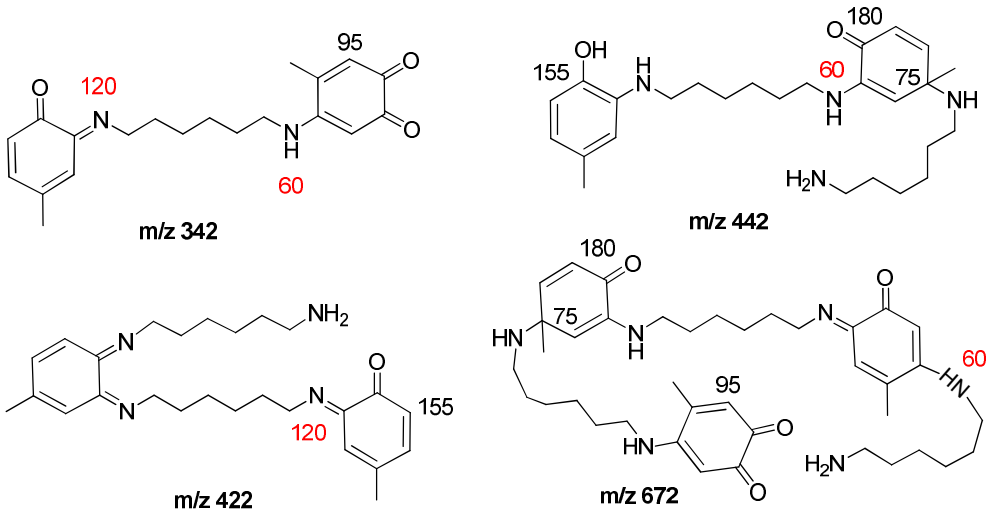

Figure 4.2.9 *Proposed structures for representative components of MC/HMDA polymer as inferred from LDI-MS. Shown are the m/z values for the pseudomolecular ions. ^{13}C NMR and ^{15}N (red) NMR resonance assignments are highlighted.*

These results unambiguously demonstrated the covalent coupling of HMDA with autoxidatively generated quinone intermediates as a general cross-linking mechanism underlying film formation. It was concluded that the nature of the catechol is not critical, but it is the combination of a long aliphatic chain and two amine groups in HMDA that is crucial to confer to catechol polymers a

suitable balance of hydrophobicity, aggregation and cross-linking, since neither simple monoamines (n-propylamine or the long chain n-dodecylamine) nor short chain diamines (1,2-ethylenediamine) were able to lead to film deposition from autoxidizing catechols.

Metal chelating and dye adsorbing properties. Subsequent experiments were directed to assess the metal binding ability of CA/HMDA coatings by means of colorimetric assays.[159–161] Experiments were conducted in comparison to pDA. CA/HMDA proved to be more efficient than pDA in binding iron and comparable to pDA for copper binding (Figure 4.4.7). On this basis the metal-binding ability of octadecylsilane silica (55-105 μm particle size), as a high surface area support, following functionalization by the CA/HMDA or pDA coating (Figure 4.2.10A) was then comparatively assessed. Almost complete (97%) removal of iron from the solution was obtained by passing it through 100 mg of CA/HMDA-coated C_{18} while the same amount of pDA-functionalized C_{18} led to 78% removal of Fe^{2+}. Lower amounts of functionalized resin (50 mg) led to the almost complete removal of copper (97% for CA/HMDA C_{18} and 93% for pDA C_{18}) (Figure 4.2.10B). Interestingly, the efficiency of the CA/HMDA C_{18}remainedvirtually unaffected after 4 passages of the fresh metal containing solution through the resin (Fe^{2+} chelation= 97%, Cu^{2+} chelation= 77%) and still effective after up to 6 passages (Fe^{2+} chelation= 47%, Cu^{2+} chelation= 47%) (Figure 4.4.8).

Figure 4.2.10C reports the metal binding capacity q_e (mg of metal/g of C_{18}) for the CA/HMDA C_{18} and pDA C_{18} calculated using the equation $q_e= (C_0-C_{eq})(V/W)$, where C_0 (mg/L) is the actual starting metal concentration as analytically determined from blank experiments, C_{eq} (mg/L) is the metal concentration remaining in solution after incubation with the resins , V (L) is the volume of the incubation mixture and W (g) is the resin dose. In all cases the curves were characterized by an increased uptake following a rise in metal concentration. With an increase of the starting metal concentration from 10 to 100 μM, the amount of Fe^{2+} binding rises up to 4.7 mg/g for CA/HMDA C_{18} vs 4.0 mg/g for pDA C_{18} and the amount of Cu^{2+} binding up to 10.1 mg/g for CA/HMDA C_{18} vs 8.3 mg/g for pDA C_{18}.

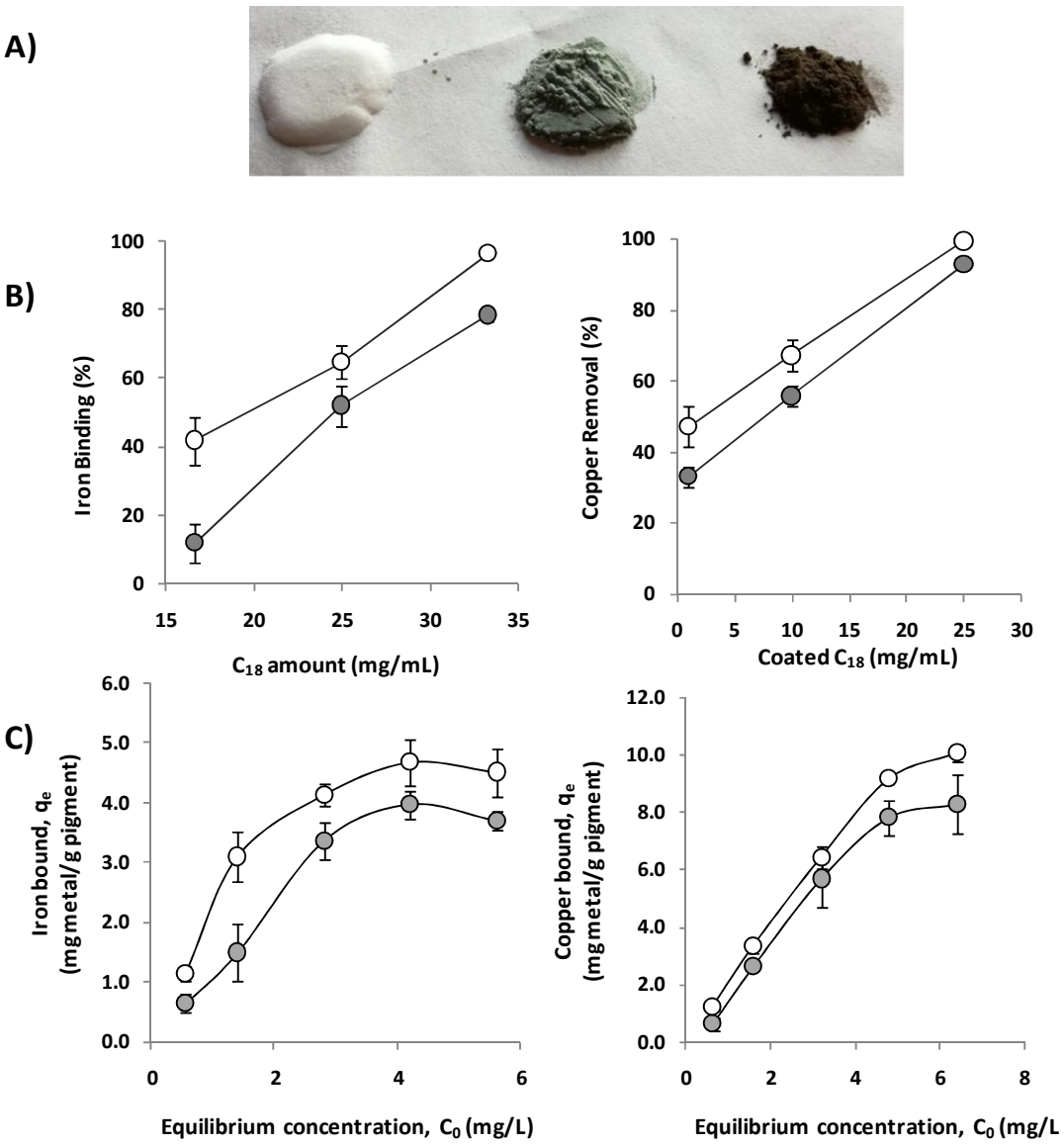

Figure 4.2.10 *A) From left to right: Uncoated C_{18} resin, CA/HMDA C_{18} and pDA C_{18}. B) Binding of iron (left) and copper (right) on different amounts of C_{18} resins coated with CA/HMDA (open circles) and pDA (full circles). C) Binding isotherms of iron (left) and copper (right) by C_{18} resins coated with CA/HMDA (open circles) and pDA (full circles). Initial concentration range, 10-100 µM for iron and copper; amount of functionalized resin, 0.25 mg/mL, temperature 37 °C, contact time 2 h. Shown are mean values of three separate experiments ± SD.*

The ability of CA/HMDA coating to interact with or retain other molecules, was also tested by immersing coated glasses into 0.4 mg/mL solutions of commercial dyes, such as Congo Red and Methylene Blue in 0.1 M phosphate buffer at pH 7. Even after extensive rinsing with water, detectable adsorption of the dye was evidenced in the UV-visible spectra (Figure 4.2.11, top) as well as by visual inspection. For comparison the same experiments are run on pDA films (Figure 4.2.11, bottom) showing some binding ability only in the case of Methylene Blue.

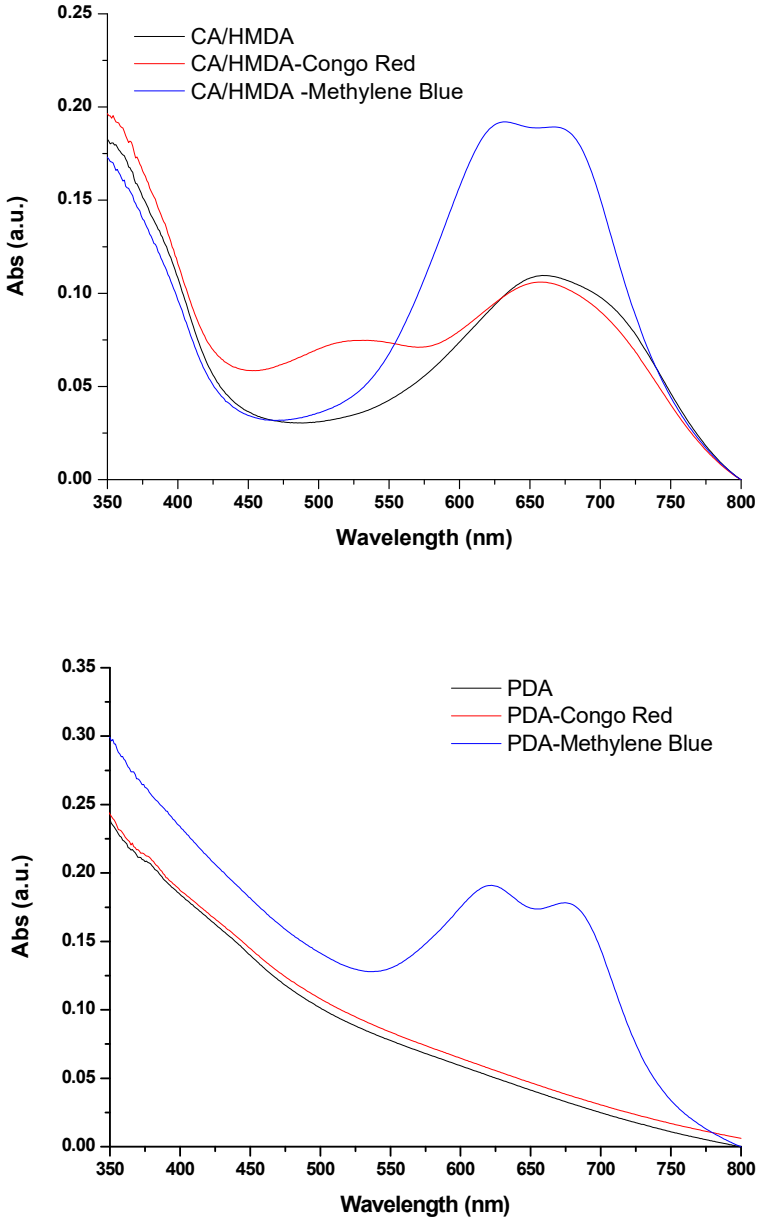

Figure 4.2.11 *UV-visible spectra of CA/HMDA (top) and pDA (bottom) coated glass after dipping into a 0.4 mg/mL solution of Congo Red or Methylene Blue in phosphate buffer pH 7.0.*

Biocompatibility. The biocompatibility of the CA/HMDA coating and the ability to support cell growth was also assessed on two different cells lines: Cultured Human Keratinocites (HaCat) and embryonic stem cells (ESCs). Experiments were carried out by Professors Pizzo and Falco and their co-workers at the biology department of the University of Naples Federico II. Briefly HaCaT cells adhered to CA/HMDA pre-treated dishes, remained viable, and showed comparable morphology as on tissue culture plates. The CA/HMDA coating efficiently supported the growth of HaCat cells (Figure 4.4.9), with a statistically significant increase in the proliferation rate at 72 h compared to pDA-coated plates ($p< 0.01$). These results showed good biocompatibility of CA/HMDA coatings and a positive effect as cell cultures surfaces and encouraged further experiments on embryonic stem cells. ESCs were cultured for 3 days in regular culture medium on cell culture plates coated with either CA/HMDA, or with PDA, or with gelatin. ESCs cultured on CA/HMDA coated plates formed round-shaped colonies (Figure 4.4.10A-a), while ESCs cultured on pDA-coated plates formed flat-shaped colonies (Figure 4.4.10A-b) consistent with high self-renewal, and low-self-renewal, respectively. As expected ESCs cultured on gelatin, as control, aggregated in spheroid cell structures floating in the medium (Figure 4.4.10A-c). Altogether, the data showed that CA/HMDA coated plates are able to improve both clonogenic and attachment capability of ESCs. Remarkably, ESCs cultured on CA/HMDA showed significantly higher number of colonies than ESCs cultured either on pDA coated plates or on gelatin coated plates (Figure 4.4.10B).

Conclusions. The autoxidative coupling of the natural catechol caffeic acid (CA) with the long-chain diamine (HMDA) at pH 9 leading to deposition of thin films was investigated an expedient strategy for surface functionalization and coating. The specific film-forming properties imparted by HMDA to autoxidizing catechols can be attributed to the efficient cross-linking properties ensuring flexibility and an optimal balance of hydrophobicity and ionic character. The two-component coating procedure reported in this study does not require organic solvents, oxidants or other additives, nor long coating deposition times, is versatile (can be extended to a range of catechols and substrates, as apparent from preliminary observations) and is based on a cheap, non-toxic and easily accessible natural compound like CA. Considering the previous studies on gallic acid and DA,[149,162] this results expand the current repertoire of catechol-based coatings with the additional advantage that HMDA is used herein in equimolar amounts with the catechol and at 1 mM concentration, much lower than in previous reports. CA/HMDA films are cyto-compatible and appear to support more efficiently stem cell growth than films obtained from pDA/Tris. Of interest in the perspectives of exploitation of these materials is the ability of CA/HMDA to efficiently bind metal ions and organic dyes.

4.3 The development of benzacridine-based green coloring agents for food related applications.

In a separate investigation the potential usefulness of the caffeic acid/amine reaction for generation of green coloring pigments for food related applications was assessed. Preliminarily, the procedures reported for the formation of the benzacridine pigments were comparatively evaluated using chlorogenic acid (CGA, Figure 4.3.1) as the catechol substrate in view of its solubility and widespread occurrence in plant-derived food preparations, while glycine (GLY) was selected as the amine component, as it was previously shown by Yabuta *et al*. to lead to most intense pigment chromophore at 680 nm.[150] Since Shilling *et al*. reported a detailed mechanistic investigation on the reaction of CGA with lysine (LYS) using reaction conditions diverging from those reported previously,[154] the investigation was extended also to this amino acid. CGA concentration varied in the range 10-20 mM and different CGA/amino acid ratios were used. In all cases the pH of the reaction medium was around 9.0-9.5 as reported.

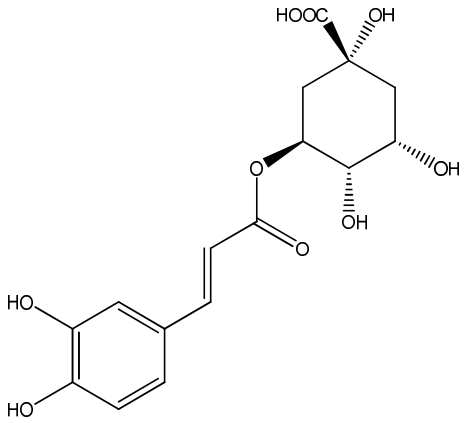

Figure 4.3.1 *5-O-Caffeoylquinic acid (chlorogenic acid, CGA) chemical structure.*

Table 4.3.1 reports the absorbance value at 680 nm due to the green pigment formation together with quantitative determination of the residual CGA by HPLC analysis.

Table 4.3.1 ***Comparative analysis of the reaction of CGA with GLY and LYS under different reaction conditions.***

Item #	CGAconc (mM)	AA	AA/CGA ratio	A_{680} *[1]	Reaction time (h)	Temp (°C)	Residual CGA*[2]	Lit
1	20	GLY	1	0.280	2	50	36.5±5.2	Yabuta *et al*. 2001
2	14	GLY	4	0.398	24	25	31.7 ± 0.6	Prigent *et al*. 2008
				0.4684	36		23.2 ± 0.8	
3	14	GLY	1	0.440	24	25	21.0± 0.7	
				0.478	36		16.1 ±0.5	
4	14	LYS	4	0.194	24	25	21.7 ± 0.6	Prigent *et al*. 2008
				0.328	36		21.4 ± 0.4	
5	14	LYS	1	0.218	24	25	17.5 ± 0.3	
				0.236	36		17.2 ± 0.1	

*[1] normalized to starting CGA concentration of 0.1 g/L; *[2]HPLC determination

The highest intensity of the visible chromophore was obtained running the reaction at room temperature (#2 and #3). An excess of amino acid with respect to CGA (# 2) did not favor pigment formation with respect to equimolar conditions (#3), while prolonging the reaction time up to 36 h increased pigment formation and consumption of the CGA under either condition (#2 and #3). Using LYS as the amino acid (#4 and #5) resulted in a chromophore with slightly less intense absorbance in the visible region, while consumption of CGA was comparable to that observed with GLY. On this basis it appears that the optimal reaction conditions in terms of pigment formation, CGA consumption and minimal excess of the reactants is achieved in either cases using a 1:1 CGA to amino acid ratio, at room temperature at pH 9.0 over 36 h reaction time. These latter conditions were therefore adopted to run the reaction of CGA with the two amino acids on a preparative scale.

Purification of the green pigment. To purify the pigment from the starting materials and saline components, dialysis through a membrane with a cut-off range of 100-500 Da was initially attempted, but without success: the pigment slowly diffused into the dialysate that was shown to contain also CGA and excess amino acid by spectrophotometric and HPLC analysis. In subsequent experiments the reaction mixtures CGA-GLY and CGA-LYS obtained using 0.5 g of CGA (1:1 amino acid ratio) were loaded on a Sephadex G10 column from concentrated water solutions and eluted with distilled water. A brownish fraction likely due to oxidation products of CGA was initially eluted followed by the green pigment appearing as a single band, and then by a fraction containing CGA (Figure 4.4.11). In addition to the broad band centered at 680 nm two maxima at 260 and 320 nm were observed in the UV region. HPLC analysis of the purified fraction showed no

residual CGA. Based on the ratio A_{680} nm by weight of material, a ca 2.5 fold purification was achieved with respect to the starting reaction mixture for the CGA-LYS pigment, but far lower (1.2 fold) for the CGA-GLY (Figure 4.4.12). The 1% extinction coefficient of the purified fraction at 678 nm was 28.67± 0.063for CGA-LYS and 19.05± 0.83for CGA-GLY. On this basis the CGA-LYS pigment was preferred for subsequent application purposes. Digital pictures of the lyophilized green pigments are reported in Figure 4.3.2.

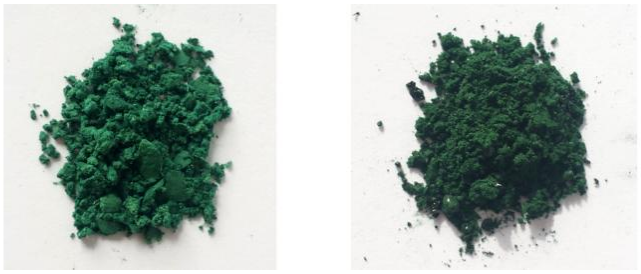

Figure 4.3.2 *Digital pictures of green pigments obtained after purification and lyophilization from CGA-GLY (left) and CGA-LYS (right).*

LC-MS analysis. The purified CGA-GLY and CGA-LYS pigments were analyzed by UHPLC with DAD and MS/MS detection using the conditions previously developed.[163] These experiments were run in collaboration with professor A. Schieber and associates of the Institute of Nutritional and Food Sciences, University of Bonn. Traces of the Figure 4.3.3-4 and data in Table 4.3.2-3 provided evidence for the presence of several compounds with the same molecular mass and absorption characteristics in line with the results of previous papers.[154,163,164] Peaks Lys 1 to Lys 4 exhibited a molecular ion peak at *m*/*z* 829 corresponding to a trihydroxybenzacridine comprising the whole lysine residue, whereas Lys 5 to Lys 10 peaks had a molecular ion peak at *m*/*z* 700 corresponding to the benzacridine system not comprising the amino acidic residue. These compounds were identical to compounds Gly 1 to Gly 6. Infact, in the case of Gly (Figure 4.3.4 and Table 4.3.4) ring closure of the benzacridine system is associated with decarboxylation and loss of the side chain. These results confirm previous observations[163] indicating that only in the case of Lys, possessing two NH_2 groups, two series of benzacridine derivatives can be obtained. Notably, those products having the ε $-NH_2$ group incorporated in the benzacridine scaffold do not undergo loss of the amino acidic residue that is invariably observed with other α-amino acids (Scheme 4.3.1). In addition, isomerization at the quinic acid moiety during the formation of the benzacridine system at the

slightly alkaline pHs of the reaction medium may likely account for the number of isomers observed for each series, as described even under milder and physiologically relevant conditions.[164–167]

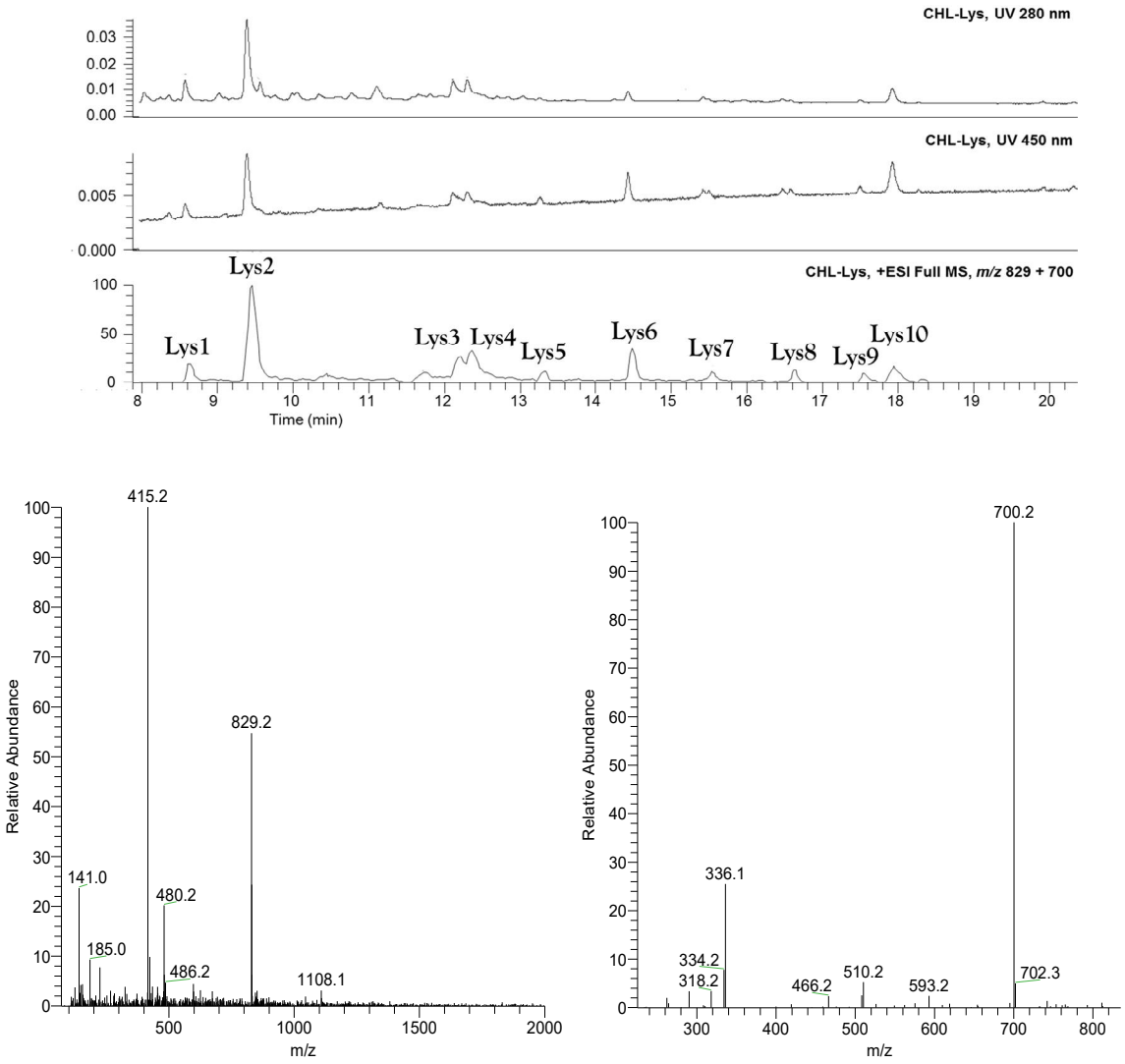

Figure 4.3.3 *Top: UHPLC chromatograms (MS m/z 700 and 829) and DAD (280 nm and 450 nm) of the CGA-LYS pigment analyzed in the Selected Ion Monitoring (SIM) mode. Bottom: Representative mass spectra of Lys 1-4.*

Table 4.3.2 ***Retention times, UV-vis absorption and mass spectrometric data for the benzacridine isomers of the CGA-LYS pigment.***

Cmp	RT_{UV} [min]	RT_{MS} [min]	UV_{max} [nm]	$[M+H]^+$	MS^2 [*m/z*, relative abundance]	MS^3 [*m/z*, relative abundance]	MS^4 [*m/z*, relative abundance]
Lys1	8.58	8.64	515/ 652	**829.2**	700.2 (100), 336.1 (26), 334.2 (7), 510.2 (5), 290.1 (3)	700.2 → 334.1 (100), 262.1 (31), 508.2 (9)	-
Lys2	9.39	9.46	519/ 647	**829.3**	700.1 (100), 336.1 (12), 510.1 (7)	700.1 → 334.1 (100), 526.1 (87), 654.2 (24), 262.0 (15), 508.1 (8), 480.1 (6), 682.2 (5), 352.1 (4)	334.1 → 262.1 (100), 334.2 (7), 306.0 (2)
Lys3	12.12	12.22	517/ 647	**829.3**	-	-	
Lys4	12.31	12.37	519/ 647	**829.2**	700.1 (100), 336.0 (12), 510.1 (6)	700.1 → 334.1 (100), 526.1 (47), 654.2 (33), 262.0 (14), 508.1 (10), 682.3 (6), 352.1 (2)	
Lys5	13.27	13.32	455/-	**700.2**	-	-	
Lys6	14.43	14.48	461/ 645	**700.1**	334.0 (100), 526.1 (83), 654.2 (21), 262.1 (13), 508.2 (7), 682.2 (5), 480.2 (3), 352.1 (3)	334.0 → 262.2 (100)	
Lys7	15.53	15.55	426/-	**700.2**	-	-	
Lys8	16.58	16.63	461/-	**700.2**	-	-	
Lys9	17.50	17.55	462/-	**700.2**	-	-	
Lys10	17.93	17.95	431/-	**700.2**	-	-	

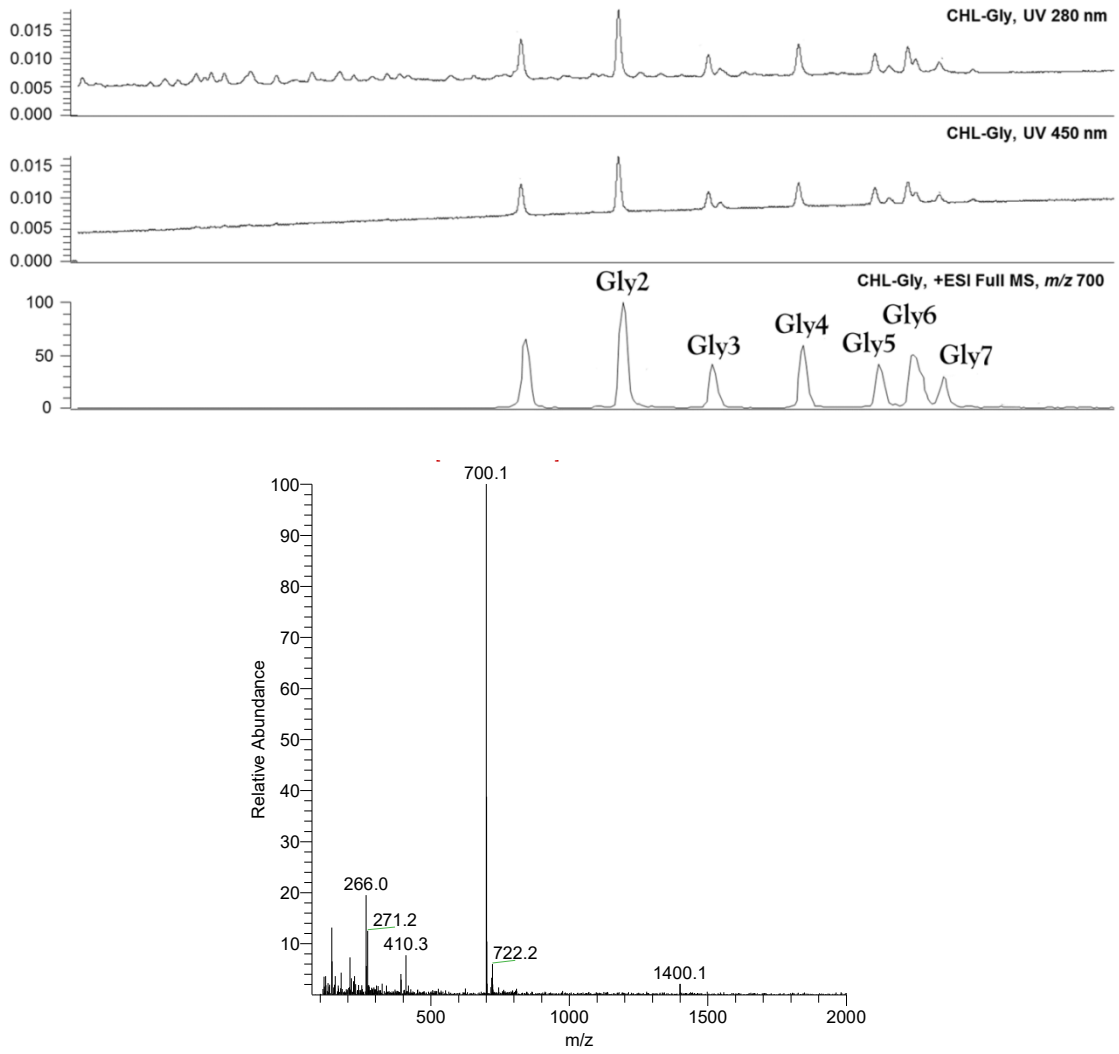

Figure 4.3.4 *Top: UHPLC chromatograms (MS m/z 700) and DAD (280 nm and 450 nm) of the CGA-GLY pigment analyzed in the Selected Ion Monitoring (SIM) mode. Bottom: Representative mass spectrum of Gly 1-7.*

Table 4.3.3 ***Retention times, UV-vis absorption and mass spectrometric data for the benzacridine isomers of the CGA-GLY pigment.***

Cmp	RT_{UV} [min]	RT_{MS} [min]	UV_{max} [nm]	$[M+H]^+$	MS^2 [*m/z*, relative abundance]	MS^3 [*m/z*, relative abundance]	MS^4 [*m/z*, relative abundance]
Gly1	13.28	13.33	462/ 643	**700.1**	334.1 (100), 526.1 (30), 508.1 (13), 262.1 (12), 654.1 (5)	334.1 → 262.1 (100)	262.1 → 262.2 (100), 206.1 (39), 234.0 (26), 178.1 (12), 216 (12),188.1 (3)
Gly2	14.44	14.49	462/ 643	**700.1**	334.1 (100), 526.1 (72), 654.2 (36), 262.1 (18), 508.1 (6)	334.1 →262.0 (100)	
Gly3	15.52	15.57	462/ 642	**700.2**	526.1 (100), 334.0 (95), 508.1 (15), 262.1 (15), 352.0 (5), 682.2 (4)	526.1 → 334.1 (100), 352.1 (62), 508.1 (5), 308.2 (3) 334.0 → 262.1 (100)	334.1 →262.1 (100), 306.2 (3)
Gly4	16.60	16.66	462/ 643	**700.1**	334.1 (100), 526.1 (26), 508.1 (18), 262.1 (12), 654.2 (6)	334.1 →262.1 (100)	262.1 →262.1 (100), 206.2 (32), 216.1 (23), 178.1 (16), 234.2 (15), 233.2 (3)
Gly5	17.51	17.55	462/ 642	**700.2**	334.0 (100), 526.1 (61), 508.2 (31), 654.2 (24), 262.1 (10), 682.2 (4)	334.1 →262.0 (100)	262.0 →262.1 (100), 206.2 (42), 234.1 (32), 178.3 (11), 216.0 (11), 207.1 (5)
Gly6	17.90	17.97	462/ 643	**700.2**	334.0 (100), 526.1 (40), 654.2 (30), 262.1 (16), 682.2 (5)	334.0 →262.1 (100)	262.1 →262.1 (100), 206.2 (32), 234.1 (20), 178.3 (15), 216.0 (13), 244.0 (2)
Gly7	18.28	18.33	462/-	**700.2**	334.1 (100), 526.2 (81), 508.2 (33), 262.1 (13), 352.1 (5), 654.2 (5), 682.3 (4)	334.1 →262.1 (100)	262.1 →262.1 (100), 206.1 (22), 216.1 (17), 234.1 (17), 178.1 (14), 151.1 (5), 188.1 (3)

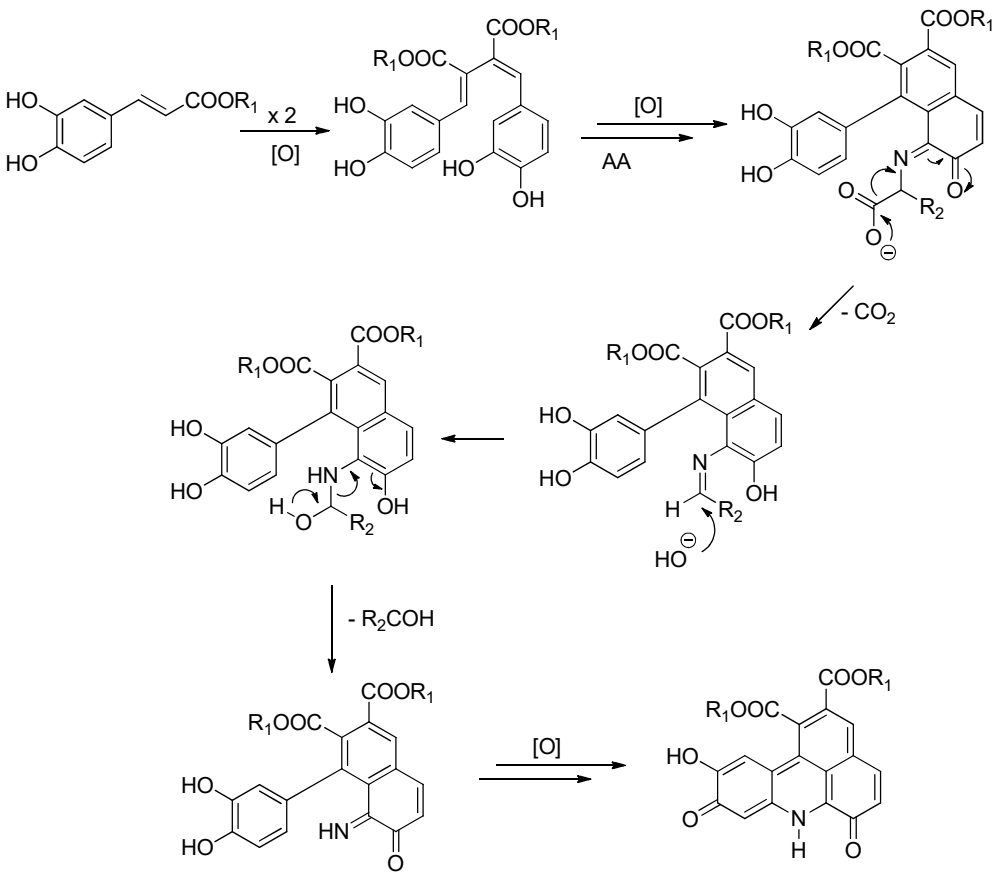

Scheme 4.3.1 *Proposed mechanicistic pathway for the decarboxylation and loss of the α-amino acid side chain occurring during the benzacridine formation steps*.

pH-dependence of the chromophore. The pH dependence of the chromophores from both the CGA-GLY and CGA-LYS pigments was systematically investigated. Figure 4.3.5 reports the absorption maxima of the purified CGA-LYS pigment at different pHs. Data indicate the existence of three prototropic forms of the benzacridine pigment: in the alkaline pH range 7-9 the species with visible absorption at 680 nm was dominant, but at pH 4 it was converted to a species with maximum at 620 nm, and at acidic pH below 2 the form with λ_{max} at 500 nm was prevalent. All the shifts proved to be reversible. The same shifts were observed in the case of the CGA-GLY pigment (Figure 4.4.13). Based on these and previously reported data, the species likely involved in the proton transfer equilibria are shown in figure 4.3.6.

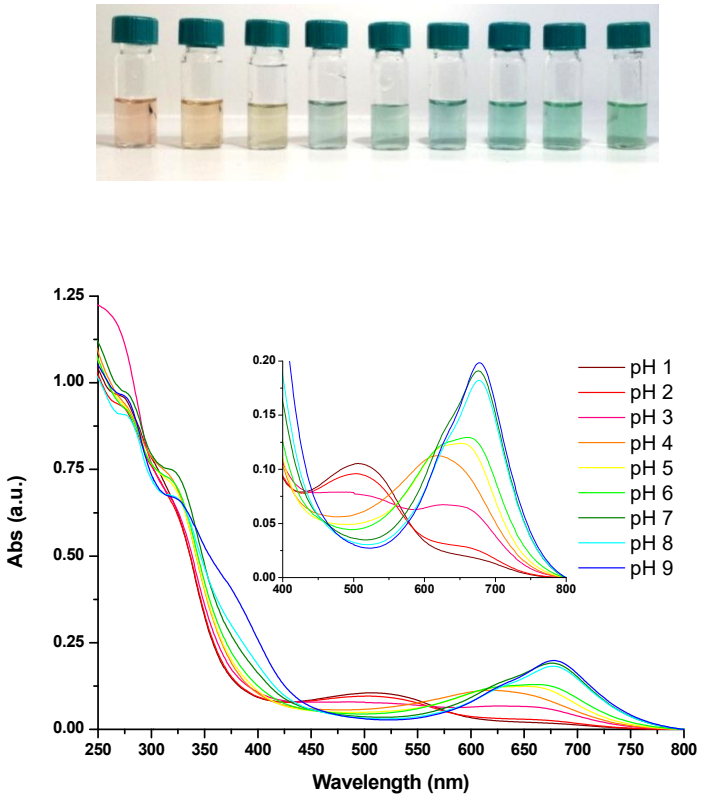

Figure 4.3.5 *Digital pictures (top) and absorption spectra (bottom) of 0.1 g/L solutions of the purified CGA-LYS pigment in 0.1 M phosphate buffers at pH ranging from 1.0 to 9.0.*

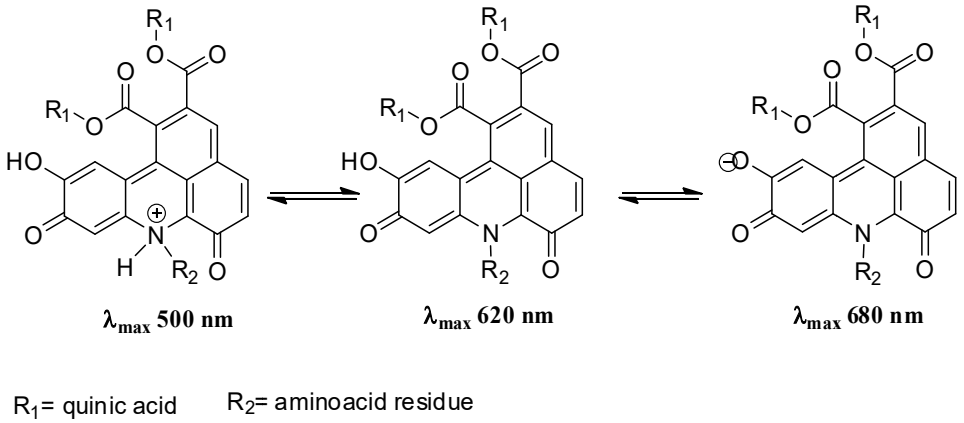

Figure 4.3.6 *Proposed prototropic species of the benzacridine pigments responsible for the absorption maxima observed at different pHs.*

Generation of the benzacridine pigment from proteins and protein-rich food matrices. The access to benzacridine pigment from low-cost easily available sources of amino acids was then explored with the view to assessing the potential of this reaction for food coloring. Initially CGA was reacted at 0.1 w/v % in the presence of bovine serum albumin (BSA) at 1% in aqueous solution pH 9 in air at room temperature. The green color increased over time showing an absorption

spectrum in the visible region almost identical to that of the pigment obtained with GLY or LYS with no further development after 24 h. At this time residual CGA was evaluated by HPLC analysis around 16%. By increasing the amount of CGA to 0.5 or to 1% the yield of the green pigment was not increased but the solution was yellow suggesting failure of the protein amino residues to divert the oxidation pathway of CGA toward benzacridine formation. Keeping the amount of CGA constant at 0.1% and varying the amount of albumin in solution, the intensity of the green color resulted to be of 0.24 and 0.38 for the reaction carried out with 1% and 5% albumin respectively (value of the absorbance at 680 nm normalized to starting CGA concentration of 0.1 g/L). Neither higher (10%) nor lower (0.5%) amounts of albumin resulted in green color development.

On this basis in further experiments chicken egg white (CEW, albumen) was used as the protein source. The intrinsically alkaline pH of this matrix allowed rapid development of the green pigment in the presence of 0.1% CGA. Solutions of albumen at different dilution in water from 1:1 (CEW50), 1:5 (CEW20) to 1:10 (CEW10) with CGA at 0.1% also yielded the green pigment with a linear increase of the absorbance at 680 nm (Figure 4.3.7, left). A significant and well appreciable development of the color was obtained using either lower or higher concentrations of CGA ranging from 0.05% to 1% (Figure 4.3.7, right). However, 5 fold excess of CGA (0.5%) did not lead to a linear increase of the absorbance at 680 nm. Residual CGA determined by HPLC analysis proved to be of 5.5% ± 1.0 in the case of the reaction carried out with 1% CGA, while it resulted under the detection limit in the other reaction conditions.

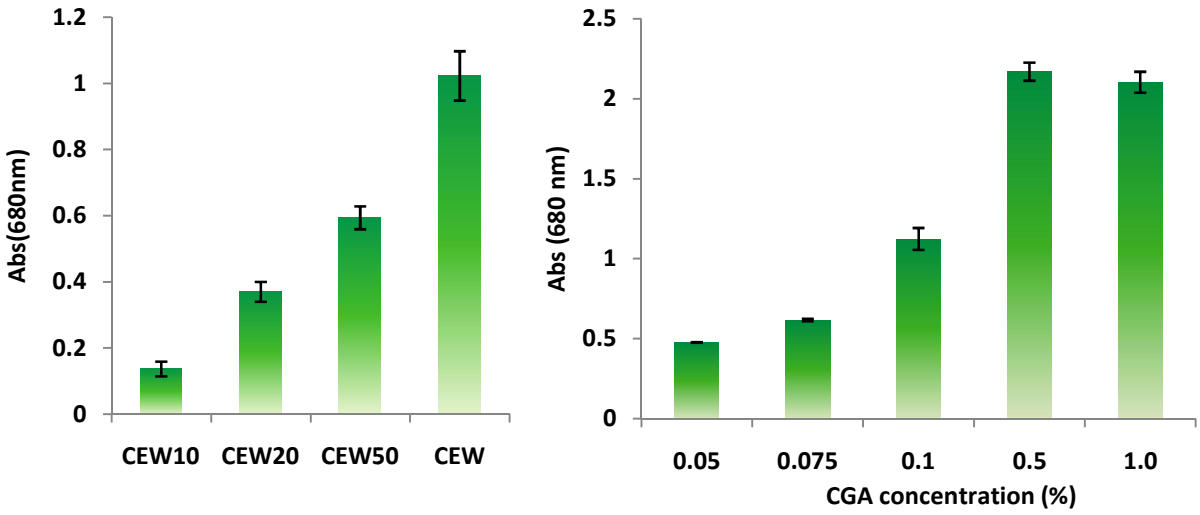

Figure 4.3.7 *Absorbance at 680 nm of CEW at different dilutions in water in the presence of CGA 0.1% at room temperature after 24 h (left) or CEW containing different amount of CGA (right). Spectra were recorded after 10-fold dilution in 50 mM carbonate buffer pH 9.*

Cytotoxicity assays. The toxicity of benzacridine pigments in on human intestinal CaCo-2 cells and hepatoma cell line (HepG2) was finally evaluated by the 3-(4,5-dimethylthiazol-2-yl)-2,5-diphenyltetrazoliumbromide (MTT) reduction assay at different times of incubation (see Methods, experiments carried out by Professor Pizzo and Dr. Valeria Pistorio, department of Biology, University of Naples Federico II). The assay was run on the pure pigments and the pigmented protein matrices as obtained from albumin or CEW. In all cases the amounts added to the cell culture was evaluated based on the absorbance at 680 nm. Different doses of CGA-LYS in the range 0.2- 5 μg/mL (A_{680} in the range 0.001-0.02) did not produce significant alteration of the cell viability in Hep G2, unless for a slight decrease only after 72 at the maximum dose tested. A similar behavior was observed in the case of CGA-GLY pigment. No toxic effects were obtained on CaCo-2 with either pigments, though also in this case after 48 h some decrease of viability was observed at the highest dose. Albumin at 1% with CGA at 0.1% and CEW-CGA 0.1% were also tested. Both pigments did not show toxicity on Hep G2 over the whole range of concentrations tested (Data not shown).

Food applications. In a final set of experiments purified benzacridine pigments were tested as food coloring agents in model systems. Figure 4.3.8A shows the CGA-LYS pigment incorporated at 0.5 % in beads of alginate hydrogels. Two different food matrices namely cow milk and soybean milk were then tested for coloring with the benzacridine pigments. An intense green color was obtained using as low as 0.05% of CHL-LYS pigment (Figure 4.3.8B,C). Similar results were obtained also with the CHL-GLY (Figure 4.4.14). A powder obtained from freeze drying of the green solution of CEW20 with CHL at 0.1% (1% extinction coefficient at 678 nm: 1.9 $\pm$ 0.085) was prepared and used at 1% to impart green coloring in cow milk (Figure 4.3.8D).

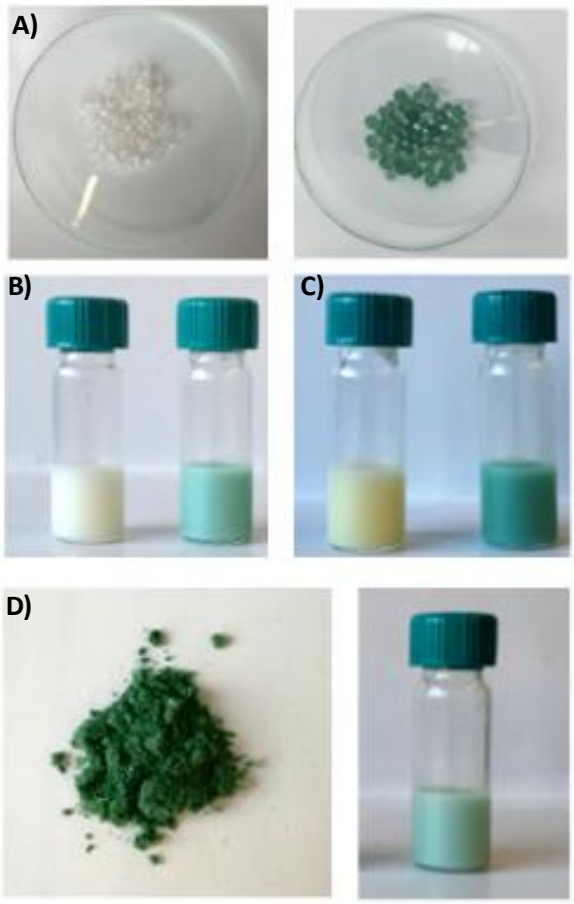

Figure 4.3.8 *Food coloring with benzacridine pigments. A) Calcium alginate hydrogel beads incorporating CGA-LYS pigment 0.5%; B)cow milk and C) soy milk, no addition (left) and with CGA-LYS (right) at 0.05%; D) Powder from CEW20 with CGA 0.1% (left) and the powder incorporated in cow milk at 1% (right).*

In order to assess the potential of the pigment as food colorant, its thermal stability was then investigated under different conditions. Figure 4.3.9A shows that the pigment developed in CEW with 0.1 % CGA does not show appreciable color changes with cooking. For thermal stability assessment, a diluted solution of CEW (CEW10) was reacted with CGA 0.1% and then exposed to a range of temperatures up to 90 degrees over 30 min no appreciable color modification occurred as assessed by visual inspection and spectrophotometric analysis (Figure 4.3.9B,C and Figure 4.4.15A). Finally also the stability in cow milk was assayed using CEW10 with CHL 0.1% as dyeing agent (Figure 4.3.9D and Figure 4.4.15B).

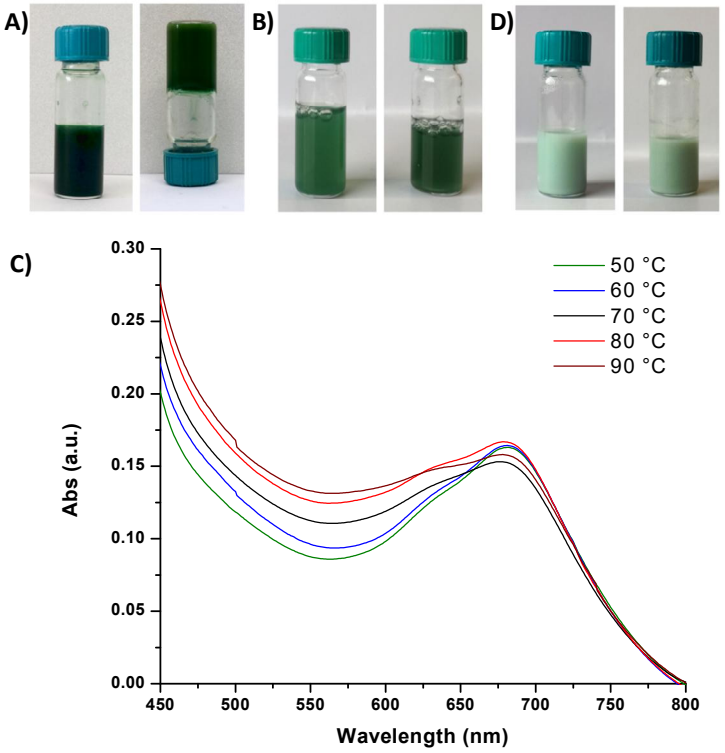

Figure 4.3.9 *A) CEW reacted with 0.05% CGA before and after cooking. Heating at different temperatures over 30 min of B) CEW10 with 0.1% CGA at r.t. (left) and 90 °C (right); C) Visible spectra of 10 fold diluted solution of CEW10-CGA 0.1% after exposure over 30 min at different temperatures; D) digital picture of CEW10 with CHL 0.1% in cow milk at 1:1 dilution at r.t. (left) and 90 °C (right).*

Sensing of food deterioration. In a final set of experiments, the utility of pH dependent color changes of the benzacridine pigments for sensing basic amine-containing volatiles (e.g., NH_3 and NMe_3) generated during food spoilage caused by microbial growth was preliminarily investigated. Filter paper sheets, silica gel plates or alginate hydrogel films loaded with an acidic aqueous solution of the CHL-LYS pigment were exposed to vapours from decomposing fish fillets at room temperature in a closed chamber. As a control, the same conditions at -20 °C under an argon atmosphere were selected. Figure 4.3.10 shows the shift after 48 h of the originally red color of the pigment at acidic pHs to the intense green associated to neutral and slight alkaline conditions.

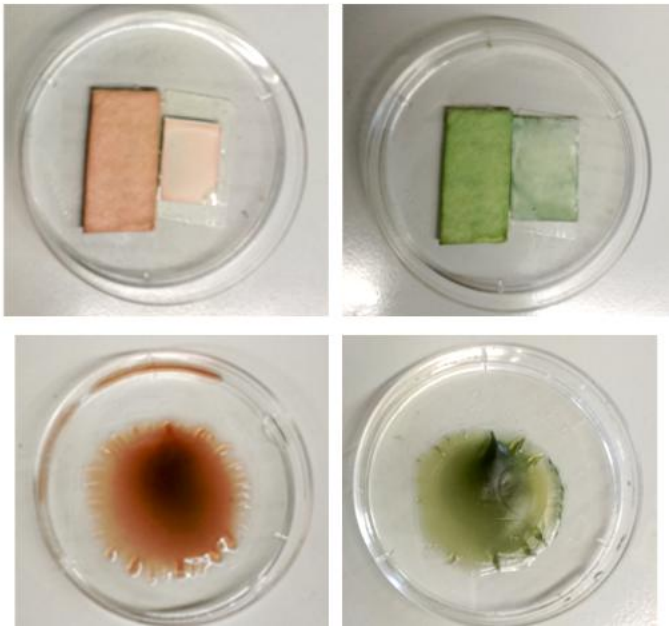

Figure 4.3.10 *Top: Filter paper sheets (left), silica gel plates (right) or Bottom: alginate hydrogel films loaded with an 1% aqueous solution of the CHL-LYS pigment at pH 3 exposed to decomposing fish fillets at T=0 (left) and T=48 h (right).*

In conclusion, the reaction leading to green trihydroxybenzacridine pigments by aerial oxidation of CGA in the presence of a source of primary amino groups under slightly alkaline conditions was re-examined and conditions were optimized. Gel filtration chromatography of the green reaction mixtures containing CGA-LYS pigment led to a satisfactory purification of the pigment with complete removal of CGA. The presence of the benzacridine components was further supported by the fragmentation pattern observed in the LC MS/MS analysis in full agreement with previous reports.[154,158,163] Green pigments were also produced from CGA and low cost proteins and protein-rich matrices such as chicken egg white CEW in the presence of very low amounts of CGA, corroborating potential use of these pigments as food coloring agent. Preliminary toxicity test indicated no toxic effect on two different cellular lines. Different food matrices commonly used for preparation of creamy desserts like cow and soy milk were imparted green hues on addition of the pure pigments or those obtained with diluted CEW. The low toxicity and thermal stability of these formulations over a range of temperature of relevance to industrial transformations or home cooking was satisfactory, at variance with what is observed in the case of the other commonly used natural green dyes like chlorophylls. In addition, benzacridine pigments hold promise also for exploitation in other food related applications such as the sensing of volatiles amines developed by fish decomposition.

4.4 Experimental methods and supporting information, *paragraph 4.2*

Materials. All reagents are purchased from commercial sources and used without further purification. Substrates (quartzes, silicon wafers and borosilicate coverslips) are cleaned by soaking in piranha solution (H_2SO_4/30% H_2O_2 5:1) overnight, then rinsed with distilled water and dried under vacuum.

General procedure for substrate coating. To a 1 mM, 10 mM or 50 mM solution of the appropiate amine (HMDA, ethylenediamine, butylamine or dodecylamine) in 0.05 M sodium carbonate buffer pH 9, CA, MC or dopamine are added under vigorous stirring in a 1:1 molar ratio. For PDA coatings a previously reported procedure is followed involving oxidation of dopamine at 1 mM concentration in 0.05 M TRIS buffer pH 8.5. Under these conditions no coating is obtained using CA or MC. In other cases the oxidation is run dissolving CA or MC in 1% NH_3 at 1 mM concentration. Substrates are dipped into the reaction mixture after complete dissolution of the catechol and left under stirring for 3~6 hours, then rinsed with distilled water, sonicated and dried under vacuum. For preparation of the coated cell culture plates, a solution of 1 mM HMDA and 1 mM CA in 0.05 M Na_2CO_3 buffer (pH 9) or 1 mM PDA in 0.05 M Tris buffer (pH 8.5, 15 mL) is poured into the plate and left overnight in air. After 24 h, the coated plates are extensively washed with water, sonicated and dried under vacuum.55-105 μm C_{18} silica gel resin (Millipore) is used as purchased. 650 mg of resin are suspended in a 1:1 solution of 25 mM HMDA and CA or 25 mM dopamine hydrochloride in 50 mM carbonate buffer (pH 9, 45 mL) under vigorous stirring. After 15 hours, the coated resins are filtered under vacuum and washed with water (4 x 10 mL) and methanol (1 x 5 mL). Washing solutions are monitored by UV-Vis spectrometry until no absorption is found in the eluates.

Sample preparation for MALDI-LDI-MS, FT-IR and CP-MAS NMR analysis. CA (540 mg, 3 mmol) is added to a solution of HMDA (348 mg, 3 mmol) in 0.05 M sodium carbonate buffer (pH 9, 300 mL) and the reaction mixture is left under stirring overnight. The deep green precipitate that separates is collected by centrifugation (5000 rpm, 4 °C, 15 minutes) and washed with distilled water (3 x 20 mL) (124 mg). MC (366 mg, 3 mmol) is dissolved in a 1% KCl solution (150 mL) and then added to a solution of HMDA (348 mg, 3 mmol) in 0.05 M Na_2CO_3 buffer pH 9 (150 mL), and the reaction mixture is left under stirring for 6 h. The orange precipitate that separates is collected by centrifugation (5000 rpm, 4 °C, 15 minutes) and washed with distilled water (3 x 20 mL) (225 mg). For LDI-MS analysis, a suspension of the solid in water (1 mg/mL), is loaded onto the target plate and allowed to dry before analysis. In the case of MALDI analysis 10 mg/mL 2,5-

dihydroxybenzoic in water is added to the suspension at a 1:1 ratio v/v. FT-IR and CP-MAS analysis are run on the solid samples after lyophilization.

Ellipsometry. Ellipsometric thickness of the films on silicon wafers is measured in air using a EL X-02C ellipsometer at a wavelength of λ = 632.8 nm and at an angle of incidence of 70°. Dry thickness values are estimated by numerical fitting of the ellipsometric data (Δ and ψ) to a four layer model (silicon/silica/film/air) taking 3.912, 1.4571 and 1 as refractive index (n) values for silicon, silica and air respectively. The films are assumed to be transparent and homogeneous with a negligible extinction coefficient (k_{film} = 0) and with an n value of 1.63. The parameters for the ellipsometry experiments are taken from our previous extensive ellipsometry studies on catechol layers. This model gave the best fit.[65]

Water contact angle. The water contact angles are measured on a KRÜSS DSA 10 Mk2 drop shape analysis system with 3 μL deionized water as the probe fluid. The average value of the water contact angle is obtained by measuring the same sample at 3-5 different locations on the modified silicon wafer.

Atomic Force Measurements. Measurements are conducted over modified silicon wafers using a Bruker Dimension Icon® with ScanAsyst in the tapping mode in air. An Olympus OMCL-AC160TS cantilever is used in non-contact mode (K = 42 N/m, range: 33.5 – 94.1 N/m, F_0 = 300 kHz, range: 278 – 389 kHz). The Root Mean Square roughness (RMS) values are determined using the following formula:

$$RMS = \sqrt{\frac{\sum_{i=1}^{N}(Z_i - Z_{ave})^2}{N}}$$

Z_{ave} is the average Z value within the given area, Z_i is the current Z value, and N is the number of points within a given area. Z_{limit}: 3 μm.

X-ray photoelectron spectroscopy. Measurements are performed on a Kratos AXIS Ultra DLD instrument using a monochromatic Al Kα x-ray source. Atomic composition (%) is measured for C, N, and O.

MALDI and LDI-MS analysis. Positive Reflectron MALDI and LDI spectra are recorded on a 4800 MALDI ToF/ToF instrument (Sciex). Spectrum represents the sum of 15,000 laser pulses from randomly chosen spots per sample position. Raw data are analyzed using the computer software provided by the manufacturers and are reported as monoisotopic masses.

Solid state CP-MAS NMR. NMR spectra are acquired on a Bruker Avance II 400 spectrometer equipped with a 4 mm Bruker MAS probe for solid samples. All spectra are recorded in cross polarization mode with a ^{1}H $\pi/2$ pulse width of 3.8 s and a relaxation delay of 5 s. For ^{13}C experiments a contact time of 2 ms and a spinning rate of 9 kHz are selected, for ^{15}N the contact time is set to 2.5 ms and the spinning rate is 6 kHz.

ATR/FT-IR analysis. Infrared spectra are acquired using a Thermo Fisher Nicolet 5700 spectrophotometer equipped with a Smart Performer accessory mounting a ZnSe crystal for the analysis of solid samples.

Metal binding.[159–161] 0.4- 1.8 mg of CA/HMDA or pDA in water (5 mg/mL) are finely suspended using a glass/glass potter and then added to 3 mL of a 100 μM solution of $FeCl_2 \bullet 4H_2O$ in water, under stirring. Control experiments are performed in the absence of material. After 5 min, the samples are centrifuged (3 min, 7500 rpm) and 100 μL of a 5 mM ferrozine aqueous solution is added to the supernatants. The absorbance at 562 nm is measured after 5 min. Experiments are run in triplicate. For the copper binding assay. 0.04- 0.18 mg of CA/HMDA or PDA are finely suspended in water (3 mg/mL) using a glass/glass potter and then added to 2 mL of a 66.7μM solution of copper(II) acetate in 50 mM phosphate buffer (pH 6.2), under stirring. After 5 minutes, the samples are centrifuged (3 min, 7500 rpm) and 75 μL of an aqueous solution of 4 mM pyrocatechol violet are added to the supernatants. Control experiments are performed in the absence of material. The absorbance at 616 nm is measured after 5 min. Experiments are run in triplicate. In other experiments, 3 mL of a 100 μM solution of Fe(II) in water or 2 mL of 66.7 μM solution of Cu(II) in 50 mM phosphate buffer (pH 6.2) are filtered through coated C_{18} silica (50- 100 mg for iron and 2- 50 mg for copper binding) using a 5 mL syringe equipped with a filter at a flux of approximately 1 mL/min. Metal concentration in eluted fractions is determined as described above. To determine the binding ability of the coated silica, 5 mg of CA/HMDA C_{18} or pDA C_{18} are incubated in solutions of Fe^{2+} in water or Cu^{2+} solutions in 50 mM phosphate buffer (pH 6.2) at concentrations of 10, 25, 50 and 100 μM (final volume of 20 mL). Suspensions are incubated for 2 h at 37 °C under stirring, then filtered through a nylon 0.45 μm membrane, and analyzed for metal concentration as described above. Metal chelation ability of the uncoated resin and of the filtering device are tested comparatively.

Organic dyes adsorption. pDA/Tris and CA/HMDA coated glasses are dipped in 0.4 mg/mL solutions of Congo Red or Methylene Blue in phosphate buffer (0.1 M, 20 mL, pH 7.0). After 15

min, the glasses are washed with distilled water and dried under vacuum, UV-vis spectra are recorded.

Cell cultures. The HaCat cell line is maintained in our laboratory. Cells are cultured in Dulbecco's Modified Eagle's Medium (DMEM, Gibco) supplemented with 10% fetal bovine serum (Euroclone) and penicillin (100 U/mL) / streptomycin (100 mg/mL). Cells are maintained at 37 °C under a 5% CO_2: 95% air humidified atmosphere. Cell growth rate experiments are performed using untreated coverslips (control), or CA/HMDA or pDA/Tris coated coverslips. All coverslips are placed in a 24 well plate and re-sterilized by UV before use. Cells are then seeded onto coverslips (30,000 cells/1 mL DMEM for each coverslip) and grown for 24, 48 and 72 hours in a 5% humidified CO_2 incubator at 37 °C. Cell counts are performed in triplicate on days 1, 2 and 3. Cell morphology is observed by inverted microscope. The murine Embryonic Stem Cells (ESCs) line E14Tg2a.4 derived from strain 129P2/OlaHsd, is cultured for two passages on feeder-free low adhesion plates coated with either gelatin, CA/HMDA or PDA/Tris. The cultures are subsequently maintained in complete Embryonic Stem (ES) medium: Glasgow Minimum Essential Medium (GMEM, Gibco), 15% Fetal Bovine Serum (FBS, EuroClone), 1,000 U/mL Leukaemia Inhibitory Factor (LIF) (EuroClone), 1.0 mM sodium pyruvate (Invitrogen), 0.1 mM non-essential amino acids (Invitrogen), 2.0 mM L-glutamine (Invitrogen), 0.1 mM β-mercaptoethanol and 500 U/mL penicillin/streptomycin (Invitrogen). ESCs are incubated at 37 °C in 6% CO_2; medium is changed daily and cells are split every 2 to 3 days routinely.

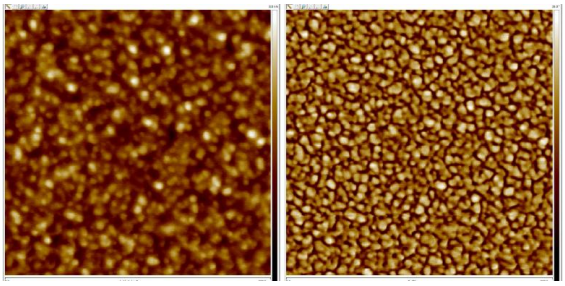

Figure 4.4.1 AFM *images of thin films from CA/HMDA on silicon wafer.Topography on the left side, phase contrast on the right side. 500 nm x 500 nm.*

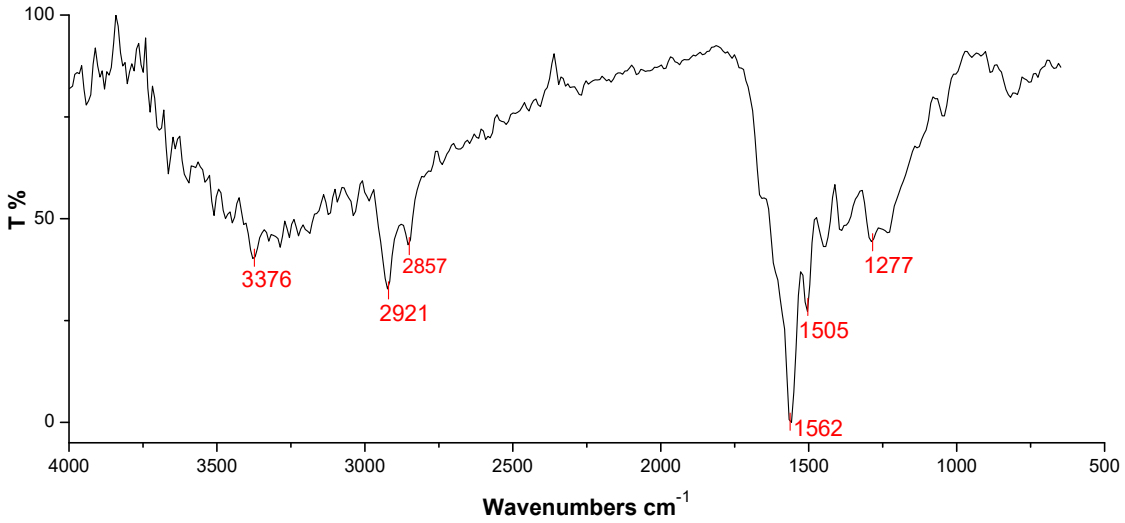

Figure 4.4.2 *ATR/FT-IR spectrum of the solid separated from the CA/HMDA mixture after centrifugation and washings with water.*

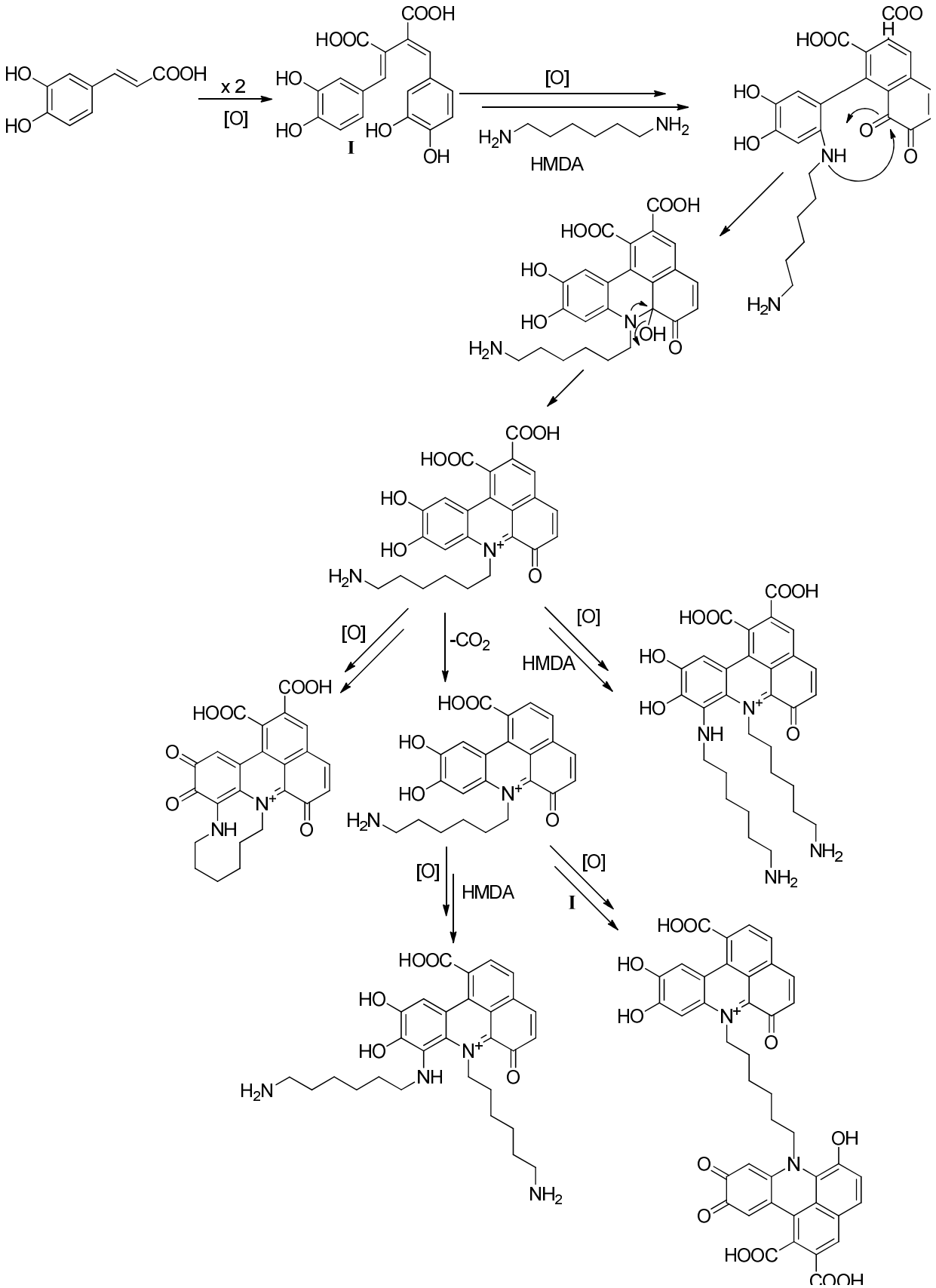

Figure 4.4.3 Proposed mechanistic route to the structures shown in Figure4.2.5.

Table 4.4.1. Characterization of thin films from MC/HMDA. Measurements performed on coated silicon wafers.

Film	Thickness (nm)	Roughness (nm)	Water contact angle (deg)	Comp.(atom, %)
Methylcatechol/ HMDA (region 1)	11.3 ±0.4	4.9	89.0 ± 1.0	C 1s 31.6 ± 6.6 O 1s 44.5 ± 3.9 N 1s 1.3 ± 0.2
Methylcatechol/ HMDA (region 2)	27.2 ± 1.2	4.1	64.0 ± 0.1	

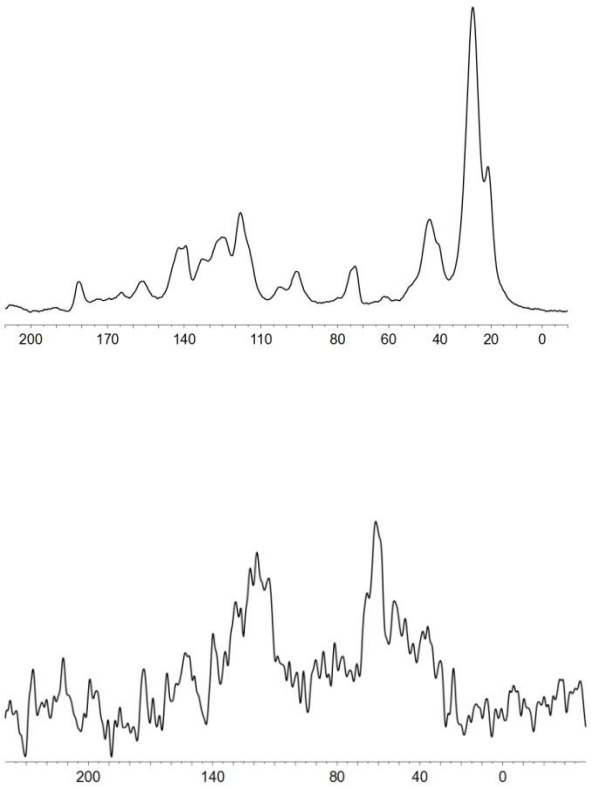

Figure 4.4.4 *(up) ^{13}C and (down) ^{15}N CP-MAS NMR spectra of MC/HMDA polymer.*

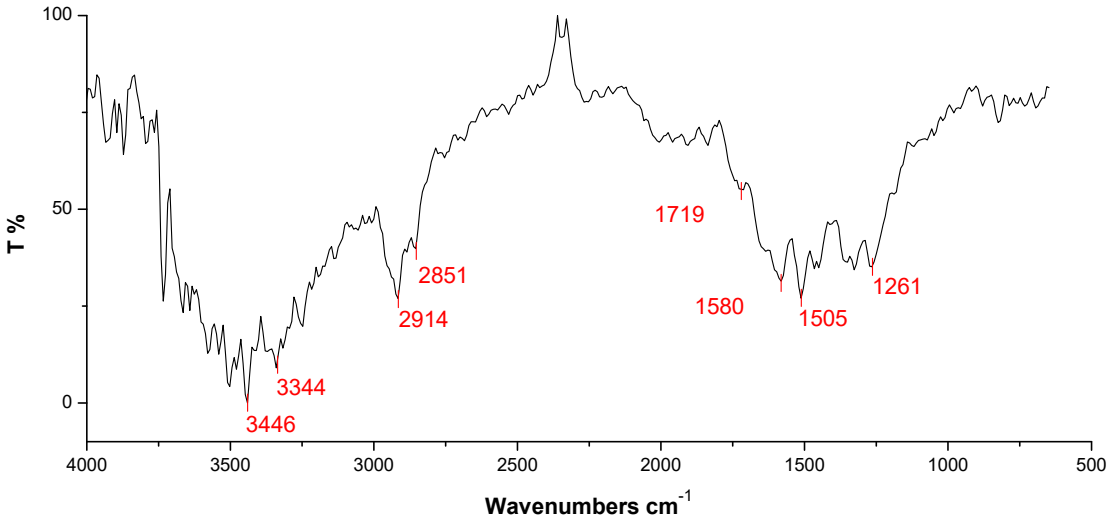

Figure 4.4.5 *ATR/FT-IR spectra of the solid separated from the MC/HMDA (down) mixture after centrifugation and washings with water.*

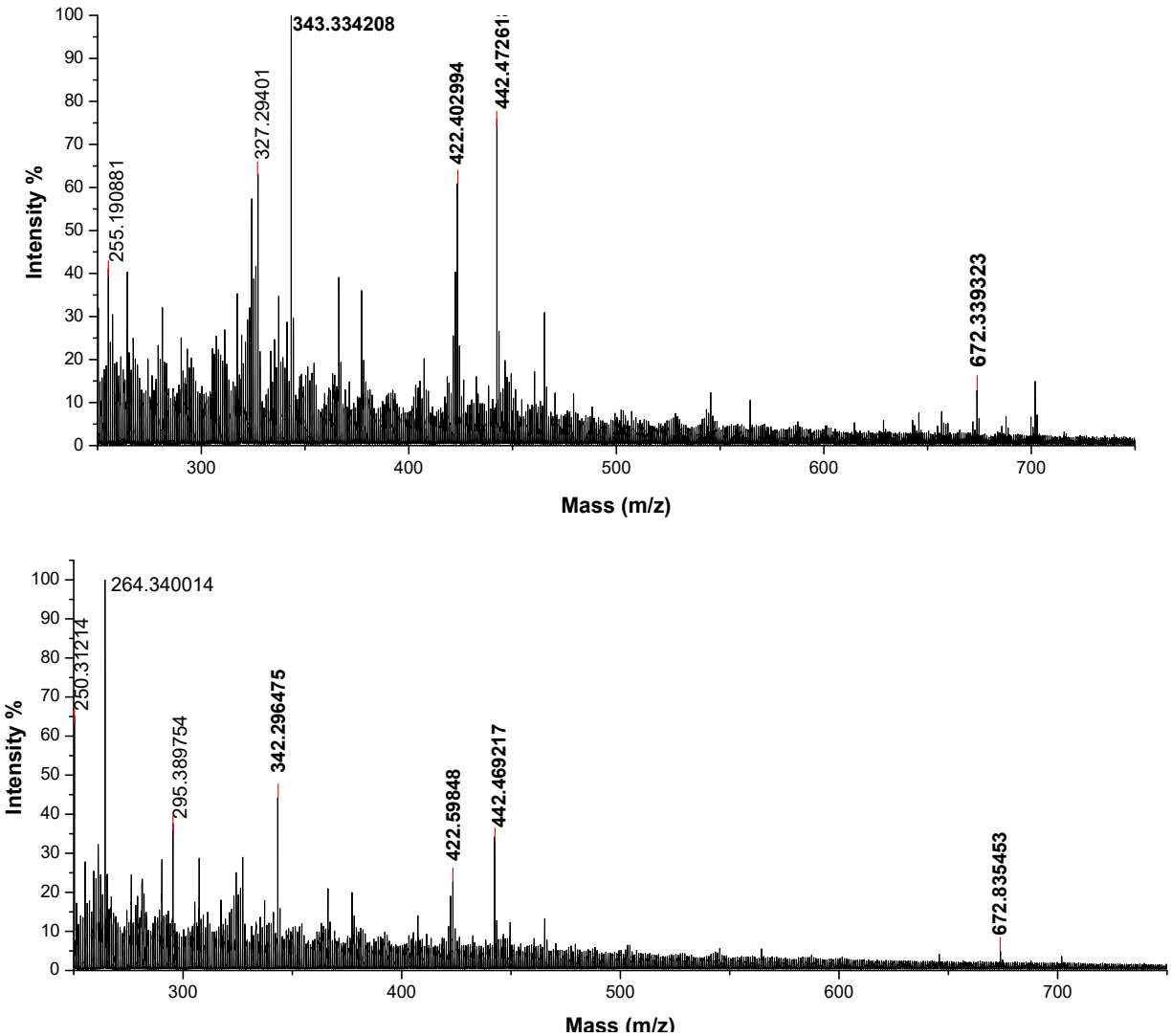

Figure 4.4.6 *MALDI-MS (top) and LDI-MS (bottom) spectra of the solid separated from the MC/HMDA mixture after centrifugation and washings with water. Enbolded are the molecular peaks that have been structurally assigned in the main text.*

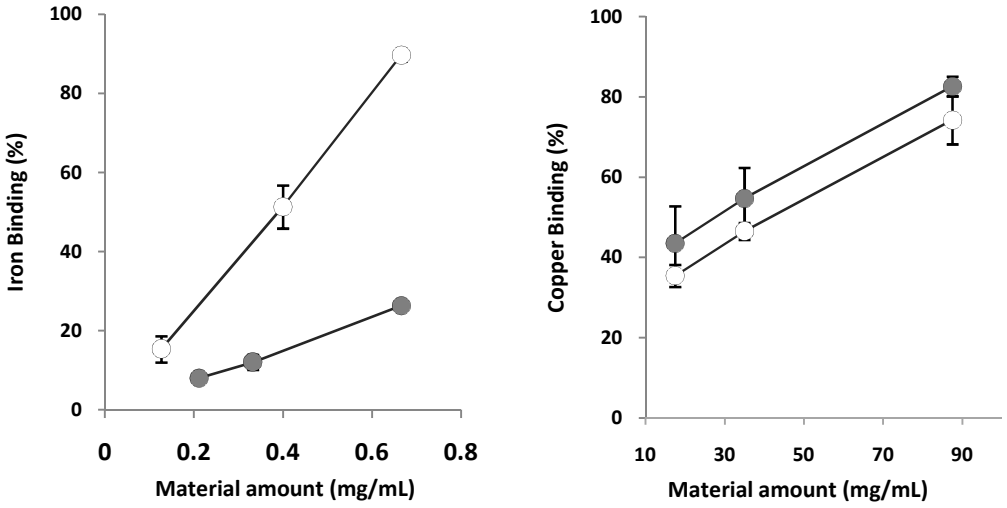

Figure 4.4.7 *Binding of iron (left) and copper (right) by CA/HMDA (open circles) and PDA (full circles) at variable solid material amounts.*

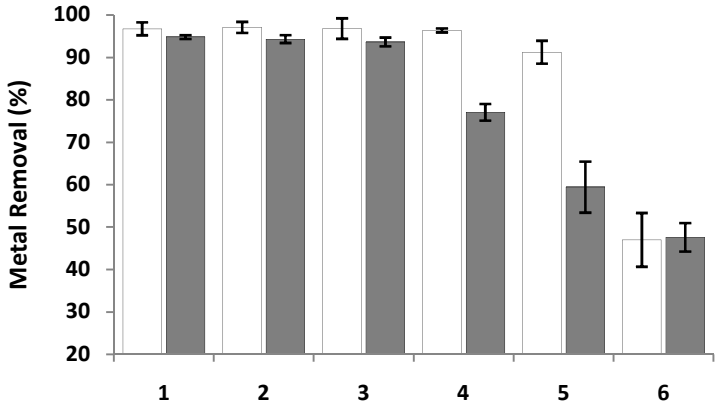

Figure 4.4.8 *Binding of iron (white bars) and copper (grey bars) by respectively 100 and 50 mg of CA/HMDA coated C_{18} during 6 elution of 3 mL 5.6 mg/L iron solution and 4.2 mg/L copper solution. Shown are mean values of two separate experiments ± standard deviation (SD).*

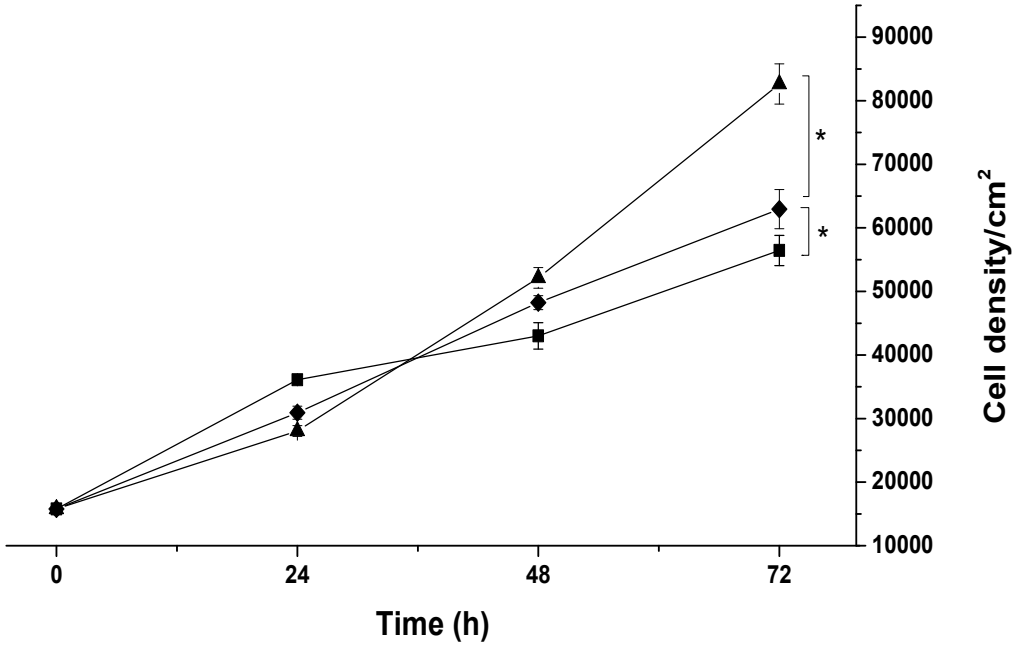

Figure 4.4.9 *Growth curve of HaCaT cells during 72 h. Cells (3x10^4) were seeded on low adhesion (■), coated PDA (♦) or coated CA/HMDA (▲) plates and triplicate cultures counted at daily intervals. (*) Welch t-test p-value < 0.01.*

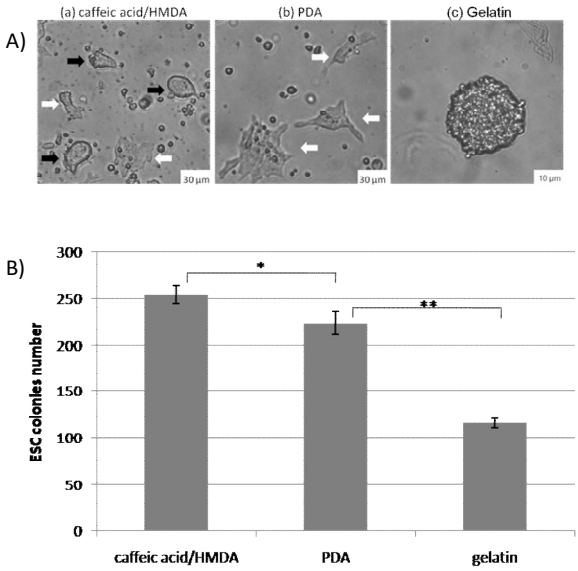

Figure 4.4.10. *(A) From left to right: ESCs grown on cell cul-ture low adhesion plates coated with: CA/HMDA (a), PDA (b), and gelatin (c). Black arrows: round-shaped, white arrows: flat-shaped ESC colonies. (B) Quantitative colony number analysis per 1.2 x 106 E14Tg2a.4 mouse ESCs on cell culture plates coated with CA/HMDA (254 ± 10), or with PDA (223 ± 12), or with gelatin (116 ± 5). ESC colonies in 3 (10×) microscopic fields are counted. Colony numbers are expressed as mean ± standard deviation (n = 3). Welch Two Sample t-test: (*) p-value = 0.02968; (**) p-value = 0.001818.*

Experimental methods and supporting information, paragraph 4.3

Chemicals. All reagents were purchased from commercial sources and used without further purification. Bovine serum albumin (BSA), chlorogenic acid (CGA) were from Sigma-Aldrich.Chicken egg white (CEW), bovine and soy milk were purchased from local markets**.**

General Experimental Methods. Gel filtration was carried out on Sephadex G-10 using water as the eluant. A LLG unistirrer 5 plate equipped with a remote PT-1000 temperature probe was used for thermostability assays. UV-vis absorption spectra were registered at room temperature on a V-560 JASCO spectrophotometer using calibrated 2 mL quartz cuvettes. HPLC analyses for reaction monitoring and determination of residual CGA were performed on an Agilent 1100 series instrument equipped with an LC-10AD VP pump and a G1314A UV-Vis detector using a Sphereclone C_{18} column (4.6 x 150 mm, 5 μm), 0.5 % formic acid – acetonitrile (ACN) from 0% to 90% in30 min was selected as the eluant, flow rate: 0.7mL min^{-1},detection wavelength 330nm.

General procedure for the preparation of the benzacridine pigments. The reactions were carried out according to previously reported procedures.[150,158] Entry #1 in Table 1: Equimolar mixture of CGA and GLY at 20 mM in 0.1 M Na_2CO_3buffer pH 9.0 was heated at 50°C for 2hunder air bubbling. Entry #2-5: Aqueous solutions of GLY or LYS(112 or 28 mM) and CGA at 28mM were mixed at a ratio of 1/1 (v/v). The resulting mixtures were adjusted to pH 9 with 0.1MNaOHat start and after 10 and 30 min. The samples were stirred up to 48 h at room temperature. In other experiments, CGA (0.1, 0.5 or 1% w/v) was added to albumin (0.1, 0.5, 1, 5% w/v) in water (10 mL) and the pH of the reaction mixture was adjusted to 9with 0.1MNaOH.Similarly, CGA was added to pure CEW (10 mL) at 0.05, 0.075, 0.1, 0.5 or 1% w/v, or, at 0.1 % concentration in CEW diluted at 1:10(CEW 10), 1:5 (CEW20), 1:1 (CEW50) in water (10 mL). Mixtures were allowed to react for 24 h at r.t., under stirring.

Purification of CGA-GLY/LYS pigments. 0.50 g of CGA were reacted with 0.12 g or 0.26 g of GLY and LYS respectively, under the reaction conditions of entry 3 and 5. After 36 h, reaction mixtures were concentrated and loaded on a Sephadex G-10column (60 x2.5 cm) using water as the eluant. 20 fractions (5 mL each) were collected and analysed spectrophotometrically. Fractions 4-8 (CGA-GLY) or 3-12 (CGA-LYS) showing the highest absorbance at 680 nm and a 680 /330 nm ratio higher than 0.4 (CGA-GLY) or 0.3 (CGA-LYS) were combined and lyophilized to give 300 mg (60% w/w yield) of the CHL LYS pigment and 100 mg (20 % w/w yield) of the CHL-GLY pigment. Purification of the pigmented material from 1% Albumin 0.1% CGA was likewise

performed by loading 2 mL of the reaction mixture on a 10x 0.5 cmSephadex G-10 column. The green fraction was analyzed by HPLC for evaluation of residual CGA and used for cellular assays.

LC-MS analysis of benzacridin derivatives were performed on an Waters Acquity UPLC system (Milford, MA, USA) including a binary pump (BSM), an autosampler (SM; cooled to 20 °C), a column oven (CM) set to 40 °C and a diode array detector (PDA) scanning from 200 to 800 nm. Separation was conducted on an AcquityHSS T3 RP 18 column (150 × 2.1 mm, 1.7 µm) and an AcquityHSS T3 RP 18 precolumn (5 × 2.1 mm, 1.7 µm) both by Waters with water (A) and acetonitrile (B) as eluents, both acidified with formic acid (0.1 %). The flow rate was set to 0.4ml/min with a gradient elution:0 min, 2%B; 20 min, 18%B; 23 min, 100%B; 25 min, 100%B; 26 min, 2%B; 28 min, 2%B. A LTQ XL linear ion trap by Thermo Scientific (Waltham, MA, USA) with an electrospray interface operating in positive ion mode was used. The MS settings were as follows: source voltage: 3.0 kV; sheath gas flow: 60 arb; auxiliary gas flow: 8 arb; sweep gas flow: 1 arb; capillary temperature: 350 °C; capillary voltage: -25.0 V; multipole 00 offset: +5.0 V; multipole 0 offset: +5.75 V; multipole 1 offset: +8.0 V; front lens: 6.25 V; normalized collision energy: 35%.

Cytotoxicity assays. Cytotoxicity of the pigments either pure or generated in the protein matrices on human epithelial colorectal adenocarcinoma cells (CaCo-2) and on human liver cancer cells (HEP-G2) was assessed by performing the (3-(4,5-dimethylthiazol-2-yl)-2,5 diphenyltetrazolium bromide (MTT) reduction inhibition assay. Both human cell lines were obtained from the A.T.C.C. (American Type Culture Collection, Manassas, VA, USA) and grown at 37°C in a humidified incubator containing 5% CO_2 in Dulbecco's modified Eagle's medium (DMEM) supplemented with 10% fetal bovine serum, 4 mM glutamine, 400 units per ml penicillin and 0.1 mg mL^{-1} streptomycin. The cells were plated on 96-well plates at a density of $5x10^3$ per well in 100 µL of medium. After 24 h, different amounts of the pure pigments or the pigmented protein matrices or of the non-pigmented matrices as a control were added. In all cases the amount of the pigmented material tested was normalized on the absorbance at 680 nm. After 24, 48 and 72 h of incubation, 10 µL of a 5 mg ml^{-1} MTT stock solution in DMEM without red phenol, corresponding to a final concentration of 0.5 mg L^{-1} in DMEM (final volume of 100 µL) were added to the cells. After 4 h incubation, the MTT solution was removed and the MTT formazan salts were dissolved in 100 µL of 0.1N HCl in anhydrous isopropanol. Cell survival was reported as the relative absorbance, with respect to control, of blue formazan measured at 570 nm with Synergy Multi Plate Reader. The contribution by the benzacridine pigments to the formazan absorption at 570 nm was negligible at

the highest concentrations tested. Cytotoxicity experiments were performed at least three times independently. Standard deviations were always <5% for each experiment.

Food related applications. For preparation of alginate hydrogels, CHL-LYS was dissolved in water at 0.5%, then sodium alginate was added (2% w/w). Beads were prepared dropping the freshly prepared gel in a 0.1 M solution of $CaCl_2$ allowing alginate reticulation for few minutes followed by beads filtration. Films were similarly fabricated spreading the gel on a smooth surface followed by dipping in the $CaCl_2$ solution for about 60 s. Exposure to decomposing fish fillets was carried out in sealed Petri dishes at room temperature.

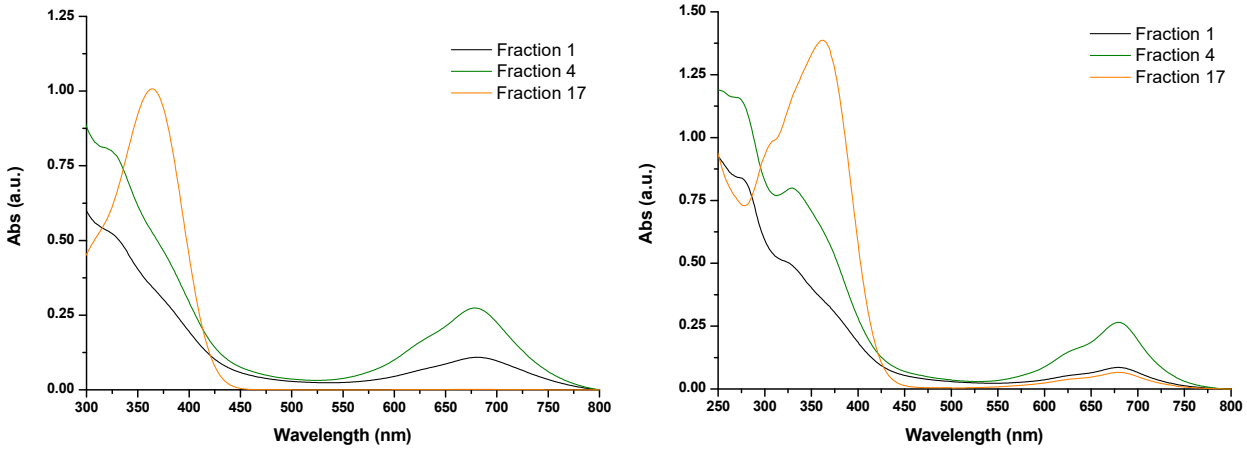

Figure 4.4.11 *UV-vis spectra of representative fractions from CGA-LYS (left) and CGA-GLY (right) chromatographic purification. Spectra were recorded after 40 fold dilution of the original solutions in 50 mM Na_2CO_3 buffer pH 9.*

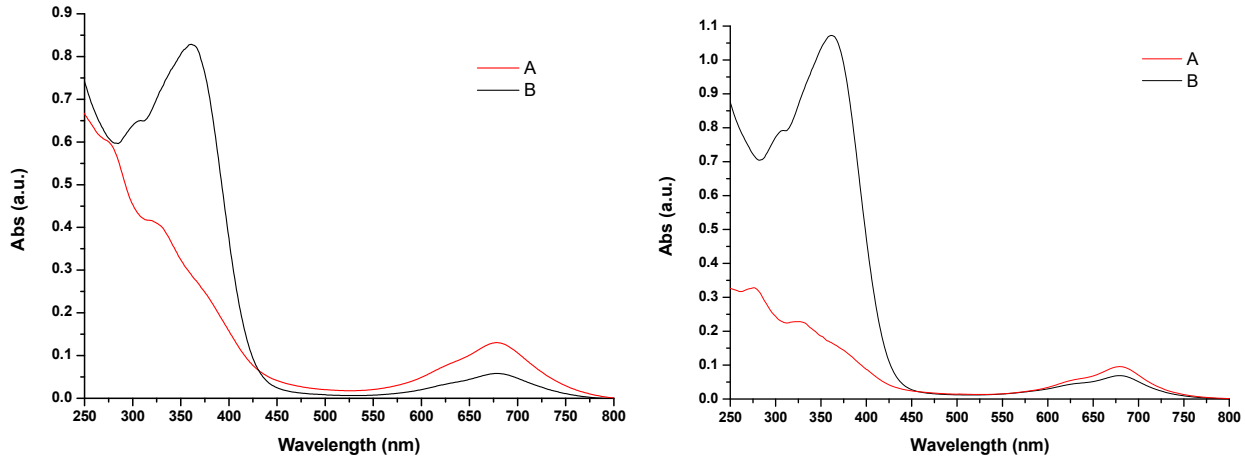

Figure 4.4.12 *UV-vis spectra of purified pigments (A) or reaction mixtures (B) of CGA-LYS (left) or CGA-GLY (right). Spectra were recorded on 0.1 g/L solutions of lyophilised samplesin 50 mM Na_2CO_3 buffer pH 9.*

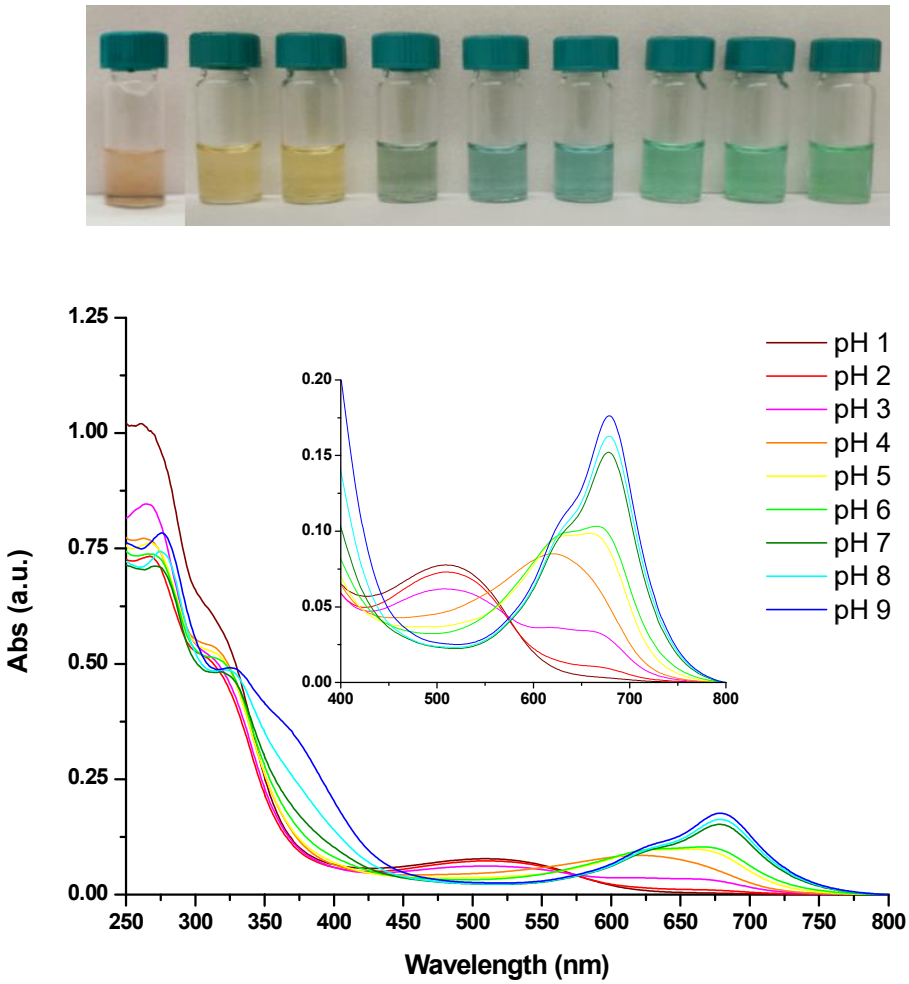

Figure 4.4.13 *Digital pictures (top) and absorption spectra (bottom) of0.1 g/L solutions of the purified CGA-GLY pigment in 0.1 M phosphate buffers at pH ranging from 1.0 to 9.0.*

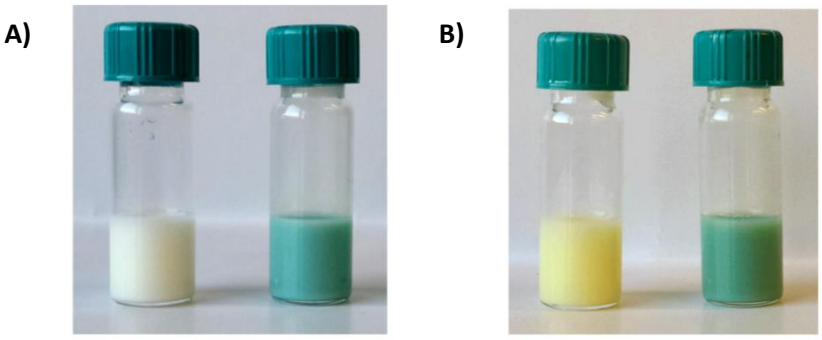

Figure 4.4.14 *Food coloring applications. A) cow milk and B) soy milk, no addition (left) and with CGA-GLY pigment (right) at 0.05%.*

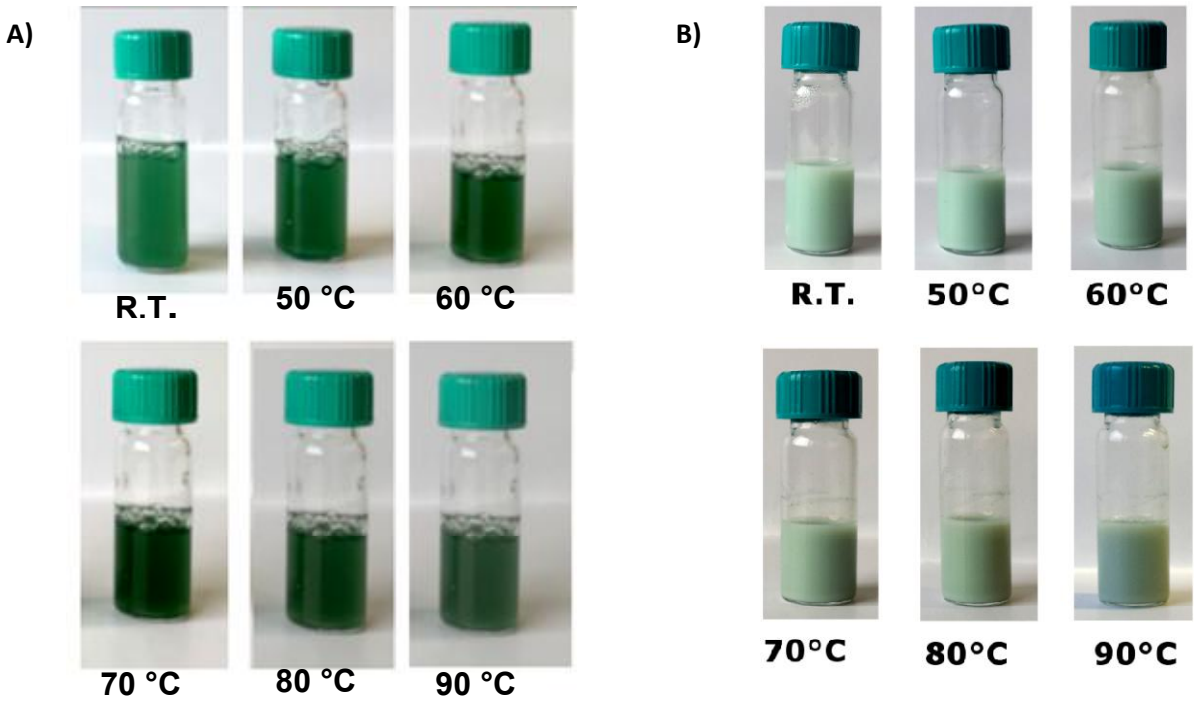

Figure 4.4.15 *Digital picture of A) CEW10 with 0.1%CGA and B) CEW10-CGA 0.1% dilute 1:1 in Cow Milk, after 30 min heating at different temperatures.*

Chapter 5

Dopamine-based multifunctional fluorescence turn-on systems

5.1 Introduction

The advancing developments in fluorescence-based analytical, imaging and functionalization techniques have spurred increasing efforts toward the design of highly efficient, robust and versatile chromophores and complexes which respond to specific recognition events or stimuli with a strong emission (the "turn-on" modality). The advantages of fluorescence "turn-on" related to "turn-off" systems are manifold and include mainly the easier determination of low-concentration contrast relative to a "dark" background, reducing the effects of false positive signals and increasing both sensitivity and specificity. Compared to the turn-off approach, which usually requires quenching or switching of a preformed fluorophore, fluorescence turn on is less straightforward and is achieved in most cases by use of preformed emitting systems, e.g. perylene or fluorescein derivatives, via removal of specific quenchers. Conversely, relatively few reports deal with reactivity-based fluorescence turn-on systems. Representative examples include the generation of fluorescent triazoles by reaction of non-emitting o-diaminoaromatics with nitric oxide-derived nitrosating systems,[168] 2-ethynyl-benzothiazolederivatized 'click-on' fluorogenic dyes for cellular imaging,[169,170] fluorogenic azide probes activated by click chemistry,[171,172] the oxidative cyclization of non emissive azo-anilines into highly fluorescent benzotriazoles for Cu(II) sensing,[173,174] and tandem reaction cascades to unmask a fluorogenicscaffold.[175] Although several modifiable platforms have become available for turn-on responses, including BODIPY,[176] fluorescein,[177] because of the increasing importance gained by reaction-based fluorescence turn on systems for a variety of applications, there is considerable interest in the development of novel efficient fluorophore-generating processes that can be triggered in response to specific stimuli and that can be applied for thin film deposition or for inclusion in hydrogels and biomatrices without significant loss of properties.

A unique, still little explored source of inspiration for novel strategies and solutions in the field of functional materials and systems is offered by the broad pool of natural products and biologically relevant systems. In line with this view, our entry to novel fluorescence turn-on systems was inspired by an early observation showing that autoxidation of natural catecholamine compounds, such as the amino acid L-dopa and the neurotransmitter dopamine (DA), in the presence of

phloroglucinol and other resorcinol derivatives, leads to the efficient formation of strongly fluorescent methanobenzofuroazocinone coupling products (Scheme 5.1.1).[72]

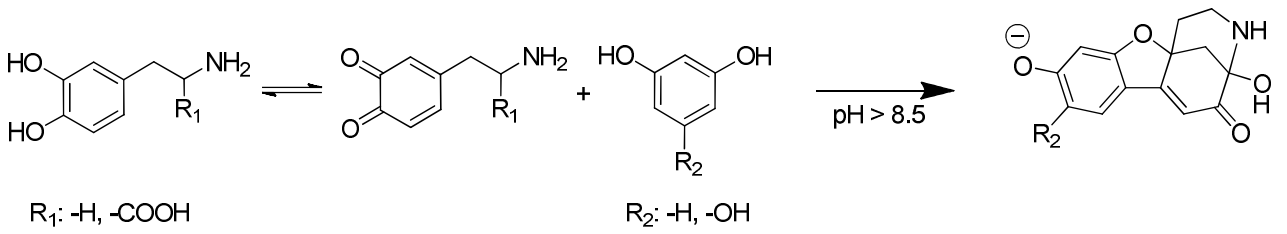

Scheme 5.1.1 *The reaction of catecholamines with resorcinol derivatives to give fluorescent methanobenzofuroazocinone coupling products.*

The first step of the reaction involves nucleophilic attack of the resorcin ring onto the electrophilic moiety of the transient o-quinone produced by oxidation of the catecholamine. A second oxidation step generates the furan ring via intramolecular attack by the OH group to an o-quinone intermediate. Finally intramolecular attack by the ethylamine side chain leads to ring closure of the azocine system and development of fluorescence.

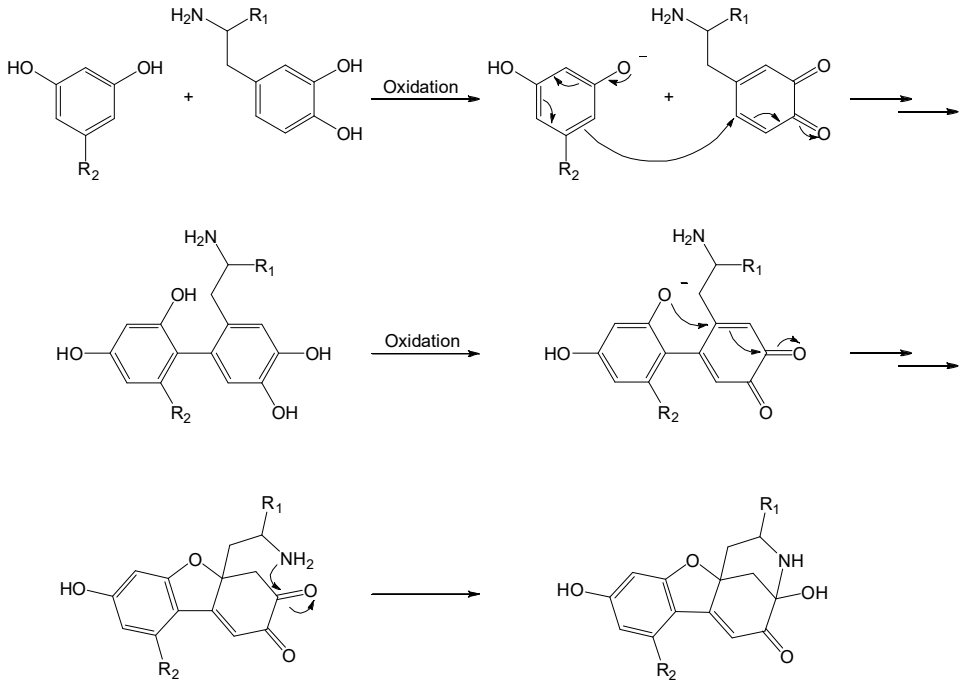

Scheme 5.1.2 *Proposed mechanism of the reaction of DOPA (R_1= -COOH) or dopamine (R_1= -H) with resorcinol (R_2= H) or phloroglucinol (R_2= -OH) to give fluorescent methanobenzofuroazocinone coupling products.*

This unusual scaffold is akin to that of matlaline, the fluorescent product produced in the infusion known as lignum nephriticum. Since many centuries ago, it was known that the alkaline infusion of the wood of a Mexican tree (*Eysenhardtia polystachya)* used by Aztecs to treat kidney diseases and later classified in Europe as *Lignum nephriticum* exhibits a strong blue fluorescence.[178,179] In 2009, Acuña *et al.* retraced the botanical history of *L. Nephriticum* and isolated from this wood two possible bio-synthetic precursors of the fluorophore: coatline A (**1**) and coatline B (**2**) (Figure 5.1.1).

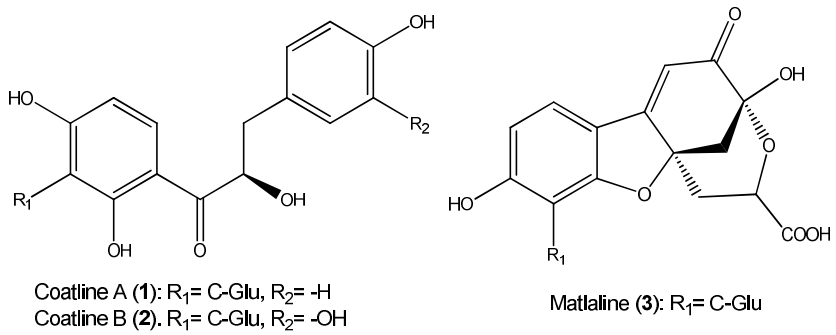

Figure 5.1.1 *Matlaline (3) and its putative biogenetic precursors*.

The authors found that an aqueous solution of **2** at slightly alkaline pH undergoes a fast, irreversible reaction giving rise to a strongly blue-emitting compound with ca. 100% yield, matlaline (**3**), which matched the fluorophore of the *L. Nephriticum* featuring a methanobenzofuroazocinonic aglycone (Scheme 5.1.3). Under the same conditions, **1** proved to be unreactive confirming the hypothesized reaction mechanism triggered by the ionization of **2** at the 4′ position in neutral or slightly alkaline medium (pK′a) 6.5 (0.2).[180]

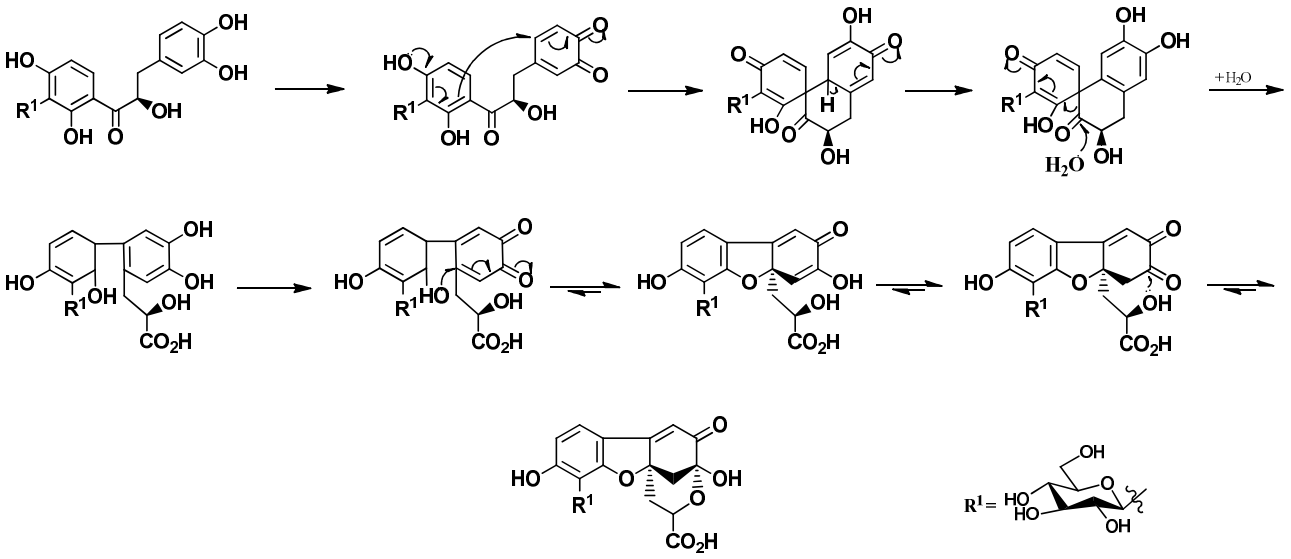

Scheme 5.1.3 *Plausible sequential reaction from Coatline B to Matlaline.*

In a recent reexamination of this chemistry, to include the aza analog described by our group, it was demonstrated that the fluorophore can exist in different prototropic species, of which only the anion form is strongly blue emitting.[181] Despite high emission quantum yield in water, pH-dependent switching between bright and dark states, and full compatibility with aqueous solvents, the potential of this fluorogenic reaction for turn-on sensing and other applications has remained virtually unexplored. The only relevant report deals with use of this chemistry for the fast and low-cost turn-on fluorescence detection of dopamine.[182]

Accordingly, in the present PhD thesis the attention was directed to the potential use of resorcinol derivatives as a means of manipulating catecholamine-based processes to implement novel reaction-based fluorescence turn on systems of biomedical and technological relevance.

Besides DOPA, other catechol-containing compounds are able to react with resorcinol to give fluorescent adducts such as: hydroxytyrosol, salvianic acid, and dopamine.[181] Noteworthy, equimolar amounts of resorcinol can efficiently inhibit the autoxidative conversion of dopamine to black, insoluble PDA at alkaline pH leading to the strong fluorophore in high yields.
The high emission quantum yield in water (~50%, pH 9), pH-controlled reversible switches between bright and dark states, and full compatibility with aqueous solvents suggested the potential of this fluorogenic reaction for turn-on sensing and other applications.

In this chapter, the design, synthesis and characterization of resorcinol-based couplers for the catecholamine dopamine will be discussed, as an entry to reaction-based fluorescence turn-on systems for novel functionalization and sensing applications.

Specific aims of this study are:

1) to investigate the scope of dopamine-resorcinol chemistry for fluorescence turn on systems;
2) to develop fluorescent surface functionalization and coating methodologies based on the rational design of resorcinol-based cross-linking compounds;
3) to probe the performance of the system in bio-based hydrogels, as a step toward implementation of amine-sensing devices and smart packaging components.
4) to develop a reaction-based fluoresce turn-on tagging system via functionalization of an amine-rich polymer with a carboxylated resorcinol derivative and subsequent “trapping” of dopamine

5.2 Results and discussions

Reexamination of the catechol-resorcinol reaction: behaviour in acids and substrate selectivity. Figure 5.2.1 shows the typical course of autoxidation of 1 mM dopamine in 0.05 M ammonium bicarbonate (pH 8.5) at room temperature in the absence and in the presence of equimolar resorcinol. Data showed complete suppression of the broadband eumelanin-like absorption profile of PDA and its replacement by a yellow chromophore at 420 nm strongly emitting at 460 nm. As expected, emission was completely quenched at acidic pH, an effect that was attributed to suppression of ionization[181] and not to any acid-promoted ring opening of the methanobenzofuro[2,3-d]azocin-5(2H)-one scaffold (Figure 5.2.2).

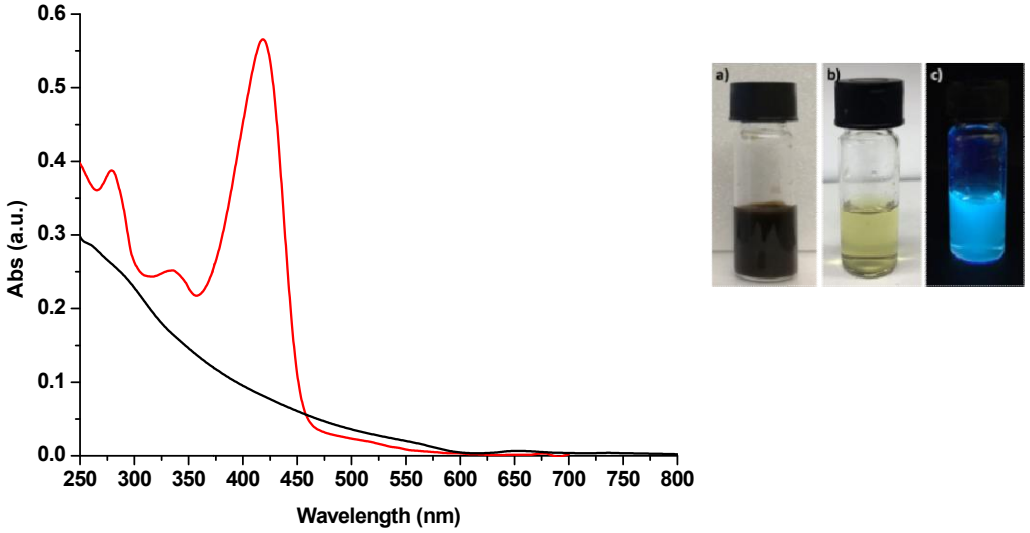

Figure 5.2.1 *UV-Vis spectra and digital pictures of DA oxidation mixtures in the absence (black trace, picture a) or in the presence of equimolar resorcinol (red trace, picture b and c, respectively under natural light and 365 nm emitting lamp).*

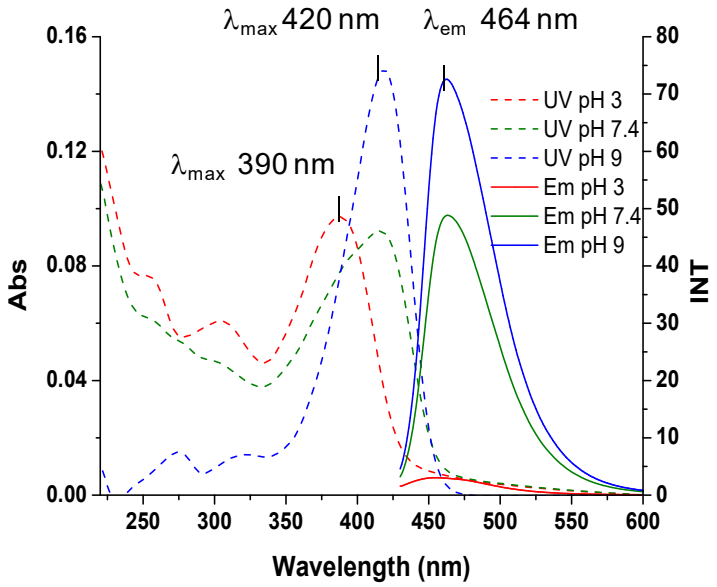

Figure 5.2.2 *UV-Vis and emission spectra of the fluorescent product from the reaction between DA and resorcin at different pH, sample concentration 50 μM.*

Interestingly, 4-methycatechol that lacks of an ethyl-substituted side chain, gave a reaction product that displayed a totally different spectroscopic behavior (Figure 5.2.3), with an absorption maximum at 480 nm (versus 420 nm) which shifted to 410 nm in acids (pH 3), and proved to be devoid of fluorescence at both alkaline and acidic pH. Although the product could not be isolated and characterized due to its instability, it was confidently assigned the structure reported in Figure 5.2.3 on the basis of previously reported literature.[72]

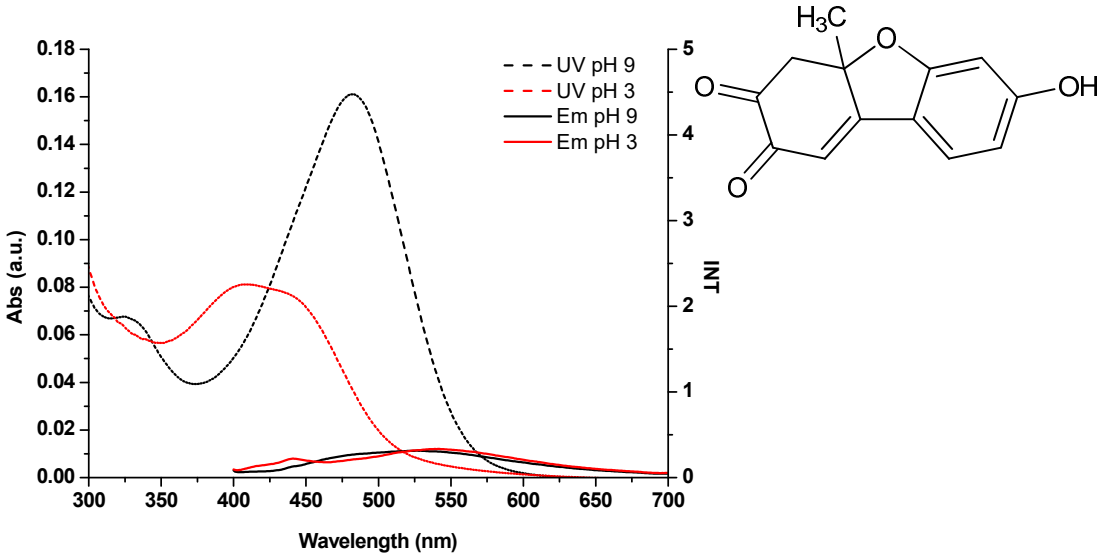

Figure 5.2.3 *UV-vis and fluorescence spectra of the reaction between resorcinol and 4-methylcatechol and putative structure of the main reaction product.*

It was concluded that the ethylamine side chain is necessary for fluorescence development.
Other biologically relevant catecholamines, such as epinephrine and norepinephrine, were also tested under similar reaction conditions. Inspection of the chromophores revealed a main peak at ca. 310 nm accompanied by a very weak absorption (inflection) around 490 nm, with no significant fluorescence (Figure 5.2.4). These results suggested that intramolecular cyclization to give orange-colored aminochrome derivatives prevails over nucleophilic attack by resorcinols.

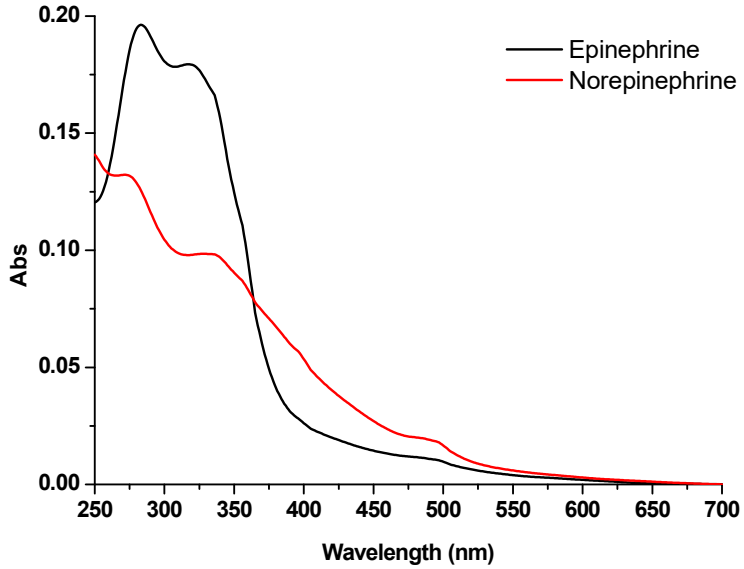

Figure 5.2.4 *UV-vis spectra of the reactions between epinephrine or norepinephrine + resorcinol.*

On the basis of these results it was concluded that the fluorogenic reaction between catecholamines and resorcinols is highly specific for dopamine and DOPA but does not proceed with beta -OH substituted catecholamines. The actual cause of this difference will be the subject of future work.

In another series of experiments the reaction of dopamine with resorcinol was carried out at various concentrations to assess the limits for fluorophore detection and linearity of response. Figure 5.2.5 shows that the minimum dopamine concentration leading to detectable fluorophore with 500 µM resorcin is 1 µM.

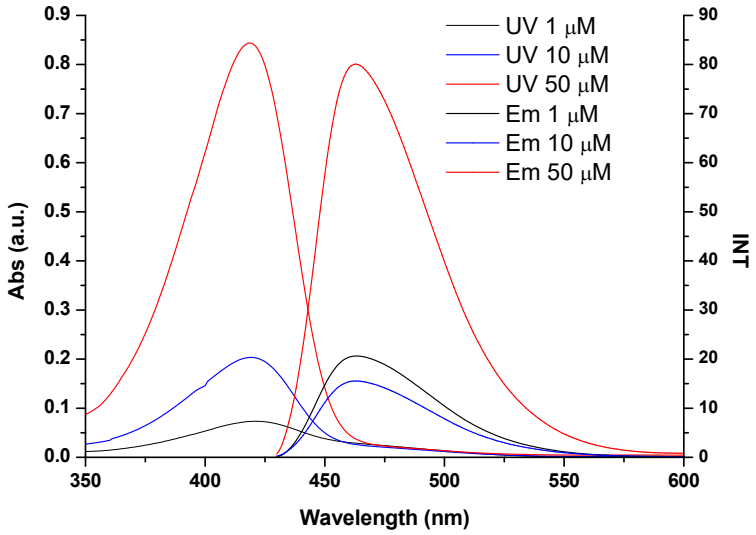

Figure 5.2.5 *Fluorophore development from reaction of dopamine with resorcin in 50 mM bicarbonate buffer, pH 8.5 (spectra recorded without dilution).*

It was concluded that the coupling reaction is efficient even under high dilution conditions and selective for dopa and dopamine versus the other catecholamines such as norepinephrine and epinephrine.

In another series of experiments, the fluorogenic reaction between resorcinol derivatives with dopamine was investigated with the aim of developing fluorescent thin films for surface functionalization via the dip-coating methodology commonly used for polydopamine (PDA).[12] While many examples have been reported of switchable and tunable fluorescent coatings obtained by self-assembled monolayer or sol−gel methodologies,[183–185] only few options are available by the dip-coating approach.[186,187] This represents a gap in the current toolbox for surface functionalization, since fluorescent coatings may have manifold potential applications, e.g. for monitoring pH changes and for sensing metabolic activity in cell cultures.[188–190] Preliminarily, deposition of dopamine-based fluorescent thin films on glass and quartz substrates was investigated by immersing the substrate into a dopamine solution at pH 8.5 in Tris buffer containing resorcinol and related derivatives, e.g. floroglucinol at various concentrations and molar ratios, but under no condition could deposition of a stable fluorescent film be observed.

With a view to imparting adhesion properties to the dopamine based fluorophores, the attention was then directed to the rational functionalization of the resorcinol coupler to increase hydrophobicity and affinity for glass, polymers and substrates with different surface properties.

To this aim, we were inspired by previous studies reporting that hexamethylenediamine, a long-chain diamine acting as a lysine mimic in mussel-inspired adhesive systems, may enable formation and deposition of adhesive films from gallic acid polymers.[12,148,162,191] Accordingly, a novel symmetrical bis-resorcinol derivative (BisRes) in which the two aromatic rings are held together by a hexamethylenediamine (HMDA) tether was designed and synthesized (Scheme 5.2.1). BisRes was prepared by mixing2,4-dihydroxybenzaldehyde (0.4 M) and hexamethylenediamine in ethanol, and leaving the reaction under stirring for 15 min. The yellow precipitate was centrifuged, washed with cold ethanol and vacuum dried to give the imine intermediate. The ^{1}H NMR spectrum exhibited one singlet at δ 8.30 (H-7), a singlet at δ 6.13 (H-3) and two doublets at δ 7.13 (H-5, J= 8.5 Hz) and 6.22 (H-6, J= 8.4 Hz) respectively, consistent with the presence of a resorcinol subunit. The aliphatic region of the spectrum was characterized by a triplet at δ 3.48 (H–8 J= 6.6 Hz), and two broad multiplets at δ 1.59 and 1.36 (H-9 and H-10). The ^{13}C NMR spectrum exhibited resonances for CH_2 groups at δ 56.4 (C-8), 30.4 (C-9) and 26.1 (C-10), beside the imine signal at δ 164.5 (C-7) and six resonances for aromatic carbons at δ 165.7 (C-2), 162.3 (C-4), 133.0 (C-6), 111.1 (C-1), 106.7 (C-5) and 102.9 (C-3), suggesting a highly symmetric structure. The imine was then dissolved in glacial CH_3COOH and reduced with $NaBH_4$. When hydrogen evolution was complete the mixture was dried under vacuum, then dissolved in distilled water, brought to pH 2 with 3 M HCl and chromatographed on a *DOWEX* resin to remove inorganic components. The fractions eluted with 6 M HCl, containing the desired product, were evaporated to dryness under reduced pressure. The brownish orange solid was identified as the desired BisRes by ^{1}H and ^{13}C NMR analysis, showing a singlet at δ 4.09 (H-7) and a signal at δ 47.8 respectively corresponding to the benzylic methylene group, while the imine resonances at δ 8.30 and δ 164 were absent.

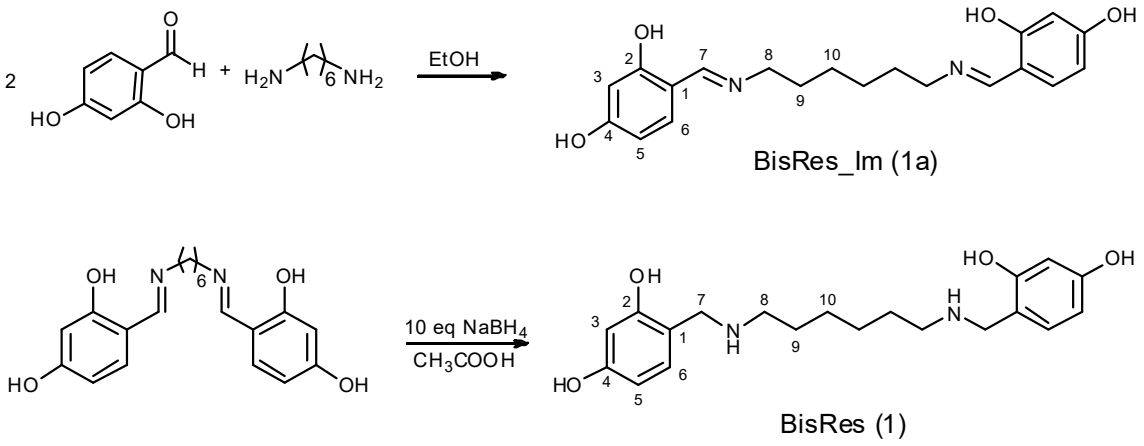

Scheme 5.2.1 *Synthetic route to BisRes.*

Stirring 1 mM BisRes with 2 mM dopamine in carbonate buffer at pH 9 (Scheme 5.2.2) led to development in solution of an intensely emitting yellow chromophore accompanied by deposition of a fluorescent thin film on a quartz substrate immersed in the reaction flask (Figure 5.2.6).

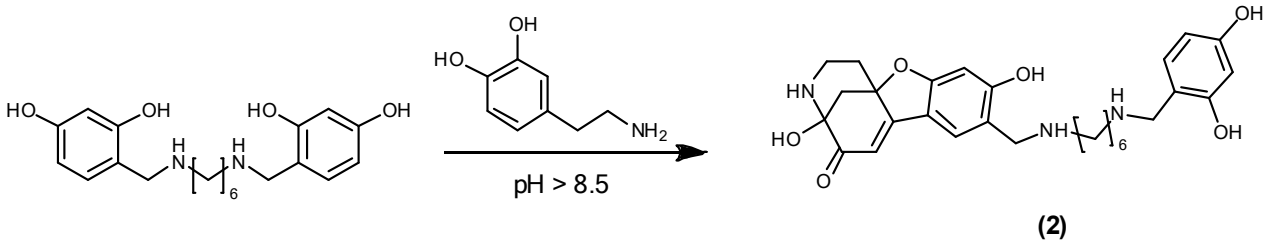

Scheme 5.2.2 *Expected structure of the reaction product of BisRes with the catecholamine dopamine, in auto-oxidative condition (1 mM in Na_2CO_3 buffer pH 9).*

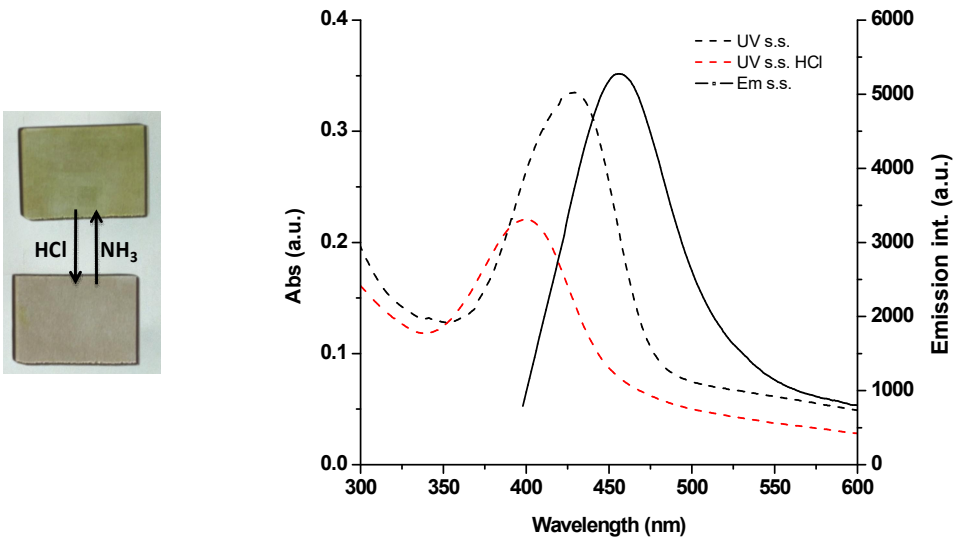

Figure 5.2.6 *Picture and UV-Vis and fluorescence spectra of a BisRes-dopamine coated quartz before and after exposure to HCl vapours.*

Profilometry data (Table 5.4.1) indicated film thickness of 55 ± 2.7 nm with a roughness of 15 nm. Spectrophotometric analysis of the coating in the solid state revealed an absorption maximum at 420 nm and an intense fluorescence emission, suggesting adduct formation of dopamine with BisRes. In support of this conclusion, LC-MS analysis of the reaction mixture (Figure 5.4.1) revealed formation of a main species with m/z = 510 $[M+H]^+$ consistent with the coupling product depicted in Scheme 5.2.2.

Exposure to HCl vapours caused a marked hypsochromic shift of the absorption maximum, a decrease in emission intensity and, most notably, a marked drop in the water contact angle of the film, from ca. 50° to values below instrumental limits, indicating conversion into a superhydrophilic material (Figure 5.2.7, left). The HCl-induced absorption shift proved to be completely reversible upon exposure to ammonia vapours over at least 5 cycles (Figure 5.2.7, right). This behaviour was attributed to acid-induced protonation of amine residues linked to the methanobenzofuroazocinone scaffold with generation of positively-charged sites increasing the hydrophilic character of the film.

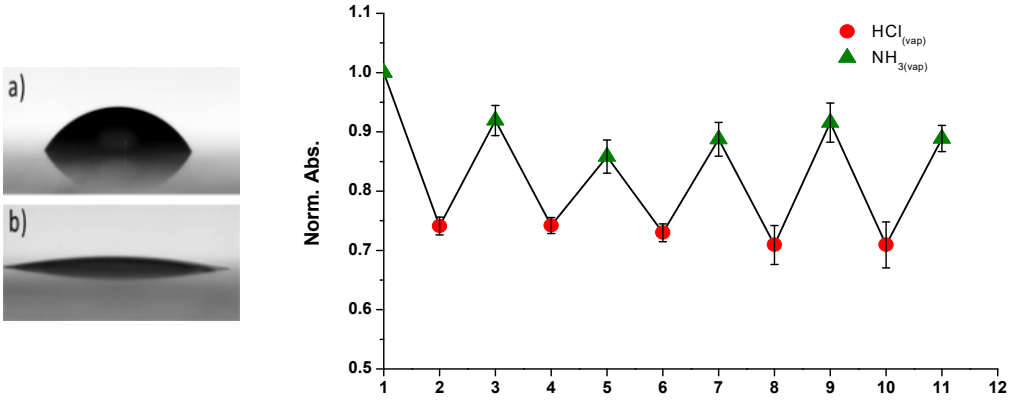

Figure 5.2.7 *Left: Water droplet on the BisRes-dopamine coating before a) and after b) exposure to HCl vapours. Right: Relative absorbance changes at 420 nm of BisRes-dopamine film following repeated sequential exposure to HCl and NH_3 vapours.*

To assess this hypothesis ATR/FT-IR spectra of the film deposed on aluminum substrate were recorded, showing at ~ 3300 cm^{-1} a broad signal attributed to the N-H and O-H stretching that, after exposure to HCl vapours, shifted to lower wave numbers (~3100 cm^{-1}); C-H stretching bands of the aliphatic chain were visible at 2900-2800 cm^{-1}. A weak band at 1735 cm^{-1} was attributed to the carbonyl group. After exposure to acid, a marked change in the low frequency bands was observed with apparent loss of the carbonyl band (Figure 5.4.2).

Toward amine-sensing, smart packaging, and polymer fluorescence-tagging applications. The dopamine resorcinol reaction described in this chapter displays several features of potential usefulness for derivatization and sensing applications, in particular the fast and efficient fluorescence response to moderately alkaline inputs and the chemical versatility deriving from decoration of the resorcinol coupler with a range of functional groups amenable to further derivatization. In this thesis, two aspects of possible relevance to applications were considered:

a) the ability of the system to respond to ammonia and volatile amines or to oxygen or the combination of the two in different supports and environments;

b) the possibility to develop fluorescent tags on polymers and other supports on demand.

Detection of basic nitrogenous volatiles is an issue of considerable importance for a variety of applications e.g. for assessment of air quality and for food spoilage determination.[192,193]

Initially, the scope of the reaction was tested using different hydrogel supports. To this aim, films or beads of alginate hydrogels prepared in the presence of 5 mM dopamine and resorcinol were exposed to gaseous ammonia in a closed chamber at room temperature. A strong fluorescence developed rapidly, accompanied by a yellow coloration, denoting in situ formation of the methanobenzofuroazocinone anion. Complete discoloration with quenching of fluorescence was induced by exposure of the yellow beads to HCl vapours (Figure 5.2.8a).

Since the generation of basic amine-containing volatiles (e.g., NH_3 and NMe_3) is also a primary index of food spoilage due to microbial growth,[194] alginate hydrogel films loaded with equimolar dopamine and resorcinol were exposed to vapours from decomposing fish fillets for 24 h at room temperature in a closed chamber. As a control, the same conditions at −20 °C under an argon atmosphere were selected. A marked fluorescence response was noticed under fish decomposition conditions, (Figure 5.2.8b) but not in the controls suggesting exploitation of this reaction in smart packaging for expedient monitoring of fish quality.

To probe the efficiency of fluorescence turn-on in a complex biological matrix with several potentially interfering species, equimolar dopamine and resorcinol (0.3 % m/v) were thoroughly mixed in raw chicken egg white (CEW) under vigorous stirring (Figure 5.2.8c). The rapid generation of a yellow colour and a strong fluorescence was direct evidence for an efficient coupling reaction even in a complex biological medium with intrinsically alkaline pH. Complete inhibition of the reaction under an argon atmosphere suggested use of this system as an all-natural oxygen sensor, e.g. to reveal leaks in a vacuum package.

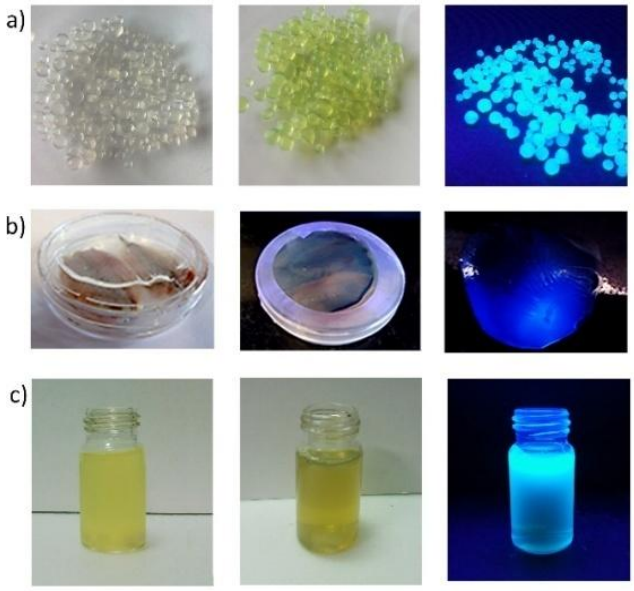

Figure 5.2.8 *a) Dopamine and resorcinol loaded alginate beads before (left) and after (middle) exposure to ammonia under natural light and 365 nm lamp (right). b) Alginate film exposed to decomposing fish fillets. Left: t = 0, middle and right: after 24 h and detail of the gel under 365 nm lamp. c) Fluorescence developed in CEW. Left: t = 0, middle and right: after 5 min under natural light and 365 nm lamp.*

Fluorescence tagging is an important application of fluorophores of both biological and technological relevance.[195] Accordingly, the potential of the dopamine resorcinol reaction for fluorescence tagging was next investigated in a simple model of polymer derivatization and tagging on demand.

A resorcinol compound substituted with a carboxyl group was selected in order to ensure facile functionalization for applications, e.g. for polymer derivatization and the amine-rich polymer polyethyleneimine (branched PEI, 25 kDa) was chose as anchoring backbone. Aim of the experiment was to assess whether polymer-bound resorcinol could efficiently trap autoxidatively generated dopamine quinone preventing melanin precipitation.

Initially, the efficiency of the fluorogenic coupling of 3-(2,4-dihydroxyphenyl)propionic acid (DHPPA) with dopamine was tested. The reaction was conducted in alkaline buffer under stirring in an open vial under the usual conditions and led to the fast development of fluorescence. Attempts to isolate and characterize the reaction product using semipreparative HPLC (eluting system: 0.1% HCOOH-acetonitrile 6:4) were however unsuccessful. In order to characterize the fluorescent adduct, DHPPA methyl ester was synthesized and reacted with dopamine in alkaline buffer (pH 9) under stirring for two days. The reaction was periodically monitored by UV spectroscopy, showing a maximum at 431 nm attributable to the fluorescent reaction product. The solution was

subsequently extracted with ethyl ether to remove unreacted reagents and subsequently desalted on a *Sephadex G10* resin using distilled water as eluting system.

^{1}H NMR of the aqueous fraction showed the conversion of the ABX system of the resorcinol ring in two singlets at δ 7.21 (H-7) and 7.15 (H-10). The six signals in the aliphatic region at δ 3.07-2.87 (m, H-2a), 2.47-2.39 (m, H-2b), 2.35 (d, H-3a), 2.22 (d, H-3b), 2.03-1.93 (m, H-1a) and 1.46 (d, H-1b) and the singlet at δ 5.95 are in accord with the methanobenzofuroazocine skeleton. The methanobenzofuroazocinone structure was also confirmed by LC-MS analysis showing $[M+H]^+$ at 346 m/z, besides $[M+Na]^+$ and $[M+K]^+$ peaks (see experimental section).

To assess the applicability of the fluorescent tagging and sensing system, a 25kDa branched PEI was functionalized with the resorcinol derivative (Scheme 5.2.3) and characterized by ^{1}HNMR (Figure 5.4.3).

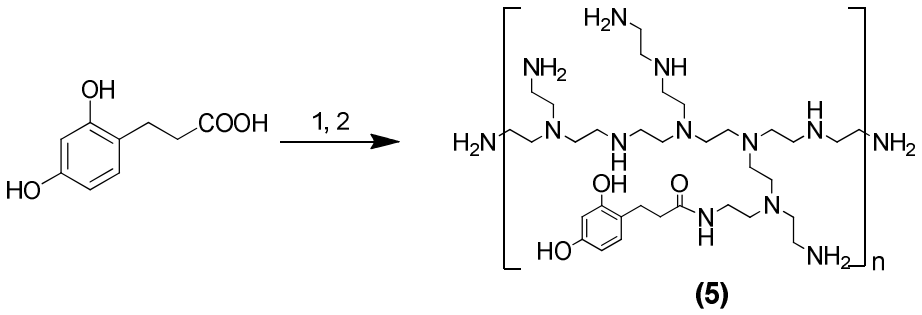

(5)

Scheme 5.2.3 *Condensation of PEI and DHPPA. 1) 1.14 eq TEA, Ethylchloroformate, DMF, 2 h, 0 °C.2) PEI, 55 °C.*

The degree of functionalization of PEI with DHPPA was determined by measuring the absorbance at 280 nm using a UV-Vis spectrophotometer.[196] DHPPA solution in methanol was used to generate a standard curve for concentration (ranging from 50 μM to 200 μM). The calculated molar absorptivity of DHPPA was ε= 2860 $M^{-1}cm^{-1}$. On this basis, the PEI/DHPPA solution in methanol (4 mg/mL) exhibited ca. 20% w/w polymer functionalization.

On this basis, DHPPA-functionalized PEI was next reacted with dopamine (Scheme 5.2.4). The reaction was conducted by mixing dissolved PEI/DHPPA and dopamine in water (173 μM) and raising pH to 9 with 2 M NaOH. The efficiency of the reaction was apparent from UV spectroscopy (maximum at 432 nm). After 1 h, the reaction was dialyzed against distilled water. No absorption

was detected in dialysis water, confirming that the reaction was complete and the methanobenzofuroazocine moiety was linked to PEI.

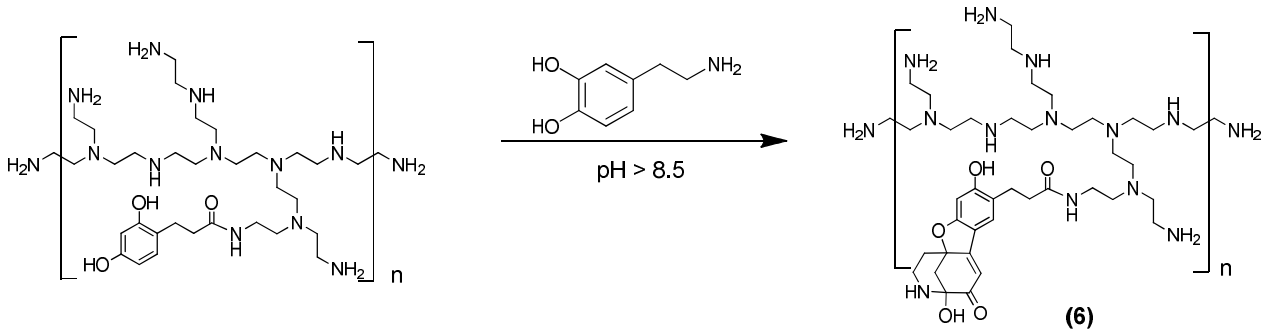

Scheme 5.2.4. *Reaction between DHPPA functionalized PEI and dopamine.*

Fluorescence measurements were performed on the functionalized polymer at three different pH values, i.e. 3, 7 and 9 in phosphate buffers. In accord with the reported behavior of methanobenzofuroazocine species, progressive quenching of fluorescence emission and an hypsochromic shift of the absorption maximum were observed with decreasing pH (Figure 5.2.9).

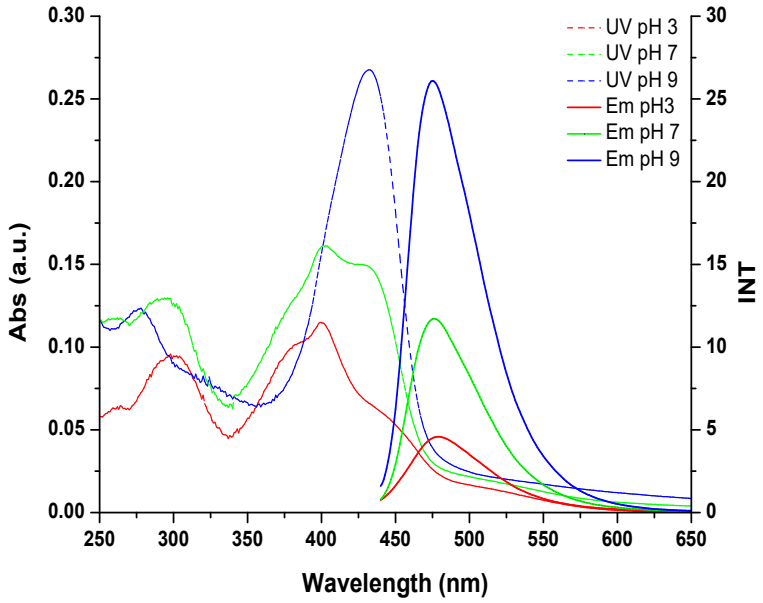

Figure 5.2.9 *Absorption and emission spectra of the fluorescent polymer measured at three different pH.*

5.3 Conclusions

The strongly fluorogenic reaction between dopamine and resorcinols is proposed as a convenient tool for surface functionalization based on fluorescent thin film deposition by dip coating, for sensing volatile amines in biocompatible hydrogels or natural matrices such as CEW, and for polymer functionalization. The reaction is efficient, develops from cheap and easily available compounds and can be extended to a range of resorcinol and catecholamine partners.

Work is now in progress to assess the scope of dopamine-resorcinol-based chemistry for biomedical and technological applications. On-demand generation of the fluorophore via a reaction-based sensing mechanism would allow to combine signal read-out with a functional process, such as cross-linking, covalent conjugation, coating deposition or synthesis of an active target, opening novel perspectives in biomedicine and materials science.

5.4 Experimental methods and supporting information

Materials. All reagents were obtained from commercial sources and used without further purification. Organic solvents were used as purchased. Water was of MilliQ® quality. Buffers were prepared by standard procedures. A Crison pH-meter equipped with a 5014 Crison electrode was used for pH measurements at room temperature. Analytical thin layer chromatography (TLC) was performed on 0.25 mm thick pre-coated silica gel plates (60 F_{254}).

Methods. UV-Vis absorption spectra were registered at room temperature on a V-560 JASCO spectrophotometer using calibrated 2 mL cuvettes and, for solid state samples, on a Cary 4000 UV-Vis spectrophotometer using the solid sample holder.

Steady-state fluorescence excitation and emission spectra of optically diluted samples were recorded with an FP-750 JASCO spectrofluorimeter.

^{1}H-NMR and ^{13}C-NMR spectra were recorded in deuterated solvents at 400 MHz on a Bruker DRX 400 or Bruker Avance DRX 400 and at 500 MHz on a Varian Inova 500, δ values are reported in ppm and coupling constants are given in Hz.

HPLC analyses for reaction monitoring were performed on an Agilent 1100 series instrument equipped with an LC-10AD VP pump and a G1314A UV-Vis detector using a Sphereclone C18 column (4.6 x 150 mm, 5 μm).

LC-MS analysis was conducted on an ESI-TOF 1260/6230DA Agilent Technologies in positive ion mode.

IR spectra were recorded on Nicolet 5700 FT-IR + Smart performer spectrometer mounting a Continuum FT-IR Microscope and on Bruker Optics TENSOR 27 FT-IR.

Oxidation of methylcatechol, noradrenaline and adrenaline in the presence of resorcinol. To resorcinol and the proper catechol (1:1 molar ratio) dissolved in 50 mM Na_2CO_3 buffer, pH 9, a solution of potassium ferricyanide (4 eq) in water was added under vigorous stirring, and the reaction mixture was allowed to stand under argon atmosphere for 1.30 h. The reaction was monitored by UV-VIS absorption and fluorescence spectroscopy. For UV-VIS analyses, aliquots were acidified to pH 3 to stop the reaction before measurement.

Synthesis and structural characterization of BisRes (1). A mixture of hexamethylenediamine (1.81 mmol, 210 mg) and 2,4-dihydroxybenzaldehyde (3.62 mmol, 500 mg) in absolute ethanol (18 mL) was stirred at room temperature for 1 h. The yellow solid that separated was centrifuged 3

times at 5000 rpm and washed with cold ethanol then dried *in vacuo* to give compound **1a** (570 mg, 88.5 % yield). The Schiff base was then rinsed in glacial acetic acid (10 mM, 160 mL) and reduced by $NaBH_4$ (16 mmol, 605 mg). When hydrogen evolution was ceased 3 M HCl was added until pH 5. The mixture was dried under vacuum, then rinsed in 1 mL of water before desalting on DOWEX resin 50W X 4 using a gradient of HCl from 0.5 M to 6 M as the eluant. Fourteen fractions of 250 mL each were collected and analyzed by UV-VIS spectrometry. The desired product eluted with 6 M HCl (7 fractions). After removal of the acid under reduced pressure, compound **1** was obtained as di-hydrochloride salt in the form of a brownish orange solid, yield= 75 %.

(1a): R_f = 0.27 ($CHCl_3$-MeOH 9:1). UV-Vis: λ_{max} (MeOH) = 301 nm (ε= 33410 $L \cdot mol^{-1} \cdot cm^{-1}$) and 371 nm ($\varepsilon$= 15879 $L \cdot mol^{-1} \cdot cm^{-1}$).m/z = 357.18 $[M + H]^+$. ATR (cm^{-1}) 1227 (phenolic C-O stretch), 1358 (phenolic C-O bend), 1637 (C=N stretch), 2932 (aliphatic C-H bend and stretch), 3065 (aromatic C-H stretches), 3509-3638 (phenolic O-H stretches). ^{1}H NMR (400 MHz, DMSO-d_6) δ 8.30 (s, H-7), 7.13 (d, *J* = 8.5 Hz, H-6), 6.22 (d, *J* = 8.4 Hz, H-5), 6.13 (s, H-3), 3.48 (t, *J* = 6.6 Hz, H-8), 1.59 (br. m, H-9), 1.36 (br. m, H-10).^{13}C NMR (101 MHz, DMSO-d_6) δ 165.7, 164.5, 162.3, 133.0, 111.1, 106.7, 102.9, 56.4, 30.4, 26.1.

(1): UV-Vis: λ_{max} (MeOH) = 279 nm (ε= 4944 $L \cdot mol^{-1} \cdot cm^{-1}$).m/z: 361.21 $[M + H]^+$.^{1}H NMR (400 MHz, MeOH-d_4) δ 7.12 (d, *J* = 8.2 Hz, H-6), 6.39 (s, H-3), 6.33 (d, *J* = 6.8 Hz, H-5), 4.09 (s, H-7), 3.01 – 2.93 (br. m, H-8), 1.73 (br. m, H-9), 1.43 (br. m, H-10).Resonance assignment follows from analysis of ^{1}H,^{1}H COSY spectrum.^{13}C NMR (101 MHz, MeOD-d_4) δ 161.4 (C-4), 158.6 (C-2), 133.5 (C-6), 109.8 (C-1), 108.1 (C-5), 103.4 (C-3), 47.8 (C-7), 47.6 (C-8), 27.1 (C-9), 26.6 (C-10). Resonance assignment follows from analysis of ^{1}H,^{13}C HSQC and HMBC spectra. ATR-FT/IR (cm^{-1})1172 (C-N stretch), 1593 (N-H bend), 2796-2935 (aliphatic C-H bend and stretch), 3041 (aromatic C-H stretches), 3235-3292 (N-H stretch), 3531-3622 (phenolic O-H stretches).

Oxidative coupling of 1 with dopamine. 1 dihydrochloride (1 mM) and dopamine (2 mM) were dissolved in 0.05 M sodium carbonate buffer, pH 9. After complete dissolution, a neat substrate (glass or quartz coverslip rinsed with piranha mixture H_2SO_4:H_2O_2 5:1) was immersed in the reaction mixture for3-6 h. The development of a blue fluorescence was rapidly observed followed by deposition of a thin layer of organic material on the substrate and concomitant separation of a brownish-green solid. Attempts to purify the reaction products by extraction with organic solvents (ethyl acetate, dichloromethane, chloroform), preparative HPLC or filtration through Sephadex G10 or other resins proved unsuccessful. However, LC-MS analysis of the reaction mixture showed a main component with a pseudomolecular ion peak corresponding to the monoadduct **2** shown in the scheme 5.2.2.

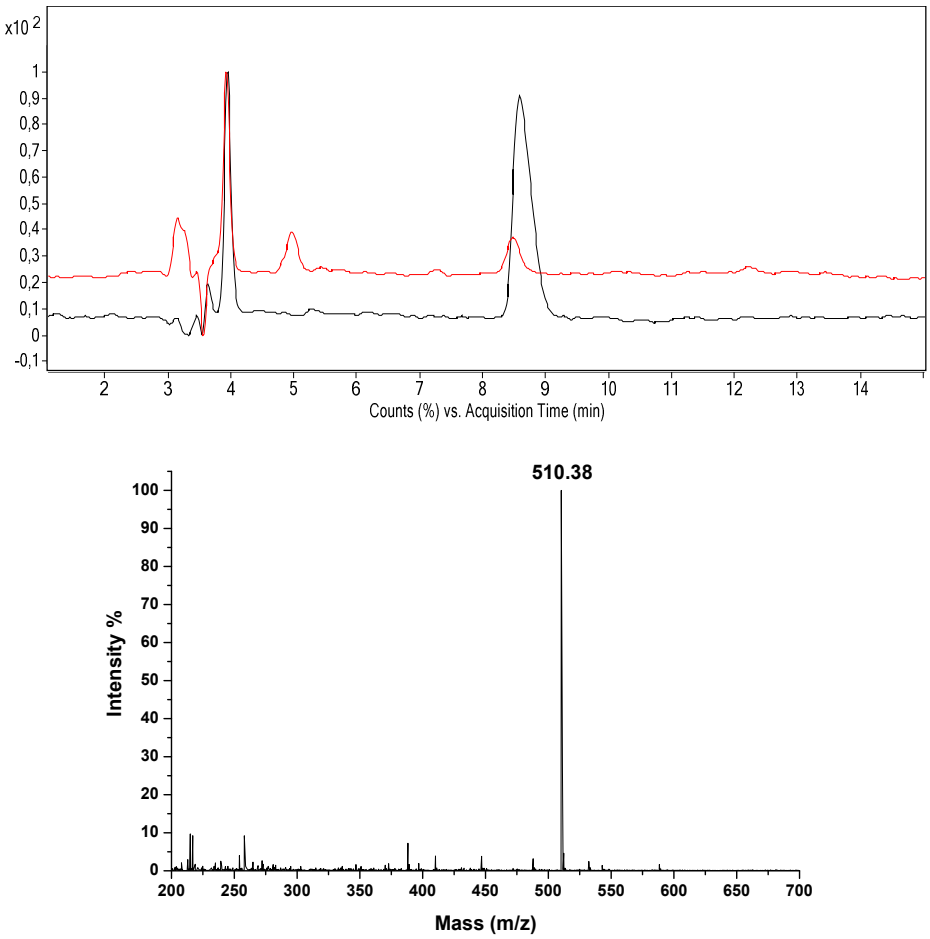

Figure 5.4.1 *LC-MS analysis of the reaction mixture between **1** (R_t: 8.9 min) and dopamine (R_t. 4 min). Top) Total ion currrent chromatogram after 0 (black) and 150 min (red). Right) Mass spectrum of the peak eluting at 5.1 min, base peak $[M + H]^+$: m/z 510.4, eluting system: 0.1 % HCOOH - MeOH 8:2.*

Table 5.4.1 ***Profilometry data of the BisRes-dopamine coating on glass before and after $HCl_{(vap)}$ exposure.***

Coating	$\lambda_{max/ex}$ (nm)	λ_{em} (nm)	Thickness (nm)	Roughness (nm)	Water Contact Angle (deg)
BisRes/DA	420	464	55 ± 2.7	15	52 ± 3.6
BisRes/DA-HCl	400	no	48 ± 0.2	16	Notcalculable

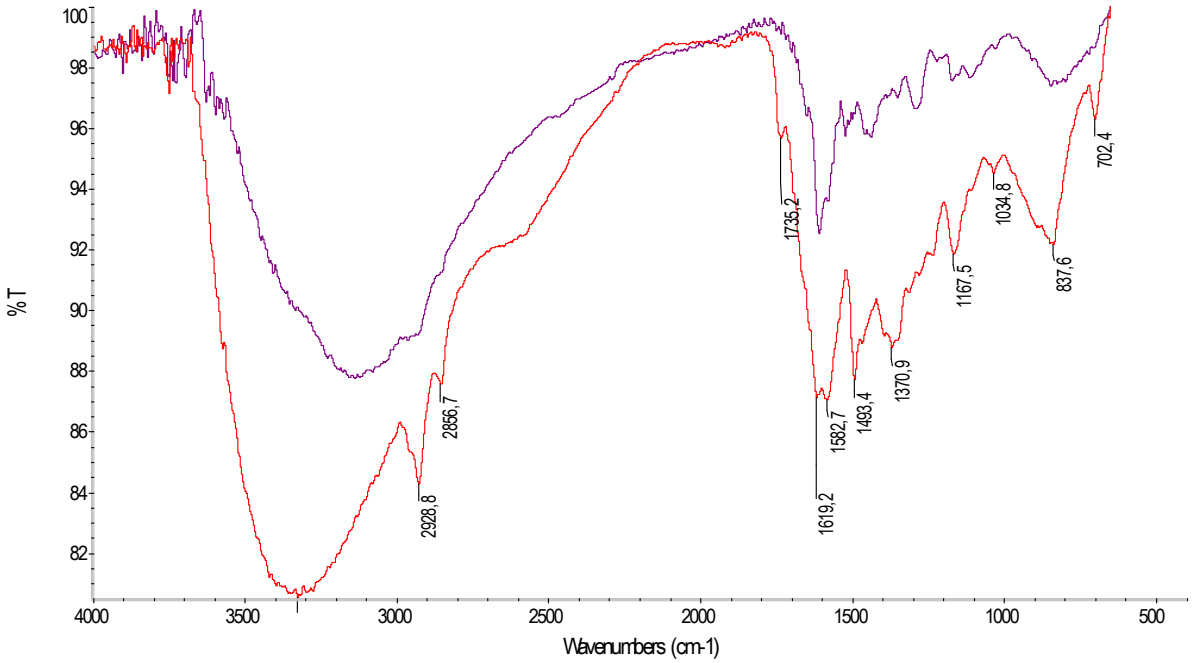

Figure 5.4.2 *ATR-FTIR of the BisRes/DA coated aluminium slide before (red trace) and after (violet trace) exposure to HC lvapours*.

Preparation of Fluorescat-alginate hydrogels. Dopamine (0.1 mmol, 19 mg) and resorcinol (0.1 mmol, 11 mg) were dissolved in distilled water (20 mL), then sodium alginate was added (2% w/w). Beads were prepared dropping the freshly prepared gel in a 0.1 M solution of $CaCl_2$ allowing alginate reticulation for few minutes followed by beads filtration. Films were similarly fabricated spreading the gel on a smooth surface followed by dipping in the $CaCl_2$ solution for about 60 sec. Exposure to acid or alkaline vapors or to decomposing fish fillets was carried out in sealed glass chambers containing aqueous hydrochloric acid (35 %) or ammonia (28%) solution or decomposing fish fillets at room temperature.

Synthesis and characterization of 3-(5,7-dihydroxyphenyl)propanoic acid (DHPPA) methyl ester. To a solution of DHPPA (0.82 mmol, 150 mg) in methanol (1.6 mL), 160 μL of H_2SO_4 were added and the reaction mixture was left under reflux and under stirring overnight. After neutralization with 1% NH_3, methanol was evaporated under vacuum and the mixture was extracted with ethyl acetate (3x 20 mL), the resulting organic layer was re-extracted with distilled water (1x 5 mL) and saturated NaCl (1x 5 mL), and the combined organic layers were dried over anhydrous Na_2SO_4. Column chromatography (hexane-ethyl acetate 1:1) purification led to isolation of the desired ester **3** (R_f 0.4) in 70 % yield, together with lower amounts of another product (R_f 0.6) that proved to be the methyl 3-(5-hydroxy-7-methoxyphenyl)propanoate (**3a**).

(3)

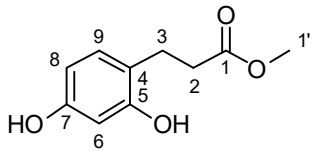

methyl 3-(5,7-dihydroxyphenyl)propanoate
3

^{1}H NMR (400 MHz, MeOH-d_4) δ 6.83 (d, *J* = 8.3 Hz, H-9), 6.26 (d, *J* = 2.0 Hz, H-6), 6.19 (dd, *J* = 8.2, 2.2 Hz, H-8), 3.63 (s, H-1'), 2.77 (t, *J* = 7.7 Hz, H-2), 2.55 (t, *J* = 7.6 Hz, H-3).^{13}C NMR (101 MHz, MeOH-d_4) δ 176.1 (C-1), 158.0 (C-7), 157.2 (C-5), 131.4 (C-9), 119.3 (C-4), 107.6 (C-8), 103.5 (C-6), 52.0 (C-1'), 35.6 (C-2), 26.5 (C-3).

(3a)

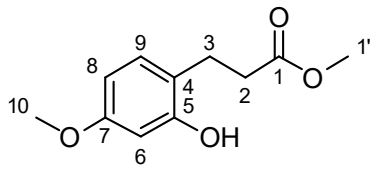

methyl 3-(5-hydroxy-7-methoxyphenyl)propanoate
3a

^{1}H NMR (400 MHz, MeOH-d_4) δ 6.92 (d, *J* = 8.1 Hz, H-9), 6.34 (d, *J* = 2.3 Hz, H-6), 6.31 (dd, *J* = 8.3, 2.3 Hz, H-8), 2.80 (t, *J* = 7.7 Hz, H-2), 2.56 (t, *J* = 7.7 Hz, H-3), 3.69 (s, H-10), 3.62 (s, H-1').^{13}C NMR (101 MHz, MeOH-d_4) δ 175.8 (C-1), 160.4 (C-5), 157.0 (C-7), 130.9 (C-9), 120.3 (C-4), 105.2 (C-8), 102.1 (C-6), 55.3 (C-10), 51.7 (C-1'), 35.0 (C-2), 26.2 (C-3).

Oxidative coupling of 3 or 3a with dopamine. 3 or **3a** and dopamine at 1 mM were dissolved in 50 mM Na_2CO_3 buffer, pH 9. The mixture was stirred at room temperature until reaction completion (UV-Vis monitoring, 3 h for **3** and 24 h for **3a**).In the case of **3**, the main reaction productwas isolated by desalting of the aqueous layer by Sephadex G10 filtration following extraction with ethyl acetate of the mixture to remove excess of the reactant. It was assigned structure **4** based on ^{1}H NMR and LC-MS spectrometry. On the other hand, **3a** did not react with dopamine as evidenced by UV-Vis, TLC and NMR analysis of the organic and aqueous layers.

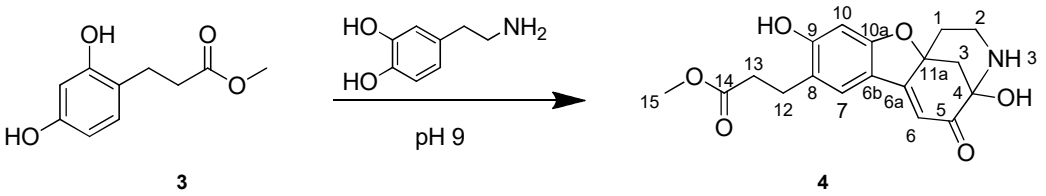

3 **4**

Scheme 5.4.1. Oxidative coupling between dopamine and **3**.

(4)^{1}H NMR (400 MHz, MeOH-d_4) δ 7.21 (s, H-7), 7.15 (s, H-10), 5.95 (s, H-6), 3.63 (s, H-15), 3.07 – 2.87 (m, H-2a), 2.80 – 2.75 (t, *J* = 7.4 Hz, H-12), 2.59 (t, *J* = 7.4 Hz, H-13), 2.47 – 2.39 (m, H-2b), 2.35 (d, *J* = 10.6 Hz, H-3a), 2.22 (d, *J* = 10.4 Hz, H-3b), 2.03 – 1.93 (m, H-1a), 1.46 (d, *J* = 12.4 Hz, H-1b).LC-MS spectrometry. base peak: m/z 368.04 = $[M + Na]^+$, m/z 346.32 = $[M + H]^+$, m/z 384.26 = $[M + K]^+$,eluting system: HCOOH 0.1 % - MeOH 8:2,R_t = 9.1 min.

Synthesis and characterization of PEI-DHPPA (5). DHPPA (20 mg, 0,11mmol) was dissolved in dry dimethylformamide (DMF, 1 mL), then triethylamine (TEA, 17 µL, 0.12 mmol) and ethylchloroformate (10.6 µL, 0.11 mmol) were added under stirring at 0 °C. The reaction was monitored by TLC ($CHCl_3$-MeOH 9:1) until consumption of the starting material. 25 kDa PEI (12.3 mg in 1 mL of dry DMF) was added after 1.30 h. The reaction was left under stirring at 55 °C for 4 h, then dried under vacuum, rinsed (10 mL) and dialysed against distilled water (500 mL x 3).The resulting material was analysed by proton NMR. A 19 % w/w functionalization of polymer was determined by measuring the absorbance at 280 nm using a calibration curve built on DHPPA (λ_{max} 280 nm, ε= 2863.5 $M^{-1}cm^{-1}$).

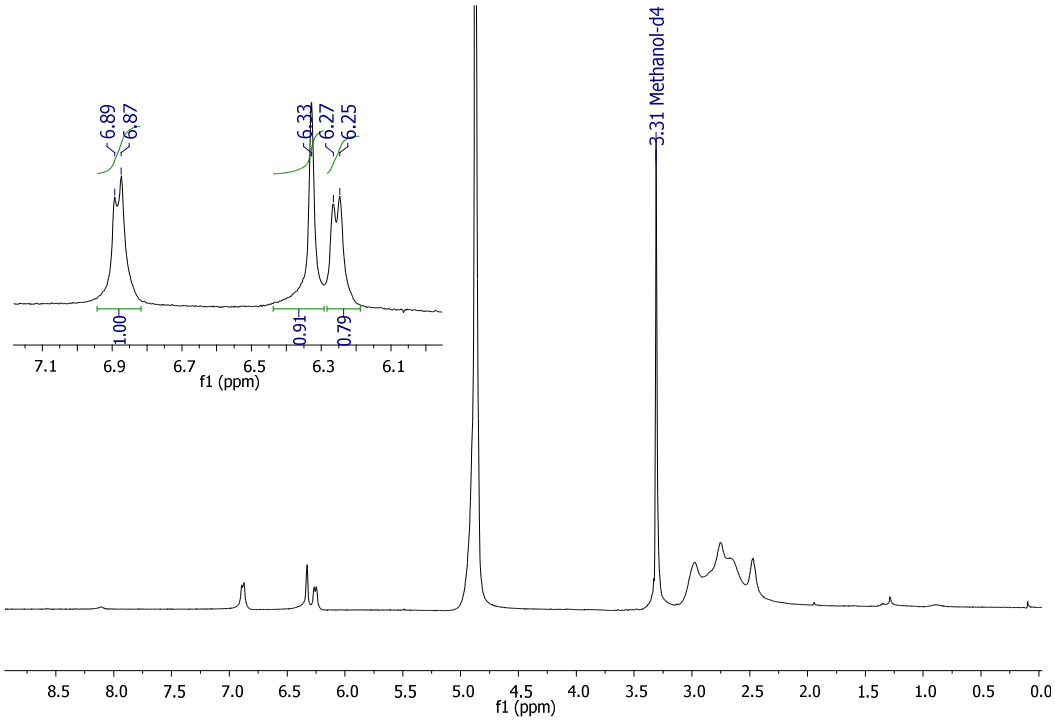

Figure 5.4.3. *^{1}H NMR (400 MHz, MeOH-d_4) δ 6.88 (d, J = 7.5 Hz), 6.33 (s), 6.26 (d, J = 7.4 Hz). The aromatic region shows the signals expected for a resorcinol moiety.*

Oxidative coupling of PEI-DHPPA with dopamine. PEI-DHPPA and dopamine (0.17 mM) were dissolved in distilled water, then the pH of the reaction was raised to 9 by addition of 2 M NaOH. The mixture was stirred at room temperature and monitored by UV-Visible spectrophotometry. After 2 h, the reaction mixture was dialyzed against distilled water (4 x 500 mL) to remove salts and unreacted dopamine. The purified polymer was subjected to UV-Visible and fluorescence analysis.

UV-Vis: λ_{max} (phosphate buffer, pH 9) = 432 nm; λ_{max} (phosphate buffer, pH 7) = 427, 400 nm; λ_{max} (phosphate buffer, pH 3) = 400 nm. Fluorescence: λ_{ex} = 420 nm, λ_{em} (phosphate buffer) = 475 nm.

LIST OF ABBREVIATIONS

AFM. Atomic Force Microscopy

BSA. bovine serum albumin

BTIB. bis(trifluoroacetoxy)iodo benzene

CAN. Ceric ammonium nitrate

CDA. Cysteinyldopamine

CEW. chicken egg white

CGA. Chlorogenic acid

DA. Dopamine

DHBT. 5,6-dihydroxybezothiophene

DHI. 5,6-didydroxyindole

DHICA. 5,6-didydroxyindole-2-carboxylic acid

DHPET. 2-(3,4-dihydroxyphenyl)ethanethiol

DHPPA. 3-(2,4-dihydroxyphenyl)propionic acid

DPPH. 2,2-diphenyl-1-picrylhydrazy

FRAP. ferric reducing antioxidant power

GLY. Glycine

GSH. glutathione

H_2-DHBT. 5,6-dihydroxy-2,3-diidrobezothiophene

HEPES. ferric chloride,4-(2-hydroxyethyl)-1-piperazineethanesulfonic acid

HMDA. hexamethylenediamine

HRP. horseradish peroxidase

L-DOPA. 3,4-Dihydroxy-L-phenylalanine

LYS. Lysine

NADH. nicotinamide adenine dinucleotide

N-MeDHI. 5,6-dihydroxy-N-methylindole

NMeDHI. N-methyl-5,6-didydroxyindole

pCDA. Polycysteinyldopamine

pDA. Polydopamine

PVA. poly(vinyl alcohol)

SEM. scanning electron microscopy

TEA. triethylamine

THF. tetrahydrofuran

Trolox. 6-hydroxy-2,5,7,8-tetramethylchroman-2-carboxylic acid

WCA. Water Contact Angle

XPS. X-ray Photoelectron Spectroscopy

References

(1) Ito, S.; Wakamatsu, K.; d'ischia, M.; Napolitano, A.; Pezzella, A. *Melanins Melanosomes Biosynthesis, Biog. Physiol. Pathol. Funct.* **2011**, 167–185.
(2) Blois, M. S.; Zahalan, A. B.; Maling, J. E. *Biophys. J.* **1964**, *4*, 471–490.
(3) Mostert, A. B.; Powell, B. J.; Pratt, F. L.; Hanson, G. R.; Sarna, T.; Gentle, I. R.; Meredith, P. *Proc Natl Acad Sci U S A* **2012**, *109*, 8943–8947.
(4) Tran, M. L.; Powell, B. J.; Meredith, P. *Biophys. J.* **2006**, *90*, 743–752.
(5) Liu, Y.; Simon, J. D. *Pigment Cell Research*. 2003, 606–618.
(6) Micillo, R.; Panzella, L.; Koike, K.; Monfrecola, G.; Napolitano, A.; d'Ischia, M. *Int. J. Mol. Sci.* **2016**, *17*, 746.
(7) Panzella, L.; Gentile, G.; D'Errico, G.; Della Vecchia, N. F.; Errico, M. E.; Napolitano, A.; Carfagna, C.; d'Ischia, M. *Angew. Chem Int. Ed.* **2013**, *52*, 12684–12687.
(8) D'Ischia, M.; Wakamatsu, K.; Napolitano, A.; Briganti, S.; Garcia-Borron, J. C.; Kovacs, D.; Meredith, P.; Pezzella, A.; Picardo, M.; Sarna, T.; Simon, J. D.; Ito, S. *Pigment Cell Melanoma Res.* **2013**, *26*, 616–633.
(9) Pezzella, A.; Napolitano, A.; d'Ischia, M.; Prota, G. *Tetrahedron* **1996**, *52*, 7913–7920.
(10) Pezzella, A.; Vogna, D.; Prota, G. *Tetrahedron* **2002**, *58*, 3681–3687.
(11) Meredith, P.; Sarna, T. *Pigment Cell Research*. 2006, 572–594.
(12) Lee, H.; Dellatore, S. M.; Miller, W. M.; Messersmith, P. B. *Science* **2007**, *318*, 426–430.
(13) Martinez Rodriguez, N. R.; Das, S.; Kaufman, Y.; Israelachvili, J. N.; Waite, J. H. *Biofouling* **2015**, *31*, 221–227.
(14) Waite, J. H.; Tanzer, M. L. *Science* **1981**, *212*, 1038–1040.
(15) Rego, S. J.; Vale, A. C.; Luz, G. M.; Mano, J. F.; Alves, N. M. *Langmuir* **2016**, *32*, 560–568.
(16) Lee, B. P.; Messersmith, P. B.; Israelachvili, J. N.; Waite, J. H. *Annu. Rev. Mater. Res.* **2011**, *41*, 99–132.
(17) Fan, D.; Wu, C.; Wang, K.; Gu, X.; Liu, Y.; Wang, E. *Chem. Commun.* **2016**, *52*, 406–409.
(18) Liu, Y.; Qiu, W.-Z.; Yang, H.-C.; Qian, Y.-C.; Huang, X.-J.; Xu, Z.-K. *RSC Adv.* **2015**, *5*, 12922–12930.
(19) Jiang, J. H.; Zhu, L. P.; Li, X. L.; Xu, Y. Y.; Zhu, B. K. *J. Memb. Sci.* **2010**, *364*, 194–202.
(20) Liu, Q.; Yu, B.; Ye, W.; Zhou, F. *Macromol. Biosci.* **2011**, *11*, 1227–1234.
(21) Mao, W. X.; Lin, X. J.; Zhang, W.; Chi, Z. X.; Lyu, R. W.; Cao, A. M.; Wan, L. J. *Chem. Commun.* **2016**, *52*, 7122–7125.
(22) Rodríguez, A. R. C.; Saiz-Poseu, J.; García-Pardo, J.; García, B.; Lorenzo, J.; Ojea-Jiménez, I.; Komilis, D.; Sedó, J.; Busqué, F.; Sánchez, A.; Ruiz-Molina, D.; Font, X. *RSC Adv.* **2016**, *6*, 40058–40066.
(23) Zhou, L.; Zong, Y.; Liu, Z.; Yu, A. *Renew. Energy* **2016**, *96*, 333–340.
(24) Kim, S.; Park, C. B. *Biomaterials* **2010**, *31*, 6628–6634.
(25) Pina, S.; Oliveira, J. M.; Reis, R. L. *Adv. Mater.* **2015**, *27*, 1143–1169.
(26) Park, H. J.; Yang, K.; Kim, M. J.; Jang, J.; Lee, M.; Kim, D. W.; Lee, H.; Cho, S. W. *Biomaterials* **2015**, *50*, 127–139.
(27) Della Rocca, J.; Liu, D.; Lin, W. *Acc. Chem. Res.* **2011**, *44*, 957–968.
(28) Neto, A. I.; Cibrão, A. C.; Correia, C. R.; Carvalho, R. R.; Luz, G. M.; Ferrer, G. G.; Botelho, G.; Picart, C.; Alves, N. M.; Mano, J. F. *Small* **2014**, *10*, 2459–2469.
(29) Zang, D.; Zhu, R.; Zhang, W.; Yu, X.; Lin, L.; Guo, X.; Liu, M.; Jiang, L. *Adv. Funct. Mater.* **2017**, *20*, 160-166.
(30) Huang, S.; Zhang, Y.; Shi, J.; Huang, W. *ACS Sustain. Chem. Eng.* **2016**, *4*, 676–681.
(31) Telford, A. M.; Hawkett, B. S.; Such, C.; Neto, C. *Chem. Mater.* **2013**, *25*, 3472–3479.
(32) Li, F.; Tu, Y.; Hu, J.; Zou, H.; Liu, G.; Lin, S.; Yang, G.; Hu, S.; Miao, L.; Mo, Y. *Polym. Chem.* **2015**, *6*, 6746–6760.
(33) Dumanli, A. G.; Savin, T. *Chem. Soc. Rev.* **2016**.
(34) Li, Q.; Zeng, Q.; Shi, L.; Zhang, X.; Zhang, K.-Q. *J. Mater. Chem. C* **2016**, *4*, 1752–1763.
(35) Wu, L.; He, J.; Shang, W.; Deng, T.; Gu, J.; Su, H.; Liu, Q.; Zhang, W.; Zhang, D. *Adv. Opt. Mater.* **2016**, *4*, 195–224.

(36) Wang, H.; Yang, Y.; Guo, L. *Adv. Energy Mater.* **2016**, *16*, 17-19.
(37) Poizot, P.; Dolhem, F. *Energy Environ. Sci.* **2011**, *4*, 2003.
(38) Fallon, K. J.; Wijeyasinghe, N.; Yaacobi-Gross, N.; Ashraf, R. S.; Freeman, D. M. E.; Palgrave, R. G.; Al-Hashimi, M.; Marks, T. J.; McCulloch, I.; Anthopoulos, T. D.; Bronstein, H. *Macromolecules* **2015**, *48*, 5148–5154.
(39) Zhuang, T.; Sasaki, S.; Ikeuchi, T.; Kido, J.; Wang, X.-F. *RSC Adv.* **2015**, *5*, 45755–45759.
(40) Wang, J.; Zhu, T.; Ho, G. W. *ChemSusChem* **2016**, *9*, 1575–1578.
(41) Wang, C.; Yu, S.; Chen, W.; Sun, C. *Sci. Rep.* **2013**, *3*, 1025.
(42) Oyama, K. I.; Yamada, T.; Ito, D.; Kondo, T.; Yoshida, K. *J. Agric. Food Chem.* **2015**, *63*, 7630–7635.
(43) De Lucia, M.; Panzella, L.; Pezzella, A.; Napolitano, A.; D'Ischia, M. *Tetrahedron* **2006**, *62*, 1273–1278.
(44) Panzella, L.; Eidenberger, T.; Napolitano, A.; D'Ischia, M. *J. Agric. Food Chem.* **2012**, *60*, 8895–8901.
(45) Weisser, J. T.; Nilges, M. J.; Sever, M. J.; Wilker, J. J. *Inorg. Chem.* **2006**, *45*, 7736–7747.
(46) Zeng, H.; Hwang, D. S.; Israelachvili, J. N.; Waite, J. H. **2010**, 10–13.
(47) Lee, H.; Scherer, N. F.; Messersmith, P. B. *Proc. Natl. Acad. Sci.* **2006**, *103* (35), 12999–13003.
(48) Harrington, M. J.; Masic, A.; Holten-Andersen, N.; Waite, J. H.; Fratzl, P. *Science* **2010**, *328*, 216–220.
(49) Holten-Andersen, N.; Harrington, M. J.; Birkedal, H.; Lee, B. P.; Messersmith, P. B.; Lee, K. Y. C.; Waite, J. H. *Proc. Natl. Acad. Sci. U. S. A.* **2011**, *108*, 2651–2655.
(50) Petrone, L.; Kumar, A.; Sutanto, C. N.; Patil, N. J.; Kannan, S.; Palaniappan, A.; Amini, S.; Zappone, B.; Verma, C.; Miserez, A. *Nat. Commun.* **2015**, *6*, 8737.
(51) Fullenkamp, D. E.; Rivera, J. G.; Gong, Y.; Lau, K. H. A.; He, L.; Varshney, R.; Messersmith, P. B. *Biomaterials* **2012**, *33*, 3783–3791.
(52) Nurchi, V. M.; Pivetta, T.; Lachowicz, J. I.; Crisponi, G. *J. Inorg. Biochem.* **2009**, *103*, 227–236.
(53) Lin, Q.; Li, Q.; Batchelor-Mcauley, C.; Compton, R. G. *J. Phys. Chem. C* **2015**, *119*, 1489–1495.
(54) Yang, J.; Cohen Stuart, M. A.; Kamperman, M. *Chem. Soc. Rev.* **2014**, *43*, 8271–8298.
(55) Fullenkamp, D. E.; Barrett, D. G.; Miller, D. R.; Kurutz, J. W.; Messersmith, P. B. *RSC Adv.* **2014**, *4*, 25127–25134.
(56) Kramer, K. J.; Kanost, M. R.; Hopkins, T. L.; Jiang, H.; Zhu, Y. C.; Xu, R.; Kerwin, J. L.; Turecek, F. *Tetrahedron* **2001**, *57*, 385–392.
(57) Wang, C. S.; Stewart, R. J. *Biomacromolecules* **2013**, *14*, 1607–1617.
(58) Burzio, L. A.; Waite, J. H. *Biochemistry* **2000**, *39*, 11147–11153.
(59) Sedõ, J.; Saiz-Poseu, J.; Busqué, F.; Ruiz-Molina, D. *Advanced Materials*. **2013**, 653–701.
(60) Abergel, R. J.; Raymond, K. N. *Inorg. Chem.* **2006**, *45*, 3622–3631.
(61) Werner, E. J.; Datta, A.; Jocher, C. J.; Raymond, K. N. *Angewandte Chemie - International Edition*. 2008, 8568–8580.
(62) Lorenzo, E.; Pariente, F.; Hernàndez, L.; Tobalina, F.; Darder, M.; Wu, Q.; Maskus, M.; Abruña, H. D. *Biosens. Bioelectron.* **1998**, *13*, 319–332.
(63) Chen, P. Y.; Nien, P. C.; Wu, C. T.; Wu, T. H.; Lin, C. W.; Ho, K. C. *Anal. Chim. Acta* **2009**, *643*, 38–44.
(64) White, E. M.; Seppala, J. E.; Rushworth, P. M.; Ritchie, B. W.; Sharma, S.; Locklin, J. **2013**.
(65) Cui, J.; Iturri, J.; Paez, J.; Shafi, Z.; Serrano, C.; d'Ischia, M.; del Campo, A. *Macromol. Chem. Phys.* **2014**, *215*, 2403–2413.
(66) González-Monje, P.; Novio, F.; Ruiz-Molina, D. *Chem. - A Eur. J.* **2015**, *21*, 10094–10099.
(67) Verma, S.; Kar, P.; Das, A.; Palit, D. K.; Ghosh, H. N. *J. Phys. Chem. C* **2008**, *112*, 2918–2926.
(68) Verma, S.; Kar, P.; Das, A.; Ghosh, H. N. *Chem. - A Eur. J.* **2011**, *17*, 1561–1568.
(69) García-Cañadas, J.; Meacham, A. P.; Peter, L. M.; Ward, M. D. *Electrochem. commun.* **2003**, *5*, 416–420.
(70) Kim, E.; Liu, Y.; Baker, C. J.; Owens, R.; Xiao, S.; Bentley, W. E.; Payne, G. F. *Biomacromolecules* **2011**, *12*, 880–888.
(71) Zhang, Y.; Thomas, Y.; Kim, E.; Payne, G. F. *J. Phys. Chem. B* **2012**, *116*, 1579–1585.
(72) Crescenzi, O.; Napolitano, A.; Prota, G.; Peter, M. G. *Tetrahedron* **1991**, *47*, 6243–6250.
(73) Zhang, X.; Zhu, Y.; Li, X.; Guo, X.; Zhang, B.; Jia, X.; Dai, B. *Anal. Chim. Acta* **2016**, *944*, 51–56.
(74) Yu, M.; Deming, T. *Macromolecules* **1998**, *31*, 4739–4745.

(75) Westwood, G.; Horton, T. N.; Wilker, J. J. *Macromolecules* **2007**, *40*, 3960–3964.
(76) Charlot, A.; Sciannaméa, V.; Lenoir, S.; Faure, E.; Jérôme, R.; Jérôme, C.; Van De Weerdt, C.; Martial, J.; Archambeau, C.; Willet, N.; Duwez, A.-S.; Fustin, C.-A.; Detrembleur, C. *J. Mater. Chem.* **2009**, *19*, 4117–4125.
(77) Falentin-Daudr, C.; Faure, E.; Svaldo-Lanero, T.; Farina, F.; Van De Weerdt, C.; Martial, J.; Duwez, A. S.; Detrembleur, C. *Langmuir* **2012**, *28*, 7233–7241.
(78) Lee, H.; Lee, K. D.; Pyo, K. B.; Park, S. Y.; Lee, H. *Langmuir* **2010**, *26*, 3790–3793.
(79) Dalsin, J. L.; Lin, L.; Tosatti, S.; Vörös, J.; Textor, M.; Messersmith, P. B. *Langmuir* **2005**, *21*, 640–646.
(80) Sileika, T. S.; Barrett, D. G.; Zhang, R.; Lau, K. H. A.; Messersmith, P. B. *Angew. Chemie - Int. Ed.* **2013**, *52*, 10766–10770.
(81) Liu, Y.; Ai, K.; Lu, L. *Chemical Reviews*. **2014**, 5057–5115.
(82) Prota, G. *Melanins and melanogenesis*; Academic Press, **1992**.
(83) Pezzella, A.; Iadonisi, A.; Valerio, S.; Panzella, L.; Napolitano, A.; Adinolfi, M.; D'Ischia, M. *J. Am. Chem. Soc.* **2009**, *131*, 15270–15275.
(84) Rienecker, S. B.; Mostert, A. B.; Schenk, G.; Hanson, G. R.; Meredith, P. *J. Phys. Chem. B* **2015**, *119*, 14994–15000.
(85) Mostert, A. B.; Hanson, G. R.; Sarna, T.; Gentle, I. R.; Powell, B. J.; Meredith, P. *J. Phys. Chem. B* **2013**, *117*, 4965–4972.
(86) Assis Oliveira, L. B.; L Fonseca, T.; Costa Cabral, B. J.; Coutinho, K.; Canuto, S. *J. Chem. Phys.* **2016**, *145*, 84501.
(87) Manini, P.; Criscuolo, V.; Ricciotti, L.; Pezzella, A.; Barra, M.; Cassinese, A.; Crescenzi, O.; Maglione, M. G.; Tassini, P.; Minarini, C.; Barone, V.; D'Ischia, M. *Chempluschem* **2015**, *80*, 919–927.
(88) Ju, K. Y.; Lee, Y.; Lee, S.; Park, S. B.; Lee, J. K. *Biomacromolecules* **2011**, *12*, 625–632.
(89) Arzillo, M.; Mangiapia, G.; Pezzella, A.; Heenan, R. K.; Radulescu, A.; Paduano, L.; d'Ischia, M. *Biomacromolecules* **2012**, *13*, 2379–2390.
(90) Clancy, C. M. R.; Simon, J. D. *Biochemistry* **2001**, *40*, 13353–13360.
(91) Ghiani, S.; Baroni, S.; Burgio, D.; Digilio, G.; Fukuhara, M.; Martino, P.; Monda, K.; Nervi, C.; Kiyomine, A.; Aime, S. *Magn Reson Chem* **2008**, *46*, 471–479.
(92) Kaxiras, E.; Tsolakidis, A.; Zonios, G.; Meng, S. *Phys. Rev. Lett.* **2006**, *97*, 1–4.
(93) Liu, Y.; Simon, J. D. *Pigment Cell Res.* **2003**, *16*, 72–80.
(94) Meng, S.; Kaxiras, E.; Pezzella, A.; Panzella, L.; Natangelo, A.; Arzillo, M.; Napolitano, A.; D'Ischia, M. *J. Org. Chem.* **2007**, *72*, 9225–9230.
(95) Stark, K. B.; Gallas, J. M.; Zajac, G. W.; Golab, J. T.; Gidanian, S.; Mcintire, T.; Farmer, P. J. **2005**, *109*, 1970–1977.
(96) Corani, A.; Huijser, A.; Gustavsson, T.; Markovitsi, D.; Malmqvist, P.-Å.; Pezzella, A.; d'Ischia, M.; Sundström, V. *J. Am. Chem. Soc.* **2014**, *136*, 11626–11635.
(97) Gauden, M.; Pezzella, A.; Panzella, L.; Neves-Petersen, M. T.; Skovsen, E.; Petersen, S. B.; Mullen, K. M.; Napolitano, A.; D'Ischia, M.; Sundström, V.; D 'ischia, M.; Sundstrom, V.; Napolitano, A; Sundström, V. *J. Am. Chem. Soc.* **2008**, *130*, 17038–17043.
(98) Slominski, A. *Physiol. Rev.* **2004**, *84*, 1155–1228.
(99) Simon, J. D.; Peles, D. N. *Acc. Chem. Res.* **2010**, *43*, 1452–1460.
(100) d'Ischia, M.; Wakamatsu, K.; Cicoira, F.; Di Mauro, E.; Garcia-Borron, J. C.; Commo, S.; Galván, I.; Ghanem, G.; Kenzo, K.; Meredith, P.; Pezzella, A.; Santato, C.; Sarna, T.; Simon, J. D.; Zecca, L.; Zucca, F. A.; Napolitano, A.; Ito, S. *Pigment Cell Melanoma Res.* **2015**, *28*, 520–544.
(101) Borovanský, J.; Riley, P. A.; Patrick A. *Melanins and melanosomes : biosynthesis, biogenesis, physiological, and pathological functions*; Wiley-Blackwell, **2011**.
(102) Tran, M. L.; Powell, B. J.; Meredith, P. *Biophys. J.* **2005**, *90*, 28.
(103) d'Ischia, M.; Crescenzi, O.; Pezzella, A.; Arzillo, M.; Panzella, L.; Napolitano, A.; Barone, V. *Photochem. Photobiol.* **2008**, *84*, 600–607.
(104) Tuna, D.; Udvarhelyi, A.; Sobolewski, A. L.; Domcke, W.; Domratcheva, T. *J. Phys. Chem. B* **2016**, *120*, 3493–3502.
(105) Pezzella, A.; Crescenzi, O.; Panzella, L.; Napolitano, A.; Land, E. J.; Barone, V.; d'Ischia, M. *J. Am. Chem. Soc.* **2013**, *135*, 12142–12149.
(106) Ascione, L.; Pezzella, A.; Ambrogi, V.; Carfagna, C.; d'Ischia, M. *Photochem. Photobiol.* **2013**, *89*,

314–318.
(107) Pezzella, A.; Panzella, L.; Crescenzi, O.; Napolitano, A.; Navaratnam, S.; Edge, R.; Land, E. J.; Barone, V.; D'Ischia, M. *J. Org. Chem.* **2009**, *74*, 3727–3734.
(108) Chen, C.-T.; Chuang, C.; Cao, J.; Ball, V.; Ruch, D.; Buehler, M. J. *Nat. Commun.* **2014**, *5*, 3859.
(109) Pezzella, A.; Panzella, L.; Crescenzi, O.; Napolitano, A.; Navaratman, S.; Edge, R.; Land, E. J.; Barone, V.; d'Ischia, M. *J. Am. Chem. Soc.* **2006**, *128*, 15490–15498.
(110) Barone, V.; Cacelli, I.; Crescenzi, O.; D'Ischia, M.; Ferretti, A.; Prampolini, G.; Villani, G. *RSC Adv.* **2014**, *4*, 876.
(111) Prampolini, G.; Cacelli, I.; Ferretti, A. *RSC Adv.* **2015**, *5*, 38513–38526.
(112) Panzella, L.; Napolitano, A.; D'Ischia, M. *Pigment Cell Melanoma Res.* **2011**, *24*, 248–249.
(113) Palumbo, P.; d'Ischia, M.; Prota, G. *Tetrahedron* **1987**, *43*, 4203–4206.
(114) Palumbo, A.; d'Ischia, M.; Misuraca, G.; Prota, G. *Biochim. Biophys. Acta* **1987**, *925*, 203–209.
(115) Palumbo, A.; Solano, F.; Misuraca, G.; Aroca, P.; Garcia Borron, J. C.; Lozano, J. A.; Prota, G. *Biochim. Biophys. Acta* **1991**, *1115*, 1–5.
(116) Tsukamoto, K.; Palumbo, A.; D'Ischia, M.; Hearing, V. J.; Prota, G. *Biochem. J.* **1992**, *286*, 491–495.
(117) Simon, J. D.; Peles, D.; Wakamatsu, K.; Ito, S. *Pigment Cell Melanoma Res.* **2009**, *22*, 563–579.
(118) d'Ischia, M.; Napolitano, A.; Pezzella, A. *European J. Org. Chem.* **2011**, *11*, 5501–5516.
(119) Pezzella, A.; Panzella, L.; Natangelo, A.; Arzillo, M.; Napolitano, A.; d'Ischia, M. *J. Org. Chem.* **2007**, *72*, 9225–9230.
(120) Corradini, M. G.; Napolitano, A.; Prota, G. *Tetrahedron* **1986**, *42*, 2083–2088.
(121) Pezzella, A.; Vogna, D.; Prota, G. *Tetrahedron: Asymmetry* **2003**, *14*, 1133–1140.
(122) Goupy, P.; Dufour, C.; Loonis, M.; Dangles, O. *J. Agric. Food Chem.* **2003**, *51*, 615–622.
(123) Benzie, I. F. F.; Strain, J. J. *Anal. Biochem.* **1996**, *239*, 70–76.
(124) Yordanov, N. D.; Gancheva, V.; Pelova, V. A. *J. Radioanal. Nucl. Chem.* **1999**, *240*, 619–622.
(125) d'Ischia, M.; Wakamatsu, K.; Napolitano, A.; Briganti, S.; Garcia-Borron, J.-C.; Kovacs, D.; Meredith, P.; Pezzella, A.; Picardo, M.; Sarna, T.; Simon, J. D.; Ito, S. *Pigment Cell Melanoma Res.* **2013**, *26*, 616–633.
(126) Napolitano, A., Corradini M.G., Prota, G. *Tetrahedron Lett.* **1985**, *26*, 2805–2808.
(127) Liu, Y.; Ai, K.; Lu, L. *Chem. Rev.* **2013**, *114*, 5057–5115.
(128) d'Ischia, M.; Napolitano, A.; Ball, V.; Chen, C. T.; Buehler, M. J. *Acc. Chem. Res.* **2014**, *47*, 3541–3550.
(129) Della Vecchia, N. F.; Avolio, R.; Alfè, M.; Errico, M. E.; Napolitano, A.; d'Ischia, M. *Adv. Funct. Mater.* **2013**, *23*, 1331–1340.
(130) Della Vecchia, N. F.; Luchini, A.; Napolitano, A.; D'Errico, G.; Vitiello, G.; Szekely, N.; d'ischia, M.; Paduano, L. *Langmuir* **2014**, *30*, 9811–9818.
(131) Hong, S.; Yang, K.; Kang, B.; Lee, C.; Song, I. T.; Byun, E.; Park, K. I.; Cho, S.; Lee, H. *Adv. Funct. Mater.* **2013**, *23*, 1774–1780.
(132) Kim, Y. R.; Bong, S.; Kang, Y. J.; Yang, Y.; Mahajan, R. K.; Kim, J. S.; Kim, H. *Biosens. Bioelectron.* **2010**, *25*, 2366–2369.
(133) Salierno, M. J.; García, A. J.; Del Campo, A. *Adv. Funct. Mater.* **2013**, *23*, 5974–5980.
(134) Wang, X.; Yuan, S.; Shi, D.; Yang, Y.; Jiang, T.; Yan, S.; Shi, H.; Luan, S.; Yin, J. *Appl. Surf. Sci.* **2016**, *375*, 9–18.
(135) Panzella, L.; Leone, L.; Greco, G.; Vitiello, G.; D'Errico, G.; Napolitano, A.; d'Ischia, M. *Pigment Cell Melanoma Res.* **2014**, *27*, 244–252.
(136) Napolitano, A.; Panzella, L.; Monfrecola, G.; d'Ischia, M. *Pigment Cell Melanoma Res.* **2014**, *27*, 721–733.
(137) Greco, G.; Panzella, L.; Verotta, L.; D'Ischia, M.; Napolitano, A. *J. Nat. Prod.* **2011**, *74*, 675–682.
(138) Takeuchi, S.; Zhang, W.; Wakamatsu, K.; Ito, S.; Hearing, V. J.; Kraemer, K. H.; Brash, D. E. *Proc. Natl. Acad. Sci. U. S. A.* **2004**, *101*, 15076–15081.
(139) Israeli, E. *Isr. Med. Assoc. J.* **2012**, *14*, 770.
(140) Ambrico, M.; Vecchia, N. F. Della; Ambrico, P. F.; Cardone, A.; Cicco, S. R.; Ligonzo, T.; Avolio, R.; Napolitano, A.; D'Ischia, M. *Adv. Funct. Mater.* **2014**, *24*, 7161–7172.
(141) Zhang, F.; Dryhurst, G. *J. Med. Chem.* **1994**, *37*, 1084–1098.
(142) Aureli, C.; Cassano, T.; Masci, A.; Francioso, A.; Martire, S.; Cocciolo, A.; Chichiarelli, S.; Romano, A.; Gaetani, S.; Mancini, P.; Fontana, M.; d'Erme, M.; Mosca, L. *J. Neurosci. Res.* **2014**.
(143) Ku, S. H.; Ryu, J.; Hong, S. K.; Lee, H.; Park, C. B. *Biomaterials* **2010**, *31*, 2535–2541.

(144) Kita, Y.; Tohma, H.; Hatanaka, K.; Takada, T.; Fujita, S.; Mitoh, S.; Sakurai, H.; Okas, S. *J. Am. Chem. Soc.* **1994**, *116*, 3684–3691.
(145) Ren, X.-F.; Turos, E. *Tetrahedron Lett.* **1993**, *34*, 1575–1578.
(146) Kita, Y.; Egi, M.; Ohtsubo, M.; Saiki, T.; Takada, T.; Tohma, H. **1996**, 2225–2226.
(147) Panzella, L.; Szewczyk, G.; D'Ischia, M.; Napolitano, A.; Sarna, T. *Photochem. Photobiol.* **2010**, *86*, 757–764.
(148) Chen, S.; Li, X.; Yang, Z.; Zhou, S.; Luo, R.; Maitz, M. F.; Zhao, Y.; Wang, J.; Xiong, K.; Huang, N. *Colloids Surfaces B Biointerfaces* **2014**, *113*, 125–133.
(149) Yang, Y.; Qi, P.; Ding, Y.; Maitz, M. F.; Yang, Z.; Tu, Q.; Xiong, K.; Leng, Y.; Huang, N. *J. Mater. Chem. B* **2015**, *3*, 72–81.
(150) Yabuta, G.; Koizumi, Y.; Namiki, K.; Hida, M.; Namiki, M. *Biosci. Biotechnol. Biochem.* **2001**, *65*, 2121–2130.
(151) Namiki, M.; Yabuta, G.; Koizumi, Y.; Yano, M. *Biosci. Biotechnol. Biochem.* **2001**, *65*, 2131–2136.
(152) Tumolo, T.; Lanfer-Marquez, U. M. *Food Res. Int.* **2012**, *46*, 451–459.
(153) Yabuta, G.; Koizumi, Y.; Namiki, K.; Kawai, T.; Hayashi, T.; Namiki, M. *Biosci. Biotechnol. Biochem.* **1996**, *60*, 1701–1702.
(154) Schilling, S.; Sigolotto, C. I.; Carle, R.; Schieber, A. *Rapid Commun. mass Spectrom.* **2008**, *22*, 441–448.
(155) Cilliers, J. J. L.; Singleton, V. L. *J. Agric. Food Chem.* **1989**, *37*, 890–896.
(156) Claramunt, R. M.; Sanz, D.; López, C.; Jiménez, J. A. *Magn. Reson. Chem.* **1997**, *35*, 35–75.
(157) Bongartz, V.; Brandt, L.; Gehrmann, M. L.; Zimmermann, B. F.; Schulze-Kaysers, N.; Schieber, A. *Molecules* **2016**, *21*, 91–99.
(158) Prigent, S. V.; Voragen, A. G.; Li, F.; Visser, A. J.; van Koningsveld, G. A.; Gruppen, H. *J. Sci. Food Agric.* **2008**, *88*, 1748–1754.
(159) Panzella, L.; Cerruti, P.; Ambrogi, V.; Agustin-Salazar, S.; D'Errico, G.; Carfagna, C.; Goya, L.; Ramos, S.; Martín, M. A.; Napolitano, A.; d'Ischia, M. *ACS Sustain. Chem. Eng.* **2016**, *4*, 1169–1179.
(160) Stookey, L. L. *Anal. Chem.* **1970**, *42*, 779–781.
(161) Su, J.; Sun, Y.-Q.; Huo, F.-J.; Yang, Y.-T.; Yin, C.-X. *Analyst* **2010**, *135*, 2918–2923.
(162) Chen, S.; Zhang, J.; Chen, Y.; Zhao, S.; Chen, M.; Li, X.; Maitz, M. F.; Wang, J.; Huang, N. *ACS Appl. Mater. Interfaces* **2015**, *7*, 24510–24522.
(163) Bongartz, V.; Brandt, L.; Gehrmann, M.; Zimmermann, B.; Schulze-Kaysers, N.; Schieber, A. *Molecules* **2016**, *21*, 91.
(164) Clifford, M. N.; Johnston, K. L.; Knight, S.; Kuhnert, N. *J. Agric. Food Chem.* **2003**, *51*, 2900–2911.
(165) Xie, C.; Yu, K.; Zhong, D.; Yuan, T.; Ye, F.; Jarrell, J. A.; Millar, A.; Chen, X. *J. Agric. Food Chem.* **2011**, *59*, 11078–11087.
(166) Dawidowicz, A. L.; Typek, R. *J. Agric. Food Chem.* **2012**, *60*, 12289–12295.
(167) Lima, J. D. P.; Farah, A.; King, B.; De Paulis, T.; Martin, P. R. *J. Agric. Food Chem.* **2016**, *64*, 2361–2370.
(168) Wang, J.; Zhao, Y.; Wang, C.; Zhu, Q.; Du, Z.; Hu, A.; Yang, Y. *PLoS One* **2015**, *10*, 1–11.
(169) MacNevin, C. J.; Gremyachinskiy, D.; Hsu, C. W.; Li, L.; Rougie, M.; Davis, T. T.; Hahn, K. M. *Bioconjug. Chem.* **2013**, *24*, 215–223.
(170) Stadler, A. L.; Delos Santos, J. O.; Stensrud, E. S.; Dembska, A.; Silva, G. L.; Liu, S.; Shank, N. I.; Kunttas-Tatli, E.; Sobers, C. J.; Gramlich, P. M. E.; Carell, T.; Peteanu, L. A.; McCartney, B. M.; Armitage, B. A. *Bioconjug. Chem.* **2011**, *22*, 1491–1502.
(171) Shieh, P.; Dien, V. T.; Beahm, B. J.; Castellano, J. M.; Wyss-Coray, T.; Bertozzi, C. R. *J. Am. Chem. Soc.* **2015**, *137*, 7145–7151.
(172) Qi, J.; Han, M. S.; Chang, Y. C.; Tung, C. H. *Bioconjug. Chem.* **2011**, *22*, 1758–1762.
(173) Shi, Z.; Tang, X.; Zhou, X.; Cheng, J.; Han, Q.; Zhou, J. A.; Wang, B.; Yang, Y.; Liu, W.; Bai, D. *Inorg. Chem.* **2013**, *52*, 12668–12673.
(174) Zhang, Y.; Liu, Z.; Yang, K.; Zhang, Y.; Xu, Y.; Li, H.; Wang, C.; Lu, A.; Sun, S. *Sci. Rep.* **2015**, *5*, 8172.
(175) Chan, J.; Dodani, S. C.; Chang, C. J. *Nat. Chem.* **2012**, *4*, 973–984.
(176) Loudet, A.; Burgess, K. *Chem. Rev.* **2007**, *107*, 4891–4932.
(177) Urano, Y.; Kamiya, M.; Kanda, K.; Ueno, T.; Hirose, K.; Nagano, T. *J. Am. Chem. Soc.* **2005**, *127*, 4888–4894.

(178) Monardes, N. *Seville* **1565**.
(179) Acuña, A. U.; Amat-Guerri, F. *Springer Se Fluoresc* **2008**, *4*, 3–20.
(180) Acuña, A. U.; Amat-Guerri, F.; Morcillo, P.; Liras, M.; Rodrìguez, B. *Org. Lett.* **2009**, *11*, 3020–3023.
(181) Acuña, A. U.; Álvarez-Pérez, M.; Liras, M.; Coto, P. B.; Amat-Guerri, F. *Phys. Chem. Chem. Phys.* **2013**, *15*, 16704–16712.
(182) Zhang, X.; Zhu, Y.; Li, X.; Guo, X.; Zhang, B.; Jia, X.; Dai, B. *Anal. Chim. Acta* **2016**, *944*, 51–56.
(183) Philip, S. *Chempluschem* **2012**, *77*, 518–531.
(184) Liu, K.; Liu, T.; Chen, X.; Sun, X.; Fang, Y. **2013**.
(185) He, M.; Peng, H.; Wang, G.; Chang, X.; Miao, R.; Wang, W. *Sensors Actuators B. Chem.* **2016**, *227*, 255–262.
(186) Jorge, P. A. S.; Caldas, P.; Rosa, C. C.; Oliva, A. G.; Santos, J. L. *Sensors Actuators B* **2004**, *103*, 290–299.
(187) Li, D.; Zhang, Y.; Fan, Z.; Yu, J. *Chem. Commun.* **2015**, *51*, 13830–13833.
(188) Long, L.; Zhang, D.; Li, X.; Zhang, J.; Zhang, C.; Zhou, L. *Anal. Chim. Acta* **2013**, *775*, 100–105.
(189) Fan, J.; Chang, X.; He, M.; Shang, C.; Wang, G.; Yin, S.; Peng, H. *ACS Appl. Mater. Interfaces* **2016**, *8*, 18584–18592.
(190) He, M.; Peng, H.; Wang, G.; Chang, X.; Miao, R.; Wang, W. *Sensors Actuators B.* **2016**, *227*, 255–262.
(191) Kord Forooshani, P.; Lee, B. P. *J. Polym. Sci. Part A Polym. Chem.* **2016**, 1–25.
(192) Veciana-Nogués, M. T.; Mariné-Font, A.; Vidal-Carou, M. C. *J. Agric. Food Chem.* **1997**, *45*, 2036–2041.
(193) Bhadra, S.; Narvaez, C.; Thomson, D. J.; Bridges, G. E. *Talanta* **2015**, *134*, 718–723.
(194) Huis In't Veld, J. H. J. H. I. *Int. J. Food Microbiol.* **1996**, *33*, 1–18.
(195) Juette, M. F.; Terry, D. S.; Wasserman, M. R.; Zhou, Z.; Altman, R. B.; Zheng, Q.; Blanchard, S. C. *Curr. Opin. Chem. Biol.* **2014**, *20*, 103–111.
(196) Kim, D.; Lee, H.; Cho, S. *Biomacromolecules* **2013**, *14*, 2004–2013.